The Synthesis and Characterisation of Macrocyclic Ligands with N, O and S Donor Atoms, and related Transition Metal Complexes of these Ligands.

by

Alison Mary Ingham
B.Sc. (Hons.), University of the Witwatersrand, 1991

A Dissertation Submitted in Partial Fulfillment of the
Requirements for the Degree of

DOCTOR OF PHILOSOPHY

in the Department of Chemistry

We accept this dissertation as conforming
to the required standard

Dr. A. McAuley, Supervisor (Department of Chemistry)

Dr. K.R. Dixon, Departmental Member (Department of Chemistry)

Dr. D.J. Berg, Departmental Member (Department of Chemistry)

Dr. G.A. Beer, Outside Member (Department of Physics)

Dr. C. Orvig, External Examiner (Department of Chemistry, University of British Columbia)

ABSTRACT

Supervisor: Dr. Alexander McAuley

The ligand 1-oxa-4,8-diazacyclodecane ([10]aneN_2O) was synthesised, along with the Cu^{II}, Ni^{II}, Pd^{II} and Co^{III} complexes. *Bis*-ligand complexes are formed with facial coordination of the ligand to the transition metals, with two nitrogen donors from each ligand forming an equatorial plane around the metal ion. The crystal structure of $[Cu([10]aneN_2O)_2](ClO_4)_2 \cdot (H_2O)$ was determined, as is described. The copper(II), nickel(II) and palladium(II) complexes have been characterised by FAB MS, electronic spectroscopy, elemental analysis and where possible by NMR and EPR spectroscopy. The nickel(II) and copper(II) complexes have distorted octahedral geometries, while the palladium(II) complex has square planar geometry with no observable axial interaction from the ether donors. The redox characteristics of the complexes formed have been determined, and are described within.

The synthesis of the novel tricyclic ligand, 7,16-dioxa-1,4,10,13-tetraazatricyclo[11.5.3.3]octadecane (tricyclo[10-14-10]N_4O_2) is described. The Cu^{II} complex has been synthesised and characterised. The complex gives an unusually stable Cu^{I} complex compared to complexes where a similar donor set is present.

A novel template synthesis was utilised to synthesise the bicyclic ligand 1,2-*bis*(1-oxa-5,8-diazacyclodecanyl)ethane ([10]aneN_2O earmuff). This synthesis involved reaction of

secondary amines which are coordinated to a copper(II) ion, a method which to our knowledge has not been used before in the synthesis of macrocyclic ligands. The copper(II) complex synthesised during this reaction has been characterised, and the redox reactions have been examined.

The synthesis of 17-oxa-1,4,8,11-tetraazabicyclo[6.6.5]tetradecane (bicyclo[12-12]N_4O) is reported. Copper(II) and nickel(II) complexes of this ligand have been synthesised and characterised. The chloride ion substitution reaction of $[Ni(bicyclo[12\text{-}12]N_4O)(OH_2)]^{3+}$ has been examined. The reaction was found to have an inverse dependence on the acid concentration. A tentative mechanism has been proposed to explain the origin of the acid dependence. The equilibrium constant for this reaction, determined by visible spectrophotometry, was found to be $170\pm10 M^{-1}$.

The cobalt(III) *bis*-ligand complex of the previously synthesised ligand, 8-aza-1,5-dithiacyclodecane ([10]aneS_2N) was synthesised. Under the conditions used, two isomers were formed - a facially coordinate *bis*-ligand complex where the equatorial plane is defined by two sulfur and two nitrogen donors, and a more symmetrical isomer where all four sulfur donors are coordinated equatorially. Isomerisation of the unsymmetrical isomer to the symmetrical isomer occurs in solution.

The Co^{II} and Co^{III} complexes of the ligand 1,2-*bis*(8-aza-1,5-dithiacyclodecanyl)ethane ([10]aneS_2N earmuff) were synthesised and characterised. The ligand coordinates to Co^{III} in

a pseudo five coordinate manner as determined by NMR spectroscopy. A solvent molecule or anion is likely to be coordinated to the Co^{III} centre in order to achieve distorted octahedral coordination. The complexes were characterised by FAB MS, electronic spectroscopy, elemental analysis and ESR spectroscopy. Although the Co^{II} centre was found to be in the low spin state, the electron transfer self exchange rate constant could not be determined by NMR spectroscopy. The Pd^{II} complex of this ligand was also synthesised and found to coordinate in a five coordinate manner. Evidence of axial coordination of nitrogen in the palladium complex was observed in the electronic spectrum, therefore a distorted square pyramidal geometry has been proposed for the $[Pd([10]aneS_2N$ earmuff$)]^{2+}$ complex.

The potentially binuclear ligand, 1,9-*bis*(4-aza-1,8-dithiacyclononane)-4,7-diaza-2,8-dione nonane, was synthesised and characterised. Preliminary results indicate that reaction with two equivalents of nickel(II) produced a binuclear complex.

Examiners:

Dr. A. McAuley, Supervisor (Department of Chemistry)

Dr. K.R. Dixon, Departmental Member (Department of Chemistry)

Dr. D.J. Berg, Departmental Member (Department of Chemistry)

Dr. G.A. Beer, Outside Member (Department of Physics)

Dr. C. Orvig, External Examiner (Department of Chemistry, University of British Columbia)

TABLE OF CONTENTS

LIST OF TABLES

LIST OF FIGURES

LIST OF SCHEMES

LIST OF ABBREVIATIONS

1,9-*bis*([10]aneS_2N amidoearmuff)	1,9-*bis*(8-aza-1,4-dithiacyclodecane)-4,7-diaza-2,8-dione nonane
[9]aneN_3	1,4,7-triazacyclononane
[10]aneN_3	1,4,8-triazacyclodecane
[10]aneN_2O	1-oxa-4,8-diazacyclodecane
[10]aneN_2O earmuff	1,2-*bis*(1-oxa-4,8-diazacyclodecanyl)ethane
[10]aneS_2N	8-aza-1,4-dithiacyclodecane
[10]aneS_2N earmuff	1,2-*bis*(8-aza-1,4-dithiacyclodecanyl)ethane
bicyclo[9-14]N_4O	17-oxa-1,5,8,12-tetraazabicyclo[10.5.2]nonadecane
bicyclo[10-14]N_4O	14-oxa-1,4,8,11-tetraazabicyclo[9.5.3]hexadecane
bicyclo[12-12]N_4O	17-oxa-1,4,8,11-tetraazabicyclo[6.6.5]tetradecane
br	broad
CI	chemical impact
cyclam	1,4,8,11-tetraazacyclotetradecane
cyclen	1,4,7,10-tetraazacyclododecane
diammac	6,13-dimethyl-1,4,8,11-tetraazatetradecane-6,15-diamine
DMF	dimethylformamide
DPPH	2,2-diphenyl-1-picrylhydrazyl hydrate
EPR	electron paramagnetic resonance
ES	electrospray ionisation
FAB	fast atom bombardment
fw	formula weight
g	gerade
IR	infra-red
L	ligand
m	multiplet
mesyl, ms	methyl sulfonyl ($CH_3SO_2^-$)

MS	mass spectroscopy
NIR	near infra-red
NMR	nuclear magnetic resonance
ppm	parts per million
PW	present work
q	quartet
s	singlet
t	triplet
tacd	1,4,8-triazacyclodecane
THF	tetrahydrofuran
TMS	tetramethylsilane
tosyl, ts	p-tolyl-sulfonyl ($p$$CH_3$-$C_6H_4$-$SO_2$-)
tricyclo[10-14-10]N_4O_2	7,16-dioxa-1,4,10,13-tetraazatricyclo[11.5.3.3]octadecane
u	ungerade
UV/Vis	ultraviolet/visible

ACKNOWLEDGEMENTS

I would like to thank my supervisor, Dr. A. McAuley, for his encouragement and guidance throughout the course of this work. I would also like to thank the members of the McAuley group: I. McKay, M. Rodopoulous, T. Rodopoulous, and K. Coulter, as well as K. Simonson, and S. Subramanian. The assistance of C. Greenwood for NMR spectroscopy, D.McGillivray and L. Schallig for mass spectroscopy and B. Chak for crystallography is greatly appreciated. Finally I would like to thank W. Ingham for proof reading this thesis.

To my husband, Wayne and my family.

CHAPTER 1

INTRODUCTION

1.1 The origins of macrocylic chemistry

Pinpointing the start of coordination chemistry as a science is a difficult task, but there is no doubt that the efforts of S.M. Jørgensen and Alfred Werner were instrumental in the development of this field. Werner's coordination theory,[1] for which he was awarded the Nobel Prize in 1913, opened the door to an entirely new theory of chemical bonding. Coordination chemistry developed rapidly once theories were proposed which could explain the bonding in complexes, leading to the development of more and more complicated ligands, and hence to the field of macrocyclic chemistry.

A macrocyclic compound, by definition, is a cyclic compound containing nine or more ring atoms with at least three or more heteroatoms which may act as donors.[2] The first macrocyclic compounds studied in detail were composed of unsaturated nitrogen containing rings with 14 - 16 members.[3] These macrocycles were the naturally occurring porphyrin rings of haeme - isolated from haemoglobin or myoglobin, chlorin - isolated from chlorophyll and corrin from Vitamin B_{12} (Figure 1.1).[4] The first synthetic macrocycles were the phthalocyanine complexes (Figure 1.2) which, due to their intense colour and stability to air, light and heat were of commercial importance as dyes and pigments.[3a] The serendipitous synthesis of [Cu^{II}phthalocyanine][5] was one of the earliest known template reactions. Several of the reactions used to synthesise phthalocyanine complexes involve the condensation of phthalamide derivatives, using a metal ion (Fe^{II}, Cu^{II}, Ni^{II}) as a template.[6] The reactants arrange around this coordination centre prior to condensation. Many different phthalocyanine complexes have now been synthesised, as the variety of metal ions that

complex with phthalocyanine, as well as coordination and oxidation states that can be achieved, is numerous.[7] Interestingly, some of the first X-ray crystal structures to be solved were the Ni^{II} and Cu^{II} phthalocyanine complexes.[8]

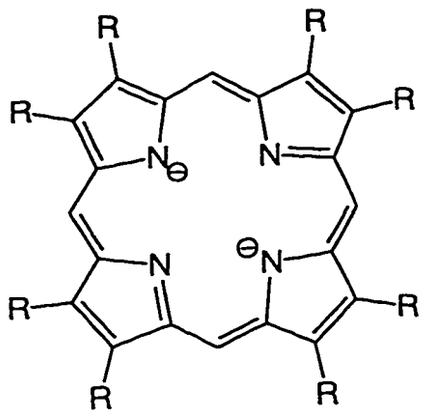

Porphyrinato dianion

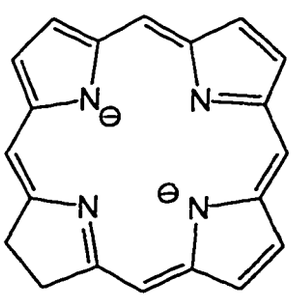

Chlorinato dianion

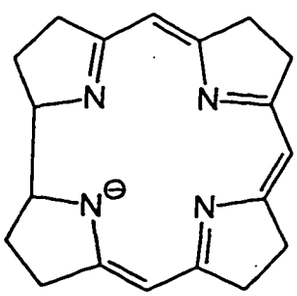

Corrinato anion

Figure 1.1: Structure of the naturally occurring macrocyclic rings

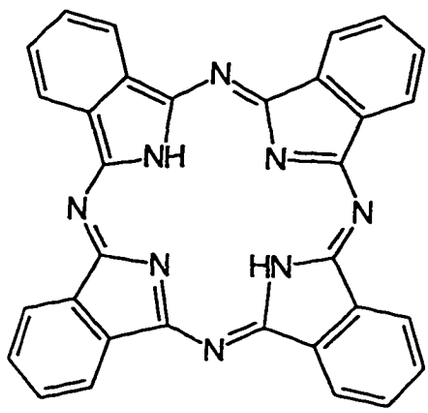

Figure 1.2: The structure of phthalocyanine

After 1960, new synthetic methods for the synthesis of macrocyclic ligands were developed[9,10] which resulted in the synthesis of both saturated and unsaturated macrocycles containing nitrogen, sulfur and oxygen donors. Most macrocycles have these atoms as donors, although phosphorus[11] and arsenic[12] have also been used as the donor atoms in certain macrocycles. The synthesis of crown ethers (cyclic polyethers)[10] during the 1960's also opened a new area of research. These macrocycles coordinate strongly to alkali and alkaline earth metals, the coordination chemistry of which had not previously been studied. Crown ethers have been used to prepare synthetic ion channels which mimic natural metal ion transportation across a lipid bilayer.

One of the most extensive fields of macrocyclic chemistry is the use of such ligands to mimic the metal-containing enzymes. Numerous ligands[13] have been synthesised in order to examine

the reactivity of Vitamin B_{12}, which has a cobalt-containing active site, shown in Figure 1.3. Macrocycles have also been used in analytical chemistry, where they are used in metal ion discrimination and sequestration, or as 'carriers' of certain substances from an aqueous to an

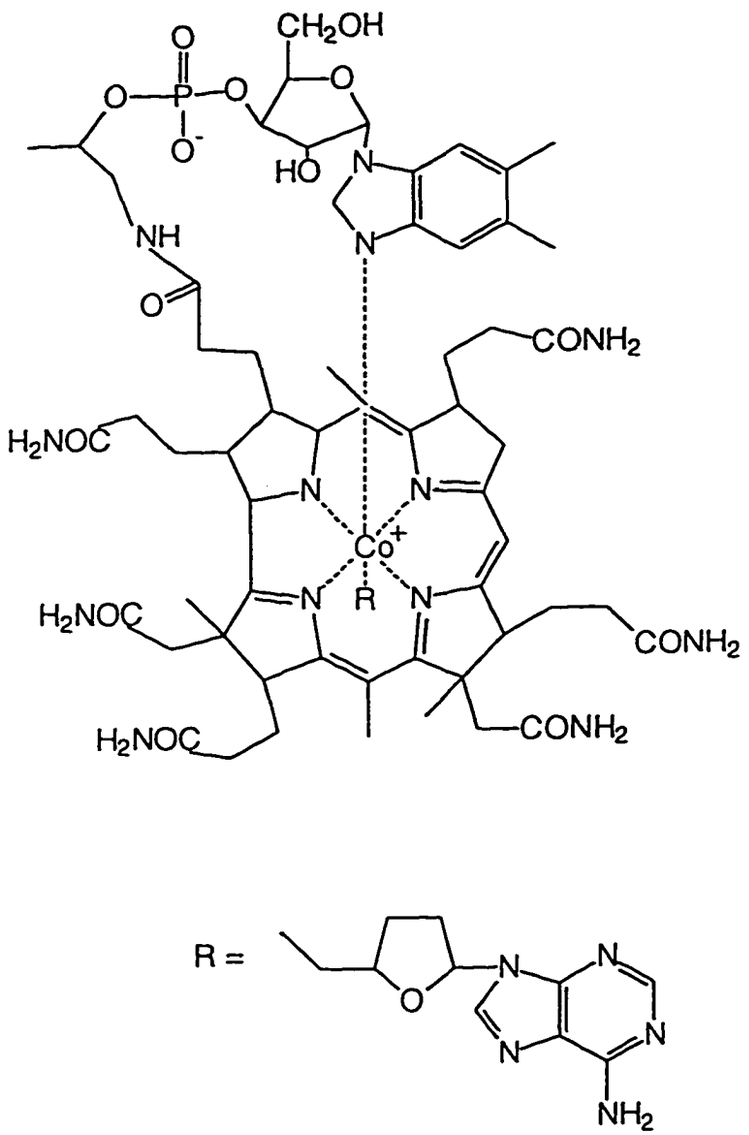

Figure 1.3: The structure of the active site of Coenzyme B_{12} (Vitamin B_{12}, R = CN)

New synthetic methodologies[14] have been developed to incorporate different donor atoms, for example nitrogen and oxygen, into a single 9 - 16 membered ring. These mixed heteroatom donor macrocycles have become increasingly important as they have the ability to stabilise differentially several oxidation states of various metals. For example, softer sulfur donors stabilise Cu^{I} preferentially, whereas the harder nitrogen donor stabilises Cu^{II}. A mixture of sulfur and nitrogen donor atoms in a macrocyclic ring could potentially stabilise both Cu^{I} and Cu^{II}, facilitating redox reactions. Larger macrocyclic rings can form binuclear metal complexes with metal : ligand ratios of 2:1.[15] Binucleating macrocycles incorporating two different metal ions offer the prospect of unusual electronic and chemical properties owing to the proximity of the two metal centres.[16]

In an effort to gain more understanding of the role of metals in biological systems, synthetic macrocycles have been used as model compounds for the more complicated, naturally occurring macrocycles. As the availability and complexity of macrocycles has increased, they have become more important in the field of catalysis.[15] In the bioinorganic field, macrocycles can be used to mimic certain enzyme-catalysed reactions. Other reactions which are of potential industrial importance have been studied, for example, metal phthalocyanine complexes catalyse the auto-oxidation of organic compounds.[7]

1.2 Nomenclature of macrocylic ligands

The nomenclature used in this thesis to describe free macrocyclic ligands is a simplified method based on ring size, saturation and type of donor atoms present. For example, the

single ring [10]aneN_2O, is named after the ten membered ring with a number of ring substituents, including heteroatoms; 'ane' implies that the ring is saturated and 'N_2O' indicates that the ring contains two nitrogen and one oxygen donor atom. The position of the substituents in the ring is not indicated, and for this purpose the IUPAC nomencluture is included in the text. For polycyclic rings, bi- and tri- indicate two and three fused rings respectively. The numbers within square brackets indicate the number of atoms per ring including donors, and the donor type and number of each atom is denoted by the atom symbol and a subscript respectively. Representative examples of the IUPAC nomenclature of macrocycles and their abbreviations used in this text are given in the list of abbreviations at the start of this text.

1.3 The thermodynamic stability and kinetic inertness of macrocyclic ligand complexes

1.3.1 Thermodynamic stability

Certain macrocyclic ligands have the ability to stabilise less common oxidation states and geometries of transition metals.[17] The term 'macrocyclic effect' was coined by Cabbiness and Margerum[18] to account for the thermodynamic stability of metal - macrocycle complexes compared to the linear anologues of the macrocyclic ligand species. The macrocyclic effect has been attributed to both thermodynamic and kinetic factors. The thermodynamic stability of the macrocyclic complexes has been ascribed to both entropic and enthalpic factors, examples of which are illustrated in Table 1.1. The origin of the thermodynamic stability appears to vary with different macrocyclic ligands, donors and metal ions.[19]

Table 1.1: The thermodynamics of complex formation with acyclic and macrocyclic ligands[2]

Ligand	logK	ΔH/kcal.mol^{-1}	$T\Delta S$/kcal.mol^{-1}
<u>Ni^{II} complex formation</u>			
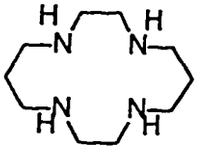	22.2	-31.0	0.6
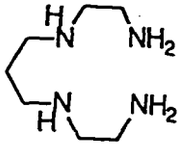	15.3	-16.8	4.1
<u>K^+ complex formation</u>			
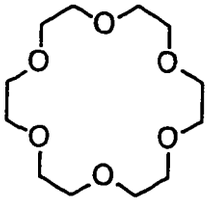	6.05	-13.21	-4.96
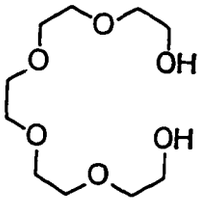	2.05	-6.37	-3.57
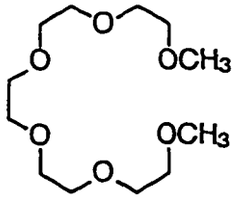	2.27	-8.16	-5.06

The entropy of formation of a macrocyclic complex is almost always favourable. This is comparable with the chelate effect[20] which results from a favourable entropy increase on metal complexation with polydentate rather than monodentate ligands. The increase in entropy is due to solvation changes involving the metal and ligand. Upon complex formation, desolvation occurs, and in the case of multidentate ligands, more molecules of solvent are released per unit of chelated ligand complexing, hence the translational entropy increases. Since the majority of the entropic stabilisation of macrocyclic complexes is a manifestation of the chelate effect, it has been concluded that the macrocyclic effect is mainly enthalpic in origin. However, there can be less loss of configurational entropy on complexation of a macrocyclic ligand, due to the preorganisation of the macrocyclic ligand compared to acyclic ligands, which may contribute to the macrocyclic effect in some ligands. An example of a preorganised macrocyclic ligand is given in Figure 1.4.[21] The open chain analogue of this macrocycle forms a low strain conformer with the piperidine ring in a chair conformation, while in the macrocycle, the ring is in a boat conformation. To form the metal complex of the open chain ligand, the ring must be in a boat conformation, therefore considerable energy is required to convert the piperidine ring from chair to boat conformation in the open chain ligand. The macrocyclic ligand is already in a suitable conformation for complexation, so no reorganisation energy is required.

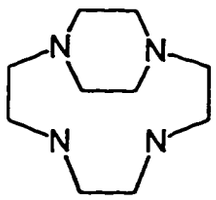

Figure 1.4: A preorganised macrocyclic ligand

Enthalpic stabilisation may be absent, in which case the macrocyclic effect is almost entirely entropic. Enthalpic stabilisation which is large in numerous cases, results from a variety of effects.[19] Ligand field factors, variations in bond energy between the metal ion and ligands involved, conformational changes on complexation, the metal size - hole size match,[22] ligand desolvation enthalpies, and steric and electrostatic interactions in the free and coordinated ligands all play a part in determining the magnitude of the macrocyclic effect.

1.3.2 Kinetic inertness

Kinetic inertness is imparted to a macrocycle complex since in non-labile systems there is no readily available site of attack on the cyclic ligand. Non-cyclic ligands are often more readily displaced by other ligands. Decomposition of complexes with chelating ligands in the presence of acid can proceed by a stepwise substitution mechanism, similar to that shown in Figure 1.5. This route is less available for cyclic compounds since there is no 'free' end, hence decomplexation rates are extremely slow as evidenced by the very high acid stability of macrocyclic complexes. $[Ni(cyclam)]^{2+}$, for example, has an estimated half life in acid solution of approximately 30 years.[23] In order to allow for protonation of a macrocyclic ligand, significant rearrangement of the cyclic ligand is often required, as illustrated in Figure 1.5 . This rearrangement of the coordination sphere essential to ligand dissociation, such as folding of the ligand, is unfavourable, hence protonation is slow. The dissociated macrocylic donor is also held in close proximity to the metal ion by the remaining complexed donors, so recomplexation can occur quite readily. Busch and co workers attributed macrocyclic kinetic stability to this concerted complexation effect,[24] and coined the phrase 'multiple

juxtapositional fixedness' to describe it.

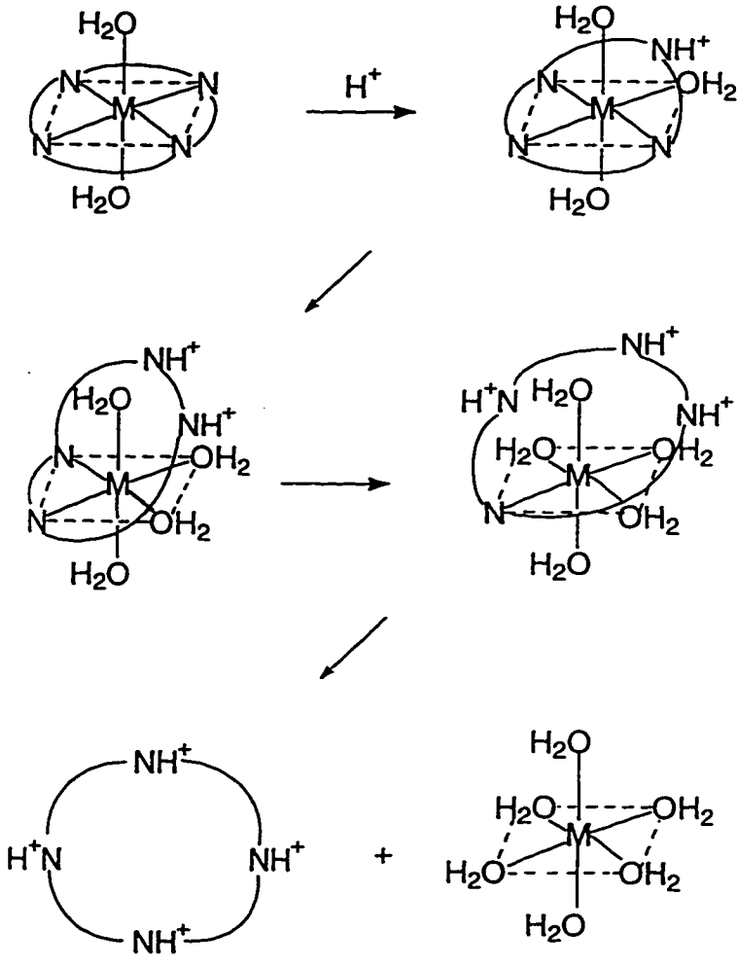

Figure 1.5: An acid catalysed dissociation mechanism for macrocyclic ligands

1.4 The implications of the macrocyclic effect

Not all ring complexes of this type exhibit the macrocyclic effect. This effect is dependent on

many factors including the match between metal size and ligand cavity (hole) size, the donor nature, ring size and rigidity, and the nature of the solvent in which the reaction occurs. If a metal ion has an effective radius larger than that of the hole of the macrocycle, complexation can occur only if the ligand either folds around the metal (Figure 1.6a), or if the metal is displaced from the plane formed by the donor atoms (Figure 1.6b).[25] If metal ions are smaller than the macrocyclic hole, contraction of the ligand is required so that favourable overlap between the ligand and metal ion is achieved. The complexation of flexible saturated ligands with metals when a slight mismatch occurs is energetically favourable in most cases, unless the folding of the ring results in sterically unfavourable intraligand interactions. Most unsaturated ligands are rigid, so folding is energetically unfavourable and a metal-ligand mismatch may result in unusual properties if complexation occurs at all. Unsaturated macrocycles, such as cyclic imines, aid the formation of less common coordination geometries.[26] An idea of the match between the macrocyclic hole size and the metal can be gained by determining the ratio of macrocyclic cavity, R_A, to the Pauling covalent radius of the metal, R_P.[27] A R_A/R_P ratio of approximately 1 indicates a good fit (Figure 1.7). Macrocyclic ligands also preferentially complex certain metals, dependent on the donor atoms present. Transition metal ions with few outer shell d electrons and the alkaline earth metals, which are hard Lewis acids, prefer hard oxygen donors, to the softer nitrogen donors. Transition metals with more d electrons prefer softer donors such as nitrogen and sulfur to oxygen. These stability trends have been rationalised by the Hard and Soft Acid Base (HSAB) principle.[28] The geometric configuration of donors in a macrocyclic ligand can result in coordination of poor donors to late transition metals. For example, oxygen donors in small

tridentate macrocycles have been found to coordinate in a facial manner to late transition metals. This coordination will be discussed further in Chapter 2. Changes in solvation of the reactants and the complex, which are charge related, during a macrocyclic coordination reaction are expected to result in enthalpy changes. Since the magnitude of the effect is solvent dependent, it can be concluded that the nature of the solvent used will determine the macrocyclic effect to a certain extent.

(a) (b)

Figure 1.6: (a) Folding of macrocycle around a metal, (b) displacement of metal from the donor atom plane

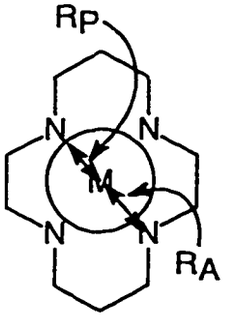

Figure 1.7: The determination of metal - ligand hole size match

Transition metal-macrocyclic complexes also have specific spectroscopic and electrochemical properties which are of interest to the inorganic chemist. Such cyclic ligands normally have much stronger ligand field strengths than related non cyclic ligands, a factor proposed initially to be due to the constrictive effect of the macrocyclic ligand on the metal ion,[29,30,31] which can result in ground electronic configurations not present with acyclic ligands. The macrocyclic ligand which is highest in the spectrochemical series for a purely σ donor ligand is diammac, the Fe^{II} complex of which has the strongest known ligand field[32] (Figure 1.8).

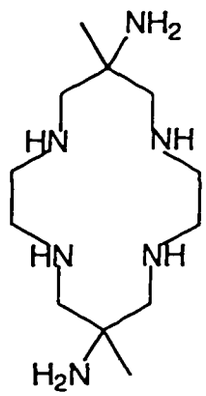

Figure 1.8: The structure of the ligand, diammac

Hancock, *et al.*,[33] have disputed the constrictive effect of the ligand on the metal. Using computer calculations, they have shown that the maximum ligand field strength corresponds to the least metal - ligand strain - ie. the metal ion 'fits' the ligand hole. They have proposed that the large number of macrocyclic secondary nitrogen donors, which supposedly form stronger M-N bonds due to their increased intrinsic basisity, combined with the low M-N bond strain contribute to the large ligand field. By varying the ligand hole size, or number

of potential donor atoms, macrocyclic complexes also have the ability to preferentially stabilise octahedral or square planar complexes. For example, the octahedral Ni^{II} ion which is paramagnetic has a radius of ~1.39 Å compared to the diamagnetic square planar Ni^{II} ion which has a radius of ~1.20 Å. The Ni^{II} ion with an ion radius closer to that of the radius of the ligand hole is usually the more stable form.[34] An interesting example of complex stabilisation is the Ni^{II} complex of the N_5 ligand shown in Figure 1.9.[35] Under alkaline conditions, Ni^{II} is a blue, octahedral complex with all five nitrogens coordinated to the metal. On the addition of acid to the complex, the nitrogen of the pendant arm is protonated and only the four ring nitrogens coordinate to the nickel. The nitrogen donors therefore form a square planar geometry around a diamagnetic Ni^{II} ion, and the complex is yellow in colour.

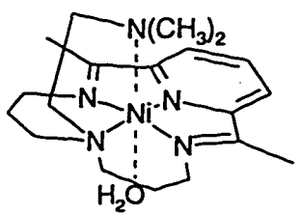

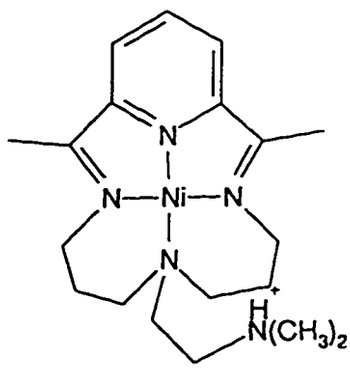

Blue Octahedral Ni^{2+} Yellow Square planar Ni^{2+}

Figure 1.9: Selective stabilisation of octahedral and square planar Ni^{II}

The above complex is also illustrative of the kinetic inertness of macrocyclic complexes, as it is only the pendant nitrogen which is protonated in acid solution and hence uncoordinated.

Jahn - Teller distortion, which occurs for high spin d^4, low spin d^7 and d^9 transition metals, can be expected for macrocyclic ligands where a mismatch between the metal ion size and the ligand hole size occurs. When the ion is larger than the hole size, axial elongation can occur compared to the equatorial bonds which are restricted. This is seen in longer axial metal - ligand bonds compared to the equatorial metal - ligand bonds. An example is given for the cobalt(II) complexes of [14]aneN$_4$.[36] The Co^{II} complex shows tetragonal distortion with two axial H_2O ligands weakly coordinated. The Co^{III} complex is less axially distorted, as Jahn - Teller distortion is absent, and the Co^{III} ion is smaller than the Co^{II} ion.

The electronic configuration of a transition metal ion in a macrocyclic complex can be determined with the use of electron paramagnetic resonance spectroscopy,[37] magnetic susceptibilities[38] as well as electronic spectra.[39] Many macrocyclic complexes are readily oxidised or reduced,[40] forming stable complexes, a feature that is uncommon with the open chain analogues of these complexes. This results in redox potentials for macrocyclic complexes which reflect the preference of the metal centre for a particular oxidation state in a complex with the macrocyclic ligand (Figure 1.10). Structural factors which favour a high oxidation state for the metal include negative charge on the ligand, increased ligand unsaturation, a match between the oxidised metal size and the ligand cavity and few ligand substituents on the chelate ring.[41]

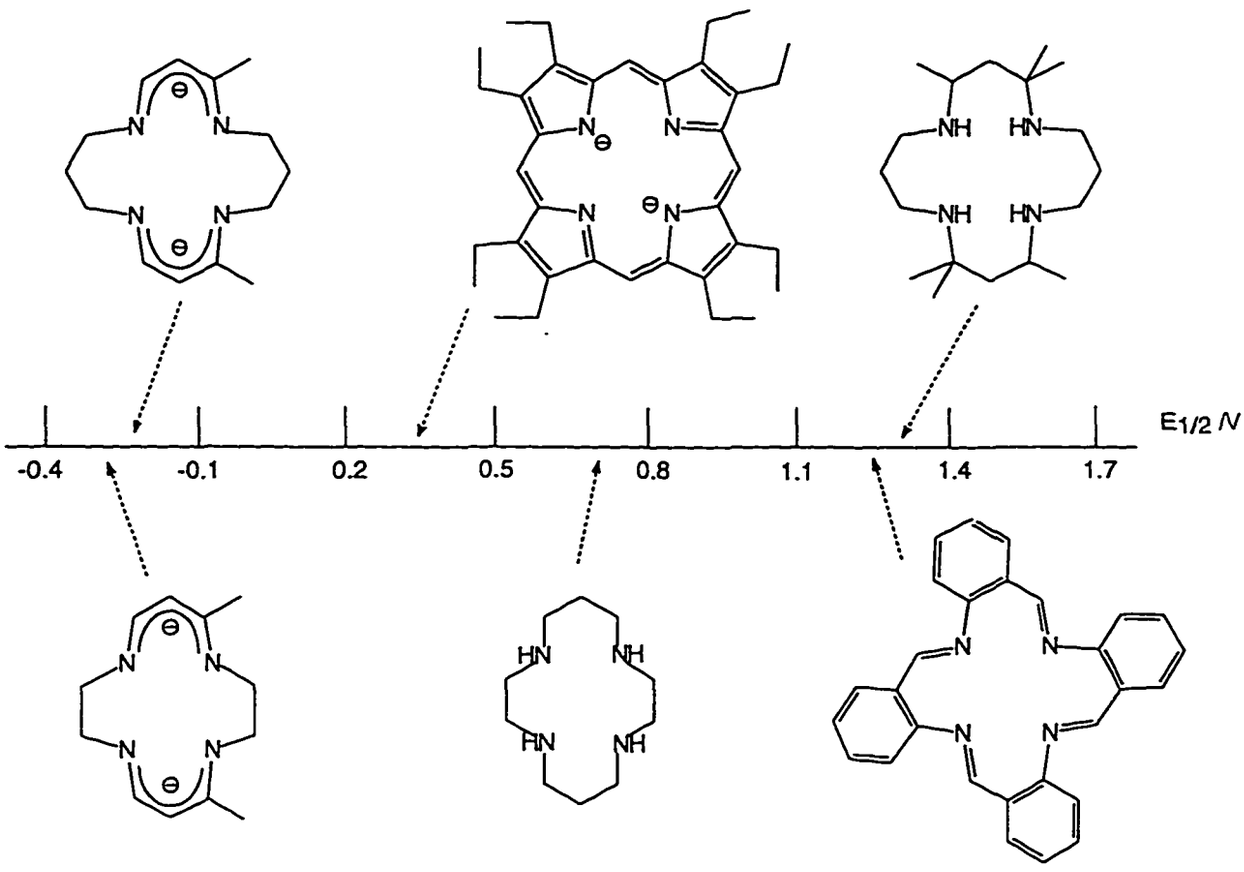

Figure 1.10: The tuning of the Ni^{III}/ Ni^{II} redox potential by variations in macrocyclic structure[42] ($E_{½}$ values vs Ag^{+}/Ag)

Initial investigations in the field of macrocyclic chemistry centred on single 12 - 16 membered rings with 4 or more donor atoms. As synthetic strategies improved, more rings were fused together to form bi- or tri-cycles. The synthesis of bi-cycles, or cryptands, led to an extension of the macrocyclic effect, as it was discovered that a concomitant increase in stability resulted on synthesis of a metal-cryptate complex. The cryptate effect[43] appears to be of enthalpic origin. Cryptands, are essentially three dimensional macrocyclic ligands, which have the ability to encapsulate metals ions within a 3-dimensional donor cage. Bi- and tri-cycles are

of interest structurally as there are a number of ways in which the donor atoms can coordinate to a metal centre, dependent on the three dimensional structure of the donors. Tricycles containing 6 donor atoms have the ability to coordinate metal atoms in two different ways: the metal atoms can be coordinated in an octahedral or tetragonal environment with four donors defining a plane and one donor coordinating above the plane and one below it (Figure 1.11a). The second possibility involves coordination of the metal ion with distorted square prismatic or trigonal prismatic geometry (Figure 1.11b).

a) Octahedral b) Trigonal prismatic

Figure 1.11: Possible coordination geometries of hexadentate macrocycles

Tricyclic ligands have the ability to induce axial coordination of the donor atoms to metals, even when the axial donor is a poor donor. This is probably due to the donor being held in close proximity to the axial site of the metal, therefore desolvation of the axial site and replacement of the solvent by the macrocyclic donor is facile. Alteration of the ring size by changing the number of carbon atoms between donor atoms can alter the geometry of the donors around the metal, partly because of steric effects caused by the increased repulsion in

the carbon bridge. Chelate rings should be generally five or six membered and form low energy conformers which minimise strain. A six membered chelate ring forms a low strain conformer similar to that of the chair form of cyclohexane. This ideal geometry results when the ring includes small metal ions. Larger metal ions form low strain rings when the chelate ring is five membered. The size of the metal imposes a particular 'bite size' or spacial separation between two donor atoms which determines the preferential size of the chelate ring[44] (Figure 1.12). Crystal structures of the complexes synthesised are therefore important in the determination of coordination effects in macrocyclic compounds.

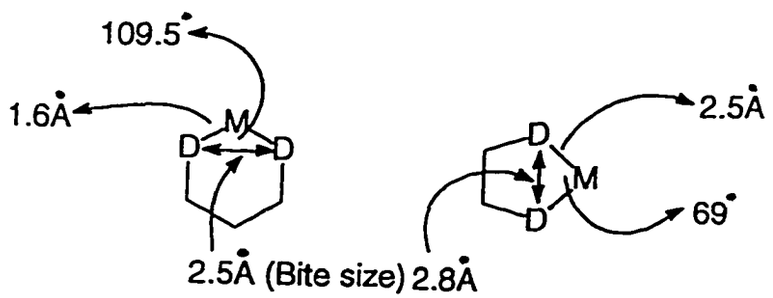

Figure 1.12: The ideal geometry of 5 and 6 membered chelate rings

1.5 Synthesis of macrocyclic ligands

Since macrocyclic ligands are cyclic in nature, their synthesis cannot in general be achieved using customary organic methods. A typical macrocyclic synthesis is depicted in Scheme1.1. In general, three procedures[42] are commonly used. These three techniques act by either promoting the rate of intramolecular cyclisation, ie. enhancing k_{intra} over k_{inter}, or by perturbing the equilibrium of the reaction in such a way that the cyclic product is favoured.

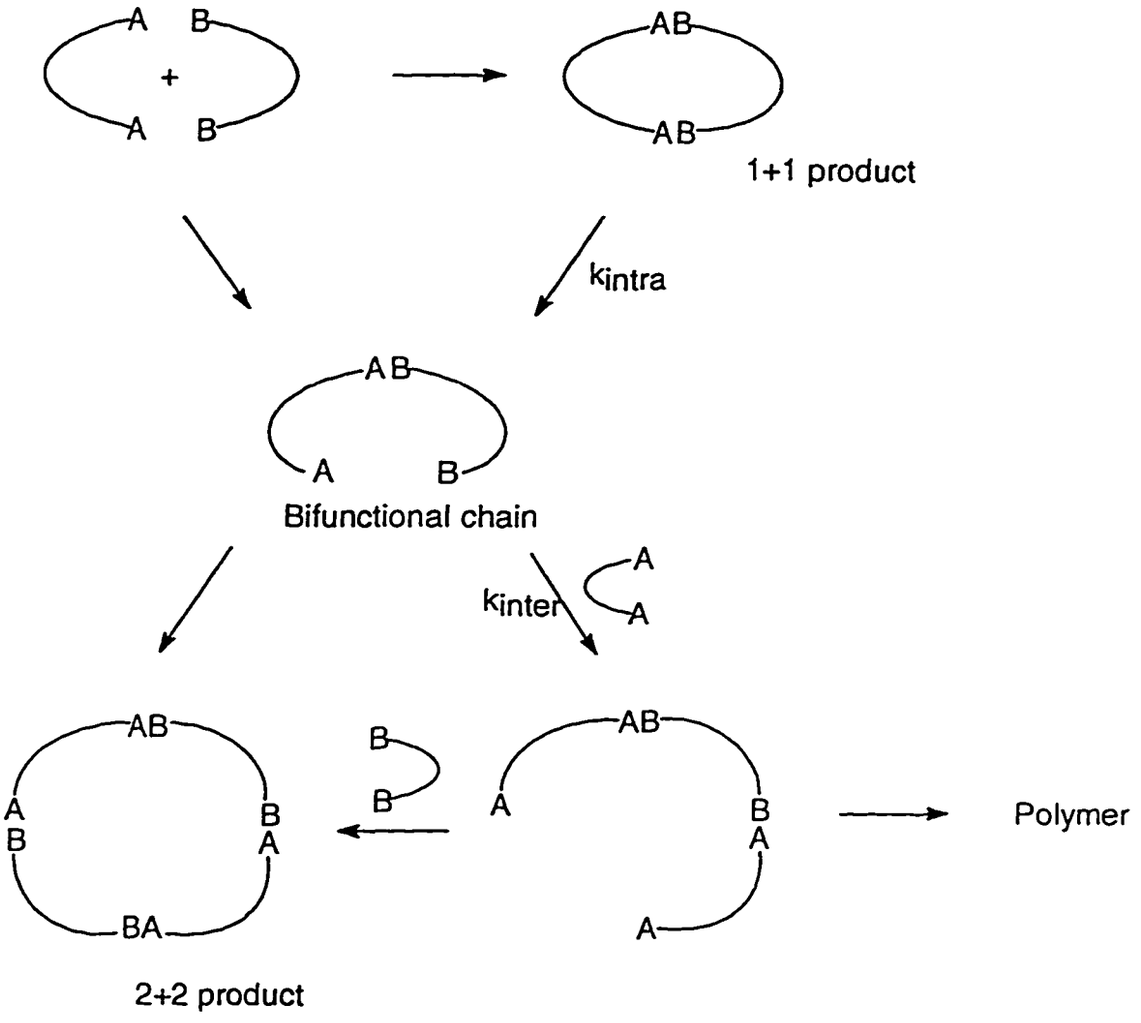

Scheme 1.1: General portrayal of a macrocyclic ring formation reaction

1.5.1 High dilution techniques

In concentrated solutions, the formation of linear polymers from bifunctional molecules is enhanced, due to the increased number of contacts the bifunctional chain has with other reagents. High dilution techniques minimise the mumber of contacts with other reagents, promoting intramolecular reactions which lead to macrocycle formation.[45] However, high

dilution reactions often give low yields of the required macrocycle even when all conditions are optimised. Specialised equipment is required to perform high dilution reactions, and ultrapure solvents are required to prevent side reactions, as concentrations of reactants are so low.

1.5.2 Template reactions

The second technique involves the use of a metal, usually in the form of a cation, which acts as a 'template' to assist in the cyclisation reaction.[46] A variety of mechanisms[47] have been proposed in order to explain the template effect. The metal can direct the course of the reaction to produce a cyclic product rather than an acyclic one by controlling the orientation of the reactants during a series of reactions - this is known as the kinetic template effect. The equilibrium template effect occurs when the metal ion perturbs the equilibrium occurring in the reaction by sequestering a particular product or reagent, forming a cyclic product preferentially. Template reactions are very specific and can seldom be used for the synthesis of more than one macrocycle. The presence of the metal may also prevent the formation of isomers in certain reactions, due to the preorganisation of the substrates during the reaction. For example, the reaction of $[Ni(en)_3]^{2+}$ with acetone[9] only forms a 14 membered macrocycle ring in two isomeric forms, shown in Figure 1.13. The major advantage of metal-directed reactions is the higher yields of cyclic products that are usually achieved. Reactions performed under high dilution conditions frequently result in the formation of the 2+2 condensation product as well as the 1+1 condensation product, which reduces yields of the desired product. For favourable reactions where condensation occurs rapidly, yields of

greater than 50% can be achieved.

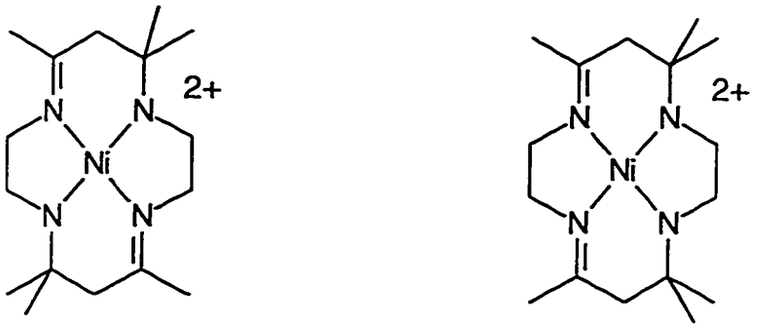

Figure 1.13: Isomeric products formed from the reaction of $[Ni(en)_3]^{2+}$ with acetone[9]

1.5.3 Rigid group synthesis

The third method, known as rigid group synthesis, can be performed at medium to low dilutions. The Richman-Atkins[14] synthesis, which involves condensation of a tosyl amide ($RTsN^-$) and a tosylated alcohol (ROTs), is an example of this type of reaction (Figure 1.14). The bulky tosyl groups are believed to prevent bond rotation and hence reduce the number of conformational degrees of freedom thereby reducing the range of possible condensation pathways.

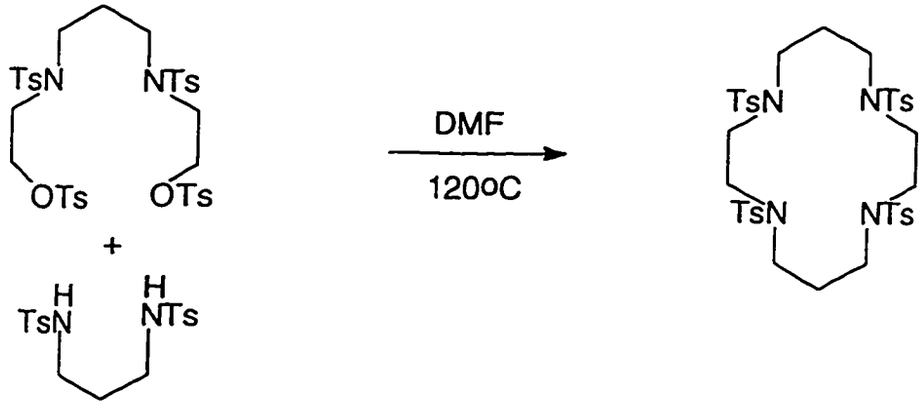

Figure 1.14: An example of the Richman-Atkins synthesis

1.5.4 Synthetic strategies used to obtain polycycles

A variety of synthetic strategies have been used to synthesise the bi- and tri-cyclic ligands.[48] Direct synthesis of the tricyclic ligand involves the formation of a donor atom containing ring which forms a 'face'. Pendant arms are then added through reaction of the heteroatoms with suitable substrates. The second ring can then be fused to the pendant arms under high dilution conditions to form a tricyclic ligand (Scheme 1.2a). A second methodology involves the capping of the major ring (face) with a bifunctional molecule to form the minor rings (Scheme 1.2b). Certain methods involve the use of metal directed reactions,[49] although direct synthesis is more common.

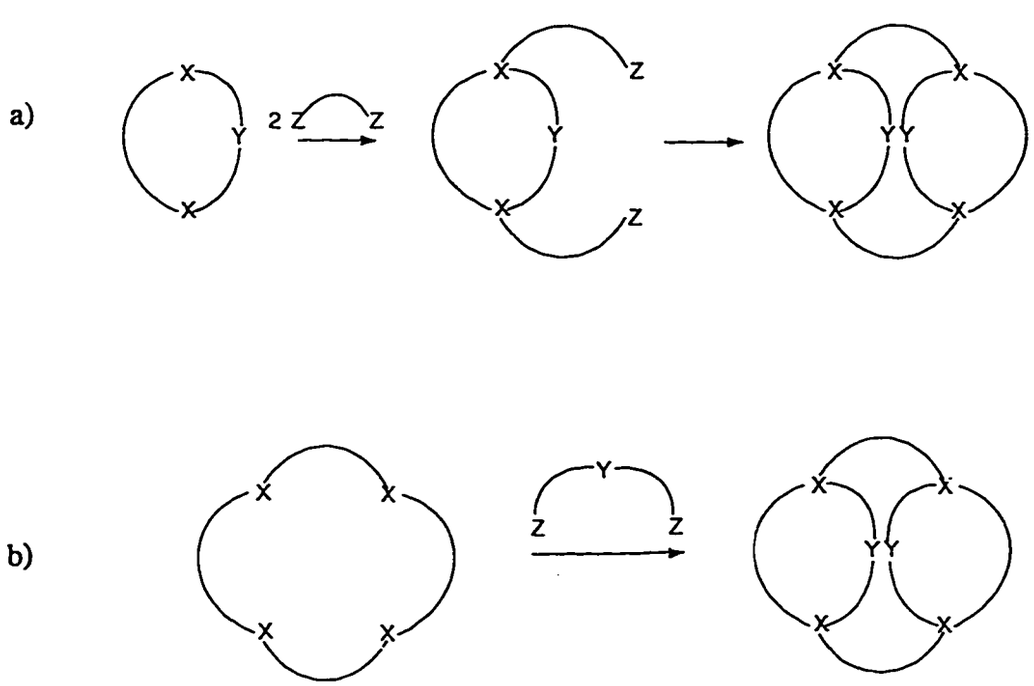

Scheme 1.2: Synthetic strategies to macrobi- and tricycles

1.6 Methods used in the characterisation and study of macrocyclic complexes

1.6.1 Nuclear magnetic resonance (NMR)

The use of NMR techniques to study macrocyclic complexes is limited to the study of those species with diamagnetic metal centres. NMR is also widely used to characterise the free ligand, as well as to determine approximate protonation constants for the uncomplexed ligand.[50] For the simpler macrocycles high field ^{1}H NMR techniques have been used to determine the structure of the macrocyclic ligand and metal ion complex[51] but, in general, it is of limited use due to the increasing complexity of macrocycles. ^{13}C NMR is used most often in the characterisation of the macrocycle. NMR line broadening techniques have also been used to determine rates of redox self exchange reactions.[52]

1.6.2 Electronic spectra

Electronic spectra of transition metal complexes are widely used to study the relative positions of the outer shell d energy levels. Information is obtained about the geometry of the donor atoms, the strength of the ligand field and the spin state of the metal atom. The d-electron energy levels are perturbed by coordination of ligands, and the relative spacings, and hence energies of electronic transitions are related to the degree and type of perturbations. This topic is covered in detail in standard inorganic textbooks and will not be discussed further here. Since electronic spectra are specific for a particular d electron configuration, relevant references to particular metal ions are given throughout the text. Electronic spectroscopy has also been used to determine equilibrium constants for reactions where there is a difference in wavelength or extinction coefficient between the products and reactants.[53]

1.6.3 Electron paramagnetic resonance spectroscopy (EPR)[54]

EPR spectroscopy is particularly useful for determining the solution state geometry of transition metals with a single unpaired spin. In the absence of a magnetic field the two spin states (±½) are degenerate. An electron in a magnetic field has spin states aligned parallel or anti-parallel to the magnetic field. The difference in energy between the two spin states (ΔE) is dependent on the magnetic field strength (H), where $\Delta E = g\beta H$. (β = Bohr magneton). Transitions of the electron from the lower to the higher energy state occur when electromagnetic radiation of frequency υ corresponding to $\Delta E = h\upsilon$ is applied. The Landé splitting factor, or g, is a function of the orbital environment of the unpaired electron, and the orientation of the molecule relative to the external magnetic field. The unpaired electron is also perturbed by spin orbit coupling of an excited state with the ground state modifying the value of g.

In an octahedral complex, the mixing is isotropic and only one g value exists. For frozen solutions of geometrically distorted metal complexes, where anisotropy exists, two or three g values can be obtained, depending on the orientation of the unpaired electron compared to the magnetic field. A tetragonal system will result in two g values, $g_{\parallel}$ and $g_{\perp}$, while a rhombic system has three values, g_x, g_y, and g_z. The numerical value of g is dependent on the ground state present. $g_{\parallel} >> g_{\perp} > 2$ indicates a $d_{x^2-y^2}$ ground state is present, while $g_{\perp} >> g_{\parallel} \approx 2$ indicates that the ground state is d_{z^2}. This provides information as to whether compressed or elongated distortions are present. Hyperfine coupling of the electron to ligand nuclei with spin (I), where present, gives information relating to the degree of delocalisation of the

unpaired electron and on the identity of the ligands coordinated to the metal. Hyperfine coupling results in splitting of the transitions into a number of lines, given by 2nI+1, where n = the number of nuclei with spin I. The extent of coupling to nuclei is measured by the hyperfine coupling constant, A, which is determined from the spacing of the relevant spectral lines.

1.6.4 Mass spectrometry(MS)

There are a variety of different techniques used to obtain mass spectra, however only those used in this project are discussed here. Chemical ionisation techniques were applied when characterising the free ligands with molecular masses less than 600amu. The technique involves bombardment of the ligand with CH_4 to produce ions and results in limited fragmentation of the molecules. This results in a characteristic spread of peaks around the molecular mass of the compound. Generally the M+1, M+29 and M+41 peaks can be identified. No attempt was made to assign and identify any fragmentation peaks observed. Metal complexes were characterised by either fast atom bombardment (FAB) or electrospray ionisation (ES) techniques. Both techniques result in minimal fragmentation of the complexes, and in general similar patterns were obtained. Using FAB techniques, only 1+ charged fragments were detected, while 2+ charges were also obtained at half the mass in the spectra obtained using ES techniques. Fragments are generated by the loss of an anion, loss of H^+ and an anion, loss of a ligand, and protonation of free ligand. Occasionally reduction of the metal-ligand cation to generate a 1+ fragment was observed. There is precedent for this in the literature.[55]

1.6.5 Electrochemistry[56]

Cyclic voltammetry is a well known technique used to determine the redox potentials and stability of the oxidation states of the metal in complexes. The shape of the cyclic voltammogram is determined by the electrochemical reversibility of the redox process. A typical cyclic voltammogram for a reversible redox process is shown in Figure 1.15. During the forward scan (increasingly positive voltage), the electrolyte in solution is oxidised at a potential dependent on the species present, the current increasing to a maximum as the voltage is increased, then decreasing as the electrolyte at the electrode is depleted. The scan potential is then reversed, and the redox product reduced in a similar manner.

The $E_{½}$ value is usually within 2-3mV of the formal potential E_o. Electrochemical reversibility is indicated by a theoretical peak to peak separation (E_a - E_c) of 57mV,[56] and equal peak currents for both the anodic and cathodic peaks. This implies that the forward and reverse electron transfer rates are in equilibrium, even at rapid scan rates. If electron transfer is slow, or a chemical reaction, or ligand rearrangement following electron transfer occurs, the equilibrium conditions are not maintained, which results in peak to peak separations greater than the theoretical 57mV and unequal peak currents.

A variety of metal complexes react via a 'square scheme'[57] (Figure 1.16). In this scheme, Ox_1 and Red_2 are more stable than Ox_2 and Red_1, and the equilibrium is shifted so that the more stable species are favoured. As a result, the forward and reverse scans do not correspond to oxidation and reduction of the same redox couple, and the cyclic voltammogram recorded will

show quasi-reversibility.

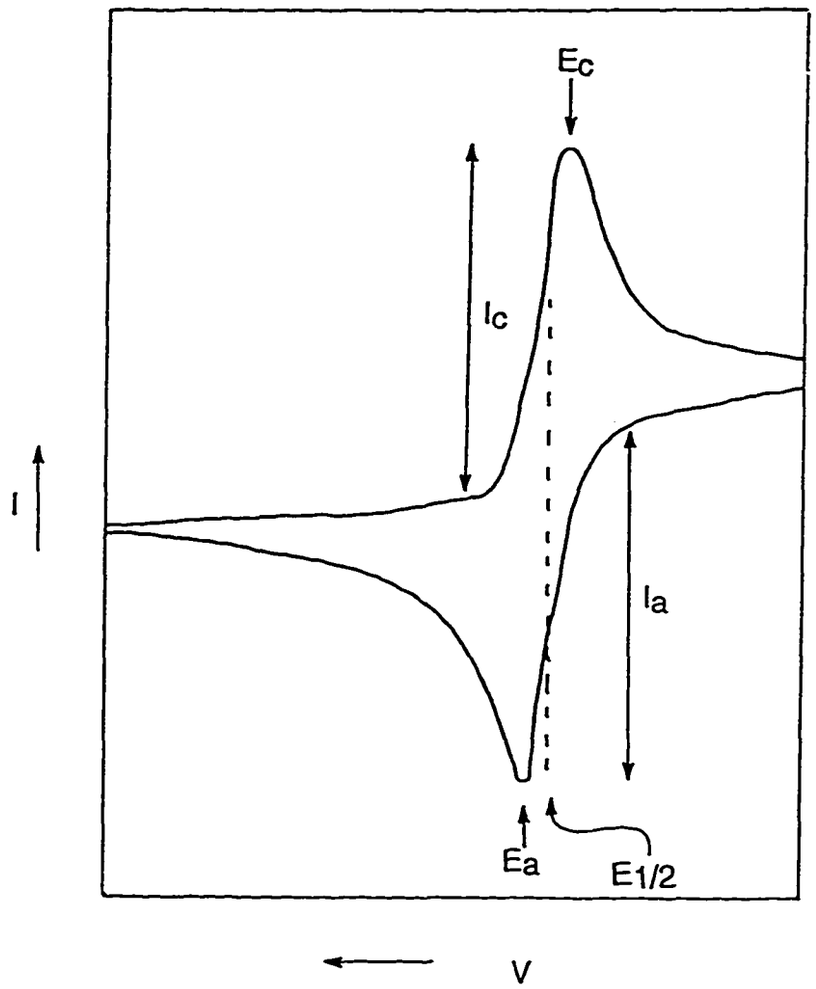

Figure 1.15: Cyclic voltammogram for a reversible redox reaction

E_a Anodic peak potential, E_c Cathodic peak potential, I_a Anodic peak current, I_c Cathodic peak current, $E_{1/2} = (E_a + E_c)/2$

$$Ox_1 + ne^- \rightleftharpoons Red_1$$

$$\uparrow\downarrow \qquad\qquad \uparrow\downarrow$$

$$Ox_2 + ne^- \rightleftharpoons Red_2$$

Figure 1.16: An electrochemical 'square scheme'

1.7 Objectives of the research

The aim of this project was the synthesis and characterisation of a variety of macrocyclic ligand complexes, with high kinetic stability, which would be suitable for use as outer sphere redox reagents. The target ligands, and other ligands studied are shown in Figure 1.17. The goal was to determine whether these ligands led to stability of less common oxidation states, or unusual geometries. Ligands synthesised fortuitously while trying to make the target ligand were also explored.

Chapter 2 details the synthesis and characterisation of complexes of the ligand [10]aneN_2O. The synthesis of tricyclo[10-14-10]N_4O_2 and other ligands ([10]aneN_2O earmuff, bicyclo[12-12]N_4O) synthesised while attempting to synthesise tricyclo[10-14-10]N_4O_2, are described in Chapter 3. The synthesis and characterisation of metal complexes of these ligands is also presented in Chapter 3. The synthesis and characterisation of the cobalt(III) complex of *bis*-[10]aneS_2N and the cobalt(II/III) and palladium(II) complexes of [10]aneS_2N earmuff are presented in Chapter 4, while the synthesis of $[Ni(bicyclo[12\text{-}12]N_4O)]^{2+}$ and $[Ni(bicyclo[12\text{-}12]N_4O)]^{3+}$ complexes, as well as the chloride substitution kinetics of $[Ni(bicyclo[12\text{-}12]N_4O)(H_2O)]^{3+}$ are presented in Chapter 5. Chapter 6 concludes the discussion with suggestions for further examination of the ligands and complexes studied. Finally detailed synthetic procedures and characterisation are given in Chapter 7.

a)

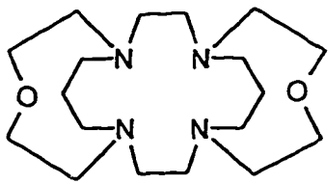

7,16-dioxa-1,4,10,13-tetraazatricyclo[11.5.3.3]octadecane (tricyclo[10-14-10]N_4O_2)

b)

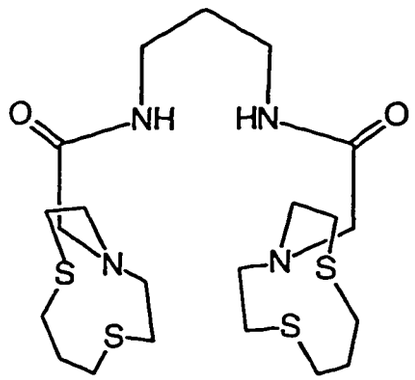

1,9-*bis*(8-aza-1,4-dithiacyclodecane)-4,7-diaza-2,8-dione nonane

(1,9-*bis*([10]aneS_2N amido earmuff))

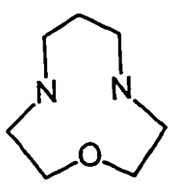

1-oxa-4,8-diazacyclodecane

([10]aneN_2O)

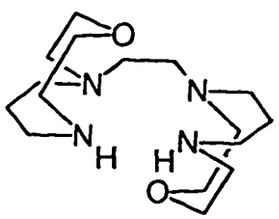

1,2-*bis*(1-oxa-4,8-diazacyclodecanyl)ethane

([10]aneN_2O earmuff)

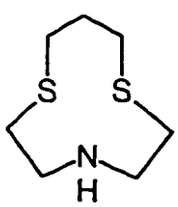

8-aza-1,4-dithiacyclodecane

([10]aneS_2N)

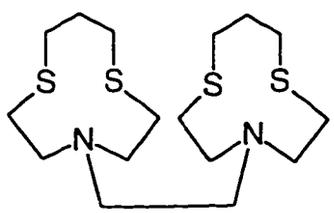

1,2-*bis*(8-aza-1,4-dithiacyclodecanyl)ethane

([10]aneS_2N earmuff)

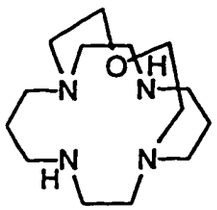

17-oxa-1,4,8,11-tetraazabicyclo[6.6.5]tetradecane (bicyclo[12-12]N_4O)

Figure 1.17: Macrocyclic ligands examined in this study

a) Target ligand, b) Other ligands explored

CHAPTER 2

SYNTHESIS AND CHARACTERISATION OF THE COPPER(II), NICKEL(II), PALLADIUM(II) AND COBALT(III) COMPLEXES OF THE [10]ANE N_2O LIGAND

2.1 Introduction

Since the development of the Richman-Atkins method of synthesis,[58] small tridentate ligands containing nitrogen, oxygen and sulfur donors have been studied in detail.[59] These macrocycles usually coordinate facially to transition metal ions[59d] as they are too small to encircle the metal ions. The thermodynamic stability of the complexes formed is high, since the entropy of formation is large, and the enthalpy of complex formation is also believed to be favourable.[33a] The mode of coordination also results in low dissociation rates[60] proposed to be due to multiple juxtapositional fixedness.[24]

Saturated tridentate macrocyclic ligands have been found to be fairly redox inactive, therefore redox changes occur at the metal centre and ligand radicals are not produced. Changes in oxidation state can occur at the metal centre with the ligand remaining coordinated to both high and low oxidation states[59d] of the metal. The complexes formed with two tridentate ligands yield coordinatively saturated octahedral complexes, which are quite resistant to decomplexation. These complexes are highly suitable therefore, as potential outer sphere electron transfer reagents in redox reactions, where decomplexation, substitution reactions or ligand-based reactions would interfere with the process. Mixed donor macrocycles are also of interest, as the combination of both hard and soft donors within a macrocycle can alter the stability of oxidation states, as well as the coordination geometry of the complex when compared to homoleptic macrocycle complexes. Although mixed sulfur-nitrogen donor macrocycles have been studied in some detail,[61] less information is available on nitrogen-oxygen donor macrocycles as potential ligands.[62]

2.2 Synthesis of 1-oxa-4,8-diazacyclodecane [10]aneN$_2$O (1)

The synthesis of [10]aneN$_2$O using Richman-Atkins methodology[58] was first published by Rasshofer *et al.*,[63] although this macrocycle has not been studied as a potential tridentate ligand. The synthetic procedure used in this project was modified as shown in Scheme 2.1. 1,3-*bis*(p-tolylsulfonyl)propylenediamine(2) was prepared according to a literature procedure.[64] *bis*(2-(p-tolylsulfonyl)ethyl)ether(3) was prepared by the addition of p-toluene sulfonyl chloride to 2-hydroxyethyl ether in the presence of triethylamine. Cyclisation was achieved by deprotonation of 1,3-*bis*(p-tolylsulfonyl)propylenediamine by sodium hydride in DMF, and subsequent slow addition of **3**. The ditosylate of [10]aneN$_2$O (**4**) was isolated as a white solid in 63% yield. Frequently yields obtained were greatly reduced by the presence of unreacted *bis*(2-(p-tolylsulfonyl)ethyl)ether, which could be removed by repeated recrystallisation. The ligand was detosylated with hot concentrated sulfuric acid to give the free ligand as a yellow oil in 50-60% yield. Although small amounts of impurities remained after detosylation, no attempt was made to purify the ligand further, as any impurities did not interfere with subsequent reactions, and could be easily removed by recrystallisation after further reaction. The ligand degraded with time, so metal complexes were prepared immediately after synthesis of [10]aneN$_2$O.

The protonated material [10]aneN$_2$O·2HCl (**5**) was formed by slow addition of 6M HCl to the free ligand, and the salt was further recrystallised from ethanol. The free ligand and the HCl salt were characterised by NMR and mass spectrometry.

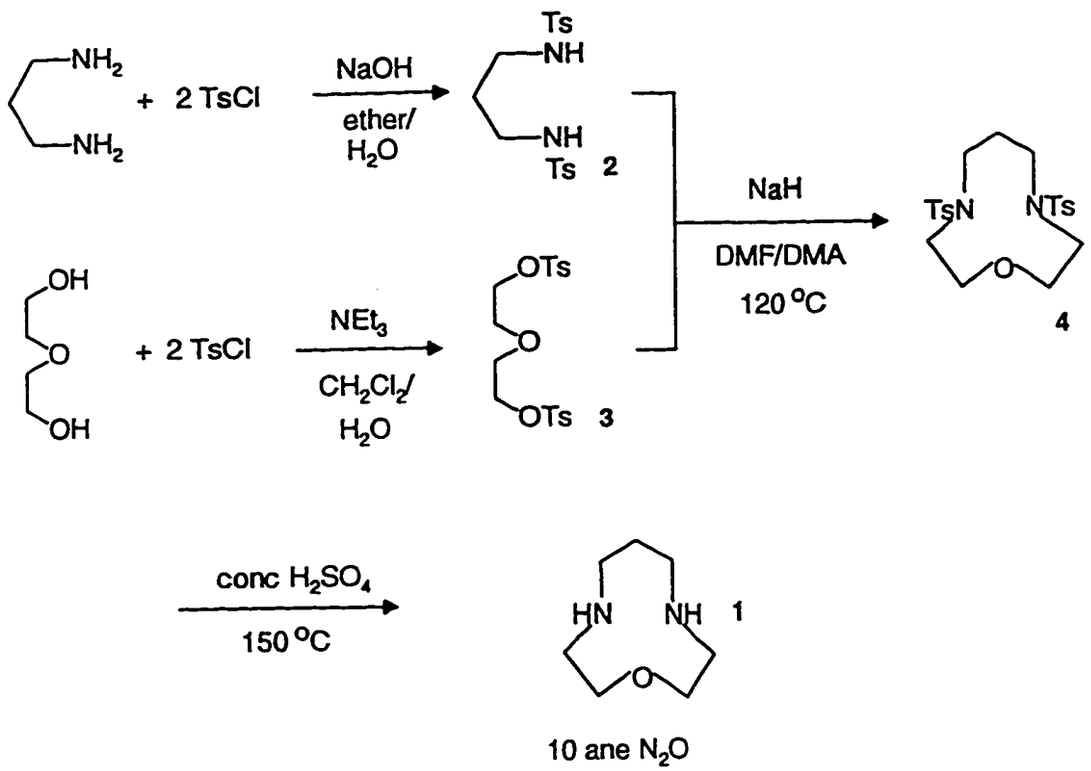

Scheme 2.1: Synthesis of [10]aneN_2O via the Richman-Atkins method

2.3 The copper(II) complex of [10]aneN_2O

2.3.1 Synthesis of [Cu([10]aneN_2O)$_2$](ClO_4)$_2$ (6)

The purple copper(II) complex was synthesised by the addition of $Cu(ClO_4)_2 \cdot 6H_2O$ in water to 2.8 equivalents of ligand **1** (Figure 2.1). The complex was characterised by mass spectrometry, elemental analysis and crystallography. X-ray quality crystals were grown by diffusion of diethyl ether into an acetonitrile solution of the complex.

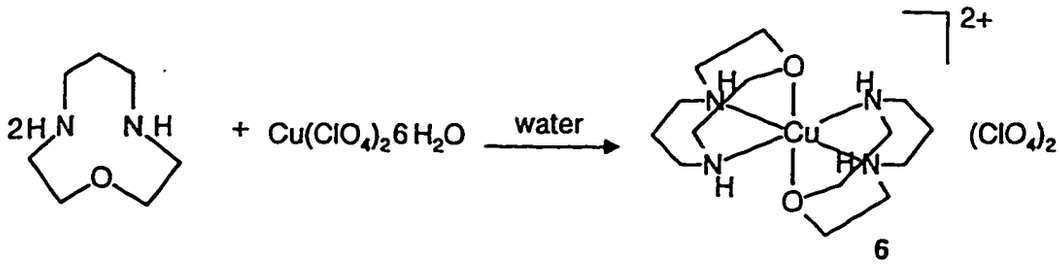

Figure 2.1: Synthesis of $[Cu([10]aneN_2O)_2](ClO_4)_2$

2.3.2 Crystallography

The molecular structure of the copper complex was determined by X-ray crystallography, and is shown in Figure 2.2. Tables of the interatomic distances, bond angles and intermolecular distances are given in Tables 2.1 - 2.3 respectively. Tables of the crystallographic parameters and fractional atomic coordinates are provided in Appendix 1.

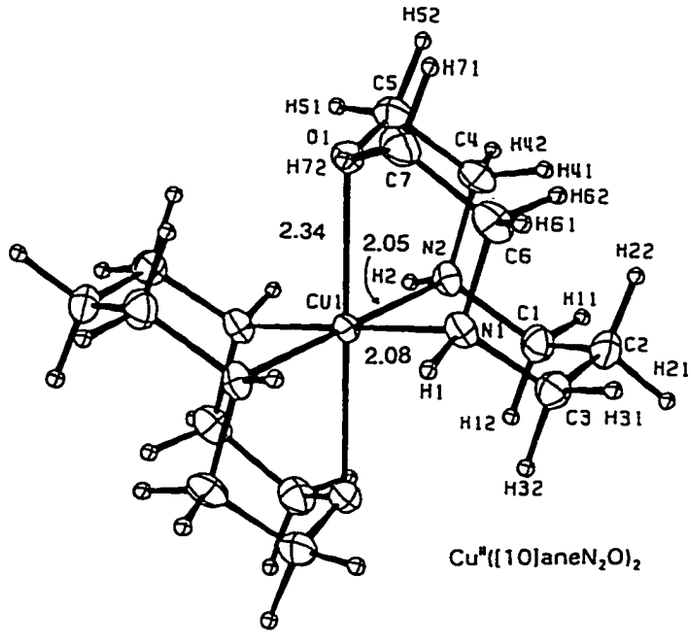

Figure 2.2: ORTEP diagram of $[Cu([10]aneN_2O)_2](ClO_4)_2 \cdot H_2O$

Table 2.1: Interatomic distances (Å) for $[Cu([10]aneN_2O)_2](ClO_4)_2 \cdot H_2O$

Atoms	Distance[a]	Atoms	Distance[a]
N(1)-Cu(1)	2.084(5)	C(2)-C(1)	1.492(10)
N(2)-Cu(1)	2.049(5)	C(3)-C(2)	1.546(11)
O(1)-Cu(1)	2.340(5)	C(5)-C(4)	1.541(11)
C(3)-N(1)	1.460(9)	C(7)-C(6)	1.534(11)
C(6)-N(1)	1.503(10)	O(11)-Cl(1)	1.338(8)
C(1)-N(2)	1.517(8)	O(12)-Cl(1)	1.312(7)
C(4)-N(2)	1.484(9)	O(13)-Cl(1)	1.366(10)
C(5)-O(1)	1.420(9)	O(14)-Cl(1)	1.310(7)
C(7)-O(1)	1.430(9)		

[a] Estimated standard deviations are given in parentheses.

Table 2.2: Bond angles (°) for $[Cu([10]aneN_2O)_2](ClO_4)_2 \cdot H_2O$

Atoms	Angle[a]	Atoms	Angle[a]
N(2)-Cu(1)-N(1)	89.3(2)	C(3)-C(2)-C(1)	115.7(6)
O(1)-Cu(1)-N(1)	80.5(2)	C(2)-C(3)-N(1)	115.6(6)
O(1)-Cu(1)-N(2)	80.4(2)	C(5)-C(4)-N(2)	110.9(6)
C(3)-N(1)-Cu(1)	113.0(4)	C(4)-C(5)-O(1)	113.5(6)
C(6)-N(1)-Cu(1)	113.1(4)	C(7)-C(6)-N(1)	111.6(6)
C(6)-N(1)-C(3)	111.7(5)	C(6)-C(7)-O(1)	113.3(6)
C(1)-N(2)-Cu(1)	112.0(4)	O(12)-Cl(1)-O(11)	113.2(6)
C(4)-N(2)-Cu(1)	114.4(4)	O(13)-Cl(1)-O(11)	102.0(8)
C(4)-N(2)-C(1)	111.4(5)	O(13)-Cl(1)-O(12)	105.7(8)
C(5)-O(1)-Cu(1)	104.5(4)	O(14)-Cl(1)-O(11)	112.4(7)
C(7)-O(1)-Cu(1)	105.1(4)	O(14)-Cl(1)-O(12)	117.1(6)
C(7)-O(1)-C(5)	118.1(5)	O(14)-Cl(1)-O(13)	104.6(8)
C(2)-C(1)-N(2)	115.3(6)		

[a] Estimated standard deviations are given in parentheses.

Table 2.3: Mean plane for $[Cu([10]aneN_2O)_2](ClO_4)_2 \cdot H_2O$

The equation of the plane containing the four nitrogens is:

$0.4125X - 0.6922Y - 0.5922Z = 0$

	Fractional atomic coordinates			
Atoms	X	Y	Z	P
Cu(1)	0.0000	0.0000	0.0000	0.0000
N(1)	1.8523	0.3416	0.8907	0.0000
N(2)	-0.3852	-1.4360	1.4102	0.0000
O(1)	1.2058	-1.7815	-0.9206	2.2757

where P is the perpendicular distance between the atom and the mean plane, given in Å.

The stucture of the geometry around the Cu^{II} cation is roughly elongated tetragonal. A water of crystallisation is present within the crystal lattice. The water molecule appears to be hydrogen bonded to N(2) (O(15)-N(2) distance = 2.948 Å). The two $[10]aneN_2O$ ligands each adopt a facial coordination around the Cu^{II} ion, as expected for small macrocyclic ligands. The symmetry of the $[Cu([10]aneN_2O)_2]^{2+}$ cation is C_i, with the copper atom located at the centre of inversion. The mean Cu-N bond length for the equatorial donor atoms is 2.07 Å, while the axial Cu-O bond length is 2.34 Å. These bond lengths are comparable to those

found in the copper(II) complex of the triaza derivative of [10]aneN$_2$O, tacd ([10]aneN$_3$).[65] In this complex, the mean equatorial Cu-N bond length is 2.09 Å, and the axial bond length is 2.29 Å. The longer axial bonds in both [Cu([10]aneN$_2$O)$_2$](ClO$_4$)$_2$ and [Cu(tacd)$_2$](ClO$_4$)$_2$ are a result of the Jahn-Teller effect,[66] however the two bond lengths cannot be directly compared, as the stereochemistry of the ten membered rings around the Cu^{II} ion (see Figure 2.3) are different, and the oxygen donor is expected to be a less suitable donor than nitrogen, due to the fact that the oxygen donor is a harder base. As a consequence, the oxygen atoms in [Cu([10]aneN$_2$O)$_2$]$^{2+}$ are predisposed to form somewhat weaker axial bonds, rather than ligating in an equatorial position. The metal ion lies within the plane of the four nitrogen donor atoms, as shown by the mean plane calculation in Table 2.5. The oxygen donor atom lies at a distance of 2.276 Å above this plane. The oxygen donor does not lie along the perpendicular axis defined by the nitrogen atom plane, but is at an angle of approximately 10.5° to this axis. This 'off-the-z-axis' bonding is quite common for complexes of this type,[67] where the axial donor is prevented from lying along the z axis by the contraints imposed by the ethylene bridge.

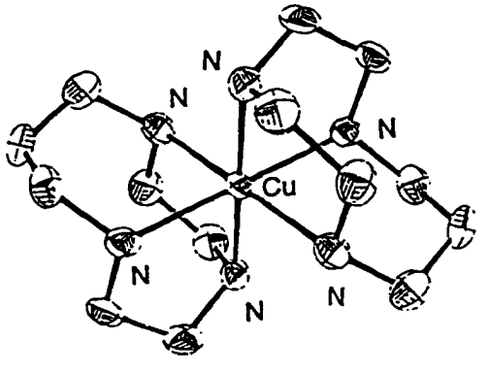

Figure 2.3: Structure of [Cu(tacd)$_2$](ClO$_4$)$_2$[65]

In the five coordinate $[Cu(bicyclo[9\text{-}14]N_4O)](ClO_4)_2$ complex[67a] (17-oxa-1,5,8,12-tetraazabicyclo[10.5.2]nonadecane) (Figure 2.4) the axial oxygen donor lies at an angle of 13.4° to the perpendicular axis described by the nitrogen donor plane. The Cu-O bond length (2.28 Å) and the mean Cu-N bond length (2.04 Å) are marginally shorter for this complex than in $[Cu([10]aneN_2O)_2](ClO_4)_2$. These differences are presumably due to the greater steric constraints imposed by the cyclam ring which cannot open up to give longer bond lengths and the fact that the 'N_2O' fragment in $[Cu(bicyclo[9\text{-}14]N_4O)](ClO_4)_2$ is now part of a nine membered ring which cannot stretch over as far as in the larger more flexible $[10]aneN_2O$ ring. Non-bonded H···H interactions between the two $[10]aneN_2O$ macrocyclic rings would also result in intramolecular repulsion, and hence the lengthening of metal donor bonds to lessen the degree of repulsion.

The bite distance[43] between the two nitrogen donors of the $[10]aneN_2O$ ring (N_1-N_2) is 2.73 Å, whereas the distance between the two nitrogens of adjacent rings (N_1-N_2') is 3.07 Å. The bite distances in the $[Cu(bicyclo[9\text{-}14]N_4O)](ClO_4)_2$ complex are shown in Figure 2.4. The N-N bite distance in the $[Cu([10]aneN_2O)_2](ClO_4)_2$ complex is smaller than that seen in the five-membered chelate rings in the $bicyclo[9\text{-}14]N_4O$ complex (Ave. 2.79 Å), and considerably smaller than the bite size for the six-membered chelate rings (Ave. 2.98 Å) in the same complex. The smaller bite distance in the $[10]aneN_2O$ macrocycles is probably the result of less steric constraints, as the cyclam ring is forced to 'open up' to include the Cu^{II} ion within the plane, where as the $[10]aneN_2O$ ring can coordinate ideally while maintaining a low strain conformation in the macrocyclic ring .

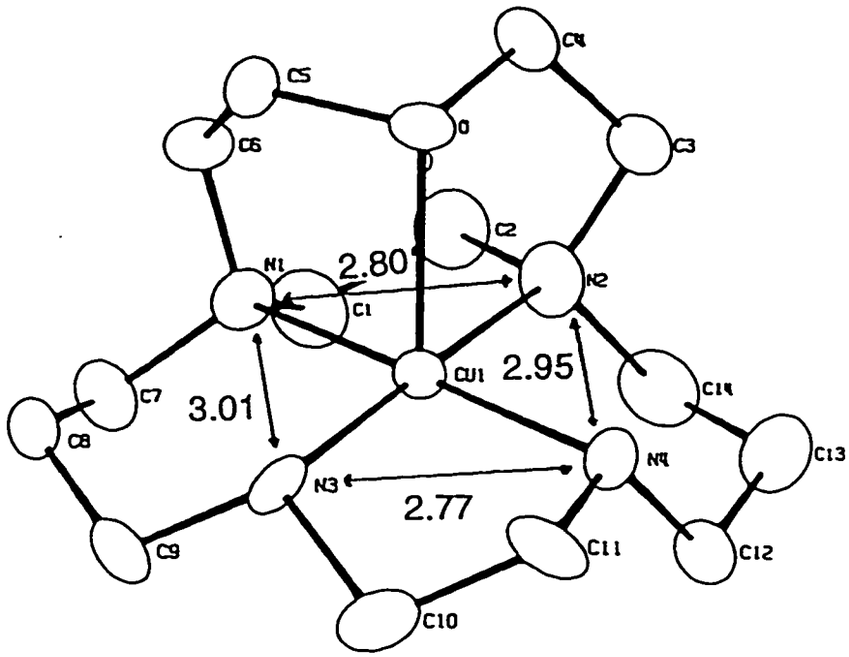

Figure 2.4: Structure of $[Cu(bicyclo[9\text{-}14]N_4O)](ClO_4)_2$ showing bite distances[67a]

2.3.3 Solution studies

2.3.3.1 Electronic spectroscopy

The UV/Vis spectrum of $[Cu([10]aneN_2O)_2](ClO_4)_2$ in water displays two absorption maxima, and is typical of a copper(II) complex with amine donor atoms. The intense absorption peak at 265.0 nm ($\epsilon = 4620\ M^{-1}cm^{-1}$) is attributable to a charge transfer band, while the absorption maximum at 581.2 nm ($\epsilon = 50\ M^{-1}cm^{-1}$) is an envelope peak encompassing the d-d transitions. Since Cu^{II} ions are Jahn-Teller distorted, the geometry of the donor atoms is expected to be axially distorted. Three d-d transitions are expected for Cu^{II} ion (d^9) in a tetragonal field, namely $^2B_{1g} \rightarrow {}^2A_{1g}$, $^2B_{2g}$, ^2E_g. The d-d band transfer peak tails off towards the low energy

side, but is completely unresolved. The peak maxima of the d-d transitions for $[Cu([10]aneN_2O)_2]^{2+}$ is at a lower energy transition than that seen for the related $[Cu(bicyclo[9\text{-}14]N_4O)]^{2+}$ (522 nm, $\epsilon = 102\ M^{-1}cm^{-1}$),[68] probably due to the increase in axial coordination for an octahedral rather than a five-coordinate complex, which is known to decrease the energy of d-d transitions in copper complexes.[69] The decrease in energy has also been found to be a function of the base strength of solvents coordinated to square planar copper complexes.[70]

The molar absorptivity is also considerably smaller for $[Cu([10]aneN_2O)_2]^{2+}$, as the inversion symmetry in the complex is likely to result in less mixing of orbitals of u symmetry with the d orbitals, resulting in a decrease in the intensity of the Laporte forbidden d-d transition.[71]

The copper(II) complex of the corresponding *bis*-[9]aneN$_3$ macrocycle has a transition at 615 nm in water.[72] This increase in wavelength is probably due to increased axial coordination from the nitrogen donors in the N_6 chromophore, which would similtaneously decrease the energy of the d-d transition envelope. The two nitrogen donors, which are of intermediate hardness are expected to be better donors than the two oxygen donors, based on the HSAB theory. The wavelength of the d-d transition is solvent sensitive, shifting to a wavelength of 575 nm ($\epsilon = 75\ M^{-1}cm^{-1}$) in acetonitrile. This is probably due to slight dissociation of the *bis*-macrocycle complex in solution, which has been noted in other copper(II) complexes with two facially coordinated tridentate macrocycles.[60b,72] Copper(II) complexes have been shown to preferentially form five rather than six-coordinate complexes, so forced octahedral

coordination by two tridentate macrocycles has a tendency to destabilise the resulting complex to a certain extent.[61b]

2.3.3.2 Electron paramagnetic resonance spectroscopy

EPR has been widely used to investigate the geometry of Cu^{II} complexes, since the d^9 configuration results in a single unpaired electron. The EPR spectrum of $[Cu([10]aneN_2O)_2](ClO_4)_2$ was obtained with the complex in a frozen glass matrix, composed of a 50%(v/v) acetonitrile/DMF solution at 77 K. Values of the isotropic EPR parameters were obtained in the same solution at room temperature. The spectra obtained are shown in Figures 2.5 and 2.6. Table 2.4 gives the values of the parameters obtained from these spectra, as well as values obtained for similar Cu^{II} complexes in CH_3CN/DMF mixtures.

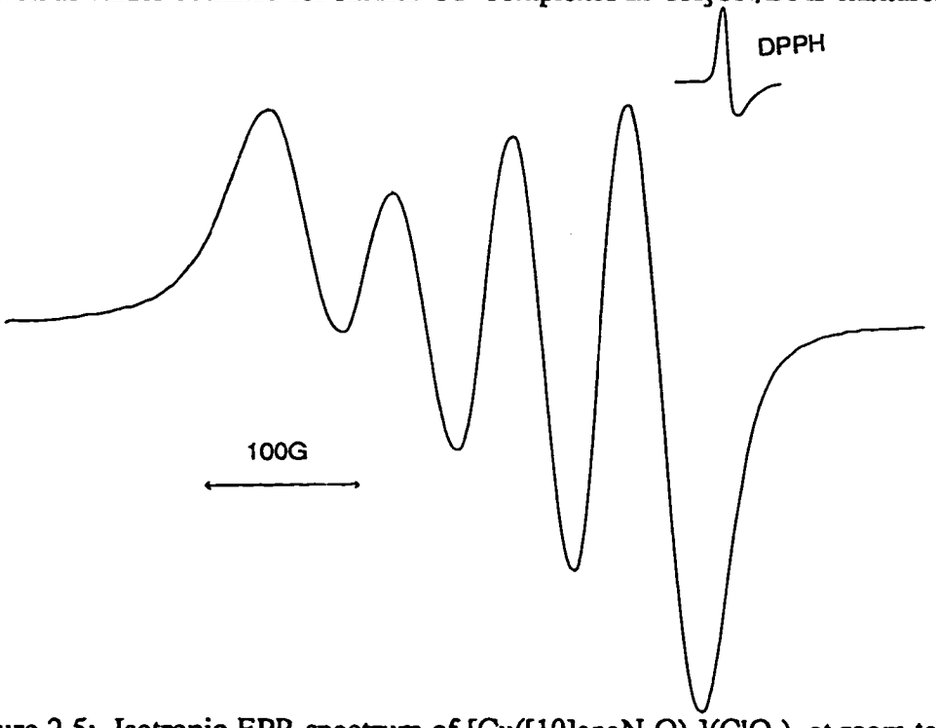

Figure 2.5: Isotropic EPR spectrum of $[Cu([10]aneN_2O)_2](ClO_4)_2$ at room temperature in CH_3CN/DMF (1:1)

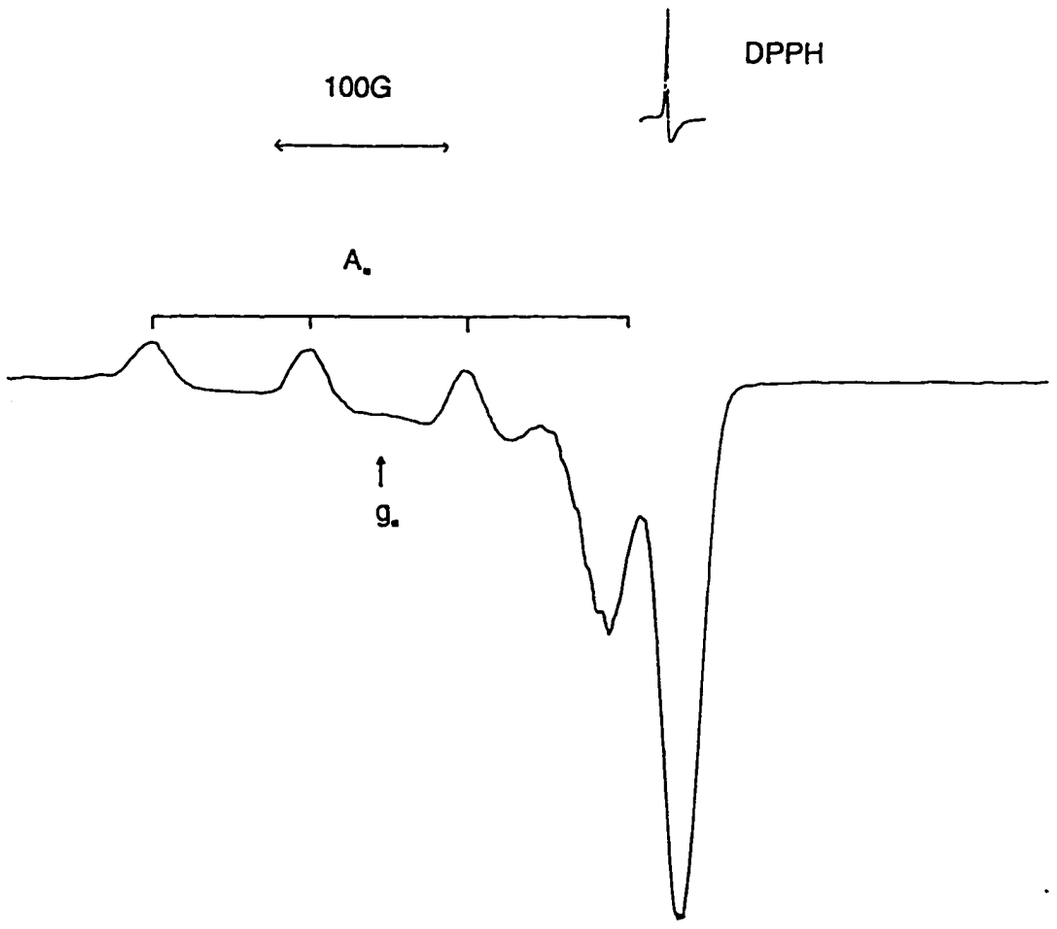

Figure 2.6: Anisotropic EPR spectrum of $[Cu([10]aneN_2O)_2](ClO_4)_2$ at 77K in CH_3CN/DMF (1:1)

The spectra obtained are characteristic of Cu^{II} complexes with tetragonal geometry. From the order of the g values, $g_{\parallel} > g_{\perp}$, the unpaired electron is in the $d_{x^2-y^2}$ orbital, and therefore the Cu^{II} ion is axially elongated. This is consistent with the bond lengths observed in the crystal structure. Coupling of the unpaired electron to the copper centre (I = 3/2), is observable in the $g_{\parallel}$ region, although the fine structure is not completely resolved, as four lines are expected. No coupling to the nitrogen donors is observed.

Table 2.4: EPR parameters for Cu^{II} complexes

Complex	g_o	A_o/G	$g_\parallel$	$A_\parallel$/G	$g_\perp$	$A_\perp$/G	Ref
$[Cu([10]aneN_2O)_2]^{2+}$	2.117	80	2.209	180	2.071	30	PW
$[Cu(cyclam)]^{2+}$	2.097	90	2.198	200	2.046	35	68, 73
$[Cu(bicyclo[9\text{-}14]N_4O)]^{2+}$	2.099	87	2.204	190	2.047	36	68

There is little variation in the overall appearance of the EPR spectra compared to spectra obtained for square planar complexes,[73,74] although the values of the EPR parameters do vary from one complex to another. There is considerable overlap between the parallel and perpendicular regions of the spectrum, so obtaining accurate values for the parameters is difficult. Approximate values were obtained using first order analysis, where $g_\perp = \frac{1}{2}(3g_o - g_\parallel)$ and $A_\perp = \frac{1}{2}(3A_o - A_\parallel)$. The use of these equations relies on the assumption that the EPR parameters, g_o and A_o, are temperature independent, however this assumption has been found to be invalid,[75] so values obtained via this method should be treated with caution.

The EPR parameters for square planar Cu^{II} complexes have been found to be dependent on the donor ability of the solvent,[76] as well as axial donor ligation.[74] The hyperfine coupling constant, A_o has been found to decrease with increasing axial ligation and g_o likewise increases. The values of the EPR parameters are dependent on the energies of the d-d

transitions which are altered by axial perturbations. Since the $g_\perp$ and $A_\perp$ values are dependent on ΔE_{xz}[76] (the energy required to couple the ground and excited state energy levels), alterations of these parameters result in changes in g_o and A_o. Unfortunately, the difficulty in determining accurate $g_\perp$ and $A_\perp$ values precludes their usage as a tool. The importance of changes in ΔE_{xz}, means that not only axial ligation but also displacement of the metal from the equatorial plane will also result in changes in g_o and A_o values. The EPR parameters therefore mirror shifts in the d-d transitions seen in the electronic spectrum. From the EPR data collected, $[Cu([10]aneN_2O)_2]^{2+}$ appears to show increased axial ligation, compared to $[Cu(cyclam)]^{2+}$ and $[Cu(bicyclo[9\text{-}14]N_4O)]^{2+}$, consistent with the two axial oxygen donor atoms being held in place by the macrocyclic rings. $[Cu(cyclam)]^{2+}$ and $[Cu(bicyclo[9\text{-}14]N_4O)]^{2+}$ have quite similar EPR parameters, indicating that coordination of DMF to $[Cu(cyclam)]^{2+}$ is similar in donor strength to that of the macrocyclic ether donor.

The EPR spectrum at 77 K of $[Cu([10]aneN_2O)_2]^{2+}$ in an acetonitrile/DMF solution to which tetraethyl ammonium chloride was added was identical to that shown in Figure 2.6. This confirms that the coordinated ether donors are relatively inert, and not substituted by the chloride ion in solution.

2.3.3.3 Electrochemistry

The cyclic voltammogram of $[Cu([10]aneN_2O)_2]^{2+}$ in acetonitrile containing 0.1 M $^tBu_4NPF_6$ as supporting electrolyte, showed an irreversible reduction wave at -1.02 V vs Ag^+/Ag, corresponding to the Cu^{II}/Cu^{I} couple. The reverse scan shows an oxidation peak at -0.38 V,

the shape of which indicates that the compound being oxidised is probably adsorbed onto the platinum electrode.

The electrochemical data for the $[Cu([10]aneN_2O)_2]^{2+}$ complex and related Cu^{II} complexes is given in Table 2.5.

Table 2.5: Redox potentials of copper(II) complexes

Complex	$E_{1/2}$/V[a]		Ref
$[Cu([10]aneN_2O)_2]^{2+/1+}$	-1.02	(irreversible)	PW
$[Cu(bicyclo[9\text{-}14]N_4O)]^{2+/1+}$	-1.04	(quasi-reversible)	68
$[Cu([9]aneN_3)_2]^{2+/1+}$	-1.31	(irreversible)	72
$[Cu(cyclam)]^{2+/1+}$	-1.46	(quasi-reversible)	77
$[Cu([10]aneN_2O)_2]^{2+/3+}$	1.23	(irreversible)	PW
$[Cu(bicyclo[9\text{-}14]N_4O)]^{3+/2+}$	1.3	(irreversible)	68
$[Cu(cyclam)]^{3+/2+}$	1.09	(quasi-reversible)	77

[a] vs Ag^+/Ag

The electrochemical data show that the copper(I) species formed by reduction is unstable, and

probably disproportionates, with the copper metal, or some other species formed, adsorbing onto the working electrode. This behaviour is similar to that observed for the $[Cu([9]aneN_3)_2]^{2+}$ ion. The irreversibility of the Cu^I species is not inconsistent with what is known about the geometry of Cu^I species.[78] Most Cu^I species adopt a tetrahedral geometry, and since the $[10]aneN_2O$ ligand is predisposed to octahedral or square planar geometry, a rearrangement of the donors would be necessary in order to stabilise the Cu^I species. The results obtained for $[Cu([10]aneN_2O)_2]^{2+}$ are comparable with those obtained for $[Cu([10]aneN_3)_2]^{2+}$.[72]

The oxidation of $[Cu([10]aneN_2O)_2]^{2+}$ also gave an irreversible wave, which occurs at 1.23 V and has been ascribe to the Cu^{III}/Cu^{II} couple. The presence of the hard oxygen donor in $[10]aneN_2O$ would be expected to increase the stability of the copper(III) species, as the smaller more highly charged ion would ligate better with the harder donor, however, Cu^{III} species are unstable in comparison to Cu^{II}, so this ligand is probably insufficient to stabilise this species. A change in geometry from octahedral to square planar, which can occur for d^8 ions, may also account for the irreversibility of the reaction.

The $[Cu([10]aneN_2O)_2]^+$ species is a strong reductant, however it is less reducing than the $[Cu(cyclam)]^+$ species. This maybe due to the increased flexibility of the tridentate ligands allowing for ligand expansion to accomodate the larger Cu^I ion.

2.4 The nickel(II) complex of [10]aneN$_2$O

2.4.1 Synthesis of [Ni([10]aneN$_2$O)$_2$](ClO$_4$)$_2$ (7)

The nickel(II) complex of [10]aneN$_2$O was synthesised in a similar manner to that of the copper complex, as shown in Figure 2.7. Nickel(II) complexes of tridentate macrocycles form more slowly than those with copper(II),[61b] so reaction times are necessarily longer. A methanolic solution of 2.2 equivalents of ligand and 1 equivalent of Ni(ClO$_4$)$_2$·6H$_2$O were refluxed for 24 hours. Initially a pale blue precipitate of the 1:1 complex was formed. However this gradually changed into the lilac 2:1 complex. The complex was isolated by filtration, and characterised by X-ray, FAB-MS and elemental analysis.

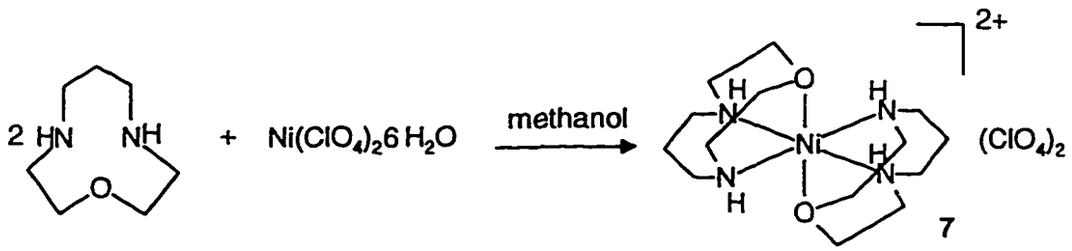

Figure 2.7: Synthesis of [Ni([10]aneN$_2$O)$_2$](ClO$_4$)$_2$

2.4.2 Crystallography

The crystal structure of [Ni([10]aneN$_2$O)$_2$](ClO$_4$)$_2$[79] (Figure 2.8) indicates that the geometry of this complex is similar to that found for the copper(II) complex, in that the oxygen atoms are coordinated to the nickel(II) ion in axial positions. The Ni^{II} ion sits at the centre of inversion for the cation, with all four nitrogen donors in a plane around the nickel centre. The Ni-O bond lengths (2.07 Å) are marginally shorter than the Ni-N bond lengths (Ave. 2.11 Å),

probably a factor of the difference in the van der Waals radii for the two donors . The Ni-O and Ni-N bond lengths are typical for octahedral Ni^{II} complexes with tetraaza ligands,[80] although the Ni-O bond length is at the short end of the range, shorter than that seen for $[Ni(bicyclo[9\text{-}14]N_4O_2)](ClO_4)_2$ (2.11 Å)[68] and for $[Ni(cyclam)](NO_3)_2$ (2.17 Å).[80b] The average Ni-N bond length at 2.11 Å is close to the 'ideal' value for Ni-N bonds (2.10 Å).[81] As a result of these bond lengths, the oxygen atom is less displaced from the perpendicular than in the $[Cu([10]aneN_2O)_2]^{2+}$ complex ion, forming an angle of approximately 7° to the z-axis. The intra-annular N-N bite size is 2.94 Å, wider than that seen in the copper complex as a result of the longer Ni-N bond lengths.

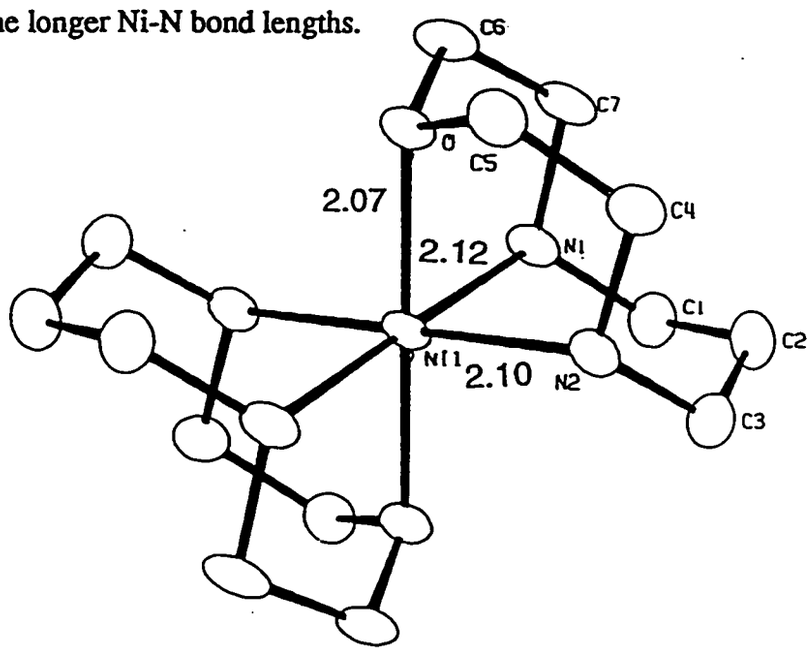

Figure 2.8: ORTEP diagram of $[Ni([10]aneN_2O)_2](ClO_4)_2$

In the $[Ni([10]aneN_3)_2](ClO_4)_2$ complex ion,[82] the nitrogen donors are trigonally distorted around the Ni^{II} centre. The Ni-N bond lengths in $[Ni([10]aneN_2O)_2](ClO_4)_2$ with Ni-N lengths of 2.10 Å and 2.12 Å, are effectively the same length as those in the $[Ni([10]aneN_3)_2](ClO_4)_2$

complex that are bridged by the propyl chain. The third Ni-N length in $[Ni([10]aneN_3)_2](ClO_4)_2$, equivalent to the axial position in $[Ni([10]aneN_2O)_2](ClO_4)_2$, is the longest bond at 2.14 Å.

2.4.3 Solution studies

2.4.3.1 Electronic spectroscopy

The data obtained from the UV/visible spectrum of $[Ni([10]aneN_2O)_2](ClO_4)_2$, along with other related complexes are given in Table 2.6.

Table 2.6: Electronic spectra and ligand field parameters for octahedral Ni^{II} complexes

Complex	λ_{max}/nm (ϵ/$M^{-1}cm^{-1}$)	Δ_o/cm^{-1}	B/cm^{-1}	ß/cm^{-1}	Ref
$[Ni([10]aneN_2O)_2]^{2+}$	359(13), 543(20), 868(6)	11522	924	0.89	PW
$[Ni([9]aneN_2O)_2]^{2+}$	354, 532, 800(sh), 862	11600	915	0.88	83
$[Ni([10]aneN_3)_2]^{2+}$	327, 513, 800, 870(sh)	12500	937	0.90	82
$[Ni([9]aneN_3)_2]^{2+}$	325, 505, 800, 870(sh)	12500	934	0.90	82,84
$[Ni(bicyclo[9\text{-}14]N_4O)]^{2+}$	337(17), 515(10), 681(5)				68

The values of 10Dq and B were calculated via the method described by Drago.[54] The Nephelauxetic ratio, ß, was calculated using B for a free Ni^{II} ion = 1038 cm^{-1}. All spectra were determined in aqueous solution.

The bands observed for $[Ni([10]aneN_2O)_2]^{2+}$ are typical of d-d transitions for octahedral Ni^{II} complexes. The ligand field strength, 10Dq or Δ_o, was obtained from the $^3T_{2g} \leftarrow ^3A_{2g}$ transition at 868 nm. The absorption at 359 nm was assigned as a $^3T_{1g}(P) \leftarrow ^3A_{2g}$ transition, and the 543 nm transition as $^3T_{1g} \leftarrow ^3A_{2g}$. The shoulder at 870 nm observed in the spectrum of $[Ni([10]aneN_3)_2]^{2+}$, was assigned as either a spin forbidden transition, or an allowed $^3T_{2g}$ transition which has been split by trigonal symmetry.[82] The latter interpretation of the origin of this shoulder has subsequently been discounted.[85,86] Hancock, *et al.*,[86] have discussed the effect of the mixing of the $^3T_{2g} \leftarrow ^3A_{2g}$ transition and the spin-forbidden $^1E_g \leftarrow ^3A_{2g}$ on the values of the ligand field parameters derived from the spectra. They contend that the anomolously large values of B derived from the spectra are caused by the mixing of the two above mentioned states, resulting in incorrect values being obtained for the $^3T_{2g} \leftarrow ^3A_{2g}$ transition, which is used in the calculation of the Racah parameter, B.

In the spectrum of the $[Ni([10]aneN_2O)_2]^{2+}$ complex, no splitting of the low energy peak was seen, however, the value of B calculated for $[Ni([10]aneN_2O)_2]^{2+}$ is of a magnitude similar to the uncorrected values calculated when the $^1E_g \leftarrow ^3A_{2g}$ transition is observed. The value of the ligand field splitting parameter, Δ_o, is greater for tridentate macrocycles containing three nitrogen donors, than for the oxa-diaza macrocyclic ligands. This is expected, since nitrogen donors are higher in the spectrochemical series than oxygen donors. The Nephelauxetic ratio, ($\beta = B_{complex}/B_{free\ ion}$), however, does not reflect the expected decrease in covalency expected in going from a nitrogen to an oxygen donor. It is generally accepted that the Nephelauxetic ratio increases with decreasing covalency of the metal-ligand bond.[87] Since oxygen is a harder

donor than nitrogen, it would be expected that the bonding between Ni^{II} and an oxygen donor would be more ionic than the bonding between Ni^{II} and nitrogen. A comparison of the solid state bond lengths around the Ni^{II} centres in $[Ni([10]aneN_2O)_2](ClO_4)_2$ and $[Ni([10]aneN_3)_2](ClO_4)_2$ suggest a possible reason for this discrepancy. The $[Ni([10]aneN_2O)_2]^{2+}$ cation is less distorted from the octahedral than the $[Ni([10]aneN_3)_2]^{2+}$ cation. This may result in reduced overlap between the nickel orbitals, and the nitrogen donor orbitals in $[Ni([10]aneN_3)_2]^{2+}$, reducing the covalency of the bond.

The use of an octahedral model to determine ligand field data for the above Ni^{II} complexes may account for discrepancies in the derived data. Clearly the geometry of the complexes is not strictly octahedral, and deviations from this geometry will induce splitting of the d energy levels, the magnitude of which will be determined by the degree of distortion from the octahedral. At best, this will induce line broadening effects in the apparently octahedral electronic spectra, but may complicate spectra by shifting band maxima, due to the presence of an increased number of d-d transitions. A more rigorous approach to obtaining ligand field data would include the use of Gaussian analysis of the experimental curves to determine band maxima, with the possible use of a tetragonal model to determine ligand field parameters.[88]

The oxidation of $[Ni([10]aneN_2O)_2]^{2+}$ with hexaaquacobalt(III) enabled the determination of the $[Ni([10]aneN_2O)_2]^{3+}$ electronic spectrum. Two transitions at 283 nm (ϵ = 1871 $M^{-1}cm^{-1}$) and 400 nm (ϵ = 1540 $M^{-1}cm^{-1}$) were observed for the bright yellow complex, typical of an octahedral Ni^{III} species. Both these bands have been assigned as metal ligand charge transfer

bands. The bands are at a higher wavelength than those observed for $[Ni(cyclam)]^{3+}$ in aqueous solution (247 nm, 309 nm).

2.4.3.2 Electron paramagnetic resonance spectroscopy of the $[Ni([10]aneN_2O)_2]^{3+}$ complex

A solution of $[Ni([10]aneN_2O)_2]^{2+}$ in water was oxidised by the addition of a solution of $[Co(H_2O)_6]^{3+}$ in 4 M $HClO_4$. The resulting Ni^{III} complex was sufficiently stable in acidic media to obtain EPR spectra. The spectra were obtained at 77 K, and show a form characteristic of a low spin d^7 ion in a rhombic environment, with g_x, g_y = 2.197, 2.182, and g_z = 2.029 (Figure 2.9). The rhombic spectrum obtained for the Ni^{III} species is probably due to trigonal distortion of the complex, which has been observed for several complexes with tridentate macrocycles.[66,82] Low spin d^7 ions are susceptible to Jahn Teller distortion. The order of the g values indicates that the complex is axially elongated, with the unpaired electron in the d_{z^2} orbital. The presence of axial elongation in the nickel complex confirms that the short length of the Ni-O bond is not unusual, and is not caused by axial compression of the the complex. No axial hyperfine coupling was seen, consistent with the nitrogen donors being equatorially coordinated.

The g values obtained are very similar to those obtained for $[Ni(bicyclo[9\text{-}14]N_4O)]^{3+}$ ion in aqueous solution with non-coordinating anions, ($g_{\parallel}$ = 2.028, $g_{\perp}$ = 2.200),[89] indicating the similarities in the coordination environment. The addition of a saturated NaCl solution did not alter the spectrum, attesting to the fact that the axial oxygen donors are sufficiently inert

that displacement by a chloride ion is not observed. This is consistent with results obtained on $[Ni([9]aneN_2O)_2]^{3+}$ where no displacement of the ether donors by fluoride anions was observed.[89] Clearly, the coordinated ether donors have spectroscopically similar characteristics to those of the oxygen atom of coordinated water molecules, but remain coordinated in the presence of stronger coordinating anions. The above data provide evidence for the maintenance of coordination of the macrocyclic ether donors both in the solid state and in solution.

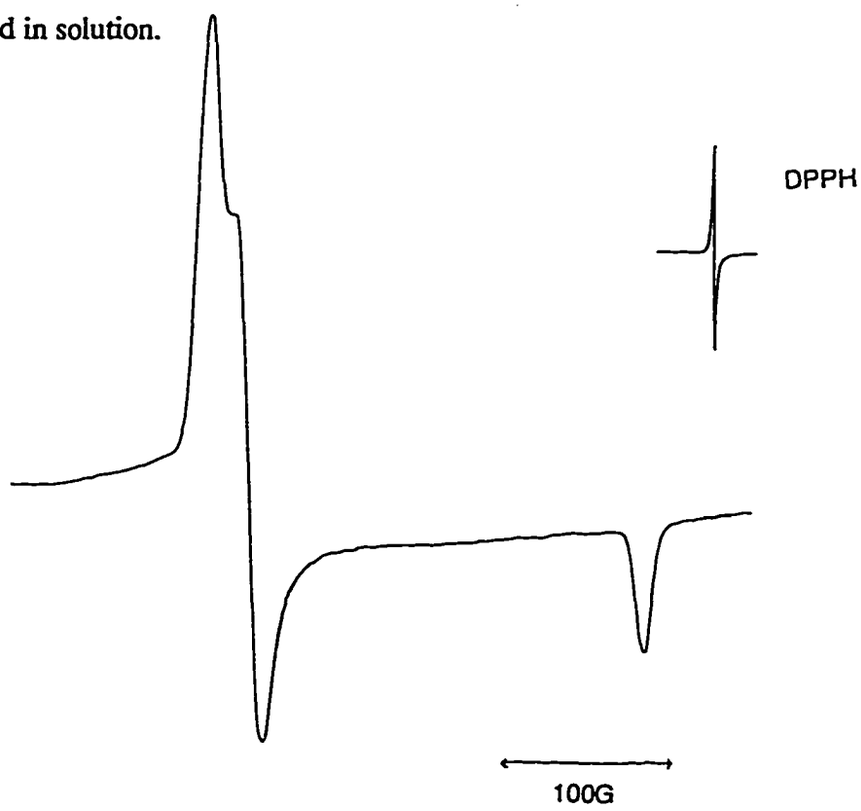

Figure 2.9: EPR spectrum of the $[Ni([10]aneN_2O)_2]^{3+}$ ion at 77 K in H_2O

2.4.3.3 Electrochemistry of $[Ni([10]aneN_2O)_2]^{2+}$

The cyclic voltammogram of $[Ni([10]aneN_2O)_2]^{2+}$ in acetonitrile, shows only one oxidation/reduction wave at 0.99 V vs Ag^+/Ag, corresponding to a one electron oxidation of

Ni^{II} to Ni^{III}. The wave is quasi-reversible, with small shifts in the peak to peak separation with varying scan rates, indicating minor changes in the coordination environment with electron transfer. This value is more positive than that for $[Ni(bicyclo[9\text{-}14]N_4O)]^{2+}$ at 0.86 V,[68] indicating a more difficult oxidation reaction, consistent with the generally observed trend[90] that the presence of secondary amines rather than tertiary amines makes oxidation reactions more difficult. In accordance with this, Kang *et al.* have observed[80a] that the redox potentials for $[Ni(L_1)]^{2+}$ were more negative than for $[Ni(L_2)]^{2+}$ (L_1 = 3,14-dimethyl-2,6,13,17-tetraazatricyclo[16.4.0.0]docosane, L_2 = 2,13-*bis*(2-hydroxyethyl)-5,16-dimethyl-2,6,13,17-tetraazatricyclo[16.4.0.0]docosane). No evidence of a Ni^{II}/Ni^{I} couple was observed.

2.4.3.4 Decomposition of nickel(II) and nickel (III)([10]aneN$_2$O)$_2$ complex ions

The rate of decompostion of the Ni^{II} and Ni^{III} species in acidic media could be determined using conventional visible spectrometry, where the rate was determined by following the rate of decay of the absorbance at a particular wavelength. The absorbance at 544 nm for the $[Ni([10]aneN_2O)_2]^{2+}$ species in 1 M $HClO_4$ was found to decay at a rate of 7.5×10^{-6} s^{-1} giving a half life of 25.7 hours for the decomposition of $[Ni([10]aneN_2O)_2]^{2+}$.

The decomposition of $[Ni([10]aneN_2O)_2]^{2+}$ is considerably more rapid than that of $[Ni(cyclam)]^{2+}$ [23] and similar cyclam based macrocycles,[67b,68] which are stable indefinitely in acidic media. This illustrates that although facially coordinating macrocyles are relatively inert, they are still open to decomposition by acid, while the equatorially coordinated macrocyles are sterically demanding, making attack by protons at the coordinated nitrogens

barely feasible.

The decomposition of the Ni^{III} species, followed at 400 nm, was found to be $2.4x10^{-3}$ s^{-1} ($t_{½}$ ~ 5 minutes). The rapid decomposition of the Ni^{III} species was not unexpected, based on the redox potential for the $Ni^{III/II}$ couple (0.99 V vs Ag^{+}/Ag). The $[Ni([10]aneN_2O)_2]^{3+}$ species is a strong oxidising agent, and by readily oxidising water, reverts to the Ni^{II} complex. This, together with the acid assisted decomplexation of the ligand, contributes to the rapid decay in the absorbance observed.

2.5 Palladium (II) complexes of $[10]aneN_2O$

2.5.1 Synthesis of $[Pd([10]aneN_2O)_2]^{2+}$ complexes

The complex, $[Pd([10]aneN_2O)_2](PF_6)_2$ (**8**) (Figure 2.10a), was synthesised from palladium acetate in acetonitrile with 2.5 equivalents of ligand present,using anion metathesis to form the hexafluorophosphate salt in 26% yield. The complex was characterised by FAB-MS, high resolution NMR and elemental analysis.

$[Pd([10]aneN_2O)_2](BF_4)_2$ (**9**) (Figure 2.10b) was synthesised by reaction of $[Pd(CH_3CN)_4](BF_4)_2$ with 2.3 equivalents of $[10]aneN_2O$ in acetonitrile, to give the complex in 16% yield. The $[Pd([10]aneN_2O)_2](BF_4)_2$ complex was more soluble in acetonitrile than that of the PF_6 salt. The complex was characterised by FAB-MS, high resolution NMR and elemental analysis.

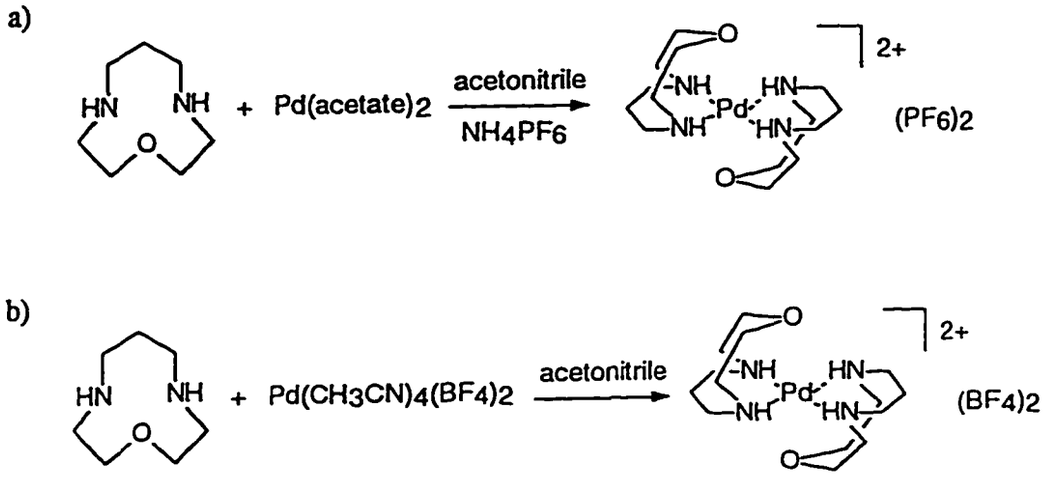

Figure 2.10: The synthesis of $[Pd([10]aneN_2O)_2]^{2+}$ complexes

2.5.2 Solution studies

2.5.2.1 High resolution nuclear magnetic resonance studies

The room temperature ^1H and ^{13}C NMR spectra for $[Pd([10]aneN_2O)_2]^{2+}$ are shown in Figures 2.11a and 2.12, respectively.

The ^1H NMR spectrum of the complex is complicated, since coordination of the ligand to the Pd^{II} centre makes each hydrogen atom of a $-CH_2-$ group inequivalent. Each proton in a methylene group is differently oriented towards the palladium, and thus experiences a slightly different environment. This results in a small difference in chemical shift, with strong coupling between the geminal methylene protons, as well as fairly strong vicinal coupling. Computer simulation of the ^1H NMR spectrum using an ABCD spin system to describe the coupling

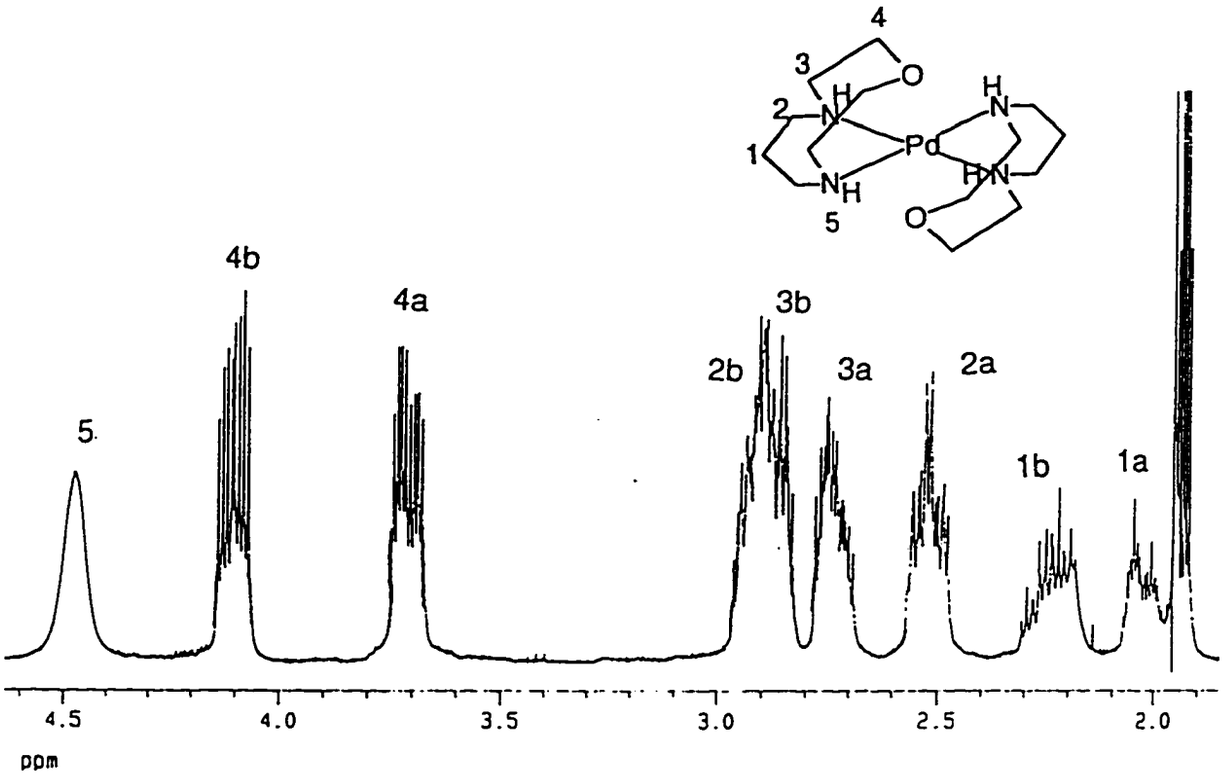

Figure 2.11a: ^{1}H NMR spectrum of [Pd([10]aneN_2O)$_2$](BF_4)$_2$ in CD_3CN (360 MHz)
Resonances attributed to each proton of a numbered methylene group have been assigned as **a** and **b**

pattern observed for the protons on the ethyl bridge gave an adequate representation of the spectrum. Using an ABCDAB spin system to describe the coupling pattern observed for the protons on the propyl bridge failed to reproduce the asymmetry of the central methylene protons of the propyl bridge (Figure 2.11b). This may suggest that on the ^{1}H NMR timescale the [10]aneN_2O ring is not symmetrical, or a second isomer with very similar chemical shifts

and coupling constants is present in solution and is contributing to the structure of the NMR spectrum. With the help of a ^{1}H COSY spectrum and a ^{1}H-^{13}C heteronuclear correlation (HETCOR) spectrum, the resonances have been assigned, as shown in Figure 2.11.

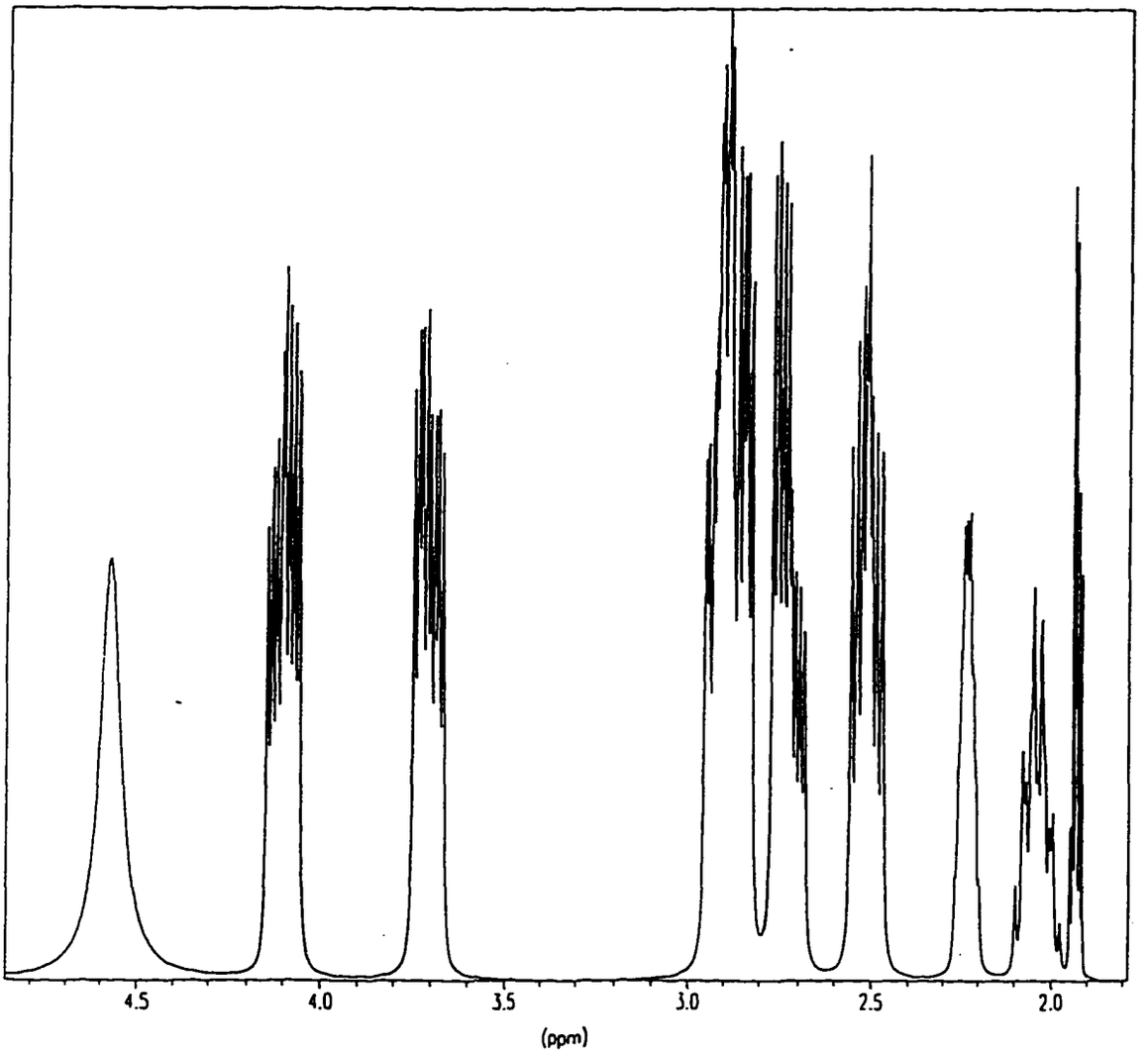

Figure 2.11b: Computer simulation of the ^{1}H NMR spectrum of $[Pd([10]aneN_2O)_2](BF_4)_2$

Each ^{13}C NMR resonance has been attributed to a set of equivalent carbon atoms, as shown in Figure 2.12. Coordination of $[10]aneN_2O$ to palladium(II) results in an upfield shift of the

^{13}C resonances. This can be attributed to the deshielding of the carbon atoms caused by donation of electron density from the donor atoms to the metal centre. The presence of only 4 peaks in the ^{13}C NMR spectrum indicates that on the NMR timescale the structure of the $[Pd([10]aneN_2O)_2]^{2+}$ cation is symmetrical, and the structure is likely to be similar to the time averaged solid state structures seen for the $[Ni([10]aneN_2O)_2]^{2+}$ and $[Cu([10]aneN_2O)_2]^{2+}$ cations. A poorly resolved crystal structure of the complex[91] (R = 0.15) indicated that the ligands may be coordinated in an endodentate fashion, rather than an exodentate manner as seen for $[Pd([9]aneN_3)_2]^{2+}$.[92]

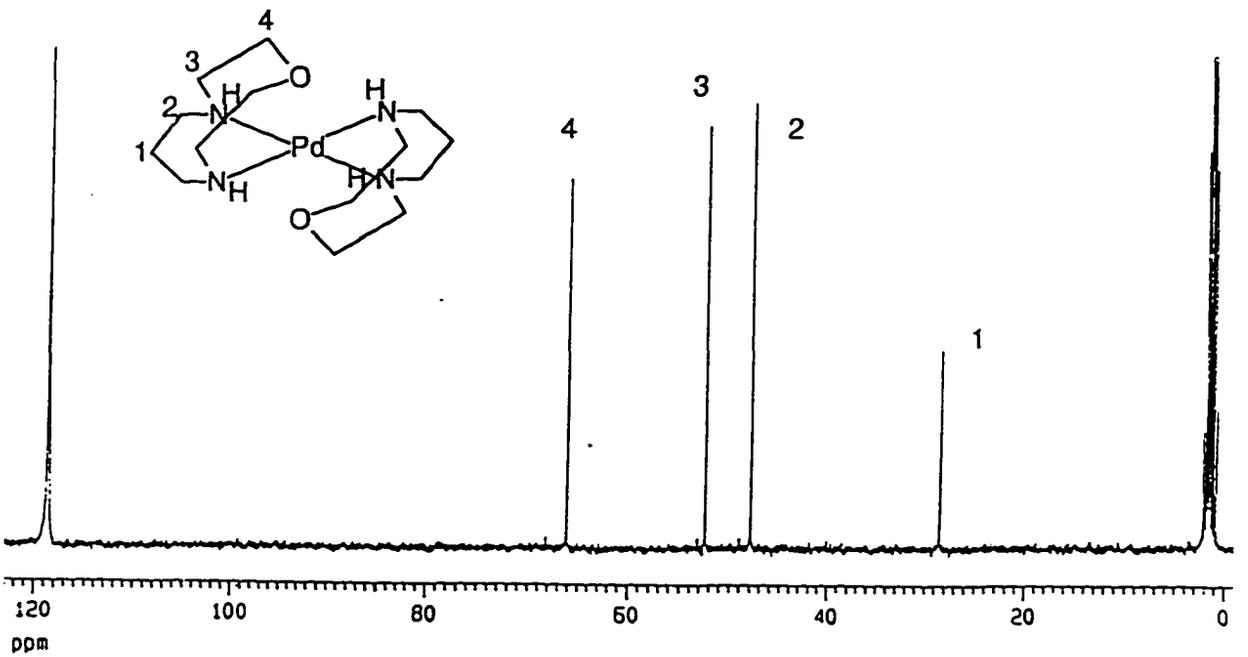

Figure 2.12: ^{13}C NMR of $[Pd([10]aneN_2O)_2](BF_4)_2$ in CD_3CN (90.6 MHz)

Fluxional processes are possible in the $[Pd([10]aneN_2O)_2]^{2+}$ cation, which may involve the interconversion of the *exo* and *endo* configurations of the $[10]aneN_2O$ ligand, as shown in

Figure 2.13. Second and third row d^8 transition metals possess large ligand field splitting parameters, therefore the gain in ligand field stabilisation energy on forming a diamagnetic Pd^{II} complex with square planar geometry is greater than that for a paramagnetic octahedral complex. For this reason, the geometry of the Pd^{II} complex is effectively square planar. The oxygen donor in the *endo* position is loosely held, and unlikely to perturb the palladium ion greatly. In solution, accordingly there would be little barrier to the interconversion between the *exo* and the *endo* forms of the complex. Variable temperature analyses of the complex did show broadening of the NMR resonances at lower temperatures, however due to the low solubility of the complex, sufficiently low temperatures could not be achieved to resolve the static spectrum.

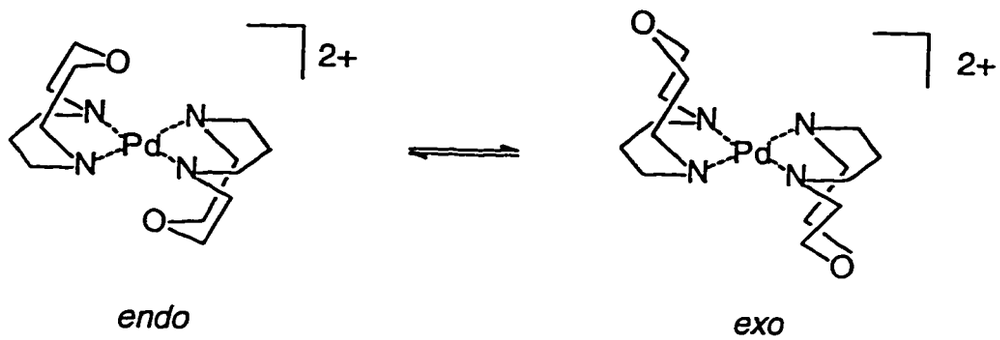

Figure 2.13: Interconversion of *exo* and *endo* configurations

Fluxional processes have been documented in the complex $[Pd([9]aneN_3)_2]^{2+}$ which involve the rapid interconversion between the *syn* and *anti* configurations of the complex[92] (Figure 2.14). Since a process similar to this in the $[Pd([10]aneN_2O)_2]^{2+}$ complex would require coordination of one oxygen and one nitrogen atom of the ligand during the cycle, it is unlikely that this process would occur with ease.

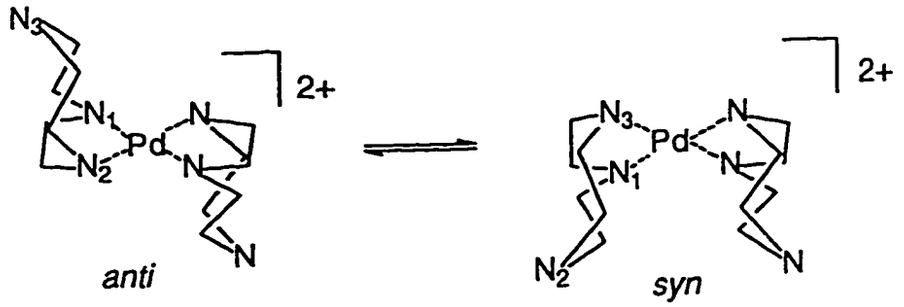

Figure 2.14: Fluxional processes in the $[Pd([9]aneN_3)_2]^{2+}$ ion

2.5.2.2 Electronic spectroscopy

The UV/Vis data for $[Pd([10]aneN_2O)_2]^{2+}$ complexes, and related palladium complexes is summarised in Table 2.7.

The UV-Visible spectrum for $[Pd([10]aneN_2O)_2]^{2+}$ was not found to be solvent sensitive which suggests that the coordination sphere does not include the weak oxygen donors, which are likely to be solvent sensitive. The spectra obtained are consistent with Pd^{II} complexes containing nitrogen donor ligands in a square planar geometry,[95] which also lends credence to the fact that the oxygen donors are poorly coordinated in the axial position, if at all. An intense, high energy transition at wavelengths less than 280 nm, is also present, and has been assigned as a metal-ligand charge transfer band. The spectra of the tetragonal Pd^{II} complexes can be assigned in a similar manner to those of square planar Pd^{II} complexes, although the labeling of the energy levels may differ. The weak d-d transitions are very similar in energy,[95] resulting in overlap of the transitions, making any definitive assignment of the transitions difficult. Hence, the band at 310 nm is assigned to the transitions $^1A_{1g} \rightarrow {}^1A_{2g}$, ^1E_g and $^1B_{1g}$. The origin of the shoulder at 414 nm is unclear; however, this peak may be caused by the shift

of one of the d-d transitions to a lower energy.

Table 2.7: UV/Visible data for Pd^{II} complexes

Complex	λ_{max} / nm (ϵ / $M^{-1}cm^{-1}$)	
$[Pd([10]aneN_2O)_2](PF_6)_2$	310 (350)	414(sh) (68)[a]
$[Pd([10]aneN_2O)_2](BF_4)_2$	309 (359)	414(sh) (31)[a]
$[Pd([9]aneN_3)_2]^{2+}$ [93]	296 (440)	440(sh) (30)[b]
$[Pd(trien)]^{2+}$ [94]	296 (1000)[b]	
$[Pd(NH_3)_4]^{2+}$ [95]	298 (212)[a]	
$[Pd([10]aneN_2O)_2]^{3+}$	315 (480)[a]	
$[Pd([9]aneN_3)_2]^{3+}$ [93]	314 (1240)	383 (590)[b]

[a] Spectrum recorded in acetonitrile, [b] Spectrum recorded in water.

2.5.2.3 Electrochemistry

The electrochemical data for the $[Pd([10]aneN_2O)_2]^{2+}$ ion is given in Table 2.8. Data for related palladium complexes have been included for comparison.

The $Pd^{IV/III}$ and $Pd^{III/II}$ couples for $[Pd([10]aneN_2O)_2]^{n+}$ were quasi-reversible, with large peak to peak separations and differences in anodic and cathodic currents, indicating that the

electron transfer was accompanied by a chemical process, probably a change in structure of the complex from square planar to distorted octahedral geometry.

It is difficult to compare the $E_{½}$ values for the redox couples with those of other complexes, mainly due to the problem in assigning accurate $E_{½}$ values for these processes. $E_{½}$ values tend to vary slightly, depending on the solvent, and the electrode system used in obtaining data. The $[Pd([10]aneN_2O)_2]^{3+/2+}$ couple is more positive than the $[Pd([10]aneS_2N)_2]^{3+/2+}$ couple. This is most likely due to the hardness of the oxygen donor being a poor donor in the Pd^{III} complex, in comparison to the softer sulfur and intermediate nitrogen donors. Although this may seem counter intuitive, since harder donor atoms are likely to stabilise higher oxidation states, the palladium(III) ion is still relatively soft, so is stabilised by the combination of nitrogen and sulfur donors.

The $[Pd([10]aneS_2N)_2]^{4+}$ is the weakest oxidant for the Pd^{IV} complexes, paralleling the results observed for the Pd^{III} complexes. The $[Pd([9]aneN_3)_2]^{n+}$ complex shows greater reversibility for both the $Pd^{III/II}$ and $Pd^{IV/III}$ couples, indicating that this complex undergoes less change on oxidation, possibly due to the symmetry of the $[9]aneN_3$ ligand which may allow for more rapid geometrical changes that occur in oxidising the Pd^{n+} centre. The more positive value of $[Pd([10]aneS_2N)_2]^{2+/1+}$ couple is due to the π acceptor capabilities of sulfur ligands, which are capable of stabilising the increased electron density on the Pd^{I} metal centre.

Table 2.8: Electrochemical data for palladium complexes

Complex[a]	$E_{½}$/V[c]		Ref
$[Pd([10]aneN_2O)_2]^{3+/2+}$ [a]	0.66	(quasi-reversible)	PW
$[Pd([10]aneS_2N)_2]^{3+/2+}$ [a]	0.53	(quasi-reversible)	96
$[Pd([9]aneN_3)_2]^{3+/2+}$ [b]	0.77	(reversible)	93
$[Pd([10]aneN_2O)_2]^{4+/3+}$ [a]	1.03	(quasi-reversible)	PW
$[Pd([10]aneS_2N)_2]^{4+/3+}$ [a]	0.93	(quasi-reversible)	96
$[Pd([9]aneN_3)_2]^{4+/3+}$ [b]	1.04	(reversible)	93
$[Pd([10]aneN_2O)_2]^{2+/1+}$ [a]	-1.63	(irreversible)	PW
$[Pd([10]aneS_2N)_2]^{2+/1+}$ [a]	-1.03	(irreversible)	96

[a] Cyclic voltammograms run in acetonitrile

[b] Cyclic voltammogram run in water

[c] vs Ag^+/Ag

2.5.2.4 Electron paramagnetic resonance spectroscopy

The $[Pd([10]aneN_2O)_2]^{2+}$ cation in acetonitrile was oxidised to Pd^{III} by the addition of NO^+. The d^7 Pd^{III} ion is low spin, and hence paramagnetic with one unpaired electron. The EPR of

the frozen solution (77 K) is typical of an axially elongated d^7 ion (Figure 2.15). The g values determined were $g_{\parallel} = 2.0013$ and $g_{\perp} = 2.1720$. The order of the g values $2 \approx g_{\parallel} < g_{\perp}$ indicates that the unpaired electron is in the d_{z^2} orbital, and hence the ground state of the complex is $^2A_{1g}$. The peaks obtained are broad, a feature that is typical of a metal centred radical, rather than a ligand centred radical. No hyperfine coupling of the spin active equatorial nitrogen donors is observed.

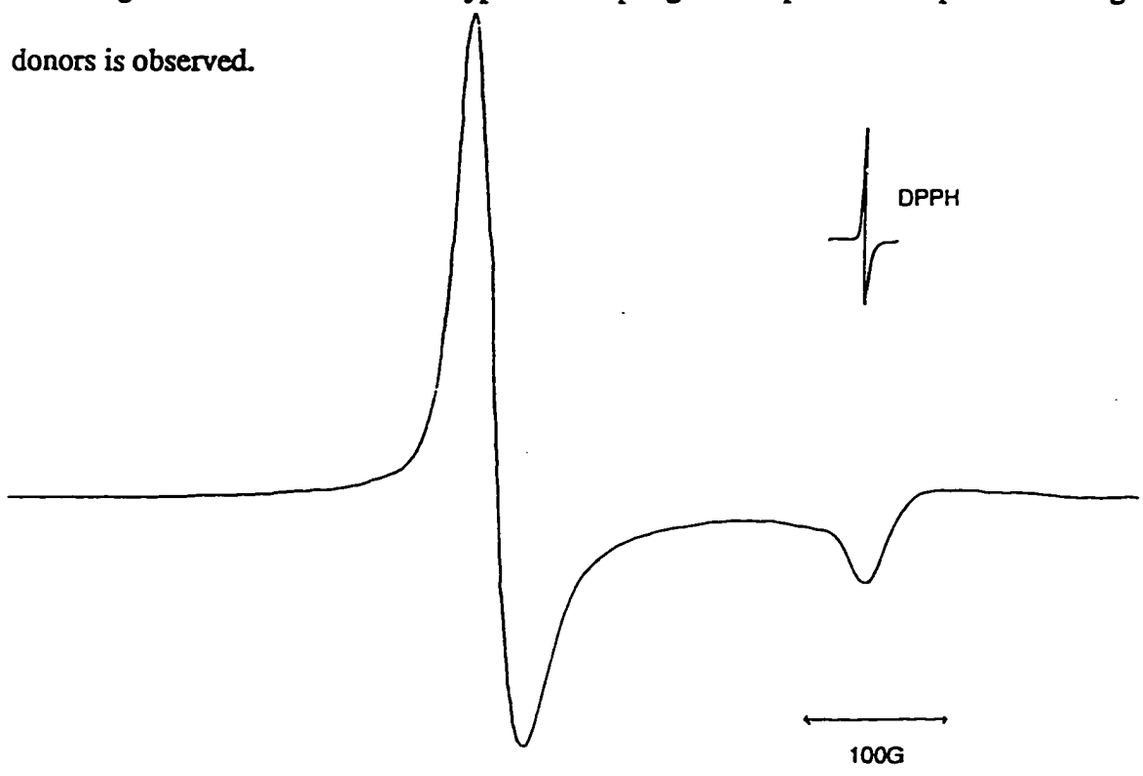

Figure 2.15: EPR spectrum of the $[Pd([10]aneN_2O)_2]^{3+}$ ion in CH_3CN at 77 K

2.6 The cobalt(III) complex of [10]aneN$_2$O

2.6.1 Synthesis of $[Co([10]aneN_2O)_2](ClO_4)_3$ (10)

Tris(carbonato)cobaltate was added directly to an aqueous solution of the HCl salt of [10]aneN$_2$O, and the resultant solution was refluxed for 5 hours to ensure complete complexation. The solution was filtered to removed any insoluble material, then loaded onto

a Sephadex CM-C25 column. The major maroon band was eluted with 0.1 M $NaClO_4$. This material will be the subject of further characterisation and reaction studies. Of interest will be the EPR spectrum of the Co^{II} d^7 ion and the potential use as an outer sphere reagent.

2.7 Conclusions

The [10]aneN_2O ligand forms complexes with the transition metals studied with a 2:1 stoichiometry. The ligand coordinates facially with the four nitrogen donors arranged equatorially. Apart from the Pd^{II} complex, the geometry of the complexes can be described as pseudo-octahedral. The complexes have been satisfactorily characterised by means of electronic spectra, NMR, EPR and elemental analysis, and the structures in the solid state confirmed for the nickel(II) and copper(II) ions by X-ray single crystal studies.

CHAPTER 3

THE SYNTHESIS OF THE TRICYCLO[10-14-10]N_4O_2 MACROCYCLE AND RELATED LIGANDS.

3.1 Introduction

A suitable candidate for an outer sphere redox reagent is a metal ion with a saturated ligand framework, so that dissociation or substitution of donor atoms is unlikely to occur during the electron transfer process. It is also required that the geometry of the metal ion remain roughly constant before and after the redox process, so that the energetics of the reaction being examined are not complicated by changes in coordination number or spin state, which would increase the barrier to electron transfer. The design of the tricyclic macrocycle, 7,16-dioxa-1,4,10,13-tetraazatricyclo[11.5.3.3]octadecane (tricyclo[10-14-10]N_4O_2) (**11**), shown in Figure 3.1, was based on the premise that a metal complex of this ligand would have a coordinatively saturated metal ion, where the donor atoms were geometrically constrained in an octahedral position. This arrangement would conceivably provide a suitable reagent for use in outer sphere redox reactions.

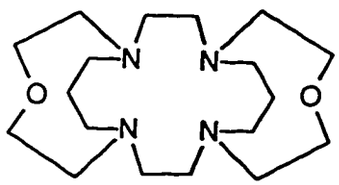

Figure 3.1: The tricyclo[10-14-10]N_4O_2 ligand (**11**)

Two isomers of tricyclo[10-14-10]N_4O_2, shown in Figure 3.2, are possible. The macrocycle can be regarded as a ring, with two 'clasps' attached to grip the metal atom. The *anti* isomer would be capable of octahedral coordination around a metal ion, and is therefore the isomer of choice. This isomer would form a 'vice'[97] around the metal, the lack of flexibility confering

steric demands on the metal which may govern some interesting chemistry. The *syn* isomer could possibly coordinate in a pseudo 5 coordinate fashion, the ligand forming a 'nest'[97] around the metal, although it may also be possible to form four coordinate tetrahedral complexes with this ligand by coordinating only two of the four nitrogen donors together with the two oxygen centres. The *anti* and *syn* isomers of tricyclo[10-14-10]N_4O_2 are illustrated in Figure 3.2.

syn *anti*

Figure 3.2: Possible isomers of the tricyclo[10-14-10]N_4O_2 ligand

3.2 Synthetic strategy

It was envisioned that the macrocycle, tricyclo[10-14-10]N_4O_2, shown above could be synthesised by a number of different routes. Since the *anti* isomer was desired, a template reaction was designed that would produce this isomer preferentially. Another reaction that was expected to produce the desired product involved capping of cyclam with a bifunctional bridge, which was expected to result in a number of possible bicyclic and tricyclic ligands. The third strategy investigated involved the use of a high dilution reaction where a smaller macrocycle was fused to the pendant arms of another macrocycle. A general schematic view of the two latter reactions is shown in Figure 3.3.

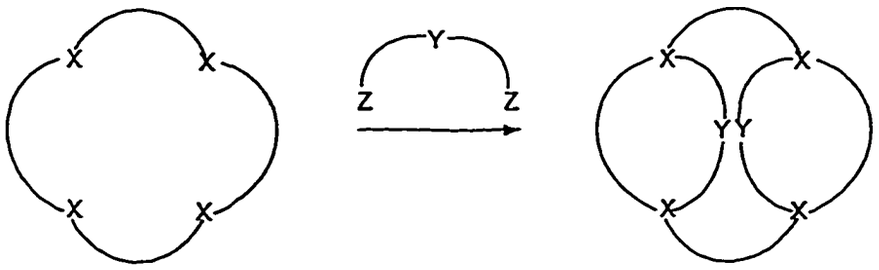

a) Capping of cyclam with a bifunctional bridge

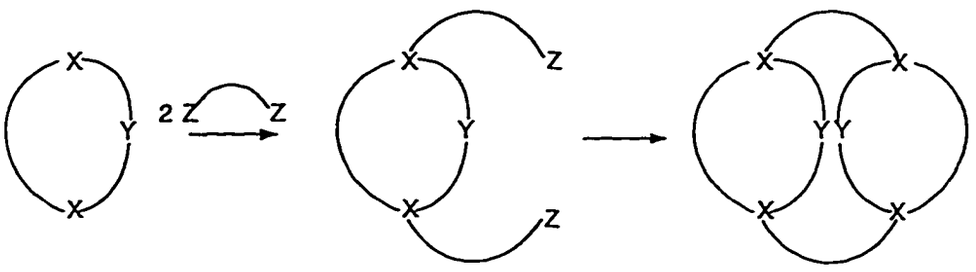

b) Fusion of a small macrocycle to a macrocycle containing pendant arms

Figure 3.3: Synthetic strategies towards the creation of the tricyclo[10-14-10]N_4O_2 ligand

3.3 The template reaction of the $[Cu([10]aneN_2O)_2]^{2+}$ complex

The proposed template molecule was the $[Cu([10]aneN_2O)_2]^{2+}$ cation, where all donors are coordinated in a manner similar to that desired in the tricycle. Reaction with two equivalents of a bifunctional molecule such as 1,2-dibromoethane would complete the cyclisation as shown in Figure 3.4. Although template reactions, where the reaction takes place at a secondary nitrogen, are unknown, it was anticipated that the ligand would be sufficiently labile so that reaction would occur. Secondary nitrogens are intrinsically more basic than primary nitrogens, so coordination to the metal is enhanced, however this results in the nucleophilicity of the reacting nitrogens being reduced,[98] resulting in slower reaction rates.

Although coordinated amides formed by deprotonation of the secondary amines are nucleophilic, their basicity precludes their usage in this reaction since they would deprotonate the ß hydrogens of 1,2-dibromoethane.[99] The solvent sensitivity of the d-d transitions for $[Cu([10]aneN_2O)_2]^{2+}$, described in the previous chapter, indicates that the complex formed is labile, and dissociates to a certain extent in solution, which led us to believe that the reaction between $[Cu([10]aneN_2O)_2]^{2+}$ with 1,2-dibromoethane should be favourable.

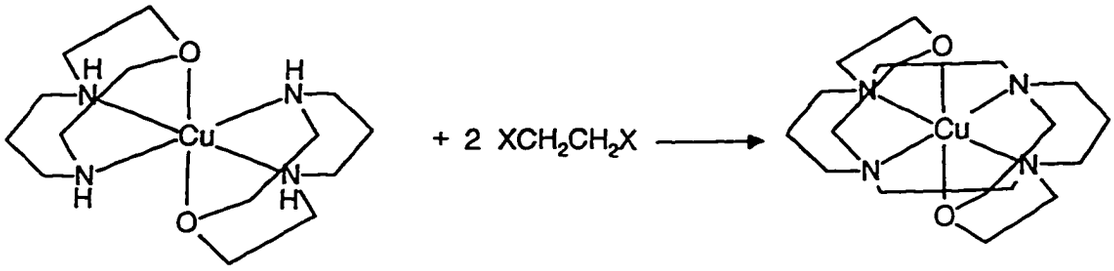

Figure 3.4: Predicted template synthesis of the tricyclo[10-14-10]N_4O_2 ligand

3.3.1 Synthesis

The $[Cu([10]aneN_2O)_2]^{2+}$ template was synthesised as previously described in Section 2.3.1. The reaction of $[Cu([10]aneN_2O)_2]^{2+}$ with 1,2-dibromoethane did not produce any detectable tricycle. The major non polymeric product of the reaction was identified as the copper(II) complex of 1,2-*bis*(1-oxa-5,8-diazacyclodecanylethane) ([10]aneN$_2$O earmuff) (**12**) (Figure 3.5). The reaction was attempted with a combination of different bases and solvent systems in an effort to promote the cyclisation of the facially coordinated [10]aneN$_2$O ligands. The copper complex was dissolved in water, and 1,2-dibromoethane and Na_2CO_3 added as base and the mixture refluxed for 24 hours. After removal of any unreacted dibromoethane, the

products were purified by separation on a Sephadex CM-C25 cation exchange column, to give the [Cu([10]aneN$_2$O earmuff)]$^{2+}$ complex as royal blue crystals by slow evaporation of the sodium perchlorate solution. Although the 1,2-dibromoethane did not dissolve in water, the reaction did proceed to completion within about 12 hours. Attempting the reaction in methanol did not improve the yields of product, but rather resulted in the production of greater amounts of polymeric material. A possible explanation for the decrease in polymeric material produced in a two-phase system is that the concentration of 1,2-dibromoethane in solution is so low that a high dilution effect is in operation, promoting cyclisation rather than polymerisation.

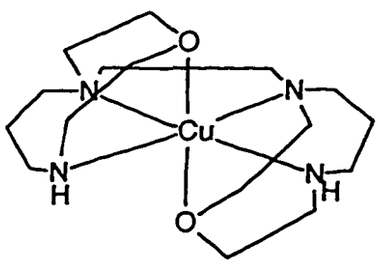

Figure 3.5: The structure of the [Cu([10]aneN$_2$O earmuff)]$^{2+}$ complex (13)

The formation of the [Cu([10]aneN$_2$O earmuff)]$^{2+}$ complex via the template method indicates that the coordinated secondary amines are sufficiently labile to react with 1,2-dibromoethane. The lack of formation of any tricyclic complex can be accounted for in two possible ways: a) the complexation of the earmuff around the Cu^{II} ion is such that the two remaining nitrogen atoms available for reaction are too far apart to be bridged by 1,2-dibromoethane. The presence of large amounts of polymeric material in the product mixture indicates that this is

likely, although a crystal structure of the copper complex is required in order to confirm this hypothesis.

b) The lability of the complex is reduced in moving from $[Cu([10]aneN_2O)_2]^{2+}$ to $[Cu([10]aneN_2O$ earmuff$)]^{2+}$ to such an extent that reaction with 1,2-dibromoethane is no longer favourable.

The free ligand was produced by decomplexation of the copper complex with sodium sulfide, and extraction of the ligand into chloroform from a basic solution.

3.3.2 NMR studies of the free ligand, $[10]aneN_2O$ earmuff (13)

The free ligand,$[10]aneN_2O$ earmuff, was characterised by high field ^1H and ^{13}C NMR spectroscopy given in Figures 3.6 and 3.7 respectively.

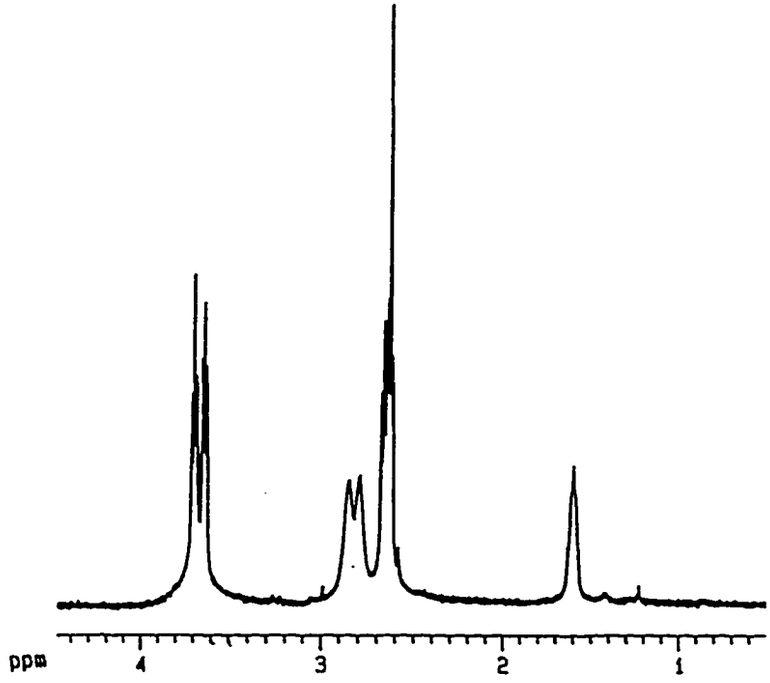

Figure 3.6: The ^1H NMR spectrum of the $[10]aneN_2O$ earmuff ligand in $CDCl_3$ (360 MHz)

The proton spectrum is relatively simple to interpret and is consistent with the ligand described. The resonances corresponding to the methylene groups adjacent to the nitrogens in the propyl bridge, as well as those of the ethyl linkage between the two [10]aneN_2O moieties, are coincident, and no coupling information can be extracted from this region. The assignment of the ^1H NMR spectrum is given in Table 3.1.

Table 3.1: Assignment of ^1H NMR resonances for the [10]aneN_2O earmuff ligand

Resonance/ppm	Multiplicity	Assignment[a]
1.60	m	2
2.65	m	1, 3, 8
2.79, 2.87	t, t	4,7
3.63, 3.68	t, t	5, 6
4.73	br	NH[b]

[a] The numbering scheme for the proton resonances is the same as that given in Figure 3.7 for the ^{13}C resonances.

[b] This resonance is not always observed in the ^1H NMR spectrum, as the presence of small amounts of H_2O in solution results in rapid proton exchange.

The ^{13}C peak assignments are given in Figure 3.7. The free ligand has an apparent plane of

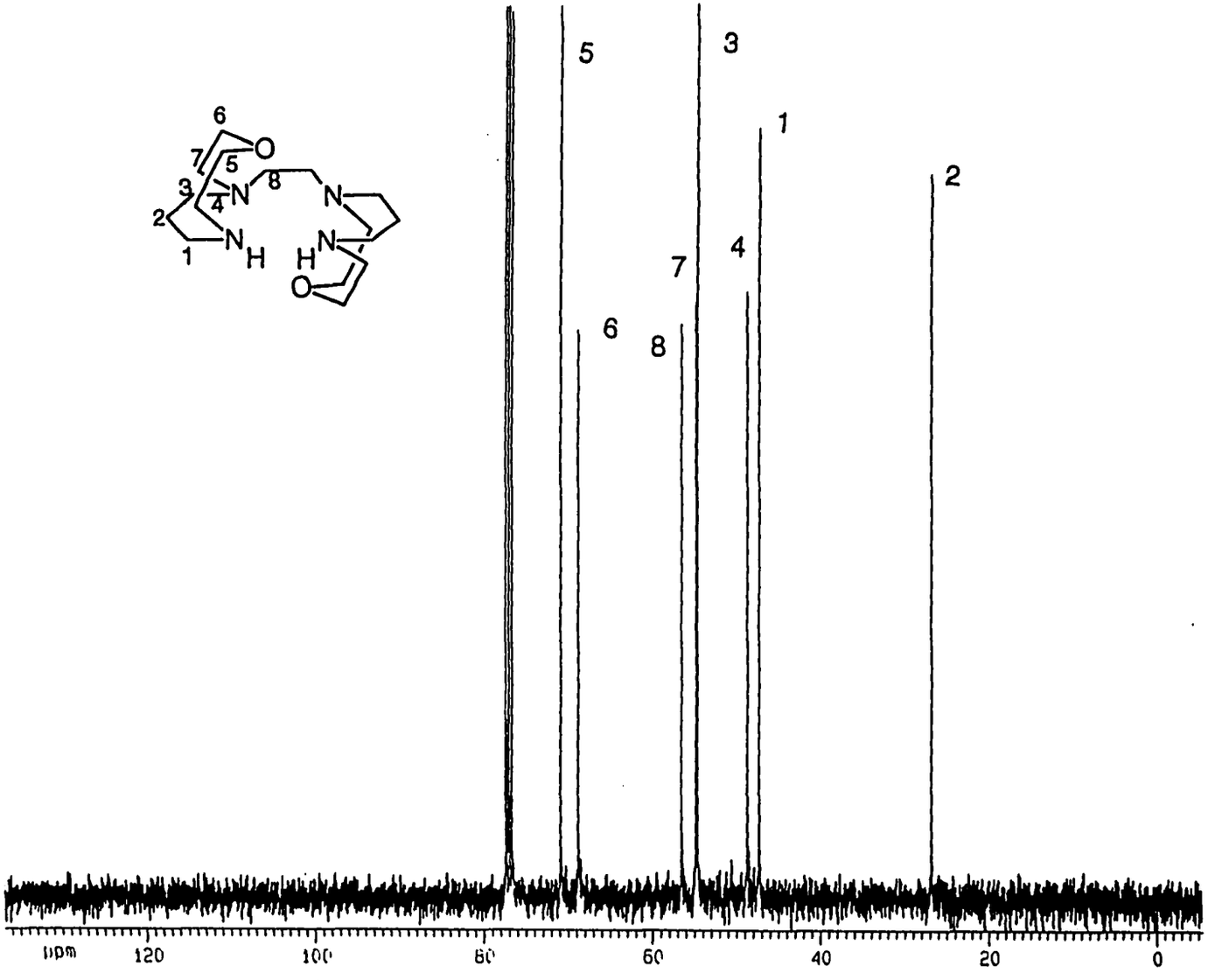

Figure 3.7: Assignment of ^{13}C NMR resonances for [10]aneN_2O earmuff in $CDCl_3$ (90.6MHz)

symmetry through the bridge linking the two [10]aneN$_2$O moieties, hence only 8 resonances are observed in the ^{13}C spectrum. The method of synthesis of [10]aneN$_2$O earmuff will produce the ligand with the two oxygen donors in an *anti* configuration. This structure is may persist in solution, as there is likely a large barrier to inversion of the tertiary nitrogens.

3.3.3 Studies of the copper complex, [Cu([10]aneN$_2$O earmuff)](ClO$_4$)$_2$

3.3.3.1 Characterisation of the copper complex by mass spectrometry

Characterisation of the copper complex by FAB MS gave peaks which were assigned to fragments caused by loss of a perchlorate anion (476.2 amu), as well as further loss of perchloric acid (377.2 amu). The data obtained from elemental analysis was also consistent with the proposed formulation.

3.3.3.2 Electronic Spectra

The UV/visible spectrum of [Cu([10]aneN$_2$O earmuff)]$^{2+}$ is characteristic of a copper(II) complex with a square planar array of nitrogen donors and weaker axial interactions (see section 2.3.3.1 for comparison with the [Cu([10]aneN$_2$O)$_2$]$^{2+}$ complex). Transitions occur at 289 nm (ϵ = 6057 M^{-1}cm^{-1}) and 587 nm (ϵ = 172 M^{-1}cm^{-1}) in water. The higher energy transition is assigned to a charge transfer band. The d-d transition at 587 nm is at a lower energy than that seen for [Cu([10]aneN$_2$O)$_2$]$^{2+}$. This is possibly due to less dissociation of the ligand which could induce more axial coordination of the oxygen donors, although the presence of tertiary amine donors would also result in a shift to a longer wavelength. Distortion of the copper atom from the plane described by the four nitrogen donors cannot

be ruled out, since this would also decrease the ligand field splitting parameter due to decreased overlap between the nitrogen donors and the metal atom. The d-d transition is less solvent sensitive than $[Cu([10]aneN_2O)_2](ClO_4)_2$, shifting to 589 nm in acetonitrile. This lack of solvent sensitivity may be a result of the increased tethering of the macrocyclic ligand as a result of bridging the two [10]aneN$_2$O moieties.

3.3.3.3 Electron paramagnetic resonance spectroscopy

The frozen glass EPR spectrum of the copper(II) [10]aneN$_2$O earmuff complex is similar to those observed for the corresponding [10]aneN$_2$O species. The EPR spectrum recorded at 77 K in DMF/CH$_3$CN (1:1) is given in Figure 3.8.

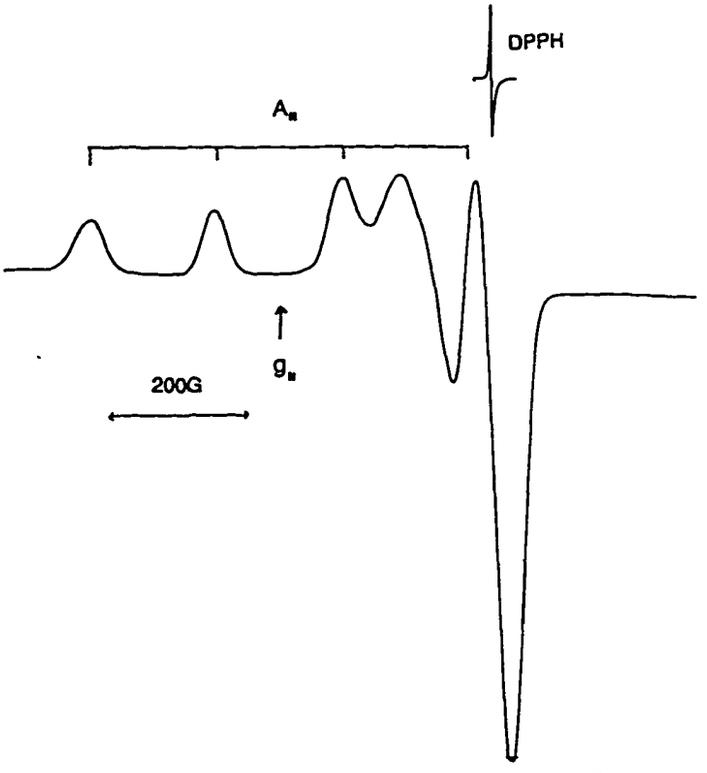

Figure 3.8: The frozen EPR spectrum of $[Cu([10]aneN_2O\ earmuff)]^{2+}$ in DMF/CH$_3$CN (1:1) at 77 K

The g_o and A_o values for the complex recorded at room temperature are 2.056 and 77 G respectively. Using first order analysis, and the $g_{\parallel}$ (2.200) and $A_{\parallel}$ (180 G) values obtained from Figure 3.8, the values of 1.984 for $g_{\perp}$ and 26 G for $A_{\perp}$ were obtained. The $g_{\perp}$ value is lower that that expected for increased axial coordination in the [Cu([10]aneN_2O earmuff)]$^{2+}$ compared to the [Cu([10]aneN_2O)$_2$]$^{2+}$ complex, however the decrease in $A_{\perp}$ is consistent with increased axial coordination for the [Cu([10]aneN_2O earmuff)]$^{2+}$ as proposed.

3.3.3.4 Cyclic voltammetry

The cyclic voltammogram of [Cu([10]aneN_2O earmuff)]$^{2+}$ exhibited two irreversible waves. The redox wave corresponding to the Cu^{III}/Cu^{II} couple was observed at 1.46 V, while the Cu^{II}/Cu^{I} couple appeared at -0.85 V. The reverse wave was complicated by a sharp peak at approximately -0.55 V attributed to the adsorption of a reduced copper species onto the electrode. The Cu^{II}/Cu^{I} couple is considerably more positive than that observed for [Cu([10]aneN_2O)$_2$]$^{2+}$ (-1.02 V). Since the structure of the two complexes is likely to be fairly similar, the ease in reduction of [Cu([10]aneN_2O earmuff)]$^{2+}$ is due to the tethering of the two macrocyclic rings, producing two tertiary amine donors. This is consistent with the trends observed for the Ni^{III}/Ni^{II} redox couple with secondary and tertiary amines,[90] and with trends observed with the Cu^{III}/Cu^{II} couple.[80a]

3.4 The capping of cyclam with *bis*-(2-(methylsulfonyl)oxyethyl)ether (14) in order to form polyclic products

3.4.1 Synthesis

The use of a bifunctional bridging molecule to cap cyclam, was expected to produce a number of bicyclic and tricyclic macrocycles, some of which are shown in Figure 3.9.

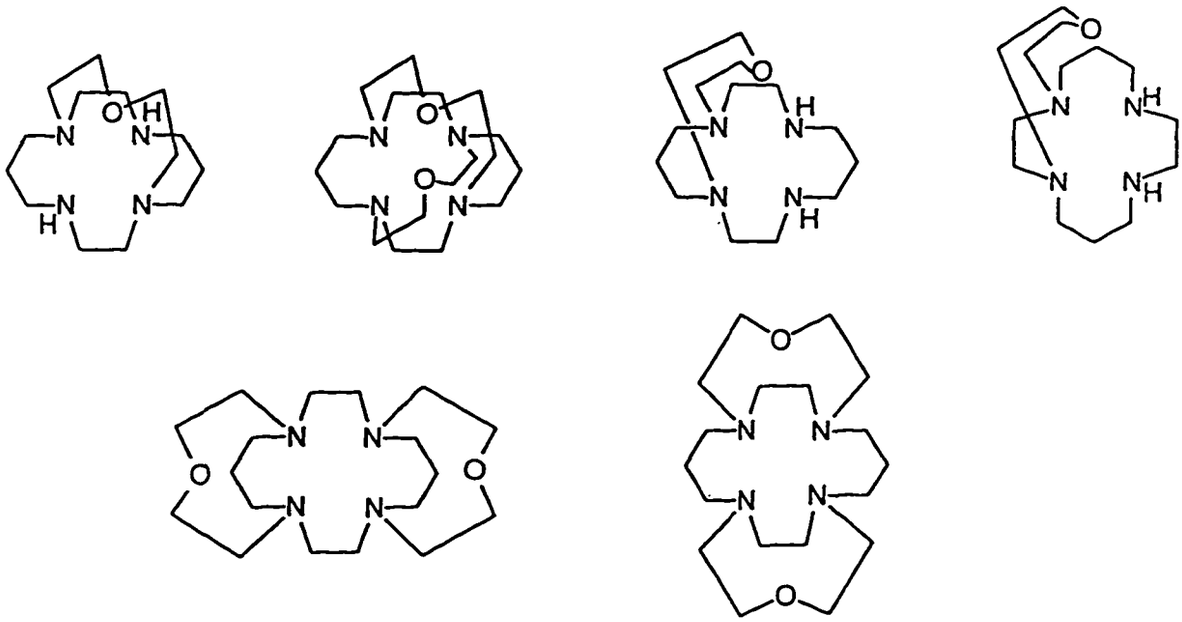

Figure 3.9: Possible bicyclic and tricyclic macrocycle products expected from the reaction of cyclam with *bis*-(2-(methylsulfonyl)oxyethyl)ether

Only one configurational isomer is shown in Figure 3.9, although in some cases other isomers are possible. In addition to these isomers, it is possible that several pendant arm type macrocycles could be formed, as well as the 2:1 and 2:2 macrocycles with two cyclam moieties linked by the bifunctional reagent. The difficulty in this synthesis is considered to be the separation of the numerous products formed, due to the structural similarity of the

isomers.

A variety of synthetic procedures was examined in an effort to optimise the production of tricyclic products. It was discovered during initial trials, with triethylamine added as base, that the cyclam moiety was itself acting as a base, resulting in low product yields, and the majority of the cyclam was recovered unreacted. Stronger bases were used in attempts to reduce the protonation of cyclam. Potassium t-butoxide and NaH in dry THF were used independently; however, both resulted in elimination of the mesylate group from the bridge, resulting in excessive side reactions. [Cu(17-oxa-1,4,8,11-tetraazabicyclo[6.6.5]tetra decane)] $(ClO_4)_2$ ([Cu(bicyclo[12-12]N_4O)]$(ClO_4)_2$) (15) (Figure 3.10) was identified as the major non polymeric product in all reactions.

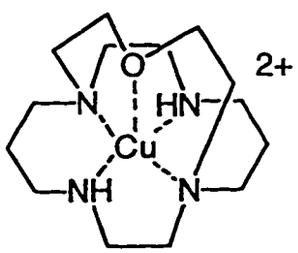

Figure 3.10: The structure of [Cu(bicyclo[12-12]N_4O)]$(ClO_4)_2$ (15)

The final reaction method chosen involved the use of large excesses of Na_2CO_3 in THF. The cyclam and mesylate bridge were added to a slurry of sodium carbonate in THF and refluxed for 10 days. After filtering the solution, and removing solvent, the crude ligand mixture was reacted with $Cu(ClO_4)_2 \cdot 6H_2O$ in acetonitrile to form the metal complexes, affording easier

separation of the reaction products. Separation of the complexes formed was achieved by column chromatography through a cation exchange resin, Sephadex CM-C25. Several complexes were isolated, and the major purple band eluted with 0.1 M $NaClO_4$ was identified as $[Cu(bicyclo[12\text{-}12]N_4O)](ClO_4)_2$. Three other minor bands eluted with increasing concentrations of $NaClO_4$ were observed. The first royal blue band could not be identified due to insufficient product being formed. The purple band eluted next was identified by FAB MS as the *bis*-copper complex of bicyclo[12-12]N_4O linked to cyclam by a diethylether linkage. The pink band eluted with 0.5 M $NaClO_4$ was identified as the *bis*-copper(II) complex of two bridged cyclam moieties. Since the minor products have only been identified by FAB MS, the exact configuration of the complexes is unknown; however the possible isomers of these two complexes are shown in Figure 3.11.

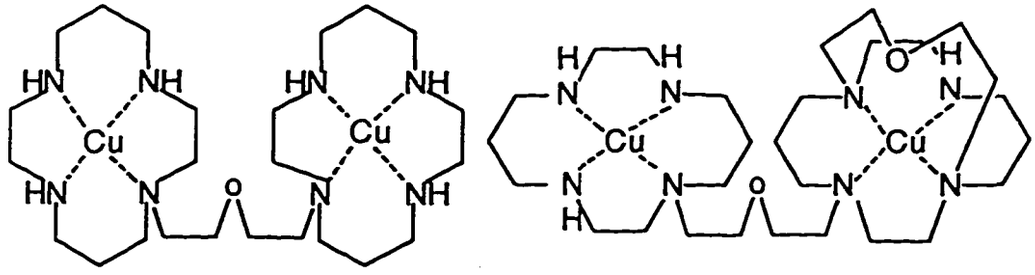

Figure 3.11: Other complexes synthesised from the reaction of cyclam with *bis*-(2-(methylsulfonyl)oxyethyl)ether

A pale blue $[Cu(N_4O_2tricycle)]^{2+}$ (**16**) was also found to co-elute with the major band. This was separated from the bicyclo[12-12]N_4O by demetallation of the $[Cu(bicyclo[12\text{-}12]N_4O)]^{2+}$ with NaS (the tricycle remains complexed to the copper), and extraction of the bicyclo[12-

12]N_4O ligand (17) and $[Cu(N_4O_2tricycle)]^{2+}$ from a basic solution into chloroform. Synthesis of the $[Ni(bicyclo[12\text{-}12]N_4O)]^{2+}$ (18) complex, by reaction of $Ni(ClO_4)_2 \cdot 6H_2O$ with the ligand, then separation of the two complexes by passing through a Sephadex CM-C25 column gave the $[Cu(N_4O_2tricycle)]^{2+}$ complex.[a] The isomeric structure of the $[Cu(N_4O_2tricycle)]^{2+}$ complex is unknown, since it has only been characterised by FAB MS (341.2 amu, LH^+; 403.2 amu, $[Cu^{II}(L\text{-}H^+)]^+$; 502.1 amu, $[Cu^{II}(L)(ClO_4^-)]^+$) and UV/Visible spectroscopy. Since the major bicyclic product from this reaction is the 1,8-annelated cyclam, it is likely that the tricyclic structure formed is the tricycle where the 1,8 position and the 5,12 position are both diagonally bridged shown in Figure 3.12. Attempts to grow X-ray quality crystals of this complex for exact structure determination have as yet been unsuccessful.

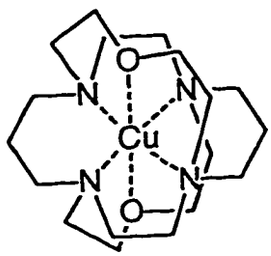

Figure 3.12: Possible structure of $[Cu(N_4O_2tricycle)]^{2+}$ (16)

The pure $[Cu(bicyclo[12\text{-}12]N_4O)]^{2+}$ complex can be synthesised by reacting the crude ligand mixture with $Cu(ClO_4)_2 \cdot 6H_2O$ in water instead of acetonitrile. In water, the tricyclic ligand appears to be protonated due to its inherent basisity, and the complex with copper is no longer formed. The $[Cu(bicyclo[12\text{-}12]N_4O)]^{2+}$ complex can be purified on Sephadex as

---

[a] This nomenclature has been employed because the structure of the macrocycle is unknown, however it is likely to be the structure shown in Figure 3.12.

described previously, and the free ligand was obtained by extraction of the copper as CuS. The ligand can then be extracted from a highly basic solution into chloroform or dichloromethane.

The origin of the stereoselectivity of the bridging reaction is possibly a function of the protonation of cyclam. The pK_a values of the conjugate acid of cyclam are 11.58, 10.62, 2.41 and 1.61,[100] which indicates that cyclam has two basic nitrogen sites, and two sites which are much less basic. To minimise electrostatic repulsion of protons within the cyclam cavity, the two basic sites are diagonally opposed in the ring. The pK_a of hydrogen carbonate is 10.5, therefore at the start of the reaction, cyclam will be protonated initially at the 1 and 8 positions, leaving the two less basic sites to react further with the bridge. A similar explanation has been proposed for the regioselectivity of the reaction of cyclen with chloroformates in acid solution.[101]

The reaction of triethylene glycol ditosylate with cyclen in acetonitrile solvent, and using sodium carbonate as base, was found to produce the 1,4-annellated isomer and the 1,7-annelated isomer in 10:1 ratios.[102] This reaction is similar to the reaction of cyclam with *bis*-(2-(methylsulfonyl)oxyethyl)ether, however the regioselectivity is opposite to that observed in this study. Previously synthesised 1,8-disubstituted cyclam compounds have generally been prepared via a bisaminal intermediate[103] (Figure 3.13), which directs further reaction regioselectively. This selectivity is due to the conformation of the compound preventing attack at two diagonally opposed nitrogen lone pairs.

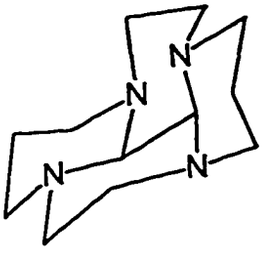

Figure 3.13: The conformation of bisaminal cyclam

The 1,4-annellated isomer of cyclam would be expected to be the most stable product thermodynamically, based on the stability of the *trans*(III) form of cyclam complexes with Ni^{II}, shown in Figure 3.14.

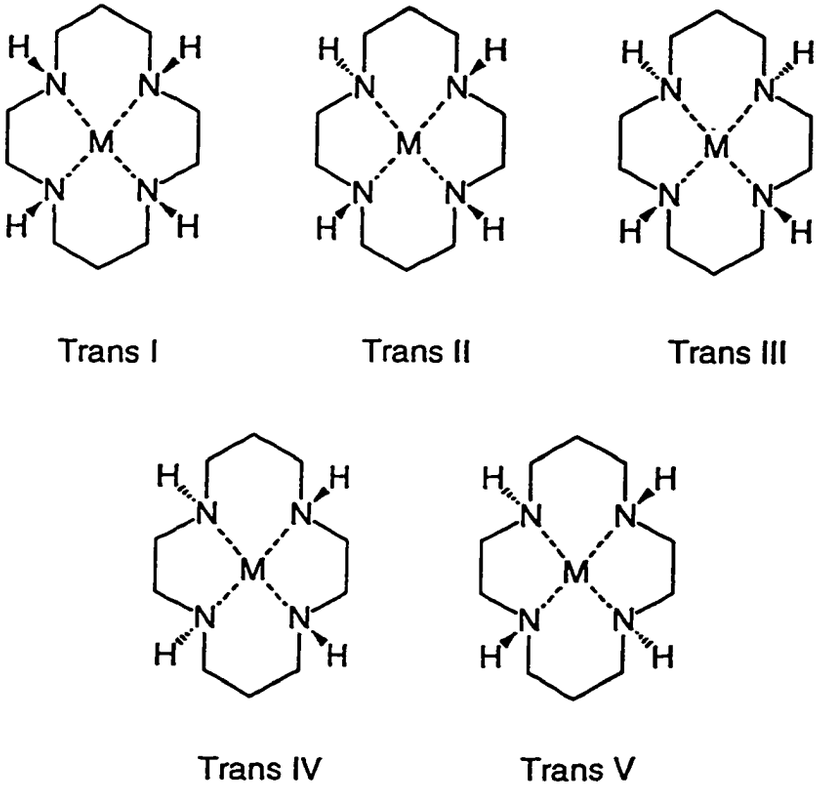

Figure 3.14: The ring conformations of cyclam

The crystal structure of the unprotonated cyclam molecule has the *trans*(III) conformation in the solid state.[104] In this form, the cyclam ring of the isomer could adopt a low energy conformation, with the propyl bridges in a 'half chair' conformation, and the ethyl bridges arranged in a gauche conformation. If this structure persists in solution, which is believed to occur in non-polar solvents, the cyclam moiety would be in the conformation required to produce the 1,4-annellated substitution product as the kinetically favoured product. Isomerisation of the product once formed is unlikely, due to severe steric hindrance.

Further study of the origin of the 1,8- regioselectivity observed in this study would be of interest, but is out of the scope of this project.

3.4.2 Characterisation of $[Cu(bicyclo[12\text{-}12]N_4O)]^{2+}$ by FAB mass spectrometry

Major peaks were observed clustered around 333.1 and 432.1 amu in the FAB mass spectrum. In order to completely characterise these peaks, theoretical isotope distributions were calculated for the fragments expected to give rise to these peaks. The peaks around 432.1 amu were expected from the $[Cu^{II}(bicyclo[12\text{-}12]N_4O)(ClO_4^-)]^+$ fragment, and a good experimental and theoretical isotope distribution match was found, confirming the assignment. The peak distribution at 333.1 amu, expected from the $[Cu^{II}(bicyclo[12\text{-}12]N_4O\text{-}H^+)]^+$ gave a poor match with the theoretical distribution. This is believed to be due to the reduction of some of the copper ion in the complex, resulting in the peak being a composite of the $[Cu^{I}(bicyclo[12\text{-}12]N_4O)]^+$ and $[Cu^{II}(bicyclo[12\text{-}12]N_4O\text{-}H^+)]^+$ fragments. Since mNBA is a weak reducing agent, and reduction of ions have been previously noted under similar

conditions,[55] reduction of Cu^{II} to Cu^{I} is a reasonable premise. The experimental and theoretical isotope distributions for the fragments are illustrated in Figure 3.15. Experimental isotopic distributions for fragments generated by electrospray ionisation were found to match adequately with the theoretical predictions.

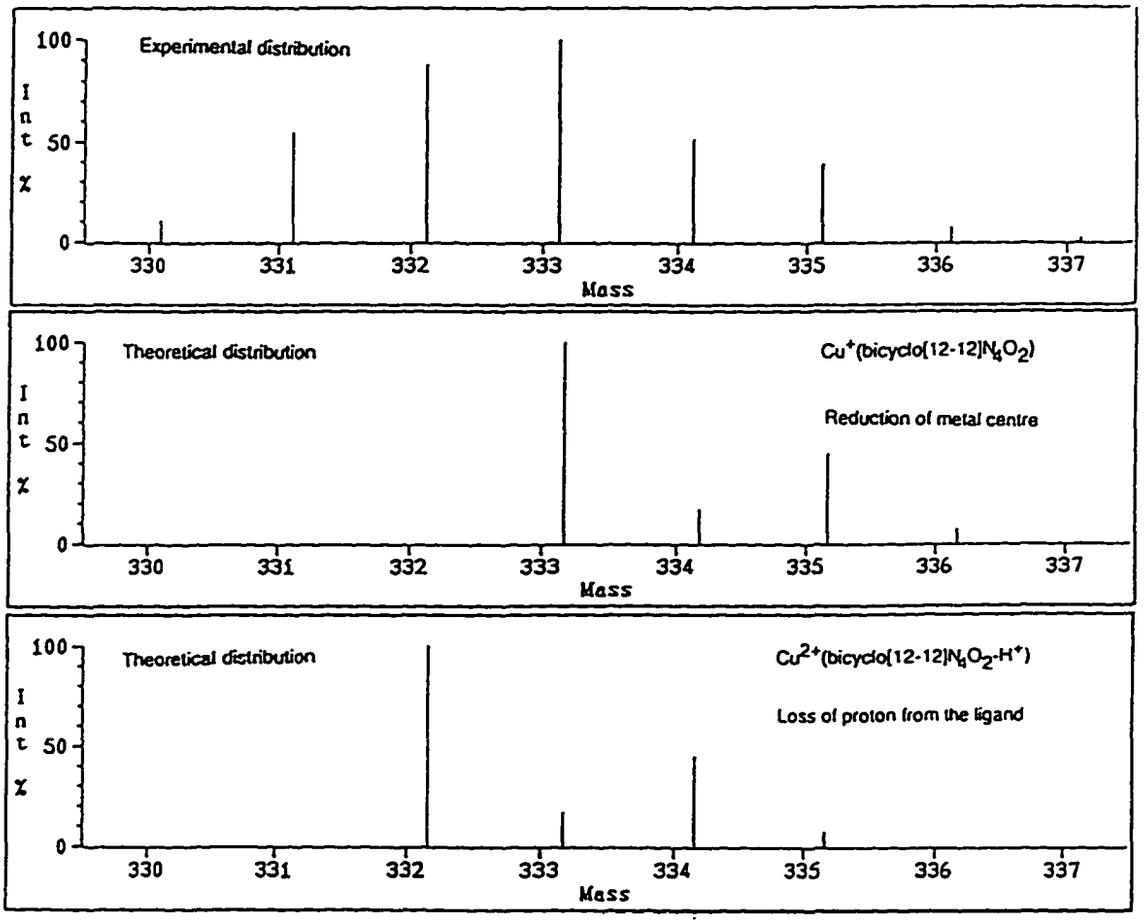

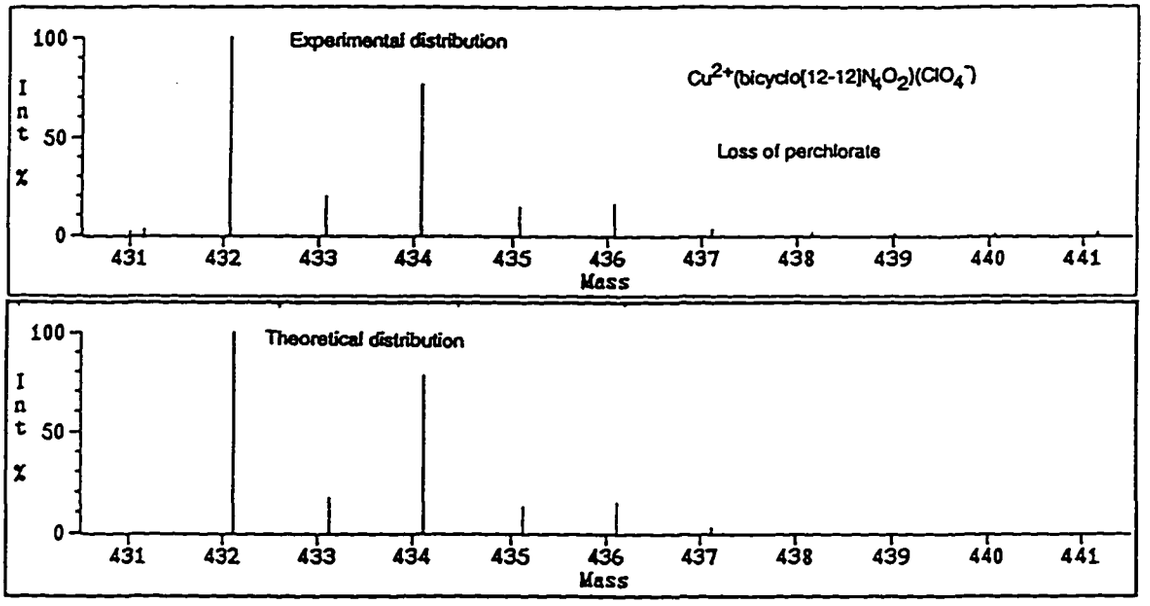

Figure 3.15: Isotopic distributions for fragments generated by FAB MS of the [Cu(bicyclo[12-12]N_4O)]$(ClO_4)_2$ complex at approximately 333 amu and 432 amu

3.4.3 Characterisation of the free bicyclo[12-12]N_4O ligand by NMR

The structure of the bicyclo[12-12]N_4O ligand was determined by ^{13}C NMR spectroscopy, and is shown in Figure 3.16. From the synthetic procedure, three possible structures with molecular weights of 270 amu are possible, namely bicyclo[12-12]N_4O, bicyclo[9-14]N_4O, and bicyclo[10-14]N_4O. . The ^{13}C NMR data for bicyclo[9-14]N_4O, bicyclo[10-14]N_4O and bicyclo[12-12]N_4O are presented in Table 3.2.

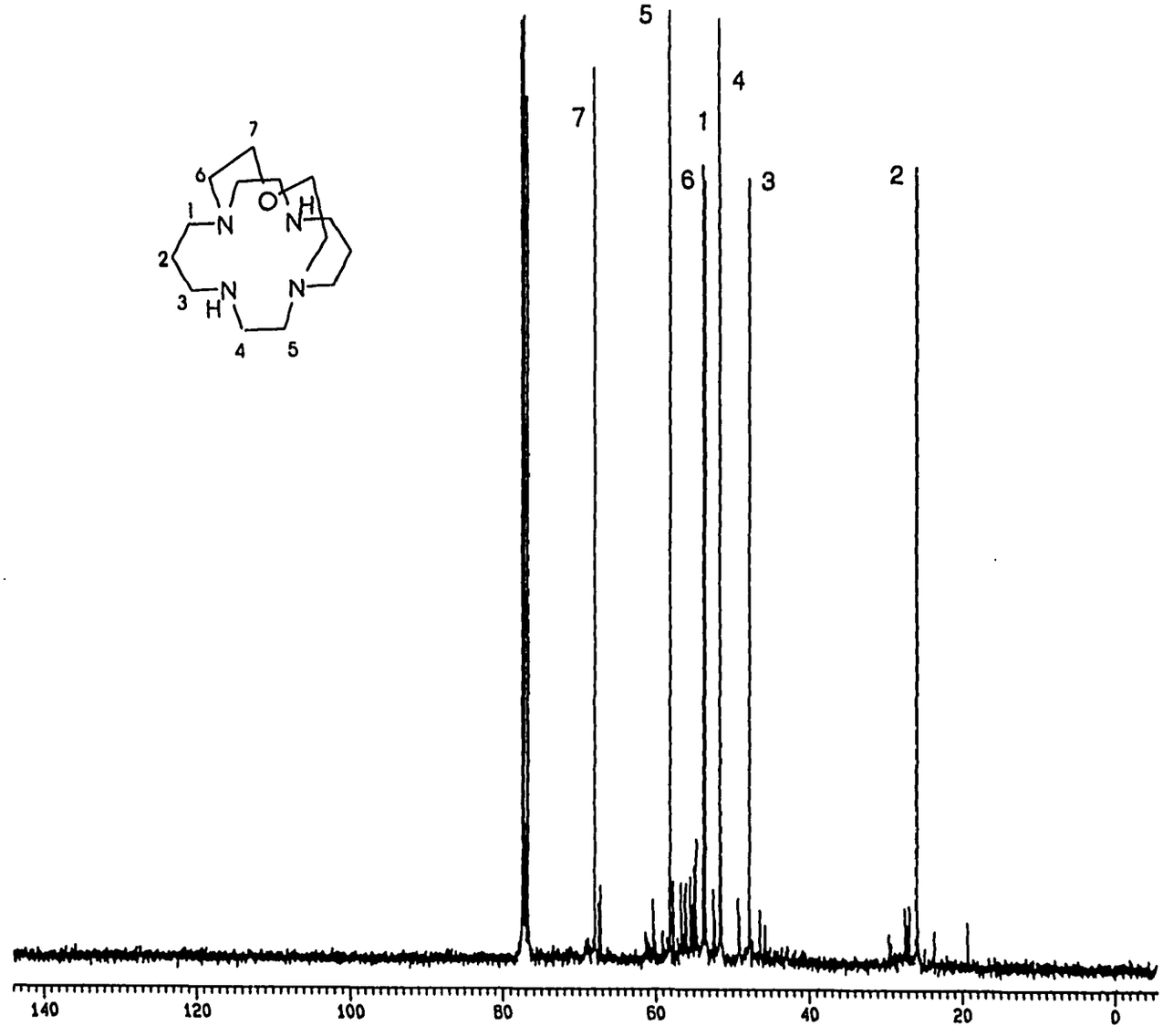

Figure 3.16: The ^{13}C NMR spectrum and structure of bicyclo[12-12]N_4O (17) in $CDCl_3$ (90.6 MHz)

Table 3.2: The ^{13}C NMR data for bicyclo[9-14]N_4O, bicyclo[10-14]N_4O and bicyclo[12-12]N_4O in $CDCl_3$ (75.5 MHz)

Bicyclo[9-14]N_4O	Bicyclo[10-14]N_4O	Bicyclo[12-12]N_4O
	^{13}C NMR/ppm	
26.8	28.2	25.5
47.8	28.4	47.9
49.2	47.4	51.0
54.6	47.9	53.3
58.5	57.0	53.6
59.0	58.1	57.6
76.6	58.5	67.5
	73.7	

Since there are only 7 resonances in the ^{13}C NMR spectrum, bicyclo[10-14]N_4O can be discounted, as 8 resonances are expected from this structure.[105] The ligand bicyclo[9-14]N_4O has been previously synthesised,[68] so can be discounted as well by comparison of the NMR spectra with known data. The major differerence in the ^{13}C NMR spectra observed for the three isomers is the shift of the resonances corresponding to the carbon atom adjacent to the ether donor. This peak is observed at 76.6, 73.7 and 67.5 ppm for bicyclo[9-14]N_4O,

bicyclo[10-14]N_4O and bicyclo[12-12]N_4O, respectively. The assignment of the peaks for bicyclo[12-12]N_4O is given in Figure 3.16.

The ^1H NMR spectrum of bicyclo[12-12]N_4O is complicated by extensive coupling. This is due to the rigidity of the ring resulting in the inequivalence of each proton of a methylene group. As a result a complex coupling pattern is seen accompanied by extensive overlap of resonances. The multiplets can be tentatively assigned to three sets of methylene resonances. The two multiplets centred at 1.4 ppm can be assigned to the methylene group at the centre of the propyl bridge, while the multiplets centred at 2.35 ppm are ascribed to methylene groups adjacent to nitrogen atoms. The set of multiplets centred at 3.23 ppm is due to the methylene groups adjacent to the oxygen atom.

3.4.4 Solution studies

3.4.4.1 Electronic spectra

The UV-Visible spectrum of $[Cu(bicyclo[12-12]N_4O)]^{2+}$ was investigated in water. Two broad bands with maxima at 537 nm (ϵ = 185 $M^{-1}cm^{-1}$) and 280 nm (ϵ = 4860 $M^{-1}cm^{-1}$) were observed. Analogous to the $[Cu([10]aneN_2O)_2](ClO_4)_2$ complex, the more intense band is assigned to a charge transfer band, while the lower energy band envelopes the d-d transitions. The effect of the 5-coordinate complexation of the ligand is clearly seen in the higher energy of this transition compared to the same band observed for $[Cu([10]aneN_2O)_2]^{2+}$. The extinction coefficient for the transition at 537 nm is relatively high compared to similar copper(II) complexes, and implies that the geometry around the copper atom is relatively

distorted, reducing the symmetry and resulting in a more favourable d-d transition. Comparison of the extinction coefficients of the 5-coordinate $[Cu(bicyclo[12\text{-}12]N_4O)]^{2+}$ with the known 5-coordinate $[Cu(bicyclo[9\text{-}14]N_4O)]^{2+}$ which has a d-d transition at 522 nm (ϵ = 102 $M^{-1}cm^{-1}$),[68] suggests that the bicyclo[12-12]N_4O isomer may be the more distorted of the two isomers.

3.4.4.2 Electron paramagnetic resonance spectroscopy

The EPR spectrum of $[Cu(bicyclo[12\text{-}12]N_4O)]^{2+}$ (Figure 3.17) was determined in the same manner as that of $[Cu([10]aneN_2O)_2](ClO_4)_2$ and gives a comparable axially elongated spectrum with $g_o = 2.099$, $g_{\parallel} = 2.173$ and $g_{\perp} = 2.062$. Coupling to ^{63}Cu (I = 3/2) gives A_o = 84 G, $A_{\parallel}$ = 186 G and $A_{\perp}$ = 33 G. These values parallel trends noted in the electronic spectra for similar compounds, with $A_{\perp}$ greater than that for $[Cu([10]aneN_2O)_2]^{2+}$ (30 G), but less than that for $[Cu(bicyclo[9\text{-}14]N_4O)]^{2+}$.[67a] The decrease in $A_{\perp}$ for $[Cu(bicyclo[12\text{-}12]N_4O)]^{2+}$ suggests that there is greater axial coordination or greater distortion of the metal atom from the donor plane in this complex. In $[Cu(bicyclo[9\text{-}14]N_4O)]^{2+}$ the copper atom is displaced from the plane circumscribed by the nitrogen donors by ~0.04 Å towards the oxygen donor, which is pulled away from the z axis by 13.4°. Since the structure of the bicyclo[12-12]N_4O ligand with the oxygen donor in the diagonal bridge tethers the oxygen donor in a specific position, the copper atom is possibly displaced from the plane of the nitrogen donors away from the oxygen in order to maintain the axially elongated geometry. The crystal structure of this complex is currently being determined, since a crystal structure analysis would be invaluable in determining the geometry of the complex, which would confirm the proposed

steric demands of the ligand.

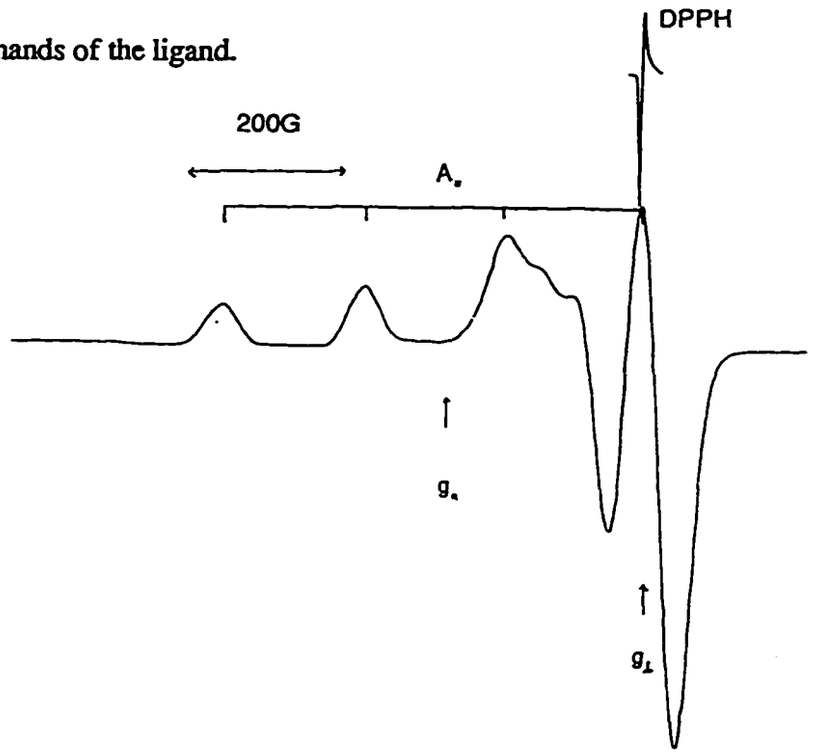

Figure 3.17: The EPR spectrum of $[Cu(bicyclo[12\text{-}12]N_4O)]^{2+}$ at 77K in DMF/CH_3CN (1:1)

3.4.4.3 Cyclic Voltammetry

Two irreversible redox waves are observed for the $[Cu(bicyclo[12\text{-}12]N_4O)](ClO_4)_2$ complex in acetonitrile. The first wave, corresponding to the Cu^{III}/Cu^{II} couple is seen at 1.25 V, approximately the same potential as the $[Cu([10]aneN_2O)_2]^{3+/2+}$ complex (Section 2.3.3.3). Similarly, the Cu^{II}/Cu^{I} couple of $[Cu(bicyclo[12\text{-}12]N_4O)]^{2+/+}$ at -1.06 V is quite close to that of $[Cu([10]aneN_2O)_2]^{2+/+}$. As observed with other copper complexes, the product of the reduction wave is adsorbed onto the electrode, and produces a spurious but reproducible reverse wave. The redox potentials for the copper cyclam complex[77] for both the Cu^{III}/Cu^{II} and Cu^{II}/Cu^{I} couples are more negative than those observed above. The $[Cu(bicyclo[9\text{-}14]N_4O)]^{2+}$ complex, with redox potentials at -1.04 V and 1.3 V for Cu^{II}/Cu^{I} and Cu^{III}/Cu^{II}

respectively, exhibits a very similar redox behavour to that of $[Cu(bicyclo[12\text{-}12]N_4O)]^{2+}$ suggesting that the change in ligand geometry does not appreciably alter the stability of the copper complexes. The effect of increasing axial coordination by oxygen in $[Cu([10]aneN_2O)_2]^{2+}$ on the redox potential appears to be similar to that seen with substitution of two secondary amine donors with tertiary amine donors, in that reduction is easier, but oxidation more difficult.

3.5 Synthesis of 7,16-dioxa-1,4,10,13-tetraazatricyclo[11.5.3.3]octadecane (tricyclo[10-14-10]N_4O_2) by fusion of [10]ane N_2O to 4,8-(dichloroacetyl)-1-oxa-4,8-diazadecane (19)

The method that produced the tricyclo[10-14-10]N_4O_2 ligand in acceptable yields involved the fusion of [10]aneN_2O to the pendant arm moiety, 4,8-(dichloroacetyl)-1-oxa-4,8-diazadecane (19). Details of the synthesis are shown in Scheme 3.1. High dilution conditions in acetonitrile were required to produce the tricyclo[10-14-10]N_4O_2 *bis*-amide (20) in approximately 60% yields. The use of DMF as a solvent, and caesium carbonate as base, resulted in the production of the self condensed moiety,[79] shown in Figure 3.18, as the major product.

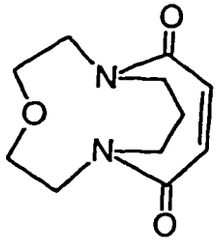

Figure 3.18: Major product of the high dilution reaction in DMF

Reduction of the amide with excess diborane in THF, with subsequent acid cleavage of the amino-boranes formed, produced the tricycle as a yellow oil in essentially quantitative yields. This method of synthesis does not preclude the synthesis of either the *syn* or *anti* isomers and a mixture of products is expected and formed.

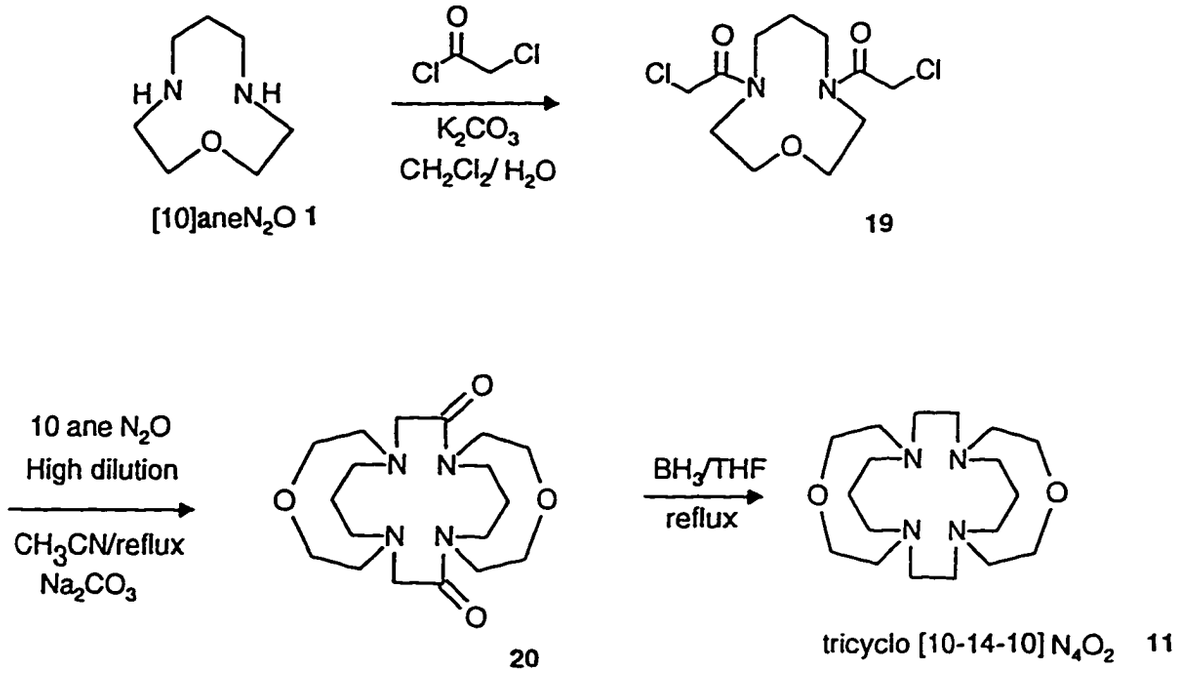

Scheme 3.1: The high dilution synthesis of tricyclo[10-14-10]N_4O_2

The increase in the yield of tricyclo[10-14-10]N_4O_2 in acetonitrile with sodium carbonate as base rather than a DMF/$CsCO_3$ slurry is indicative of a possible template effect. Indeed, when the reaction was performed under less dilute conditions, a 15% yield of tricyclo[10-14-10]N_4O_2 was obtained. Similar results have been obtained in the cyclisation of bifunctional iodides with bifunctional amines, where the greatest yields were obtained using sodium carbonate as base in acetonitrile.[106]

3.5.1 Nuclear magnetic resonance studies

The ^{13}C NMR of the pendant arm moiety **(19)** (Figure 3.19) shows the presence of three isomers. These isomers are due to restricted rotation of the amide which results in the differentiation between the two isomers with both pendant arms oriented on one or other side of the ring, and the isomer with the pendant arms oriented on either side of the macrocyclic ring.

High field ^{13}C NMR studies of the tricyclo[10-14-10]N_4O_2 ligand formed show the presence of 5 major peaks. A second minor set of 5 peaks is also seen, and are ascribed to a second isomer. The ratio of the major to minor isomer is not consistent, and varies erratically from one reduction reaction to another. The ^{13}C NMR chemical shifts, with approximate assignments of the peaks are given in Table 3.3.

Both the *syn* and *anti* isomers would be expected to give 5 peaks, due to the high degree of symmetry, as well as fluxional averaging on the NMR timescale. The minor isomer appears to be present as an impurity of the amide, although it has not been possible to purify this compound in sufficient quantities to enable complete characterisation. The mass spectra of both the amide and the tricycle show the presence of only one molecular weight product, making it likely that the two products are isomers.

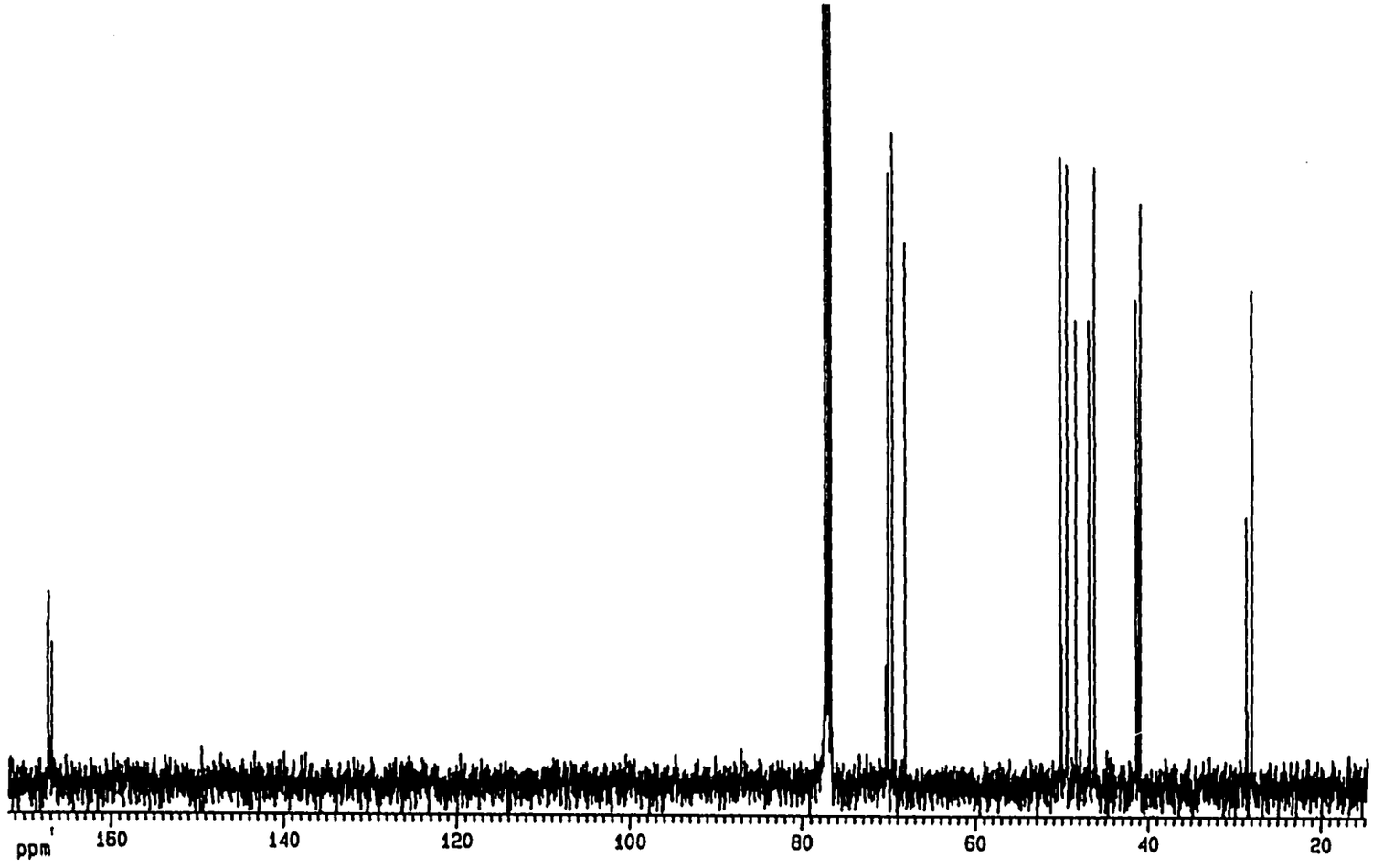

Figure 3.19: The ^{13}C NMR spectrum of 4,8-(dichloroacetyl)-1-oxa-4,8-diazadecane (**19**) in $CDCl_3$ (90.6 MHz)

Table 3.3: Chemical shifts for isomers of tricyclo[10-14-10]N_4O_2 in $CDCl_3$ (300 MHz)

Isomer	C-CH_2-C	CH_2-N	CH_2-O
		ppm	
A (major)	28.1	53.2, 53.4, 54.5	65.7
B (minor)	27.2	56.8, 57.3, 58.3	73.3

The interconversion of the two isomers after formation of the tricycle seems most unlikely, since isomerisation would require nitrogen inversion, a process that would be highly restricted by the interlinking carbon chains. Homeomorphic isomerisation, as shown in Figure 3.20, where a conformational change takes place by the passing of one chain through the ring formed by two other chains, is only believed to occur when the three chains connecting two bridgehead nitrogens each contain at least 8 members, although the energy required to overcome the barrier to interconversion is large.[107]

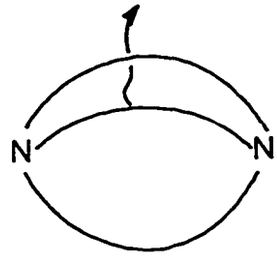

Figure 3.20: Homeomorphic isomerisation of a bicyclic ligand

The five resonances have been assigned for the major isomer, as shown in Figure 3.21, although the assignments are likely to be similar for the minor isomer. The two isomers have been tentatively assigned, based on the shielding of the carbon atom adjacent to the ether

atom. Isomer A, the major product, is assigned as the *syn* isomer since the carbon atoms adjacent to the ether oxygen would be more shielded by close presence to the oxygen atom in the second ring. This results in the ^{13}C resonance being shifted to a lower frequency in the *syn* than in the *anti* isomer, as observed in the spectra.

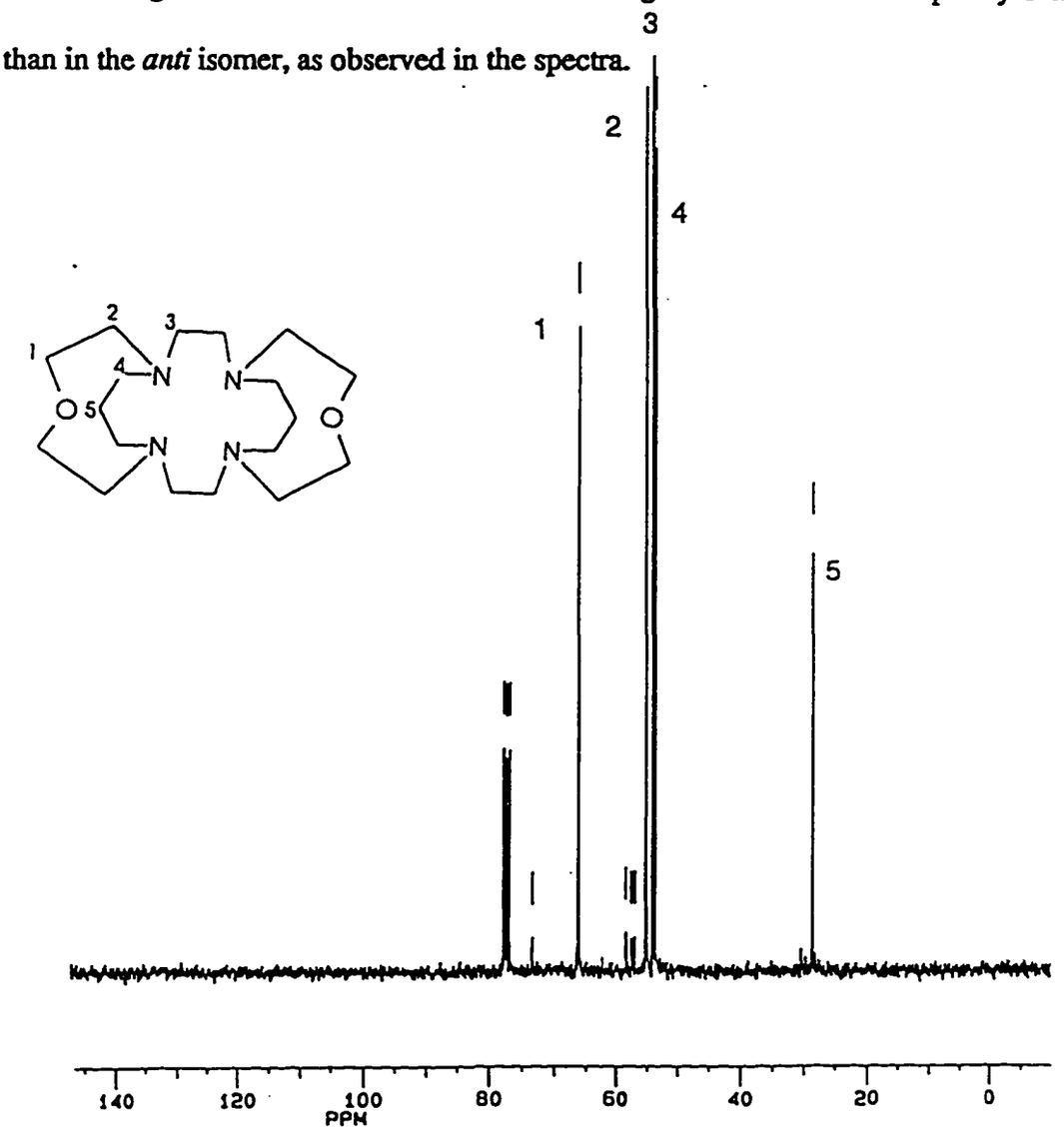

Figure 3.21: The ^{13}C NMR spectrum of the major tricyclo[10-14-10]N_4O_2 product in $CDCl_3$ (75.5 MHz)

Attempts to model the high field ^1H NMR spectra (Figure 3.22) have been unsuccessful due

to the high degree of overlap of the CH_2-N resonances. It was anticipated that by determining the proton coupling constants for the isomers, the Karplus equation could be used to determine the dihedral angles of the protons attached to the carbon chains. The dihedral angles may have assisted in the determination of the absolute configuration of the two isomers.

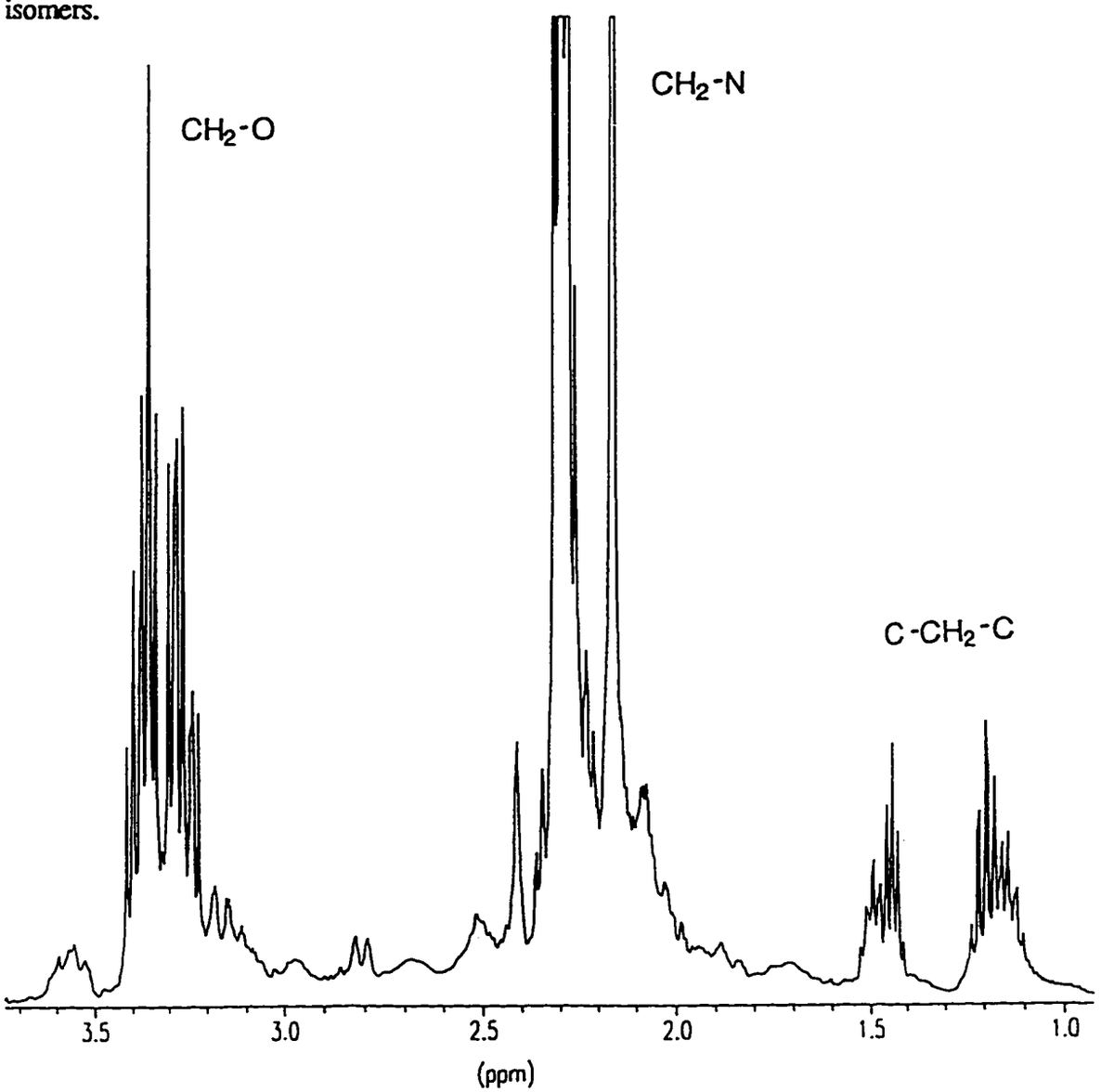

Figure 3.22: The ^{1}H NMR spectrum of the major tricylo[10-14-10]N_4O_2 isomer in $CDCl_3$ (300 MHz)

3.5.2 Protonation of the tricyclo[10-14-10]N_4O_2 ligand

The basisity of tricyclo[10-14-10]N_4O_2 results in the free amine being readily protonated in aqueous solution. The pK_a of [H tricyclo[10-14-10]N_4O_2]$^+$ is expected to be > 11, based on similar bridged molecules.[103,108] Addition of a 0.1 M perchloric acid solution to the free amine gave the diprotonated species, tricyclo[10-14-10]N_4O_2·2$HClO_4$, which crystallised readily from aqueous solution. The colourless crystals were recrystallised from hot aqueous solution, and satisfactory analytical results were obtained. The analytical data has been listed in Section 7.1.11.4. The assignment of the ^{13}C NMR resonances obtained for the tricyclo[10-14-10]N_4O_2·2$HClO_4$ salt are tabulated in Table 3.4, and ^1H NMR spectra are shown in Figure 3.23. Similar spectra were obtained for the compound in CD_3CN and D_2O, with only slight shifts in peak positions. The two peaks observed in the ^{13}C NMR spectrum at approximately 54 ppm in CD_3CN are not resolved in aqueous media.

Table 3.4: ^{13}C NMR data obtained for the tricyclo[10-14-10]N_4O_2·2$HClO_4$ salt (75.5 MHz)

Assignment	Resonance(D_2O)/ppm	Resonance(CD_3CN)/ppm
C-CH_2-C	19.0	20.0
C-C-CH_2-N	50.1	51.3
N-CH_2-C-N, O-C-CH_2-N	53.1	53.8, 54.0
O-CH_2-C-N	66.3	66.7

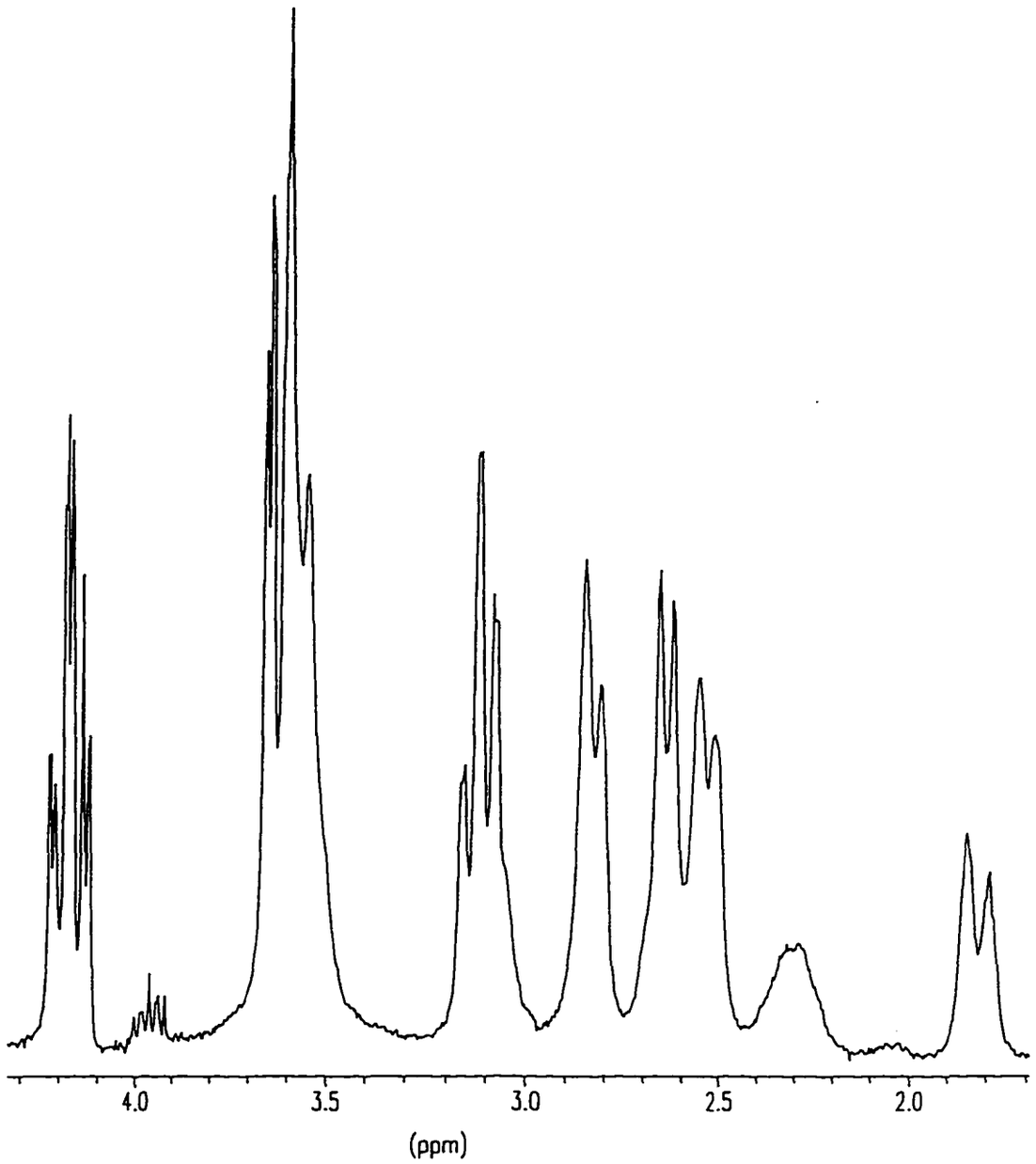

a)

Figure 3.23: ^{1}H NMR spectra of the tricyclo[10-14-10]N_4O_2.2$HClO_4$ salt in a) D_2O and b) CD_3CN (300 MHz)

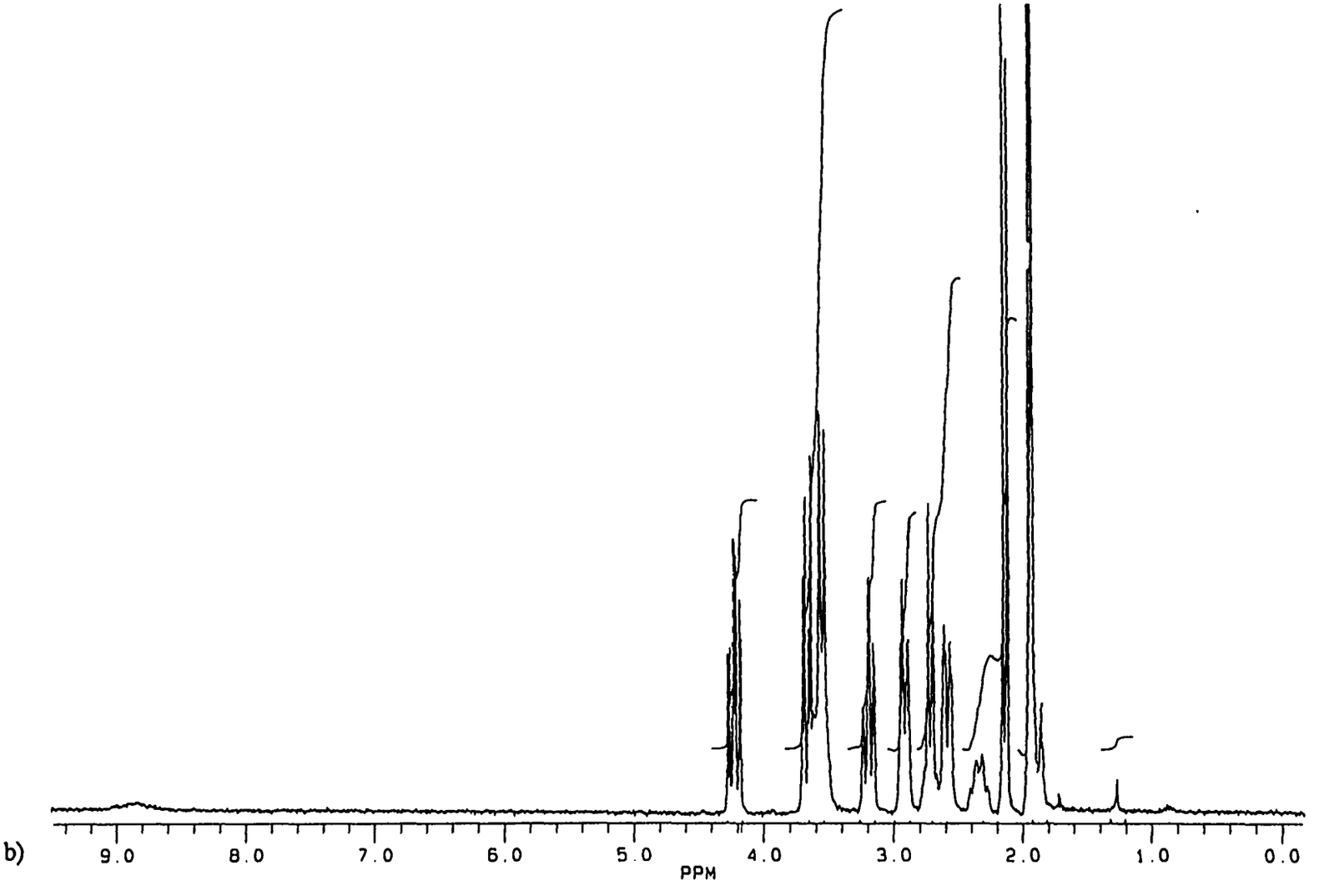

Figure 3.23: ^{1}H NMR spectra of the tricyclo[10-14-10]N_4O_2.2$HClO_4$ salt in a) D_2O and b) CD_3CN (300 MHz)

The presence of only 5 resonances in the ^{13}C spectra in CD_3CN suggests that the symmetry of the tricycle is maintained when protonated. Two possibilities which could account for this are: 1) The two protons are symmetrically hydrogen bonded between two nitrogens, as shown in Figure 3.24.

2) The protons within the cavity are undergoing rapid exchange on the NMR timescale, so that an averaged signal is observed. The broad resonance at 8.8ppm observed in the ^1H NMR spectrum of tricyclo[10-14-10]$N_4O_2 \cdot 2HClO_4$ in acetonitrile is attributed to the NH^+ proton, consistent with what has been observed for other protonated amines.[50,109] The resonance integrates approximately to 2 protons. The absence of the broad NH^+ resonance in D_2O indicates that the protons associated with the ligand exchange with the bulk D_2O solvent, an exchange which is rapid on the NMR timescale. In acetonitrile, this exchange is slower due to the small quantities of water present in solution. The addition of water to the acetonitrile solution results in the disappearance of this resonance. The protons can be removed from the cavity, but only in very basic NaOH solutions (pH ≈ 14), placing the pK_a of tricyclo[10-14-10]N_4O_2 at approximately 13. An attempt to obtain a better estimate of the pK_a of tricyclo[10-14-10]N_4O_2 by NMR methods was unsuccessful due to the poor solubility of tricyclo[10-14-10]N_4O_2 in aqueous solution.

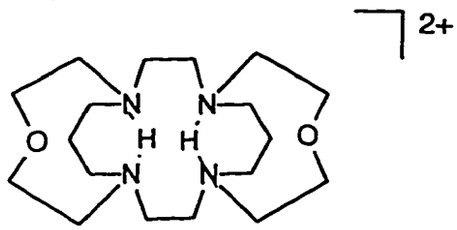

Figure 3.24: Symmetrical hydrogen bonding of two protons in the $[H_2$tricyclo[10-14-10]$N_4O_2]^{2+}$ ligand cavity

The *anti* isomer of tricyclo[10-14-10]N_4O_2 appears to be more readily protonated than the *syn* isomer. A mixture of *syn* and *anti* isomers, when stored for several weeks, was found to be only partially soluble in chloroform. A white water soluble solid was removed by filtration and gave the same ^{13}C NMR spectrum as that of tricyclo[10-14-10]$N_4O_2 \cdot 2HClO_4$ in D_2O. The chloroform extract showed resonances attributed to the *syn* isomer only. Although this technique gave a fairly pure sample of the *syn* isomer, it was uncertain as to whether the protonated species was a pure sample of the *anti* isomer, or a mixture of both isomers.

3.5.3 Synthesis of [Cu(tricyclo[10-14-10]N_4O_2)]$(ClO_4)_2$ (22)

A solution of $Cu(ClO_4)_2 \cdot 6H_2O$ in methanol was added to a methanolic solution of tricyclo[10-14-10]N_4O_2. Initially, a green precipitate formed but this disappeared on refluxing for 30 minutes. The solution was refluxed for a further 30 minutes and then filtered. The solvent was evaporated and the residue recrystallised from an acetonitrile/ether solution. An initial crop of less soluble pale blue solid recrystallised initially, followed by royal blue crystals. Further purification of the royal blue crystals was performed by column chromatography on sephadex CM-C25. Only one royal blue band was observed on the column, even when both isomers were present in the starting material. Elution of the sephadex column with L-disodium tartrate gave no separation of the band. The sephadex column may be insufficient to resolve the isomeric products of the complex, or only one isomer forms a complex. X-ray quality crystals of the copper complex, [Cu(tricyclo[10-14-10]N_4O_2)]$(ZnCl_3H_2O)_2$ (**23**) were synthesised, and structure determination is currently underway.

3.5.3.1 Characterisation of [Cu(tricyclo[10-14-10]N_4O_2)]$(ClO_4)_2$

The pale blue crystals obtained were initially identified by FAB MS as the protonated free ligand tricyclo[10-14-10]N_4O_2·2$HClO_4$, however, the UV/Vis spectrum (λ_{max} = 304 nm, 860 nm) suggests that a copper complex may be present. Unfortunately the yield of this product was too low to characterise fully this product. The royal blue copper crystals gave satisfactory FAB and ES mass spectra. Apparent reduction of the Cu^{II} ion, in a manner similar to that described for the [Cu(bicyclo[12-12]N_4O)]$(ClO_4)_2$ complex, was noted. A large peak corresponding to the protonated ligand was observed in the mass spectrum. Whether this originated from decomplexation of the macrocycle during the ionisation process or from contamination with uncomplexed ligand from the formation reaction is unclear. Elemental analysis of the royal blue crystals was satisfactory, and is included in Section 7.1.13.

3.5.3.2 Solution Studies

3.5.3.2.1 Electronic spectra

The observed wavelength of the d-d transition for the [Cu(tricyclo[10-14-10]N_4O_2)]$(ClO_4)_2$ (22) complex is fairly solvent sensitive, shifting from 600 nm (ϵ = 147 $M^{-1}cm^{-1}$) in water to 615 nm (ϵ = 162 $M^{-1}cm^{-1}$) in acetonitrile. The transition is of lower energy than any of the other compounds synthesised in this work, except for the $[Cu(N_4O_2tricycle)]^{2+}$ (Figure 3.12) synthesised during the cyclam annelation reaction, which has a d-d transition at 754 nm (ϵ = 162 $M^{-1}cm^{-1}$). The shift to lower energy is indicative of either strong axial coordination, or distortion of the copper complex by displacement of the copper atom from the plane defined

by the four nitrogen donors. The charge transfer bands observed for the two complexes were found to be 308 nm (ϵ = 3465 $M^{-1}cm^{-1}$) for the $[Cu(N_4O_2tricycle)]^{2+}$ (Figure 3.12) and 314 nm (ϵ = 4930 $M^{-1}cm^{-1}$) for $[Cu(tricyclo[10\text{-}14\text{-}10]N_4O_2)](ClO_4)_2$ (*Vide infra*). The shift in the d-d transition for the $[Cu(N_4O_2tricycle)]^{2+}$ to lower frequencies is extremely large for a copper amine complex, and suggests that the structure of this compound may be unusual. The structure proposed for this complex is consistant with a shift to lower frequency, because the structure of the ligand constrains the oxygen donors in the axial position, increasing the perturbation by axial coordination. Lengthening of the axial bonds due to Jahn - Teller distortion would be unfavourable, and may result in an axially compressed structure for the complex.

Both the *syn* and *anti* isomers of $[Cu(tricyclo[10\text{-}14\text{-}10]N_4O_2)](ClO_4)_2$ would exhibit the shifts in wavelength observed for this complex. The *syn* isomer would be expected to have a distorted trigonal prismatic geometry (Figure 3.25), with the copper atom displaced from the plane defined by the nitrogen donors, towards the oxygen donors in order to minimise electrostatic repulsion between the two oxygen donor atoms. Copper(II) complexes frequently favour five coordinate geometry, therefore a fluxional structure may result, where only one of the two arms are coordinated at any moment in time. This fluxionality would be similar to the *exo - endo* isomerism proposed for the $[Pd([10]aneN_2O)_2]^{2+}$ complex where the oxygen atoms are uncoordinated. The *anti* isomer would be expected to exhibit distorted octahedral geometry (Figure 3.26), with increased axial coordination due to the ligand structure tethering the ether donor atoms in the axial position, similar to the coordination of

the tridentate ligand [10]aneN$_2$O which coordinates in a facial manner. This structure will not be as resistant to lengthening of the axial bonds as the [Cu(N$_4$O$_2$tricycle)]$^{2+}$ since the oxygen atoms can be pulled away from the z axis by the constraints imposed by the ethylene bridges, resulting in longer Cu-O bonds.

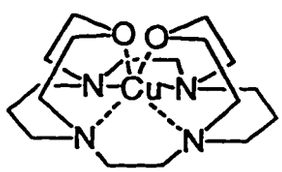

Figure 3.25: Distorted trigonal prismatic geometry of *syn*-[Cu(tricyclo[10-14-10]N$_4$O$_2$)](ClO$_4$)$_2$

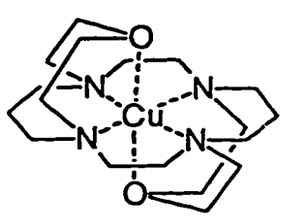

Figure 3.26: Distorted octahedral geometry of *anti*-[Cu(tricyclo[10-14-10]N$_4$O$_2$)](ClO$_4$)$_2$

3.5.3.2.2 Electron paramagnetic resonance spectra

The EPR spectrum of [Cu(tricyclo[10-14-10]N$_4$O$_2$)]$^{2+}$ (Figure 3.27) is typical of an axially elongated Cu^{II} centre with an equatorial array of nitrogen donors, and weaker axial donors. The g and A values, (g_o = 2.118, $g_{\parallel}$ = 2.209 and $g_{\perp}$ = 2.073 and A_o = 66 G, $A_{\parallel}$ = 156 G and $A_{\perp}$ = 21 G) are expected for a complex with a low energy d-d transition, as noted in the electronic spectrum.

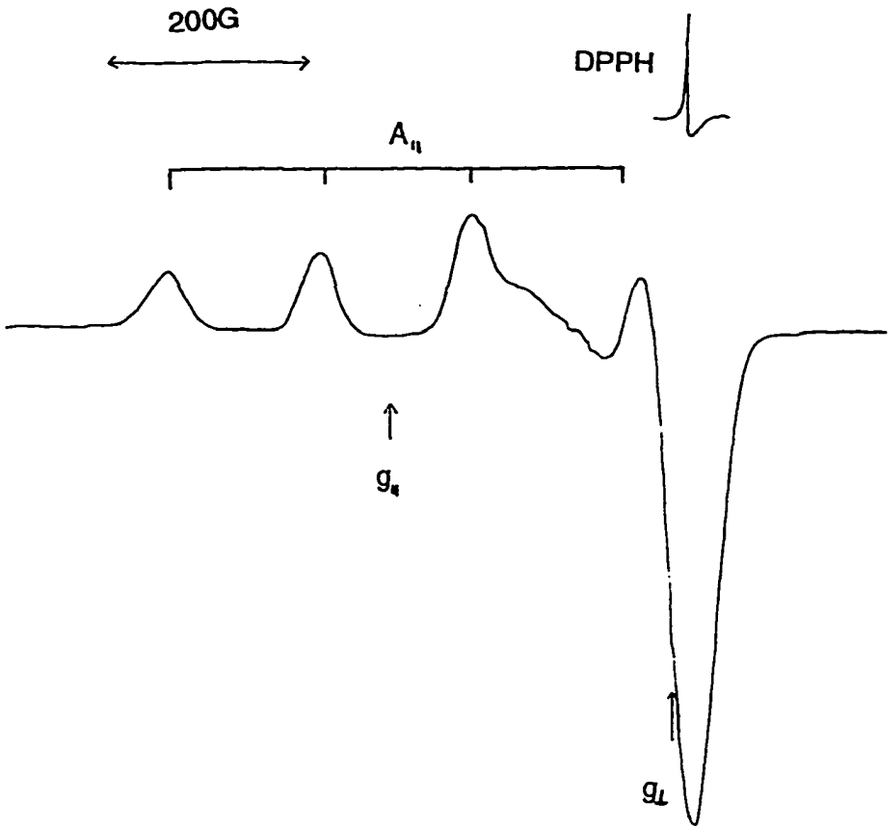

Figure 3.27: EPR spectrum of $[Cu(tricyclo[10\text{-}14\text{-}10]N_4O_2)](ClO_4)_2$ at 77 K in DMF/CH_3CN (1:1)

The EPR spectrum of the $[Cu(N_4O_2tricycle)]^{2+}$ (Figure 3.12) appears to be composed of two compounds (Figure 3.28). The values of $g_{\parallel} = 2.23$ and $A_{\parallel} = 138$ G were obtained from this spectrum. Unfortunately no room temperature spectrum could be recorded, possibly due to broadening of the signal caused by two complexes being present. The spectrum is typical of an axially elongated Cu^{II} species, which refutes the argument that the structure of the (N_4O_2tricycle) might impose axially compressed geometry.

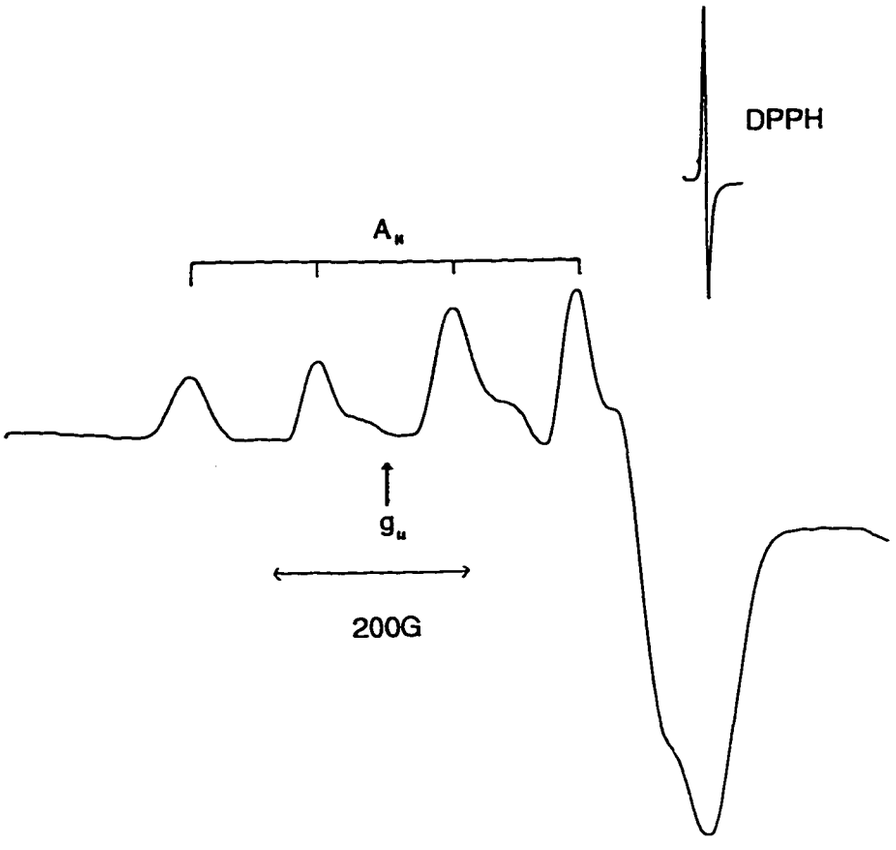

Figure 3.28: EPR spectrum of $[Cu(N_4O_2tricycle)](ClO_4)_2$ at 77 K in DMF/CH_3CN (1:1)

3.5.3.2.3 Cyclic voltammetry and chemical reduction of the tricyclic copper(II) complexes

The cyclic voltammogram of $[Cu(tricyclo[10\text{-}14\text{-}10]N_4O_2)](ClO_4)_2$ shows a quasi-reversible redox wave at -0.77 V corresponding to the Cu^{II}/Cu^{I} couple. Although the peak to peak separation varies slightly with different scan rates, the ratio of the anodic and cathodic peak currents is almost unity, indicating that the system is approaching electrochemical reversibilty. The corresponding couple for similar ligands studied in this work, where the Cu^{II} to Cu^{I} process occurs at a considerably more negative potential and is irreversible, establishes that the ease in reduction to the Cu^{I} ion is a function of the molecular topology of the macrocycle,

and not of the donor set. If the structure of $[Cu(tricyclo[10\text{-}14\text{-}10]N_4O_2)](ClO_4)_2$ is *syn*, then the increased stability of Cu^I may be due to the ability of this isomer to stabilise Cu^I in a tetrahedral manner, as illustrated in Figure 3.29. The change in geometry from an octahedral donor set to a tetrahedral one, will result in a set of equilibria in the form of a 'square scheme' (Scheme 3.2). See section 1.6.5 for a discussion of 'square schemes'. The presence of these equilibria account for the quasi-reversibility of the Cu^{II}/Cu^I redox process.

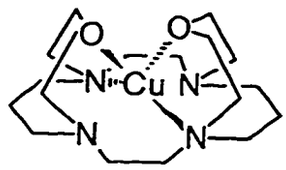

Figure 3.29: Tetrahedral geometry of $[Cu(tricyclo[10\text{-}14\text{-}10]N_4O_2)]^+$

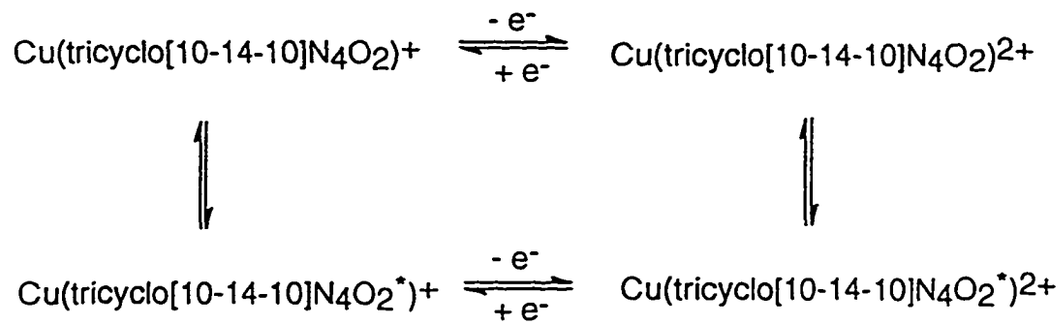

Scheme 3.2: 'Square scheme' for the $Cu[(tricyclo[10\text{-}14\text{-}10]N_4O_2]^{2+/+}$ redox process

Cyclic voltammetry studies on $[Cu(N_4O_2tricycle)]^{2+}$ (Figure 3.12) indicated that the Cu^{II}/Cu^I couple occurs at a potential of -0.44 V, and was quasi-reversible. It is possible that the quasi-

reversibility of the process is due to the molecular topology of the ligand which encapsulates the Cu^{I} ion minimising the decomposition of the complex. The redox potential for this compound is interesting as it is considerably more positive than any of the other copper complexes studied in this work.

The Cu^{III}/Cu^{II} couple for $[Cu(tricyclo[10\text{-}14\text{-}10]N_4O_2)]^{3+/2+}$ at 1.6 V is more oxidising than that of the $[Cu(N_4O_2tricycle)]^{3+/2+}$ at 1.15 V. Both redox processes are irreversible. The trends observed for macrocycles with tertiary amine donors rather than secondary amine donors where reduction is easier and oxidation more difficult, holds for $[Cu(tricyclo[10\text{-}14\text{-}10]N_4O_2)](ClO_4)_2$, but not for $[Cu(N_4O_2tricycle)](ClO_4)_2$. Further studies on the oxidation of this complex to Cu^{III} are required to elucidate why the redox potential for this species is lower than might be expected. The $[Cu(N_4O_2tricycle)]^{2+}$ ion also showed evidence of an irreversible Cu^{I}/Cu^{o} couple at -1.04 V upon reduction.

Chemical reduction of the copper tricycles with either $NaBH_4$ or Na_2S gave fairly stable water insoluble pale grey complexes. The Cu^{I} complex would be expected to be colourless. These complexes were readily oxidised back to the original Cu^{II} complexes by the addition of oxygenated water. The complexes appeared to slowly disproportionate to Cu^{o} and Cu^{II}, the Cu^{II} being rereduced when excess reducing agent was present. The black precipitate formed by this process readily dissolved in nitric acid to give the blue colour characteristic of copper. The enhanced stability of these copper complexes is unusual, as most Cu^{I} amine complexes readily disproportionate in aqueous solution. The stability of the tricyclic copper complexes

is reminiscent of tetrahedral copper(I) complexes with biphenyl nitrogen donor macrocycles.[110] These macrocycles induce a nearly tetrahedral geometry around the Cu^{I} ion, stabilising this state. Higher redox potentials were obtained in the macrocycles which could easily distort to form tetrahedral rather than planar geometry on reduction of Cu^{II}.

3.5.4 Synthesis of [Cu(tricyclo[10-14-10]N_4O_2 *bis*-amide)]$(ClO_4)_2$

Refluxing tricyclo[10-14-10]N_4O_2 *bis*-amide with $Cu(ClO_4)_2 \cdot 6H_2O$ in acetonitrile gave pale blue crystals which were recrystallised from water. The solubility of these crystals indicated that they were neither the $[Cu(H_2O)_6]^{2+}$ species, nor tricyclo[10-14-10]N_4O_2 *bis*-amide, however the FAB MS was inconclusive, giving a fragment corresponding to the protonated amide and an unidentified fragment. The electronic spectrum showed a d-d transition at 571 nm, again implicating the formation of a complex, but providing no further infomation as to the nature of the complex. Further analysis of the complex formed will be undertaken at a later date.

3.5.5 Synthesis of nickel(II) and cobalt(III) complexes of the tricyclo[10-14-10]N_4O_2 ligand

Attempts at synthesising nickel and cobalt complexes of tricyclo[10-14-10]N_4O_2 were unsuccessful.

The reaction of $Ni(ClO_4)_2 \cdot 6H_2O$ with tricyclo[10-14-10]N_4O_2 in acetonitrile produced an unidentified material, which could not be dissolved in any of the solvents tried. After 48

hours of refluxing the free ligand in methanol with $Ni(acetate)_2 \cdot 4H_2O$, and purification by column chromatography on Sephadex CM-C25, eluting with $NaClO_4$, gave a white solid identified as tricyclo[10-14-10]$N_4O_2 \cdot 2HClO_4$. Electronic spectra and FAB MS of the reaction mixtures did not appear to show the presence of any new complex.

The structure of *syn* and *anti* - $[Ni(tricyclo[10\text{-}14\text{-}10]N_4O_2)]^{2+}$ would not be expected to be highly distorted, as these conformations would be equivalent to the *trans*-I and *trans*-III structures of $[Ni(cyclam)]^{2+}$ respectively, which are relatively close in energy.[111] It is possible that the bulky arms in the ligand prevent the approach of the nickel atom. The nickel(II) ion would also be competing with the protonation of the tricycle due to the presence of water, and since nickel(II) generally coordinates slower than copper(II), complex formation may be unfavourable since the Ni^{II} cannot fully displace the protons present. Micheloni[112] has reported the formation of nickel(II) and cobalt(II) complexes with the proton sponge 12,17-dimethyl-5-oxo-1,9,12,17-tetraazabicyclo[7.5.5]nonadecane, which suggests that the transition metals should be able to replace the protons in the macrocycle.

Wainwright[113] has synthesised square planar nickel(II) complexes with the tetrasubstituted cyclam molecule shown below in Figure 3.30. No octahedral complexes of this ligand could be formed with additional ligands, either due to the bridges imposing a steric barrier to axial coordination, or due to the macrocyclic hole being incapable of expanding to fit the larger octahedral Ni^{II} species.

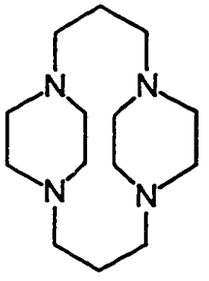

Figure 3.30: A reinforced cyclam ligand

Addition of $Co(ClO_4)_2 \cdot 6H_2O$ to a solution of the ligand in acetonitile produced a bright blue solution characteristic of a tetrahedral cobalt species. This solution was hygroscopic, reverting to the pink hexaaqua cobalt(II) species on addition of water. The blue species formed was possibly a complex of the tricycle, however the FAB MS of this species did not show the presence of any $[Co(tricyclo[10\text{-}14\text{-}10]N_4O_2)]^{2+}$, or any other related fragments. Attempts at oxidising the Co^{II} to Co^{III} with air/activated charcoal were unsuccessful. An attempt to synthesise the Co^{III} species by adding tris(carbonato)cobaltate to an aqueous solution of protonated $tricyclo[10\text{-}14\text{-}10]N_4O_2$ did not produce any product, but resulted in the recovery of the protonated tricycle.

Further studies are required to elucidate the reasons for the lack of complex formation with nickel(II) and cobalt(II).

3.6 Conclusions

The copper complexes of the macrocycles synthesised show interesting coordination behavior.

Crystal structures are required in order to further interpret the results obtained. The bicyclo[12-12]N_4O ligand shows some promise as a five coordinate ligand, with the oxygen donor held in the axial position, suitable for examining the substitution reactions in the sixth site. Although the tricyclic ligands appear to be suitable structurally as cage ligands, the difficulty in complexing to transition metals will hinder their usefulness.

CHAPTER 4

SYNTHESIS AND CHARACTERISATION OF THE COBALT(III) COMPLEX OF [10]ANE S_2N, AND THE COBALT(II/III) AND PALLADIUM(II) COMPLEXES OF [10]ANE S_2N EARMUFF

4.1 Introduction

Extensive investigation of the transition metal complexes of homoleptic tri-aza[59d,114] and tri-thia[115] macrocycles has been undertaken. The heteroleptic analogues of these macrocycles are of great interest,[59b,c,61,116] because of the differing properties imposed on the coordinated transition metal by the hard and soft donors. Nitrogen, a base of intermediate hardness, is known to stabilise a great variety of transition metals,[59d] including less common higher oxidation states.[117] Sulfur donors, which are soft, are much more suitable for stabilising the softer late transition metals, especially those in the second and third rows, which tend to be softer metals due to the increased diffuseness of the d orbitals. The empty d orbitals of sulfur can also act as π acceptors, and are therefore capable of stabilising the reduced form of several transition metals. The combination of hard and soft donors in a macrocycle consequently has the ability to stabilise both higher and lower oxidation states, facilitating electron transfer in complexes that function as one electron outer sphere reagents. There is also the possibility that mixed donor macrocycles could result in distorted geometry around the metal centre.

Recently, the coordination chemistry of *bis*-(4-aza-1,5-dithiacyclodecane) ([10]aneS_2N) with nickel(II) and palladium(II) has been investigated.[61a,96] It has been suggested[96] that the blue coloured isomer of the palladium(II) complex, shown in Figure 4.1, is capable of stabilising octahedral palladium(II) at low temperatures. Since the geometry of palladium(II) is generally square planar, the possibility of forming an octahedral palladium(II) complex is very exciting. Octahedral palladium(II) complexes could be regarded as an entatic state[118] between

square planar palladium(II) and octahedral palladium(III) states, facilitating rapid electron transfer between the two species. With this in mind, the palladium(II) complex of the related ligand, 1,2-*bis*(8-aza-1,5-dithiacyclodecanyl)ethane ([10]aneS_2N earmuff), has been synthesised and characterised. The results are presented in Section 4.4.1.

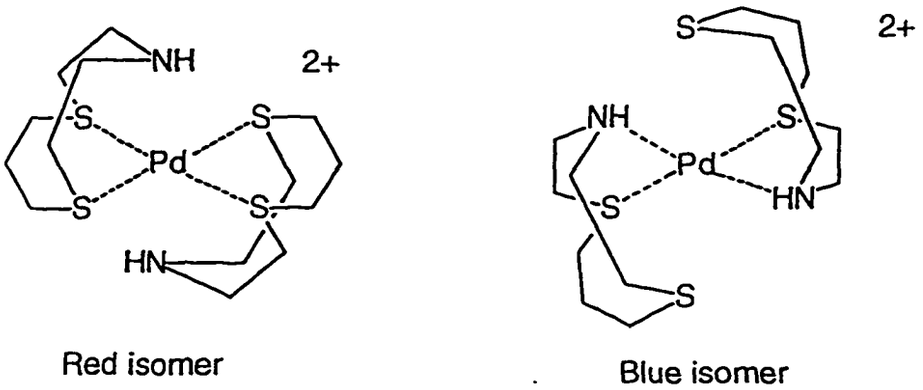

Figure 4.1: The structure of the isomers of $[Pd([10]aneS_2N)_2]^{2+}$

The cobalt(III) complexes of *bis*-[10]aneS_2N and [10]aneS_2N earmuff have also been synthesised. The cobalt(III) ion, with an ionic radius of 0.69 Å, is relatively small compared to the octahedral nickel(II) and square planar palladium(II) ions, with ionic radii of 0.83 Å and 1 Å[119] respectively. The complex formed with [9]aneN_3 has been found to have a higher ligand field than that with [10]aneN_3,[120] a function of interligand repulsion between hydrogen atoms on the two macrocycles lengthening the metal-donor bonds. Sulfur donors tend to lengthen the metal - donor bond, which should decrease interligand repulsion. Interligand repulsion in $[Co([9]aneN_3)_2]^{3+}$ and *bis*-([9]aneS_3) complexes is believed to be the cause of the minor changes in M-L bond length in the cobalt(II) and cobalt(III) complexes.[121] This is

important in electron transfer reactions, since minimal inner sphere reorganisation energy is required to alter bond lengths. The $[Co([9]aneS_3)_2]^{2+}$ is also in the low spin state,[121] therefore the barrier to electron transfer is further reduced, as the Co^{III} species is also in the low spin state and no electon spin reorientation is required. Rates of self-exchange in complexes of this form are therefore enhanced, and lead to a better understanding of the effect of inner sphere reorganisation on the rate of electron transfer. The mixed donor macrocycles were therefore synthesised with the expectation that the Co^{II} complexes formed would be in the low spin state, allowing for the determination of the self exchange electron transfer rate constants for the Co^{III}/Co^{II} couple.

4.2 Synthesis of the ligand, [10]aneS$_2$N (25)

The synthesis of [10]aneS$_2$N (Section 7.1.15) was based on a modification of the previously published procedure,[61a] and will not be discussed further.

4.3 Synthesis of $[Co([10]aneS_2N)_2](ClO_4)_3$ (26)

The complex of $[Co([10]aneS_2N)_2](ClO_4)_2$ was synthesised by addition of $Co(ClO_4)_2 \cdot 6H_2O$ in acetonitrile to a refluxing acetonitrile solution of 2.3 equivalents of the ligand. Attempts to purify the Co^{II} species at this stage by Sephadex CM-C25 column chromatography failed, as the complex oxidised readily to the corresponding Co^{III} complex in aqueous solution. Therefore, on dissolving the cobalt(II) complex obtained in hot water, the solution was aerated before passing through the column. Two orange bands were eluted from the column with 0.1M $NaClO_4$. The first band was recrystallised to give brown crystals of Isomer A

(26A), while the major band, Isomer B (26B), recrystallised to give orange crystals. Both bands gave satisfactory elemental analyses. The results are given in Chapter 7.

4.3.1 Solution studies

4.3.1.1 Characterisation of Isomers A and B by NMR spectroscopy

Due to the inequivalence of methylene protons on the [10]aneS_2N ring, as a consequence of coordination to the cobalt atom, the ^1H NMR spectra for the two isomeric complexes showed numerous unresolved multiplets. No chemical shift or coupling information could be extracted from either of the spectra. The spectra obtained are illustrated in Figures 4.2 and 4.3.

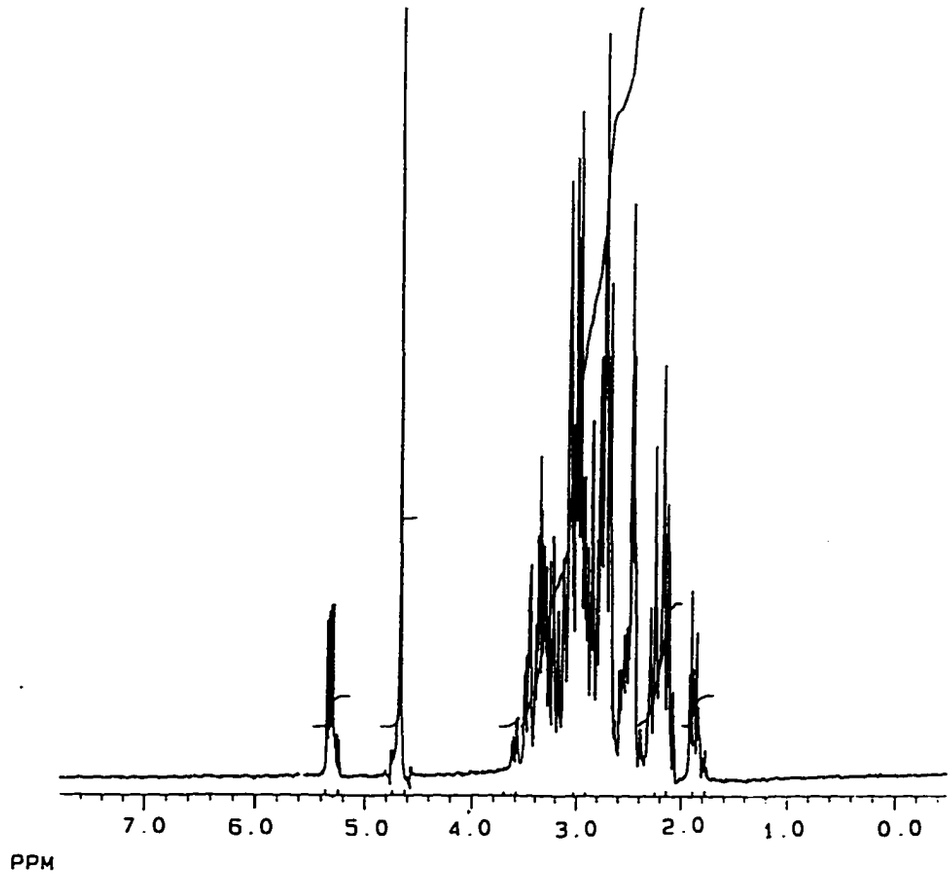

Figure 4.2: ^1H NMR spectrum of $[Co([10]aneS_2N)_2](ClO_4)_3$, Isomer A, in D_2O (300 MHz)

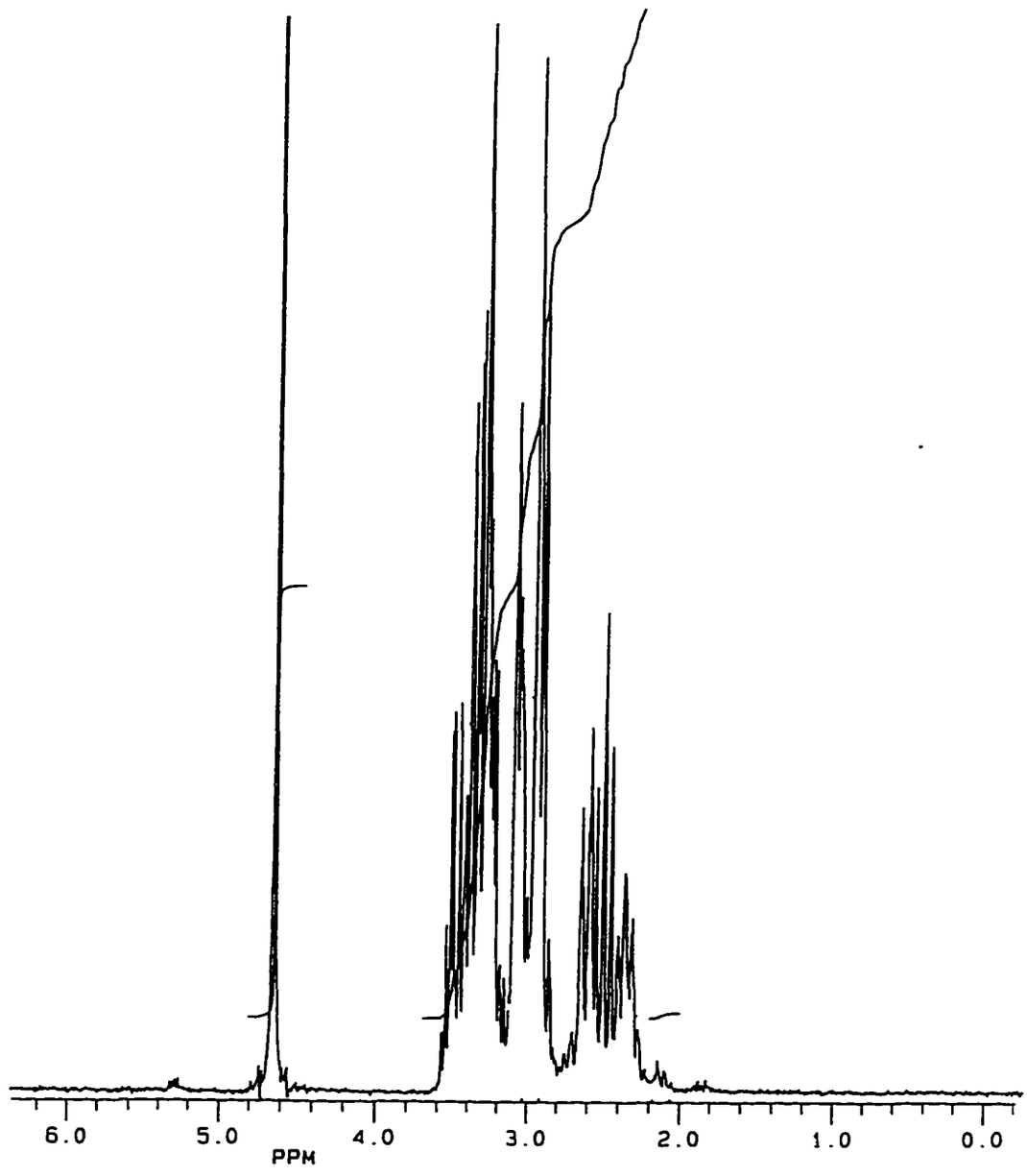

Figure 4.3: ^{1}H NMR spectrum of $[Co([10]aneS_2N)_2](ClO_4)_3$, Isomer B, in D_2O (300 MHz)

The ^{13}C spectra for the two isomers were obtained (Figures 4.4 and 4.5), and were considerably simpler than the corresponding ^{1}H spectra. From the number of resonances in each spectrum, the two isomers could be identified as the unsymmetrical isomer, Isomer A, and the symmetrical isomer, Isomer B. The proposed geometry of the two isomers is shown

in Figure 4.6.

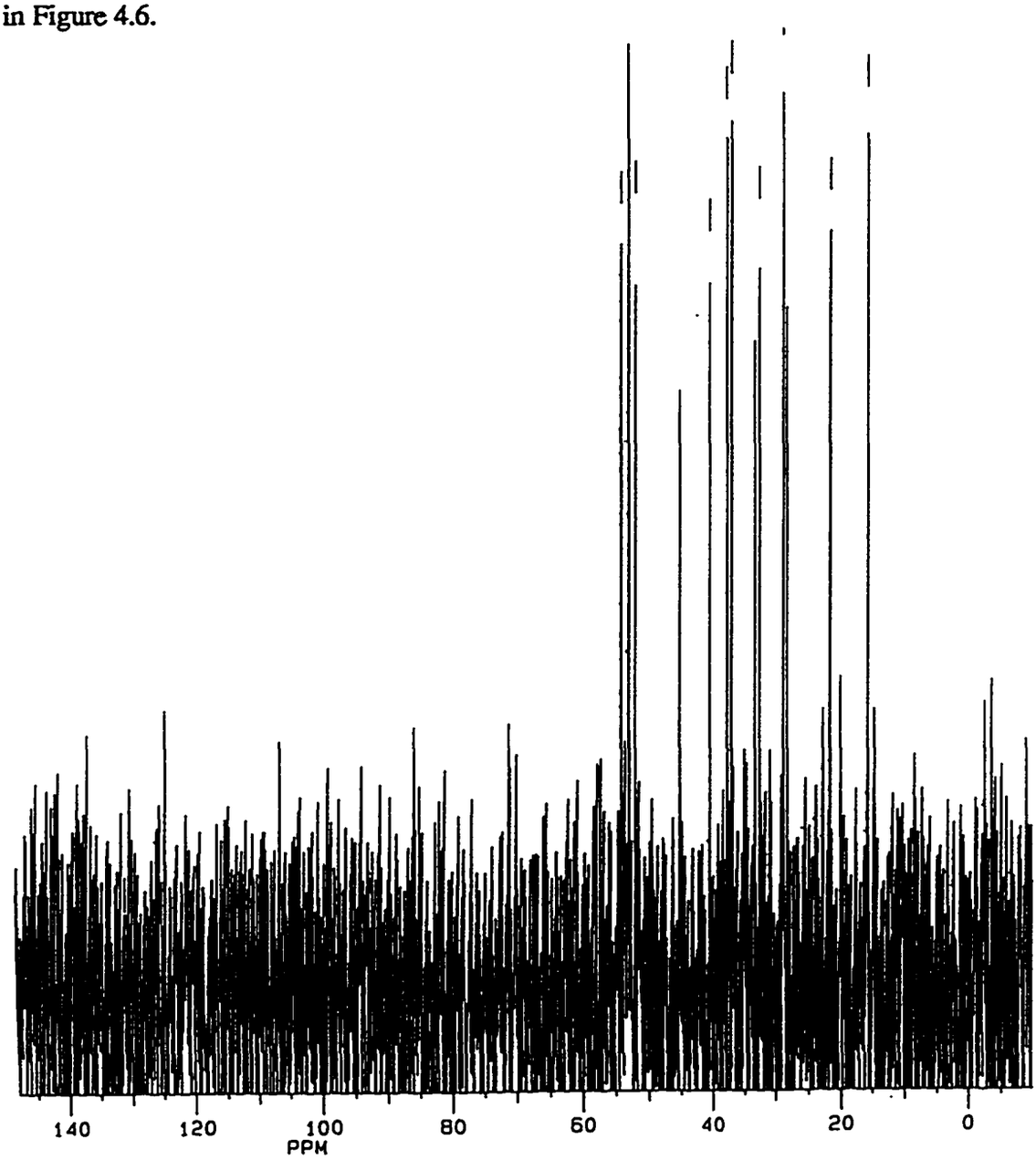

Figure 4.4: ^{13}C NMR spectrum of $[Co([10]aneS_2N)_2](ClO_4)_3$, Isomer A, in D_2O (75.5 MHz)

The ^{13}C NMR spectrum of Isomer B is relatively simple, consisting of only 7 resonances corresponding to the seven carbon atoms in the $[10]aneS_2N$ ring. Unlike the Pd^{II} isomers of

this ligand,[95] which show only 4 resonances in the ^{13}C NMR spectrum, Co^{III} is not labile, and the time averaged spectrum of the [10]aneS_2N ligand is not observed. The tentative assignment of the ^{13}C NMR resonances for Isomer B is shown in Figure 4.5. The ^{13}C NMR spectrum of Isomer A has 13 peaks. Presumably 2 of the peaks overlap, since 14 resonances would be expected for the unsymmetrical isomer of $[Co([10]aneS_2N)_2]^{3+}$. Unfortunately, without additional information, it has not been possible to positively assign any of the NMR resonances observed.

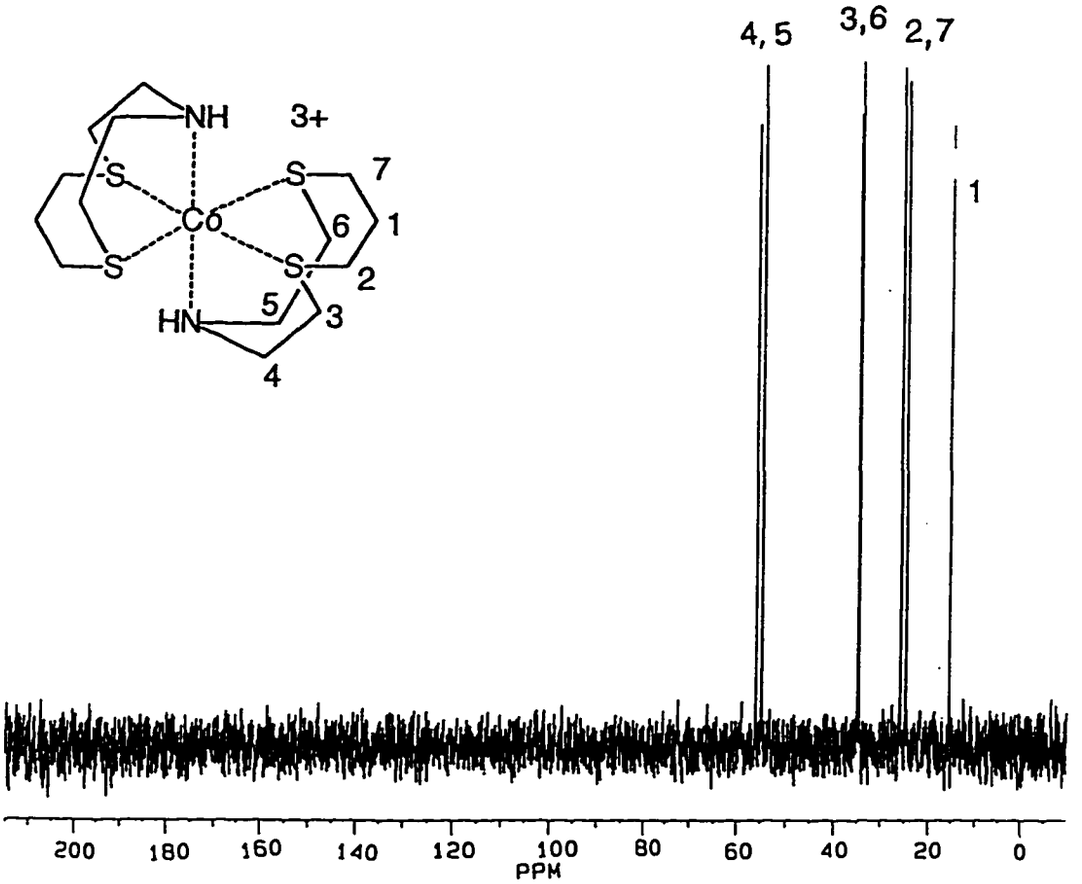

Figure 4.5: ^{13}C NMR spectrum of $[Co([10]aneS_2N)_2](ClO_4)_3$, Isomer B, in D_2O (75.5 MHz)

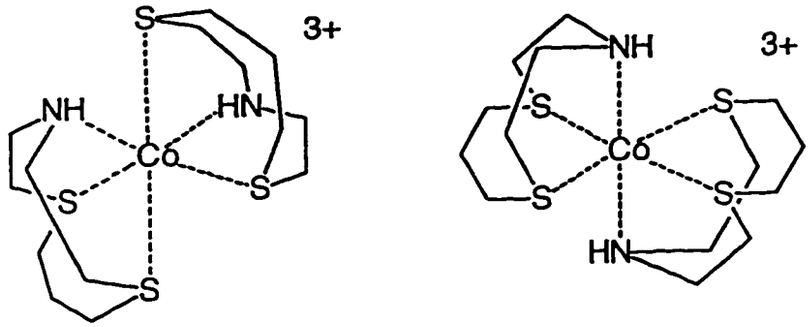

Figure 4.6: The structure of the two $[Co([10]aneS_2N)_2](ClO_4)_3$ (26) isomers obtained

In solution, Isomer A was found to isomerise readily to Isomer B, therefore attempts to purify Isomer A by repeated recrystallisation failed, and Isomer B was recovered from the solution.

4.3.1.2 Electronic spectra

Octahedral low spin d^6 transition metals undergo two spin allowed d-d transitions, which have been assigned to $^1T_{1g} \leftarrow {}^1A_{1g}$ and $^1T_{2g} \leftarrow {}^1A_{1g}$. In amine and hexaaqua complexes[122] of Co^{3+}, these transitions are sufficiently well resolved to allow for the determination of the ligand field splitting parameter, Δ, as well as the nephelauxetic parameter, B. In complexes with sulfur donors, the charge transfer bands are shifted to a lower energy,[121] and frequently obscure the $^1T_{2g} \leftarrow {}^1A_{1g}$ transition, rendering complete analysis of the spectrum impossible. Splitting of the $^1T_{1g} \leftarrow {}^1A_{1g}$ transition has been observed[122b] for complexes with less than octahedral geometry, however no splitting is observed in this case.

Table 4.1: UV/Visible Absorption data for the isomers of $[Co([10]aneS_2N)_2](ClO_4)_3$ and related complexes.

Complex	λ_{max}/nm (ϵ/$M^{-1}cm^{-1}$)
Isomer A	273(~10000), 350(~8000), 485(~200)
Isomer B	230(10900), 275(8875), 326(sh), 355(7210), 500(235)
$[Co([9]aneN_3)_2]^{3+}$ [121]	333(89), 458(100)
$[Co([9]aneS_3)_2]^{3+}$ [121]	330(22000), 476(320)
$[Co([10]aneS_3)_2]^{3+}$ [123]	295(6004), 356(13077), 374(sh), 493(398)
$[Co(daes^a)_2]^{3+}$ [124]	234(14500), 279(14000), 359(215), 485(274)

[a] daes = di(2-aminoethyl)sulfide (H_2N-CH_2-CH_2-S-CH_2-CH_2-NH_2)

The UV/Visible spectra of the two isomers in water are very similar. A comparison of the absorption bands for Isomers A and B is given in Table 4.1. The main difference observed in the spectra is a shift in the wavelength for the lower energy $^1T_{1g}$←$^1A_{1g}$ transition at around 450 to 500 nm. The λ_{max} values of the d-d transition are comparable with other Co^{III} complexes with sulfur and nitrogen donor ligands. The complex with the two nitrogen donor atoms *trans* to each other (Isomer B) would be expected to have a lower energy $^1T_{1g}$←$^1A_{1g}$ transition[122b], which is indeed observed.

The increased resolution of the spectrum for Isomer B, compared to Isomer A, is probably due to the isomerisation of Isomer A in solution. Only approximate values of ϵ were determined for this isomer due to the difficulty in determining the concentration in solution.

4.3.1.3 Electron paramagnetic resonance spectroscopy

Initial attempts to reduce $[Co([10]aneS_2N)_2]^{3+}$(Isomer B) to Co^{II} with $NaBH_4$ in H_2O appeared to produce a purple solution of Co^{I} species which rapidly decomposed to a brown solution, presumably the Co^{II} species. To prevent the formation of the Co^{I} species, very small amounts of the $NaBH_4$ were added to an excess of the $[Co([10]aneS_2N)_2]^{3+}$ in water, forming a brown solution.

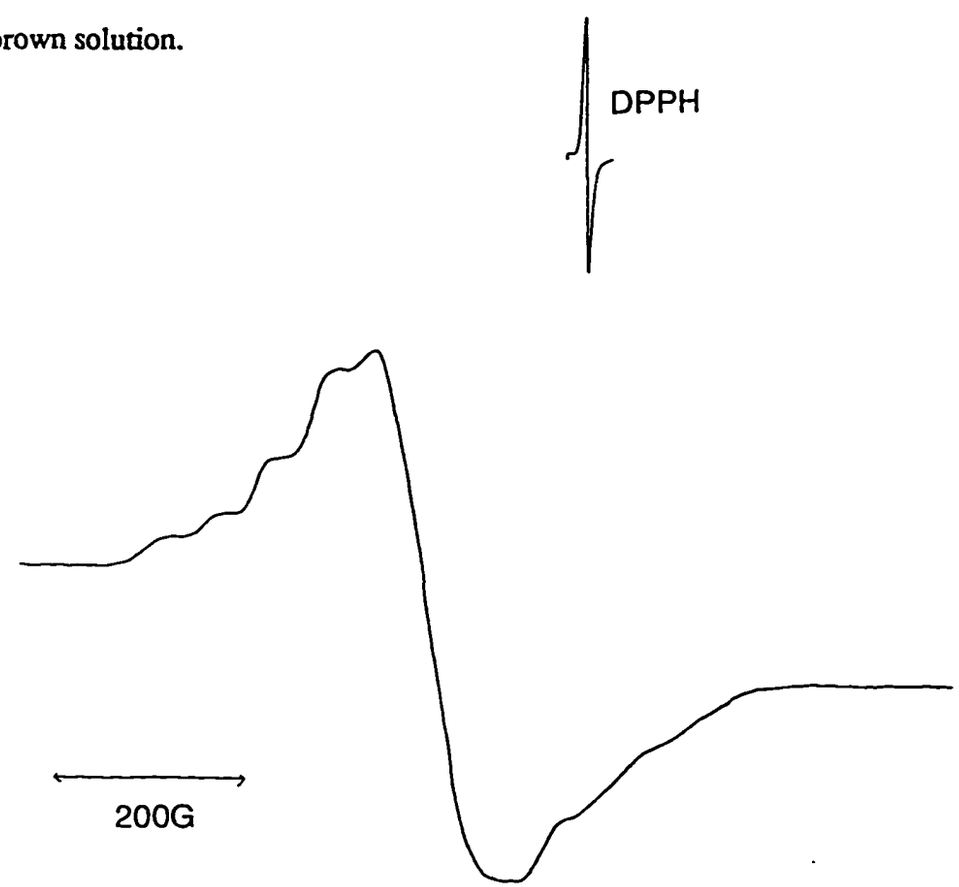

Figure 4.7: EPR spectrum of $[Co([10]aneS_2N)_2]^{3+}$ in water at 77 K

The EPR spectrum at 77 K observed for this solution gave an apparently isotropic g_o value of 2.107 (Figure 4.7). Coupling to ^{59}Co (I = 7/2) can be observed, but is not well resolved.

4.3.1.4 Cyclic voltammetry

Electrochemical data obtained for the symmetrical isomer, Isomer B, of $[Co([10]aneS_2N)_2](ClO_4)_3$, along with other related complexes of Co^{III} are presented in Table 4.2.

Table 4.2: Redox potential of aza- and thia- macrocyclic complexes of Co^{III}

Complex	Couple	$E_{½}$(vs NHE)/V		Ref
$[Co([10]aneS_2N)_2]$ Isomer B [a]	3+/2+	0.27	(quasi-reversible)	PW
	2+/1+	-0.90	(quasi-reversible)	PW
$[Co([10]aneS_3)_2]$ [b]	3+/2+	0.41	(quasi- revesible)	123
	2+/1+	-0.45	(reversible)	123
$[Co([9]aneN_3)_2]$ [b]	3+/2+	-0.41	(quasi-reversible)	121
$[Co([9]aneS_3)_2]$ [b]	3+/2+	0.42	(quasi-reversible)	121
	2+/1+	-0.48	(quasi-reversible)	121

[a] in acetonitrile, Ag^+/Ag reference electrode

[b] in water, AgCl/Ag reference electrode

The two quasi-reversible redox waves observed in the cyclic voltammogram of $[Co([10]aneS_2N)_2](ClO_4)_3$ were identified as the $Co^{III/II}$ couple at 0.27 V and the $Co^{II/I}$ couple at -0.90 V. Both observed couples are more negative than the respective couples for the tri-thia macrocycles, indicating a decrease in the ease of reduction for the mixed donor macrocycle. On the other hand, the potential of the $Co^{III/II}$ couple for $[9]aneN_3$ is considerably more negative, demonstrating the capacity of the softer sulfur ligands to stabilise low oxidation states, while the triaza macrocycle stabilises the apparently harder Co^{III} ion. The potential of the $Co^{III/II}$ couple for the $[Co([10]aneS_2N)_2]$ complex, is slightly less than that for the tri-thia macrocycles, however the potential for the $Co^{II/I}$ couple is considerably lower. This potential difference is significant in that it illustrates that the effect of a minor change in donor ability does not significantly effect the stability of Co^{II}, but considerably reduces the stability of Co^{I}, which may require the π acceptor capability of the sulfur donors to stabilise the Co^{I} state.

4.4 Synthesis of $[10]aneS_2N$ earmuff (27)

The synthesis of $[10]aneS_2N$ earmuff[61a] via the literature method, gave less than satisfactory yields of the product. The reaction conditions were therefore altered to improve yields. A solution of $[10]aneS_2N$, 1,2-ethanediol ditosylate, and Na_2CO_3 were refluxed in acetonitrile for 60 hours, before partial purification by washing with aqueous media. Rigorous purification was achieved by formation of the Ni^{II} complex. The crude yield of $[10]aneS_2N$ earmuff, based on integration of the product peaks in the NMR spectrum, was approximately 70%, however the yield of $[Ni([10]aneS_2N\ earmuff)](ClO_4)_2$ (28) was only 30%. The overall yield, from

[10]aneS_2N, was therefore 29%. This compares with the published yield of 24% overall.[61a]

4.4.1 Synthesis of [Pd([10]aneS_2N earmuff)]$(PF_6)_2$ (29)

The palladium complex of [10]aneS_2N was accomplished by adding Pd(acetate)$_2$ to a refluxing acetonitrile solution of the ligand. The addition of ammonium hexafluorophosphate and diffusion of ether into the solution gave red crystals. These were further recrystallised from acetonitrile/ether, and analysed as [Pd([10]aneS_2N earmuff)](acetate)$(PF_6)(½CH_3CN)$ (30). The crystals were characterised by ^{13}C NMR as the unsymmetrical isomer of [Pd([10]aneS_2N earmuff)]$^{2+}$. Further addition of ammonium hexafluorophosphate, and repeated recrystallisation, by diffusion of ether into an acetonitrile solution at low temperatures, gave red crystals characterised as the symmetrical isomer. Addition of ether directly to the acetonitrile solution gave a yellow precipitate that gradually turned into a red oil. It is likely therefore, that the yellow solid initially formed is the kinetic product which isomerises into the red thermodynamic product. The red crystals analysed as [Pd([10]aneS_2N earmuff)]$(PF_6)_2$ (29) (See Chapter 7).

4.4.2 Solution studies of [Pd([10]aneS_2N earmuff)](acetate)$(PF_6)(½CH_3CN)$ (30)

4.4.2.1 Nuclear magnetic resonance spectroscopy

The room temperature ^1H and ^{13}C NMR spectra of [Pd([10]aneS_2N earmuff)](acetate)(PF_6) are shown in Figures 4.8 and 4.9. Several of the peaks in the spectrum were broadened, and since recrystallisation did not alter this, the broadening was assumed to be the result of a fluxional process. In order to investigate this process, variable temperature NMR spectra

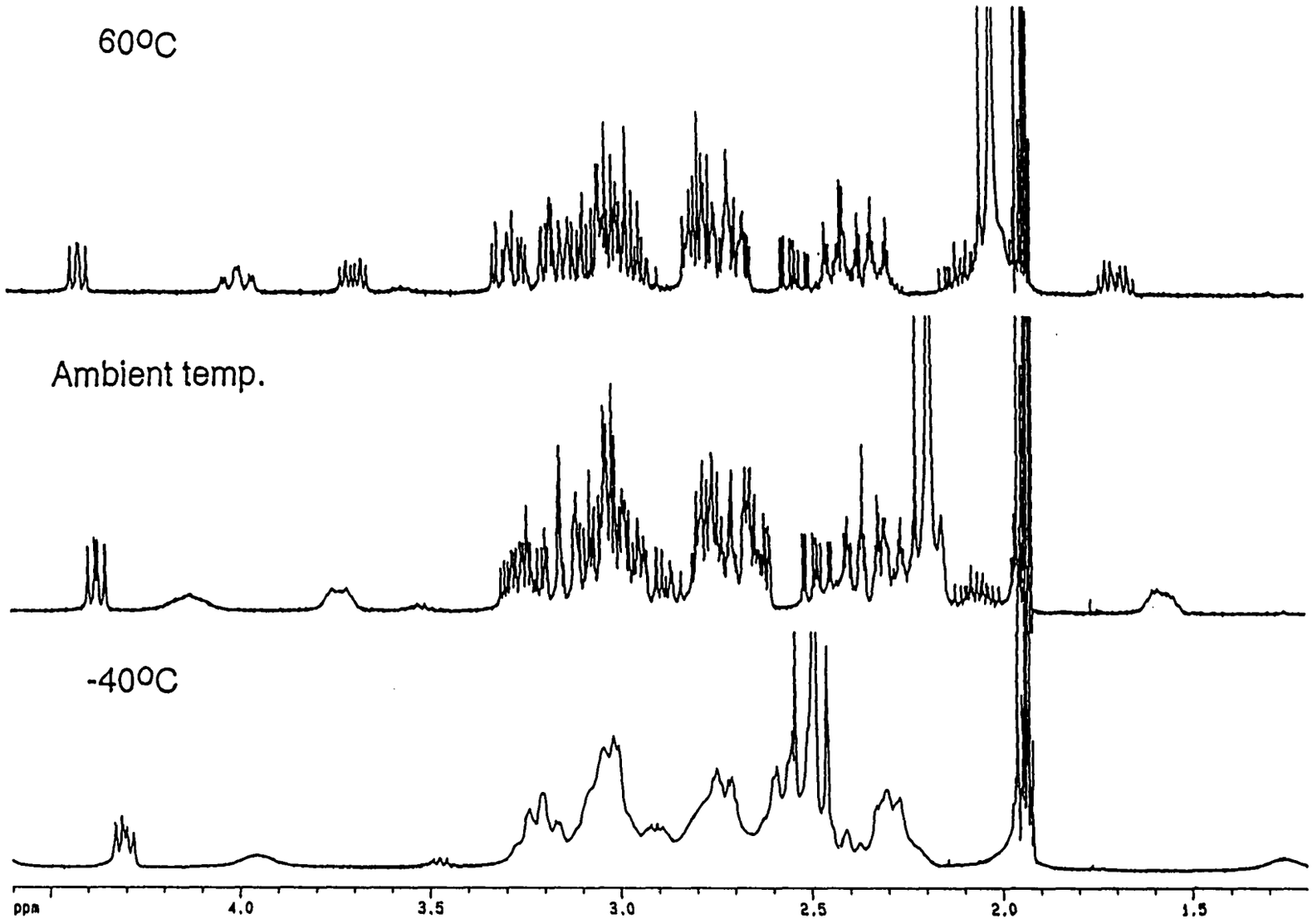

Figure 4.8: Variable temperature ^1H NMR spectra of [Pd([10]aneS_2N earmuff)](acetate)(PF_6) in CD_3CN (360 MHz)

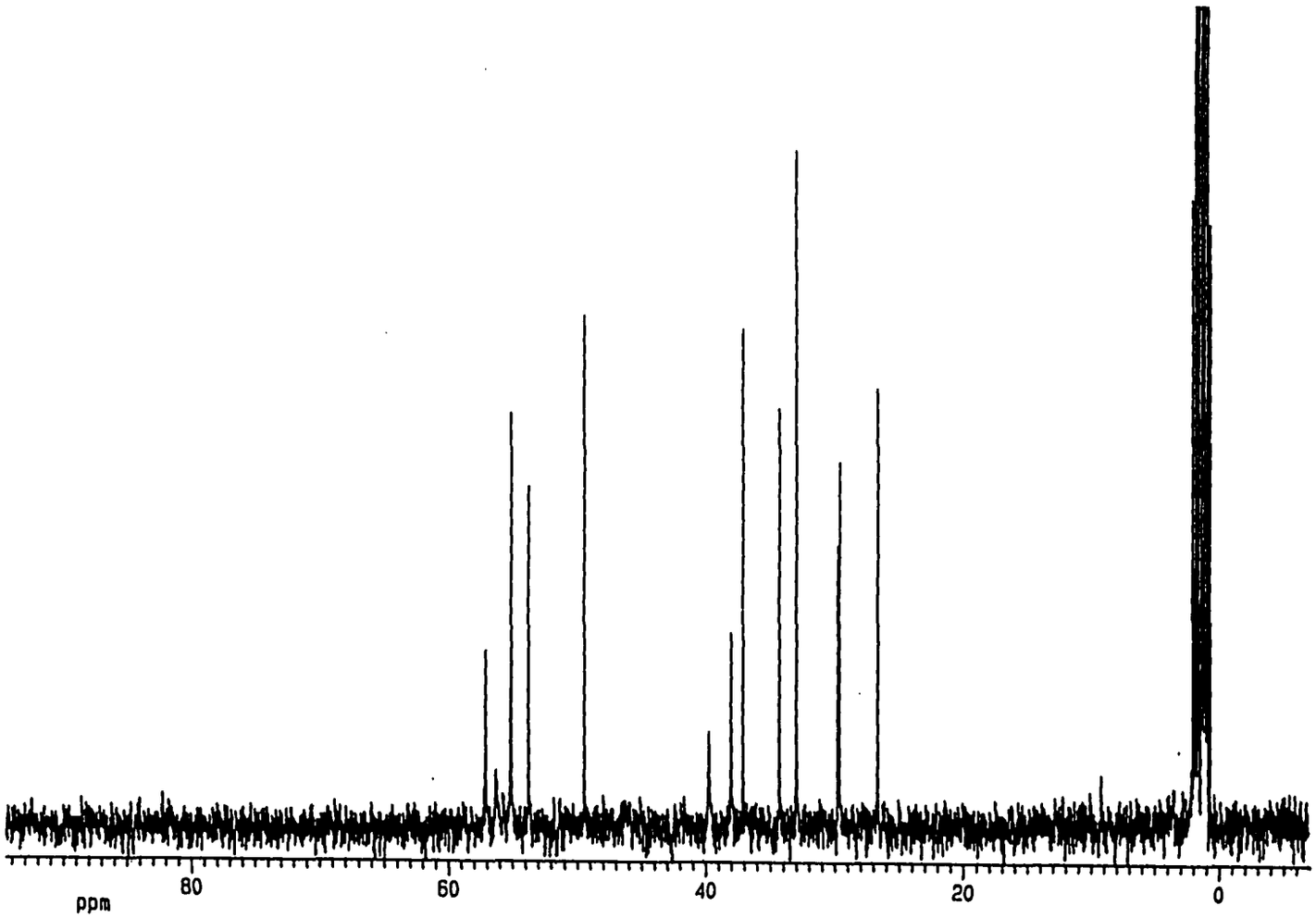

Figure 4.9a: Ambient temperature ^{13}C NMR spectra of [Pd([10]aneS_2N earmuff)](acetate) (PF_6) in CD_3CN (90.6 MHz)

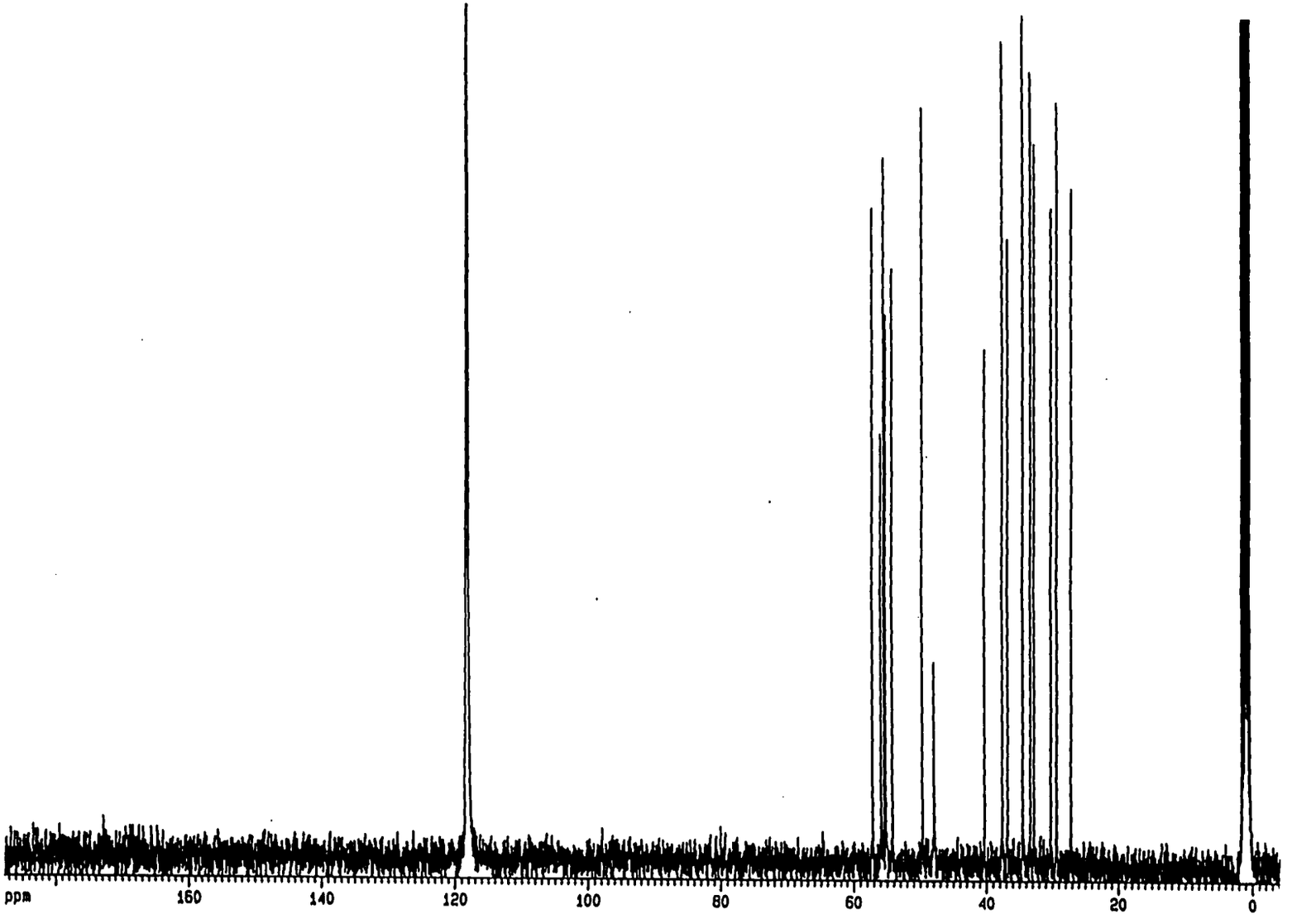

Figure 4.9b: Variable temperature (+60°C) ^{13}C NMR spectra of [Pd([10]aneS_2N earmuff)](acetate) (PF_6) in CD_3CN (90.6 MHz)

were obtained, which are shown in Figures 4.8 and 4.9. Unfortunately, due to the solubility of the complex, the lowest temperature obtainable was -40°C. At this temperature, the low temperature limit of the fluxional process was not achieved. However, at +60°C, all peaks were sharp and well resolved, indicating that the high temperature limit has been reached.

The ^{13}C NMR spectrum at 60°C shows 16 resonances, indicating that the earmuff is unsymmetrical. To form a complex with the two nitrogen atoms and two sulfur atoms coordinated in a planar fashion, the two bridged nitrogen atoms are required to be in a *cis* conformation, which would result in the destruction of the symmetry of the [10]aneS_2N earmuff once coordinated. The geometry of this conformation is shown in Figure 4.10.

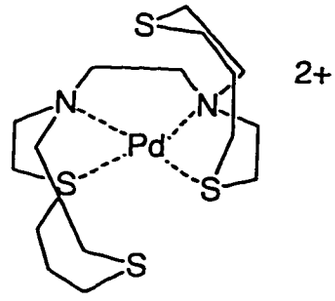

Figure 4.10: The unsymmetrical coordination geometry of [Pd([10]aneS_2N earmuff)]$^{2+}$ (30)

One thing to be noted from the low temperature NMR spectrum is that although the ligand resonances are appreciably broadened, the solvent peaks are still sharp, indicating that a diamagnetic - paramagnetic equilibrium is unlikely to be involved. If the fluxional process

occurring was a diamagnetic - paramagnetic equilibrium, as has been suggested for the blue isomer of $[Pd([10]aneS_2N)_2]^{2+}$, then it would be expected to exhibit some paramagnetic broadening of the solvent peaks as well as the ligand peaks. The two isomers obtained for $[Pd([10]aneS_2N)_2](PF_6)_2$ [96] are shown in Figure 4.1 .

In order to investigate whether any diamagnetic Pd^{II} - paramagnetic Pd^{II} equilibrium was in effect, the magnetic susceptibility of the complex was determined by the Evan's method[125] at various temperatures. Although the determination of mass susceptibility using this method is fraught with difficulty, it was expected that sufficiently large changes in the magnetic moment would occur if any paramagnetic palladium(II) was present. Although a very slight shift in the NMR resonance was noted at room temperature, this was probably caused by the change in density of the solution with the palladium(II) complex present. The shift with temperature of this resonance was also very slight, and paralleled the shifts expected for changes in solvent density with temperature. Since a square planar - octahedral equilibrium for palladium(II) would involve the d^8 metal altering from no unpaired electrons to two unpaired electrons, it is highly unlikely that a square planar - octahedral equilibrium exists.

4.4.3 Solution studies of the symmetrical isomer $[Pd[10]aneS_2N$ earmuff$)]^{2+}$ ion (29)

4.4.3.1 Nuclear magnetic resonance spectroscopy

Repeated recrystallisation, as described above, gave a second isomer of $[Pd([10]aneS_2N$ earmuff$)]^{2+}$. The ^1H NMR spectrum of this isomer is given in Figure 4.11.

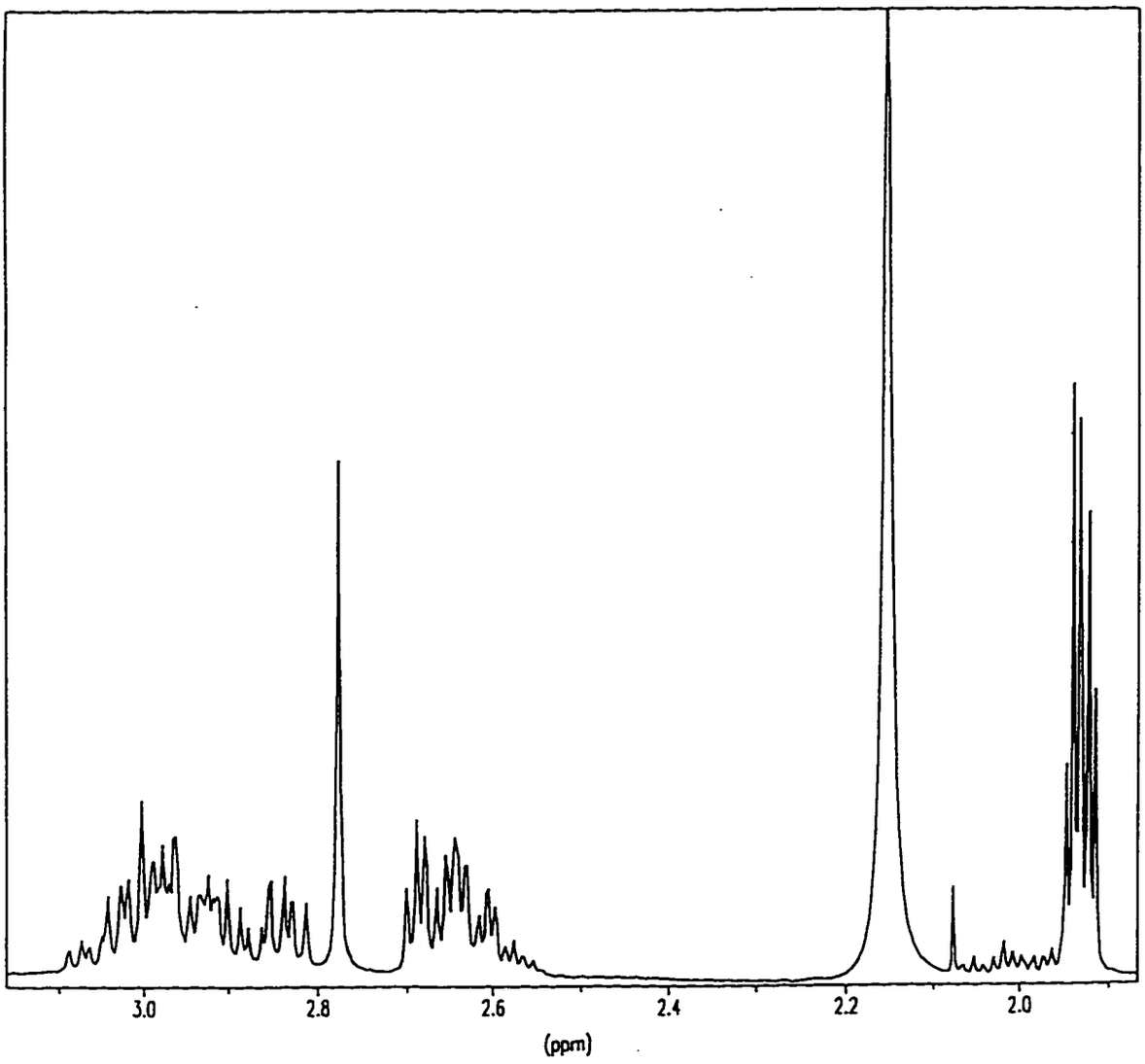

Figure 4.11: ^{1}H NMR spectrum of [Pd([10]aneS_2N earmuff)]$(PF_6)_2$ in CD_3CN (300 MHz)

Like the isomers of [Co([10]aneS_2N)$_2$]$(ClO_4)_3$ the ^{1}H NMR spectrum (Figure 4.11) exhibits several multiplets in the 1.8 to 3.2 ppm region that could not be assigned. The five intense peaks at approximately 1.9 ppm are due to the solvent. The smaller multiplet at ~2 ppm is assigned to the protons of the central methylene group of the propyl bridge. The large singlet

at ~2.15 ppm appears to be an impurity of unknown origin. The ^{1}H COSY spectrum (Figure 4.12) was recorded; however, this did not help to resolve the coupling.

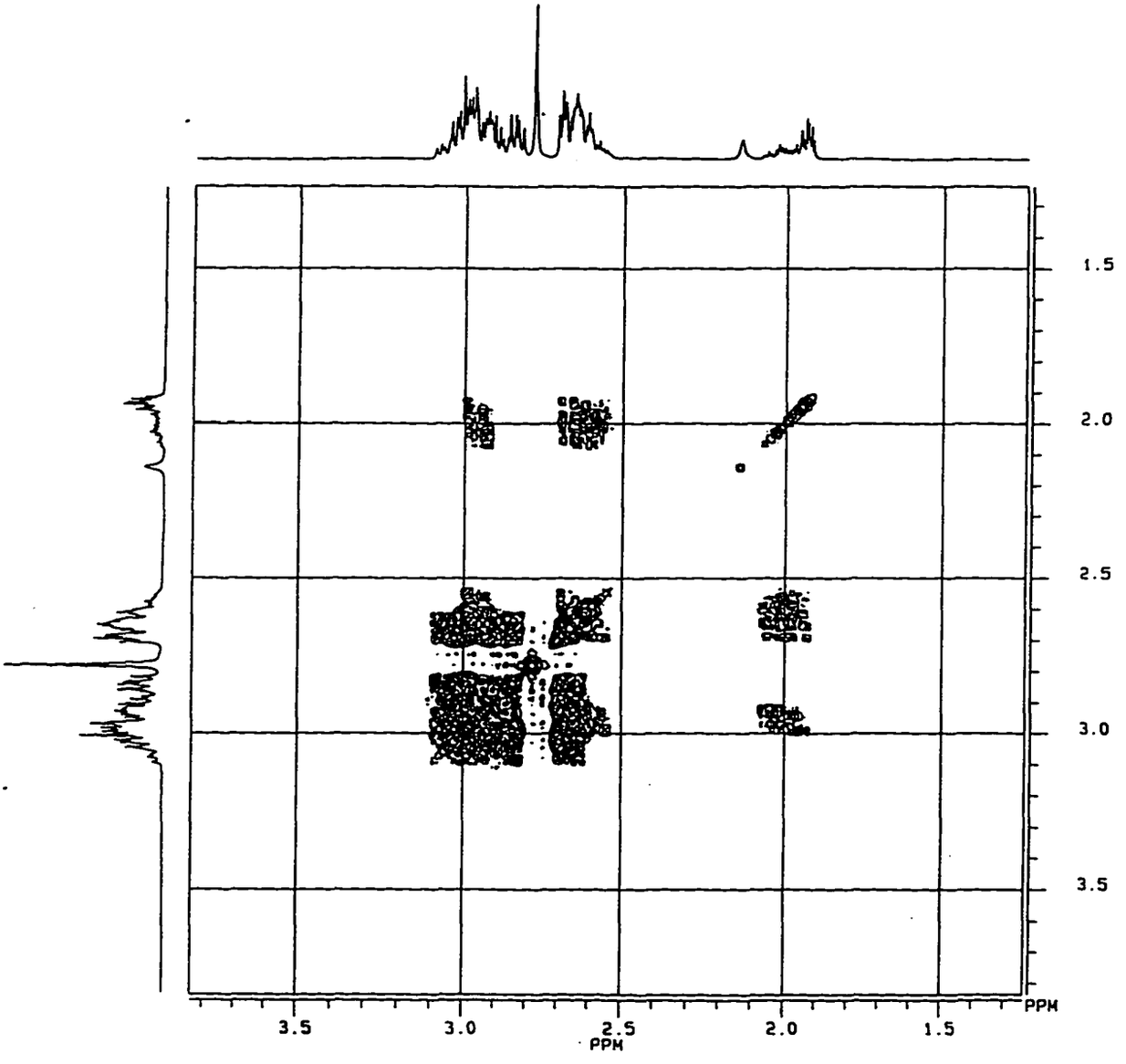

Figure 4.12: ^{1}H COSY spectrum of [Pd([10]aneS_2N earmuff)]$(PF_6)_2$ in CD_3CN (300 MHz)

The ^{13}C spectrum is considerably simpler with 5 resonances, signifying that the structure of the complex has C_{2v} symmetry on the ^{13}C NMR timescale. A tentative assignment of the resonances has been made and is given in Figure 4.13.

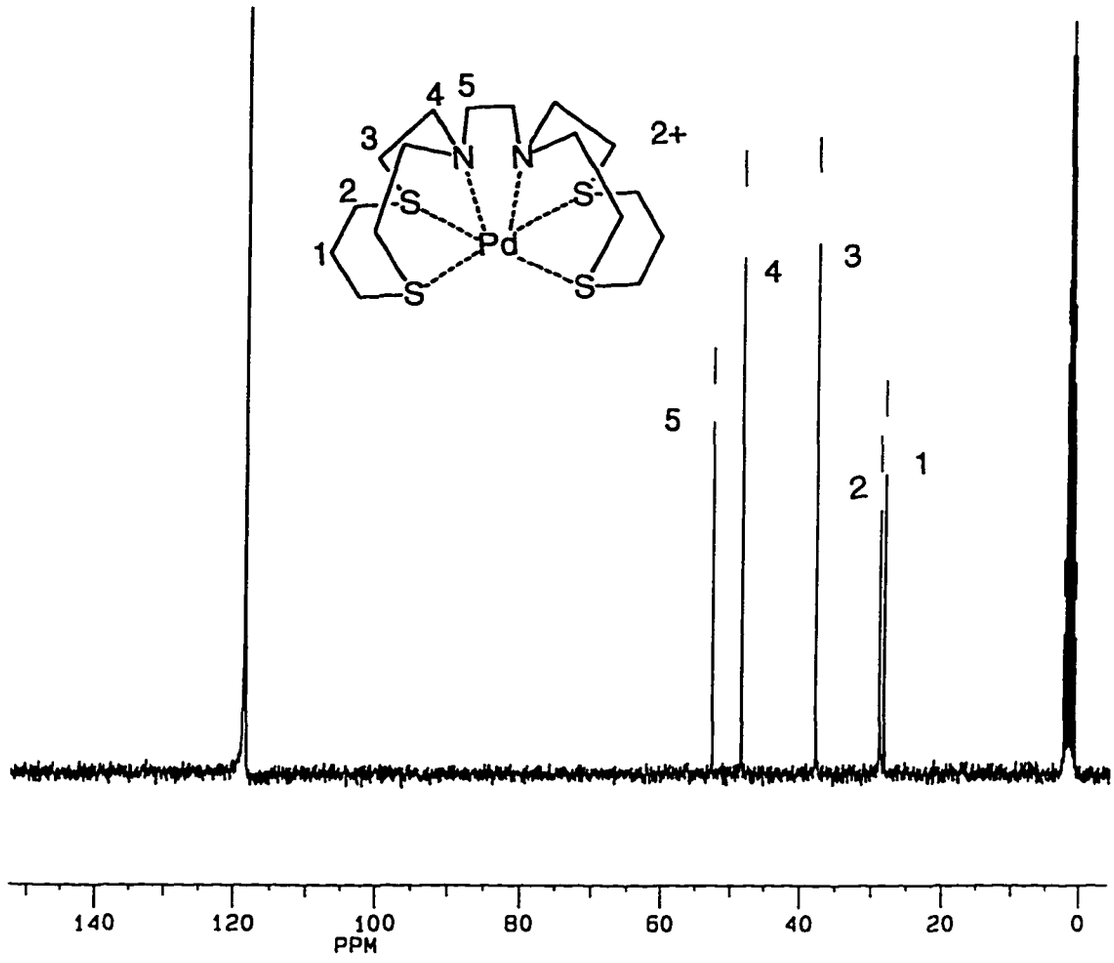

Figure 4.13: ^{13}C NMR spectrum in CD_3CN and proposed structure of [Pd([10]aneS_2N earmuff)]$(PF_6)_2$ (29) (75.5 MHz)

The proposed structure of the [Pd([10]aneS_2N earmuff)]$(PF_6)_2$ complex, based on the ^{13}C NMR is shown in Figure 4.13. This structure is pseudo five-coordinate, and is likely to be

fluxional, with only one nitrogen donor coordinated at any one time. This structure can be regarded as the analogue of the *syn* isomer of $[Pd([9]aneN_3)_2]^{2+}$,[92] shown in Figure 2.15. It is conceivable that the unsymmetrical isomer is the kinetic product of the reaction of palladium(II) with [10]aneS_2N earmuff ligand, which then isomerises into the symmetrical isomer where all four sulfur donors are in the equatorial plane. Since sulfur is a soft base, and palladium(II) is a soft acid, it is postulated that this conformation would be thermodynamically more stable than the conformation where the nitrogen donors are present in the equatorial position.

4.4.3.2 Electronic spectra

The UV/visible absorbtion data obtained for the symmetrical $[Pd([10]aneS_2N\ earmuff)]^{2+}$ ion are presented in Table 4.3, along with data for other related compounds. The red colour of $[Pd([10]aneS_2N\ earmuff)]^{2+}$ is much more intense than that observed for similar amine macrocyclic complexes, suggesting that the geometry of the complex was five coordinate, rather than square planar, since complexes of the latter type are generally pale yellow in colour.

The data presented in Table 4.3, except for $[Pd([9]aneN_3)_2]^{2+}$, are all representative of UV/Visible absorptions of square based pyramidal or penta- coordinated palladium(II) compounds.[126-128] Five coordinate Pd^{II} compounds have more intense d-d transitions at a lower energy than square planar compounds with similar ligands. The band at 459 nm in $[Pd([10]aneS_2N\ earmuff)]^{2+}$ is assigned to the d-d transitions, $^1A_{1g} \rightarrow {}^1A_{2g}, {}^1E_g, {}^1B_{1g}$.[95] The

two more intense bands have been assigned to charge transfer transitions.

The implication of five coordinate geometry in $[Pd([10]aneS_2N\ earmuff)]^{2+}$ is consistent with the structure proposed. The structure may be fluxional, so that only one of the apical nitrogens is coordinated, although a distorted trigonal prismatic geometry may exist in the solid state.

Table 4.3: UV/visible absorbtion data for Pd^{II} complexes with nitrogen and sulfur donor ligands

Complex	λ_{max}/nm (ϵ/$M^{-1}cm^{-1}$)	Ref
$[Pd([10]aneS_2N\ earmuff)]^{2+}$	273(10750), 335(14700), 459(841)	PW
$[Pd([9]aneN_3)_2]^{2+}$	296(440), 440(sh)(30)	92
$[Pd([10]aneS_2N^a)_2]^{2+}$	550(114)	96
$[Pd(TSP^b)_2]^{2+}$	360(13000), 420(4000)	126
$[Pd([10]aneS_3)_2]^{2+}$	277 (11300), 314(10800), 598(84)	96
$[Pd(L^{*\,c})]^{2+}$	453 (76)	127

[a] Blue isomer, with N_2S_2 equatorial donors, S_2 axial donors

[b] TSP = $P(o\text{-}C_6H_4SCH_3)_3$

[c] L^* = 1,4,7-tris(2-pyridylmethyl)-1,4,7-triazacyclononane

4.4.3.3 Electron paramagnetic resonance spectroscopy

The Pd^{I} (d^9) and Pd^{III} (low spin d^7) ions are both EPR active, with one unpaired electron. $[Pd([10]aneS_2N\ earmuff)]^{2+}$ was reduced with $NaBH_4$ in water, to produce the Pd^{I} complex. The complex was unfortunately very unstable, and precipitated out of solution, hence the EPR spectrum shows a broad ill defined resonance at approximately g = 2.1. Oxidising the $[Pd([10]aneS_2N\ earmuff)]^{2+}$ in acetonitrile with $NOBF_4$ gave a very unusual spectrum at 77 K, shown in Figure 4.14.

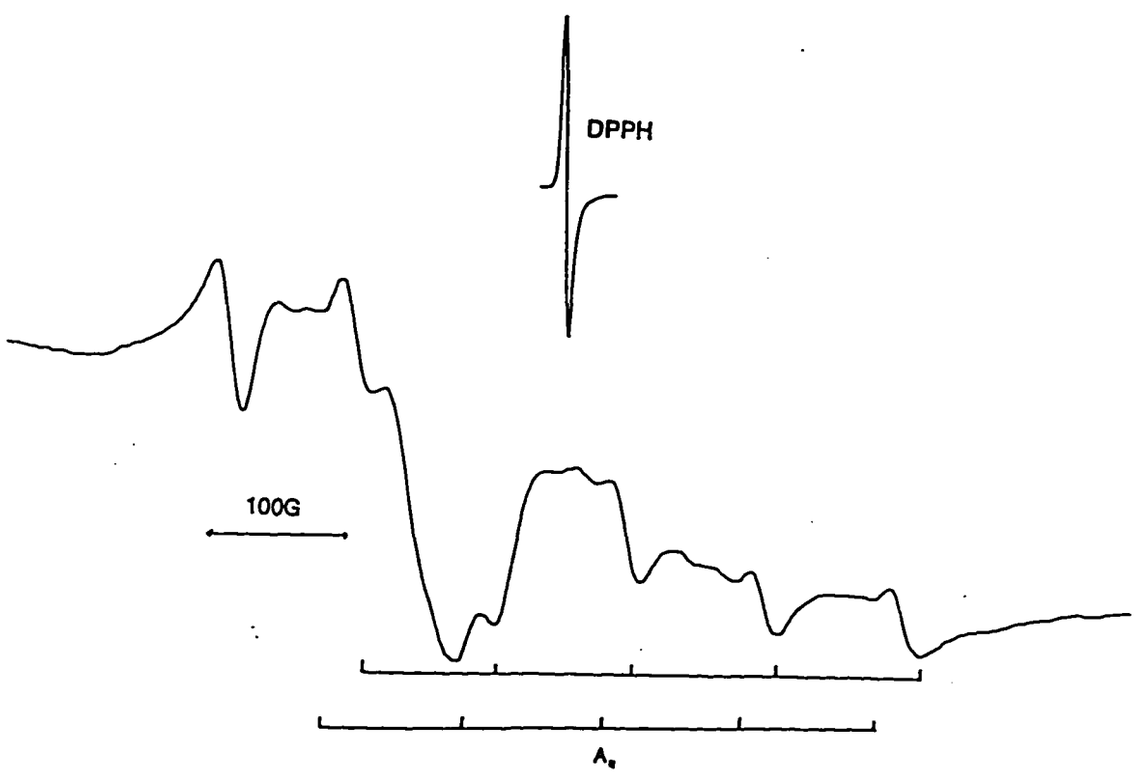

Figure 4.14: EPR spectrum of $[Pd([10]aneS_2N\ earmuff)]^{3+}$ in acetonitrile at 77K

Overlap of hyperfine structure from the axial region with the equatorial region complicates interpretation of the spectrum, however, a tentative interpretation of the features is possible.

The spectrum has a $g_\perp$ value of 2.065. Two sets of fine structure, caused by hyperfine coupling presumably to the nitrogen atoms (I = 1), appears to be present. The coupling constant, A, for both sets of hyperfine coupling appears to be about 100 G. There are 6 intense peaks, and four less intense peaks due to hyperfine coupling, one of which is believed to be obscured by the $g_\perp$ resonance. Since Pd^{III} is expected to have octahedral geometry, it is likely that coordination of NO^+ or acetonitrile is occuring in the vacant site, contributing to the fine structure. In order to clarify the fine structure, a spectrum of aqueous $[Pd([10]aneS_2N\ earmuff)]^{2+}$ oxidised with hexaaquacobalt(III) was run (Figure 4.15). Unfortunately, $[Pd([10]aneS_2N\ earmuff)]^{2+}$ is not very soluble in water so the spectrum is of poor quality, however the spectrum has several similarities with that seen in acetonitrile.

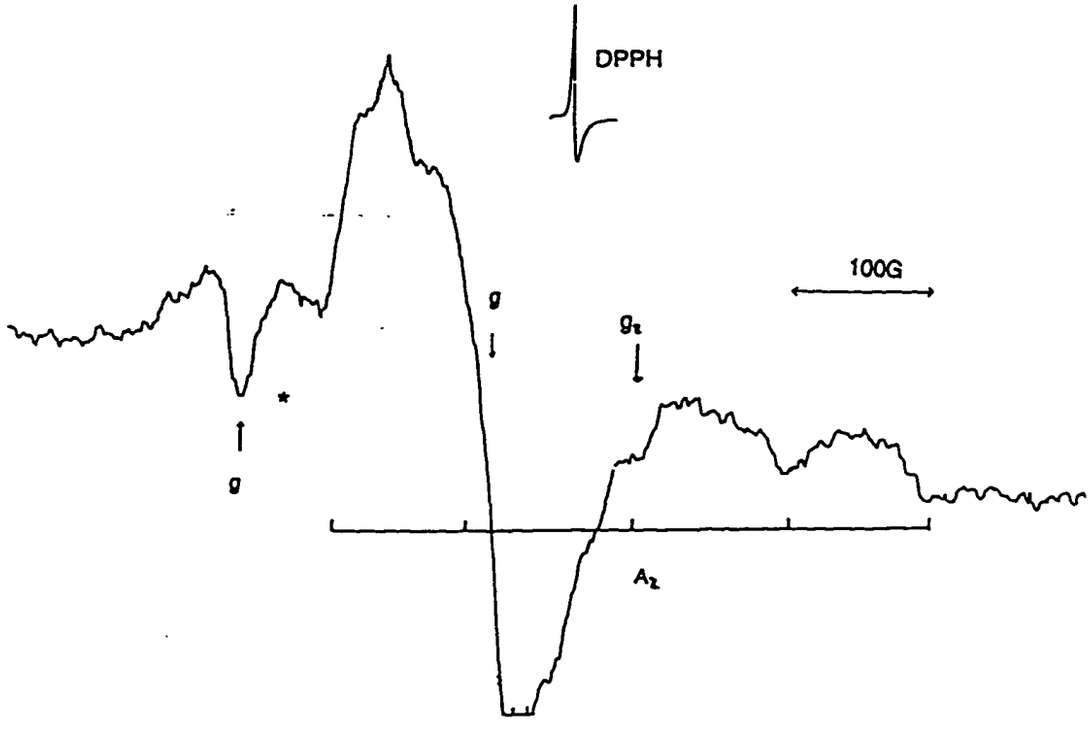

Figure 4.15: EPR spectrum of $[Pd([10]aneS_2N\ earmuff)]^{3+}$ in aqueous solution at 77K

The intensity of the peak labelled (*) is considerably greater than the intensity of the other peaks due to hyperfine structure, which are poorly resolved, if at all, in the aqueous media. For this reason, the structure of the palladium complex has been assigned as rhombic, with g_x, g_y = 2.16, 2.04 and g_z = 1.95. The five peaks due to hyperfine coupling to g_z are attributed to coupling with the two nitrogen atoms, 2nI + 1 = 5. The five smaller peaks in the acetonitrile solution are similarly determined and are therefore assigned to a second structure present in the solution.

The EPR spectrum obtained for the red $[Pd([10]aneS_2N)_2]^{3+}$ cation is nearly isotropic at 77 K, with no coupling to the nitrogens observed. The geometry imposed by the $[10]aneS_2N$ earmuff is clearly quite different to that of the similar bis-$[10]aneS_2N$ species, where pseudo octahedral geometry was observed.

4.4.3.4 Cyclic voltammetry

Three redox waves are observed in the cyclic voltammogram of the $[Pd([10]aneS_2N$ earmuff$)]^{2+}$ ion. The most positive, irreversible wave at 1.06 V vs Ag^+/Ag has been assigned to the $Pd^{III/II}$ couple. The $Pd^{II/I}$ couple is observed at -0.88 V and is electrochemically quasi-reversible, based on the peak to peak separation, however the i_p/i_a ratio is unity, suggesting that the couple is very close to attaining electrochemical reversibility. The third peak, corresponding to an irreversible $Pd^{I/0}$ couple occurs at -1.24 V. Table 4.4 gives representative examples of similar palladium(II) complexes for comparison.

From the electrochemical data, it appears that the [Pd([10]aneS$_2$N earmuff)]$^{3+}$ state is not easily attained, probably due to the inability to form octahedral coordination geometry, which could occur readily in the [Pd([10]aneS$_2$N)$_2$]$^{2+}$ complex. The lack of stability of the [Pd([10]aneS$_2$N earmuff)]$^{3+}$ species may account for the unusual EPR spectrum observed for this complex. The Pd^{I} complex on the other hand is easily reduced from Pd^{II}. The five coordinate geometry, combined with the soft sulfur donors is clearly efficient at stabilising the Pd^{I} d^9 geometry.

Table 4.4: Redox potentials for palladium complexes with nitrogen and sulfur donor ligands

Complex	couple	$E_{½}$/V (vs Ag$^+$/Ag)	Ref
[Pd([10]aneS$_2$N earmuff)]	3+/2+	1.06 (irreversible)	PW
	2+/+	-0.88 (quasi-reversible)	PW
	+/0	-1.24 (irreversible)	PW
[Pd([10]aneS$_2$N)$_2$] (*blue*)	3+/2+	0.54[a] (quasi-reversible)	96
	2+/+	-1.03 (irreversible)	96
[Pd([9]aneS$_3$)$_2$]	3+/2+	0.71 (quasi-reversible)	129

[a] This value was quoted as 0.93, however, from the figure included in the thesis, the value appears to be 0.54V

4.4.4 Cobalt complexes of the [10]aneS_2N earmuff ligand

4.4.4.1 Synthesis of [Co([10]aneS_2N earmuff)]$(ClO_4)_2$ (31)

The cobalt(II) complex of [10]aneS_2N earmuff was synthesised by reacting $Co(ClO_4)_2 \cdot 6H_2O$ with the ligand in refluxing acetonitrile in an inert atmosphere. The addition of ether to the solution gave brown crystals which analysed satisfactorily as [Co([10]aneS_2N earmuff)]$(ClO_4)_2$.

4.4.4.2 Synthesis of [Co([10]aneS_2N earmuff)]$(ClO_4)_3$ (32)

The cobalt(III) complex of [10]aneS_2N earmuff was synthesised by oxidation of [Co([10]aneS_2N earmuff)]$(ClO_4)_2$ with $NOBF_4$ in acetonitrile, which resulted in orange/red crystals. Oxidation of [Co([10]aneS_2N earmuff)]$(ClO_4)_2$ with excess $Na_2S_2O_8$ gave a new pink/red product, which has been tentatively characterised as a disulfide bridged dimer, $[(Co^{III}([10]aneS_2N\ earmuff))_2S_2](ClO_4)_4$. The mechanism of formation of the disulfide bridged dimer is unclear, although the formation of the dimer appeared to be dependent on the presence of excess $S_2O_8^{2-}$. This dimer will be discussed collectively with [Co([10]aneS_2N earmuff)]$(ClO_4)_3$.

4.4.5 Mass spectroscopy of [Co([10]aneS_2N earmuff)]$^{2+/3+}$ complexes

The FAB mass spectrum of [Co([10]aneS_2N earmuff)]$(ClO_4)_2$ gave predicted peaks, at 438.1 amu ($[Co^{II}(L\text{-}H^+)]^+$) and 537.0 amu ($[Co^{II}L(ClO_4^-)]^+$) (L = [10]ane$S_2$N earmuff); however, the mass spectrum for [Co([10]aneS_2N earmuff)]$(ClO_4)_3$ gave peaks at 439.0 and 538.0 amu. Both spectra give the same experimental isotopic distributions for the two peaks. Since the

spectrum of [Co([10]aneS$_2$N earmuff)](ClO$_4$)$_3$ is considerably weaker than that of [Co([10]aneS$_2$N earmuff)](ClO$_4$)$_2$, the peaks may be due to residual amounts of the cobalt(II) species present, or alternatively to the reduction of the cobalt(III) ion *in situ*.

The cobalt species formed by oxidation of cobalt(II) with $S_2O_8^{2-}$ gave a FAB MS with an intense peak at 471.1 amu. This corresponds to the fragment [Co([10]aneS$_2$N earmuff)S]$^+$, and gave a satisfactory match between the experimental and theoretical isotopic distribution. The Co^{III} species undoubtably has been reduced *in situ*. Whether this fragment formed from cleavage of the dimer during the ionisation process, or if it is the doubly charged dimer at half the mass, is unclear. Although FAB ionisation is generally regarded as a mild ionisation technique, fragmentation of compounds synthesised in this work was regularly seen. The doubly charged ion has only been noted in mass spectra where fragments were generated by ES, therefore it is likely that fragmentation of the dimer occurs under the experimental conditions. Elemental analysis of this complex gave satisfactory results. The percentages theoretical (and experimental) for [(Co^{III}([10]aneS$_2$N earmuff))$_2$S$_2$](ClO$_4$)$_4$ were C 28.66% (28.57) H 4.81%(4.56) N 4.18%(4.14).

4.4.6 Nuclear magnetic resonance spectra

The Co^{III} ion is diamagnetic (d^6), so low spin complexes of this ion can be characterised by NMR spectroscopy. The ^{1}H and ^{13}C NMR spectra are shown for [Co([10]aneS$_2$N earmuff)](ClO$_4$)$_3$, produced by oxidation with NO$^+$, in Figures 4.16 and 4.17.

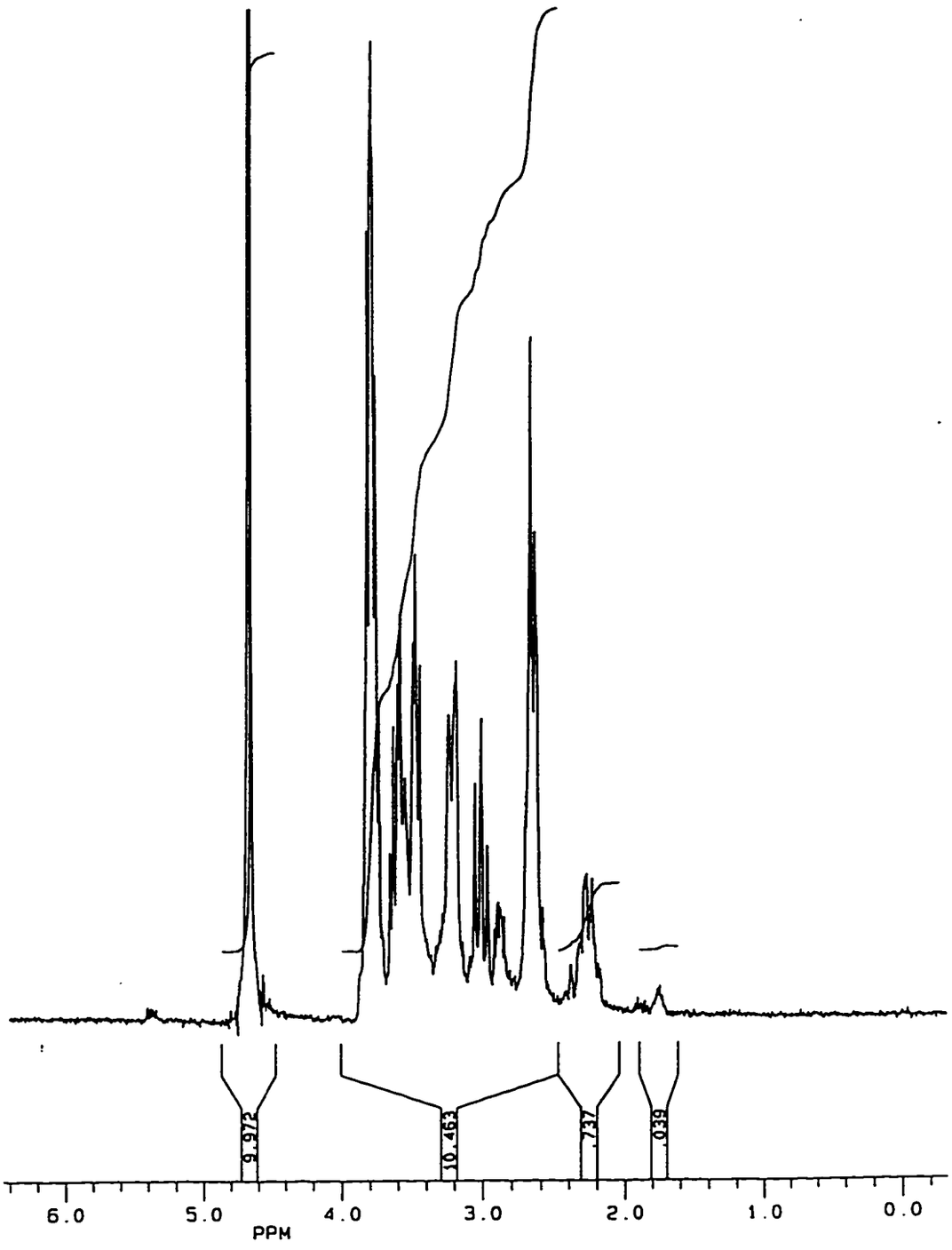

Figure 4.16: The ^{1}H NMR spectrum of [Co([10]aneS_2N earmuff)]$(ClO_4)_3$ in D_2O (300 MHz)

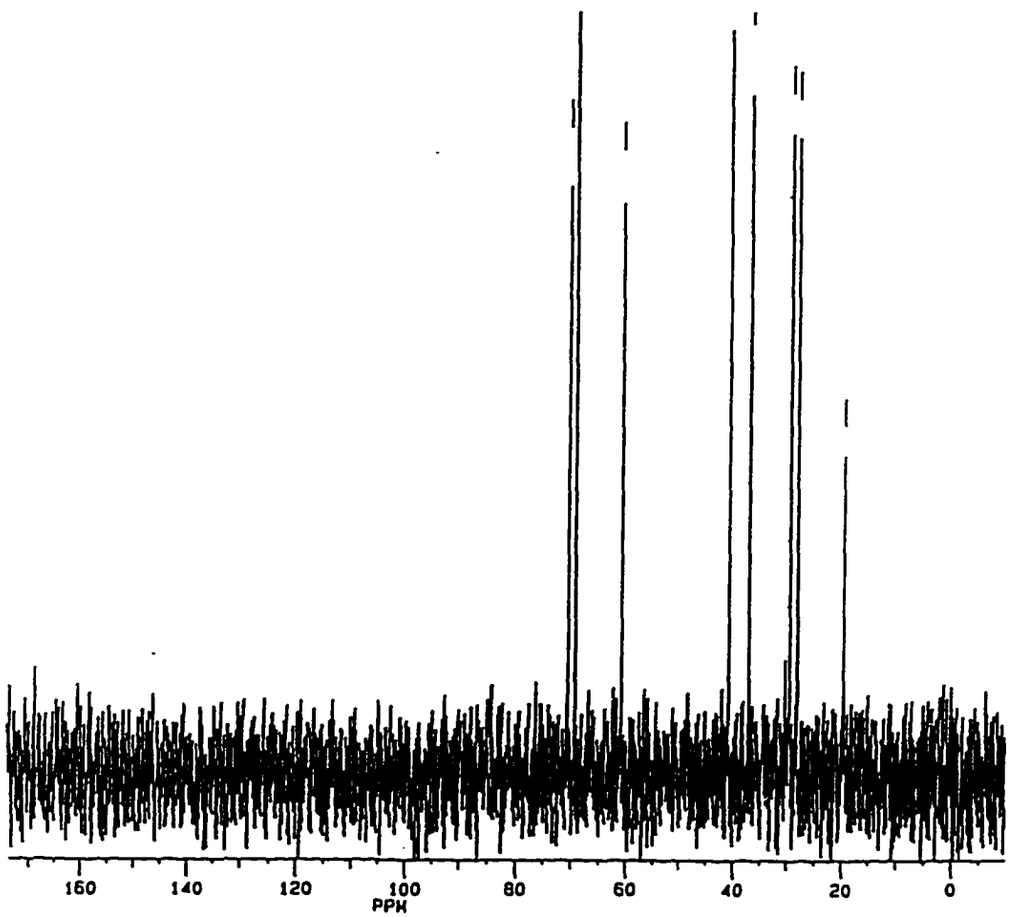

Figure 4.17: The ^{13}C NMR spectrum of [Co([10]aneS_2N earmuff)]$(ClO_4)_3$ in D_2O (75.5MHz)

Eight resonances are observed in the ^{13}C NMR spectrum, implying that a plane of symmetry is present in the macrocyclic complex, generating chemically equivalent pairs of carbon atoms. For this reason, a ligand structure similar to that proposed for the [Pd([10]aneS_2N earmuff)]$^{2+}$ is suggested for [Co([10]aneS_2N earmuff)]$^{3+}$ (Figure 4.18). Since Co^{III} species are generally six coordinate octahedral, a solvent molecule or anion is likely to be present in an axial position to produce a distorted octahedral structure.

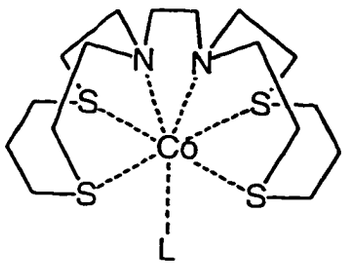

L = OH_2 (3+) or ClO_4^- (2+)

Figure 4.18: The proposed structure of [Co([10]aneS_2N earmuff)]$(ClO_4)_3$ (32)

The ^{13}C NMR spectrum of the [(Co([10]aneS_2N earmuff))$_2S_2$]$^{4+}$ dimer is quite different from that of the [Co([10]aneS_2N earmuff)]$(ClO_4)_3$ complex, suggesting that the coordination of the ligand in the dimer is unsymmetrical. The ligand is potentially six coordinate, however in order to form the disulfide bridge, it is likely that one of the donors is uncoordinated.

The ^{59}Co NMR of the two Co^{III} species have also been collected and are illustrated in Figure 4.19.

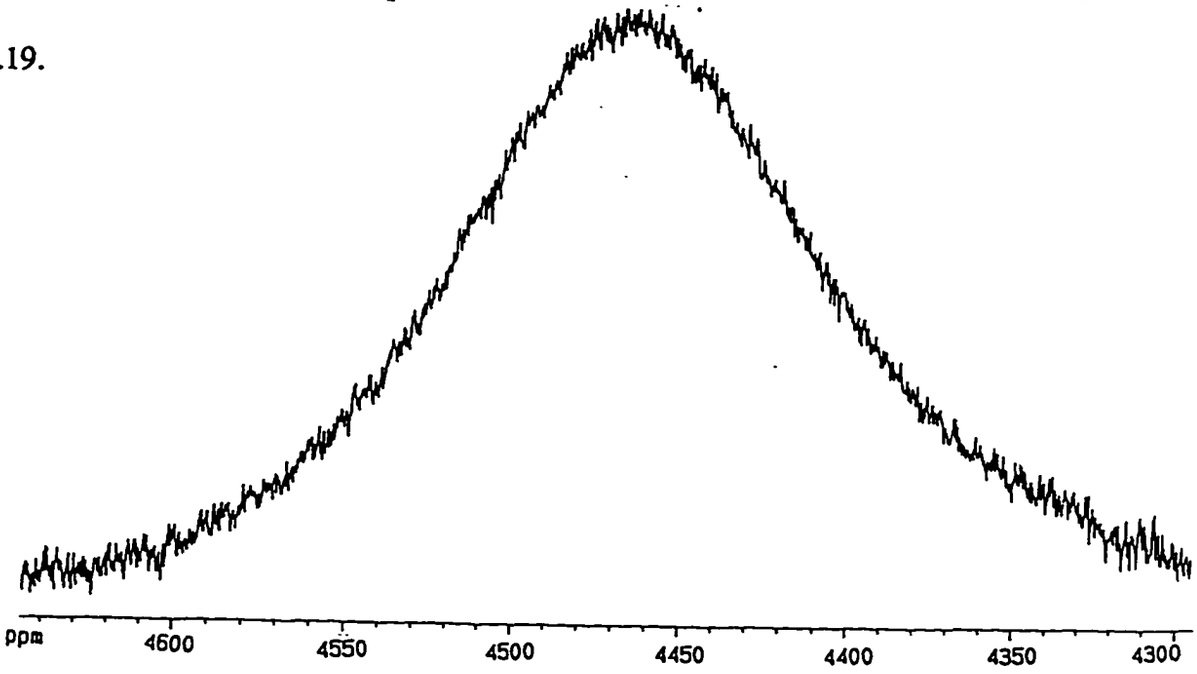

a) [Co([10]aneS_2N earmuff)$_2S_2$]$^{4+}$ dimer in D_2O (85.8 MHz)

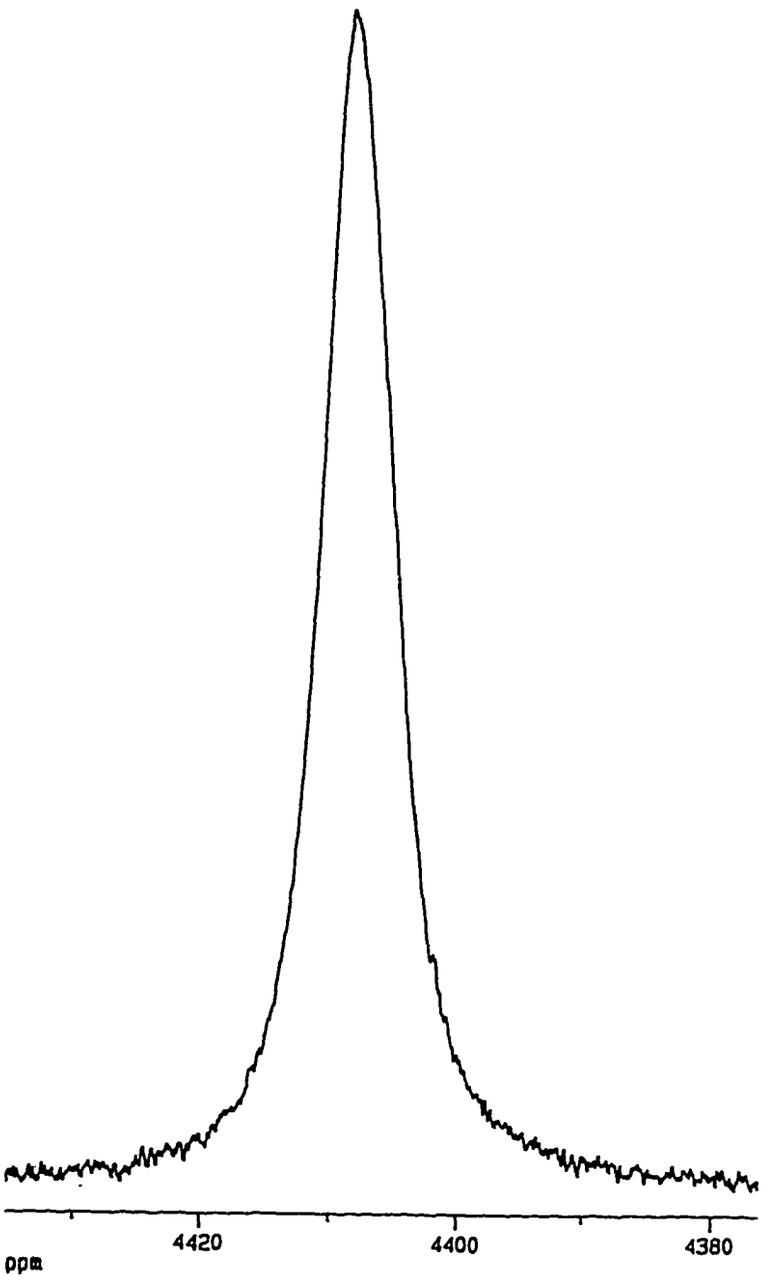

b) $[Co([10]aneS_2N\ earmuff)]^{3+}$ in D_2O (85.8 MHz)

Figure 4.19: ^{59}Co NMR spectra for the Co^{III} complexes of $[10]aneS_2N$ earmuff

The chemical shifts vs 0.1M $K_3[Co(CN)_6]$ in D_2O were 4409 ppm for the [Co([10]aneS_2N earmuff)]$(ClO_4)_3$, and 4464 ppm for the dimer. The second product gave an extremely broad resonance, the cause of which is not known.

4.4.7 Electronic spectra

The UV/visible absorption data for [Co([10]aneS_2N earmuff)]$(ClO_4)_2$ and [Co([10]aneS_2N earmuff)]$(ClO_4)_3$, and related complexes is given in Table 4.5.

Table 4.5: UV/Visible absorption data for cobalt complexes.

Complex	λ_{max}/nm (ϵ/$M^{-1}cm^{-1}$)	Ref
[Co([10]aneS_2N earmuff)]$^{2+}$ [a]	234(6880), 281(5550), 319(4100), 503(139)	PW
[Co([9]aneS_3)$_2$]$^{2+}$ [a]	264(6500), 338(6600), 480(92), 560sh, 730(11)	121
[Co([9]aneN_3)$_2$]$^{2+}$ [b]	318sh, 462(6), 545sh, 630(2), 850(2.4)	121
[Co([10]aneS_2N earmuff)]$^{3+}$ [a]	269(7460), 350(12296), 511(478)	PW
[Co([10]aneS_2N)$_2$]$^{3+}$ [b]	230(7210), 275(8875), 355(10900), 500(235)	PW

[a] Complex in acetonitrile [b] Complex in water

Low spin cobalt(II) complexes have an outer shell electron configuration of d^7, and are

therefore susceptible to Jahn - Teller distortion. Most cobalt(II) complexes are high spin, however with some macrocyclic ligands, low spin complexes or complexes which undergo a high spin - low spin equilibrium are found. For example, the $[Co([9]aneN_3)_2]^{2+}$ complex is high spin, while the tri-thia analogue is low spin.[59a] Both the high spin and low spin states of Co^{II} are expected to have several transitions in the visible region.[59a] However, in the spectrum of $[Co([10]aneS_2N$ earmuff$)](ClO_4)_2$ a broad band is observed, presumably encompassing the unresolved d-d transitions. The intensity of this band compared with other Co^{II} complexes indicates a lack of inversion symmetry in the complex making the Laporte forbidden d-d transition more favourable.

4.4.8 Electron paramagnetic resonance spectroscopy

Cobalt(II) is d^7 and is therefore a low spin complex which should be EPR active. This is the case with $[Co([10]aneS_2N$ earmuff$)](ClO_4)_2$ which gives an EPR spectrum in a 1:1 acetonitrile/DMF solution at 77 K.

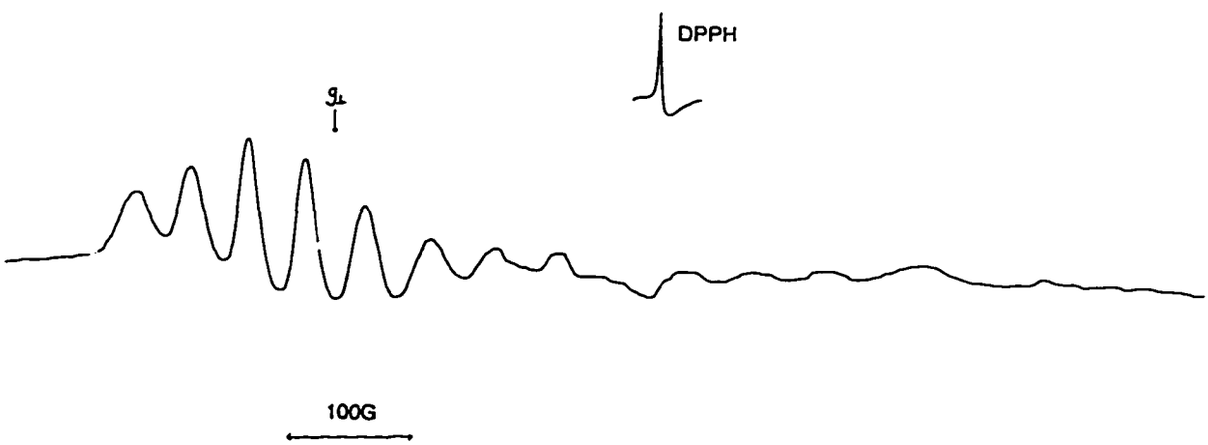

Figure 4.20: EPR spectrum of $[Co([10]aneS_2N$ earmuff$)](ClO_4)_2$ in CH_3CN/DMF (1:1) at 77 K

The spectrum, shown in Figure 4.20, is typical of a tetragonally elongated Co^{II} geometry. The Co nucleus is spin active with I = 7/2, therefore hyperfine coupling is seen for both the $g_{\parallel}$ and $g_{\perp}$ resonances. The $g_{\parallel}$ resonances are very weak, so only approximate parameters could be obtained for $g_{\parallel}$ and $A_{\parallel}$. The values of the EPR parameters are $g_{\perp} = 2.177$, $A_{\perp} = 47$ G and $g_{\parallel} \approx 1.88$, $A_{\parallel} \approx 50$ G

4.4.9 Cyclic voltammetry

The $[Co([10]aneS_2N$ earmuff$)]^{3+}$ complex in acetonitrile gave two quasi-reversible redox waves. The $Co^{III/II}$ couple was observed at -0.27 V (vs Ag^+/Ag), while the $Co^{II/I}$ couple was observed at -1.5 V. Both couples were found to be more negative than the corresponding couples for the symmetrical $[Co([10]aneS_2N)_2]^{3+}$ isomer (-0.17 V and -1.30 V respectively), hence the Co^{III} complex is stabilised by $[10]aneS_2N$ earmuff relative to the lower oxidation states compared to $[Co([10]aneS_2N)_2]^{3+}$.

4.4.10 Electron transfer studies

The ^{59}Co NMR spectrum of a solution of $[Co([10]aneS_2N$ earmuff$)]^{3+}$ from the NO^+ oxidation (I = 0.1 M adjusted with $NaClO_4$) was recorded. Addition of a solution of $[Co([10]aneS_2N$ earmuff$)]^{2+}$ (I = 0.1 M ($NaClO_4$)) to this solution did not result in any appreciable broadening of the resonance, therefore the rate of electron transfer could not be determined by this procedure. NMR has been used sucessfully to determine the rate of Co^{III}/Co^{II} self exchange for $[Co([9]aneN_3)_2]^{3+/2+}$ and $[Co([10]ane\ S_3)_2]^{2+}$ complexes.[96] It is possible that the rate of electron transfer is accompanied by an isomerisation reaction resulting in a

slow exchange rate.

To ensure that the Co^{II} complex was in a low spin state, the mass susceptibility was determined via the Evan's method. The value of μ_{eff} was calculated to be 2.09 BM, placing the Co^{II} complex in the low spin state.[59a]

4.5 Synthesis of 1,9-*bis*(8-aza-1,4-dithiacyclodecane)-4,7-diaza-2,8-dione-nonane (1,9-*bis*([10]aneS_2N) amidoearmuff) (33) and the binuclear Ni^{II} complex(34)

The potentially binuclear macrocycle, 1,9-*Bis*([10]aneS_2N) amidoearmuff, (Figure 4.21) is of interest, as the two sites could result in different geometry for each Ni^{II} ion. The two [10]aneS_2N rings are potentially six coordinate, while the two amide nitrogens plus the two [10]aneS_2N nitrogens form a potentially four coordinate site. Two four coordinate sites are also possible if the two amide nitrogens and the two nitrogens from the [10]aneS_2N rings form one site, and the four sulfur donor atoms form a second site. The two sites are in reasonably close proximity, hence the two Ni^{II} atoms which would be expected to have different redox potentials might show unusual redox behaviour as a result of 'communication' between the two redox centres.

The synthesis of 1,9-*bis*([10]aneS_2N) amidoearmuff, was achieved in a similar manner to that of [10]aneS_2N earmuff. 1,3-*bis*(chloroacetyl)propyldiamine was synthesised by the reaction of excess chloroacetyl chloride with 1,3-propyl diamine. This was purified and characterised by NMR spectroscopy. The assignment of the NMR resonances and other spectroscopic data

are given in Section 7.1.20.1. The 1,3-*bis*(chloroacetyl)propyldiamine was reacted further with two equivalents of [10]aneS_2N in acetonitrile using sodium carbonate base. The resulting ligand was purified as the nickel complex. Two equivalents of $Ni(ClO_4)_2 \cdot 6H_2O$ were reacted with the crude ligand mixture in methanol. The teal coloured complex, [Ni_2(1,9-*bis*([10]aneS_2N) amido earmuff)]$(ClO_4)_2$, was separated from [Ni([10]aneS_2N)$_2$]$(ClO_4)_2$ by Sephadex CM-C25 column chromatography. Unfortunately, it has not been possible to crystallise the binuclear Ni^{II} complex, therefore elemental analysis of the complex was not performed.

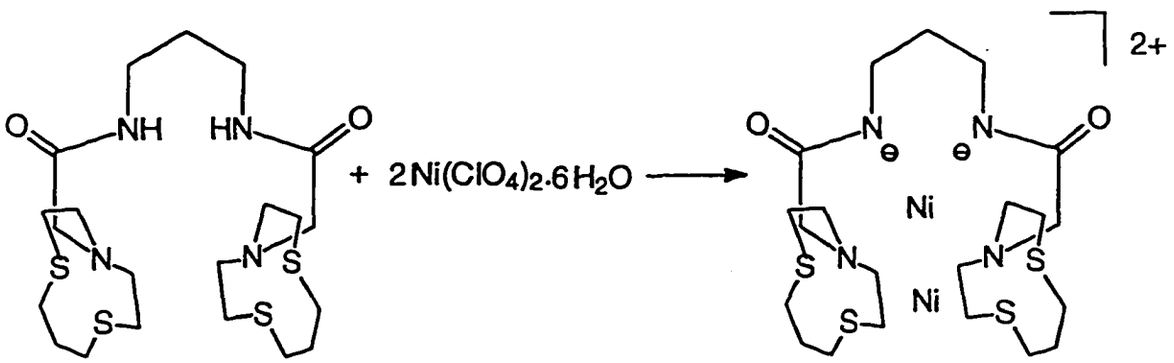

Figure 4.21: The synthesis of [Ni_2(1,9-*bis*([10]aneS_2N) amidoearmuff)]$(ClO_4)_2$ (34)

4.5.1 Nuclear magnetic resonance spectroscopy of the 1,9-*bis*([10]aneS_2N) amido earmuff ligand

The high field ^1H and ^{13}C NMR spectroscopy of the 1,9-*bis*([10]aneS_2N) amidoearmuff ligand was run in $CDCl_3$ after purification via the binuclear nickel complex. The free ligand was obtained by sequestering the nickel using cyanide, and extraction of the free ligand from a basic solution into chloroform. The assignments of the ^1H and ^{13}C NMR spectra are given in Table 4.6.

The ^{13}C spectrum is well resolved, however some overlap occurs in the ^{1}H spectrum, and as a result not all resonances have been assigned in the proton spectrum.

Table 4.6: The ^{1}H and ^{13}C NMR spectra of the 1,9-*bis*[10]aneS_2N amidoearmuff ligand

Assignment	^{13}C resonance/ppm	^{1}H resonance/ppm
N-C-CH_2-C-N	29.4	1.80 (m)
S-C-CH_2-C-S	30.1	
S-CH_2-C-N	31.6	2.69 (br)
C-C-CH_2-S	33.3	
C-C-CH_2-NH	36.6	3.28 (t)
S-C-CH_2-N	57.8	3.20 (t)
CH_2-C=O	59.3	3.10 (s)
C=O	170.5	-
NH	-	8.3 (br)

4.6 Conclusions

Although the S_2N donor ligands are capable of stabilising lower oxidation states, the presence of an amine donor makes these ligands less suitable than the homoleptic sulfur donor ligands. No evidence of Pd^{II} stabilisation with octahedral geometry was observed, indicating that these

ligands have a sufficiently large ligand field strength that the diamagnetic state of palladium(II) is maintained.

CHAPTER 5

THE SYNTHESIS AND CHARACTERISATION OF THE [Ni(BICYCLO[12-12]N_4O)]$(ClO_4)_2$ COMPLEX AND SUBSTITUTION REACTIONS OF THE CATIONIC Ni(III) SPECIES

5.1 Synthesis of [Ni(bicyclo[12-12]N_4O)]$(ClO_4)_2$ (18)

The [Ni(bicyclo[12-12]N_4O)]$(ClO_4)_2$ complex was synthesised by reacting $Ni(ClO_4)_2 \cdot 6H_2O$ in acetonitrile with the crude bicyclo[12-12]N_4O ligand mixture in acetonitrile (Figure 5.1). Long reaction times, usually in the order of 24 hours, were required to form the complex. The complex was purified readily by cation exchange column chromatography using Sephadex CM-C25, and eluting with 0.1 M $NaClO_4$. The lilac crystals were obtained after slow evaporation of the aqueous $NaClO_4$ solution.

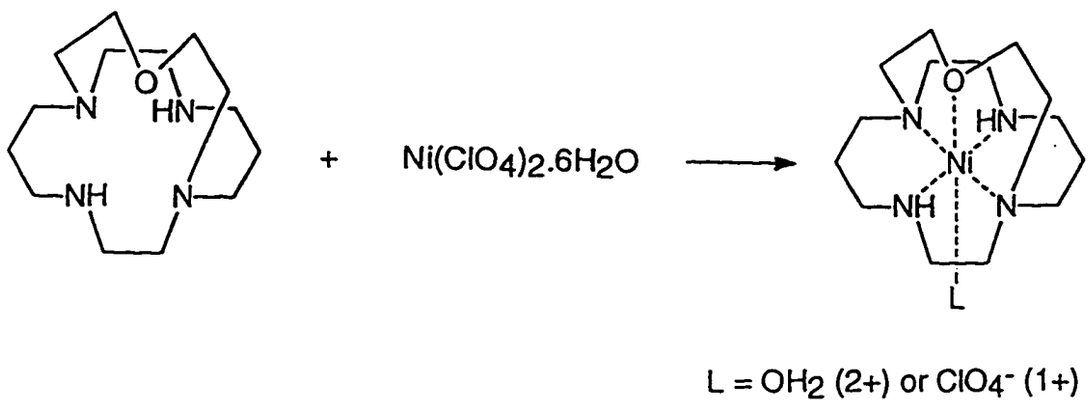

Figure 5.1: Synthesis of [Ni(bicyclo[12-12]N_4O)(L)]$(ClO_4)_n$ (18) L = OH_2 (n = 2) or ClO_4^- (n = 1)

5.2 Electronic spectroscopy

The d-d transitions of octahedral Ni^{II} complexes have already been discussed in general terms in Section 2.4.3.1, so only the relevant points with respect to [Ni(bicyclo[12-12]N_4O)]$(ClO_4)_2$ will be discussed. The spectra obtained for [Ni(bicyclo[12-12]N_4O)]$(ClO_4)_2$ in water and acetonitrile are given in Table 5.1. The spectra are typical of Ni^{II} (d^8) complexes in an

octahedral ligand environment. The apparent symmetry of the [Ni(bicyclo[12-12]N_4O)]$(ClO_4)_2$ complex is surprising, since tetragonal geometry would be expected for a five coordinate ligand.

Table 5.1: UV/visible data for [Ni(bicyclo[12-12]N_4O)]$(ClO_4)_2$

Complex	Solvent	λ_{max}/nm (ϵ/$M^{-1}cm^{-1}$)
[Ni(bicyclo[12-12]N_4O)]$^{2+}$	Water	339(7), 520(4.9), 1077(2.5)
	Acetonitrile	326(17), 398(8), 722(3), 953(4)
[Ni(bicyclo[12-12]N_4O)]$^{3+}$	Water	317(2157), 394(1440)

The solvent sensitive nature of the d-d transitions for [Ni(bicyclo[12-12]N_4O)]$(ClO_4)_2$ is expected for an octahedral complex with a five coordinate ligand, as the solvent is expected to coordinate in the sixth site, and will influence the transition energy.

The absorption peaks were ascribed to d-d transitions as previously described in Section 2.4.3.1. The weak transition seen in acetonitrile solution at 722 nm is believed to be the spin forbidden transition $^1E_g \leftarrow {}^3A_{2g}$. The ligand field splitting parameter (10Dq) was calculated and determined to be 9285 cm^{-1} in aqueous solution and 10493 cm^{-1} in acetonitrile, values considerably lower than those found for Ni([10]ane$N_2O)_2(ClO_4)_2$ (11522 cm^{-1}). Two factors

may contribute to this decrease in 10Dq. The main reason for the decrease in ligand field strength is likely to be due to the fact that bicyclo[12-12]N_4O is a five coordinate ligand. The morphology of the ligand may result in a severely distorted Ni^{II} structure, which would also result in a decrease in the ligand field observed. In water, the value of B, the Racah parameter, determined from Tanabe-Sugano diagrams,[130,131] was 970 cm^{-1}, which gave a nephelauxetic ratio of 0.93. This value is considerably greater than for the tridentate macrocycles described in Chapter 2, which ranged from 915 to 937 cm^{-1}. Calculating B using the method described by Drago[54] gave the value of 1152 cm^{-1} and $\beta > 1$. The B values calculated for [Ni(bicyclo[12-12]N_4O)]$(ClO_4)_2$ in acetonitrile were 1050 cm^{-1} (calculated using Tanabe-Sugano tables) and 1106 cm^{-1} (By the method of Drago). It is highly likely that the absolute validity of the value is suspect, since the geometry of [Ni(bicyclo[12-12]N_4O)]$^{2+}$ is not strictly octahedral, although with water as the sixth ligand, the geometry will approximate octahedral geometry. The transitions observed are likely to be split because of the reduction in symmetry, and the resulting peaks seen will encompass several transitions. The value calculated is therefore a possible estimate of the value of B at best.

The spectrum of [Ni(bicyclo[12-12]N_4O)]$^{3+}$ shows two strong transitions at energies below 400nm, which can be ascribed to charge transfer transitions.

5.3 Electron paramagnetic resonance spectroscopy

The Ni^{III} ion (d^7) has an unpaired electron which is EPR active. The spectrum obtained for [Ni(bicyclo[12-12]N_4O)]$^{3+}$ is shown in Figure 5.2. The [Ni(bicyclo[12-12]N_4O)]$^{3+}$ ion was

produced by oxidation of $[Ni(bicyclo[12\text{-}12]N_4O)](ClO_4)_2$ in aqueous solution with hexaaquacobalt(III). The EPR spectrum is characteristic of a tetragonally elongated Ni^{III} species with $g_{\parallel} = 2.027$ and $g_{\perp} = 2.195$.

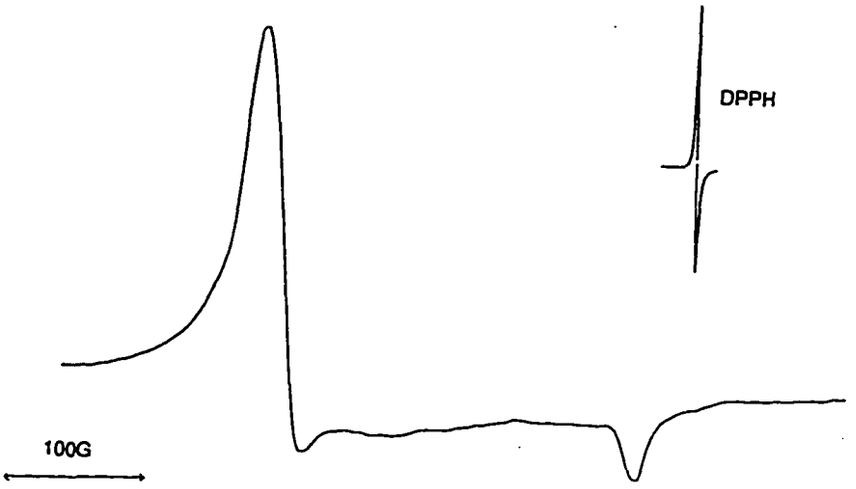

Figure 5.2: EPR spectrum of the aqueous frozen glass $[Ni(bicyclo[12\text{-}12]N_4O)(H_2O)]^{3+}$ complex, T= 77K

Addition of HCl to the aqueous solution results in substitution of the axially coordinated solvent molecule with a chloride ion. This results in hyperfine coupling of the unpaired electron to the chloride ion (I = 3/2) in the axial position and the $g_{\parallel}$ resonance is split into four peaks, with $A_{\parallel} = 28$ G (Figure 5.3). In Figure 5.3, it can also be seen that the spectrum is characteristic of rhombic rather than tetragonal geometry about the metal centre, with a shoulder being present on the $g_{\perp}$ resonance. It has been observed that tertiary amine - metal bond lengths in Ni^{II} complexes are longer than secondary amine - metal bond lengths,[132] which may explain the origin of the rhombic structure since two diagonally opposed bonds in the structure may be longer. The g values obtained from this spectrum are g_x, $g_y = 2.187, 2.165$

and $g_z = 2.029$.

Addition of NaF to a $[Ni(bicyclo[12\text{-}12]N_4O)(H_2O)]^{3+}$ solution gives a spectrum as shown in Figure 5.4. In this spectrum coordination of F^- in the axial position results in both the g_x,g_y resonance and the g_z resonance coupling to the fluoride ion ($I = ½$) giving rise to two peaks for each resonance. No evidence is observed that more than one fluoride ion is attached, even at high concentrations of F^-, so it can be concluded that the oxygen donor remains axially coordinated under these conditions. From the spectrum the values of $g_x,g_y \approx 2.217$, $g_z = 2.024$ and $A_{x,y} = 67G$ and $A_z = 199$ G were obtained.

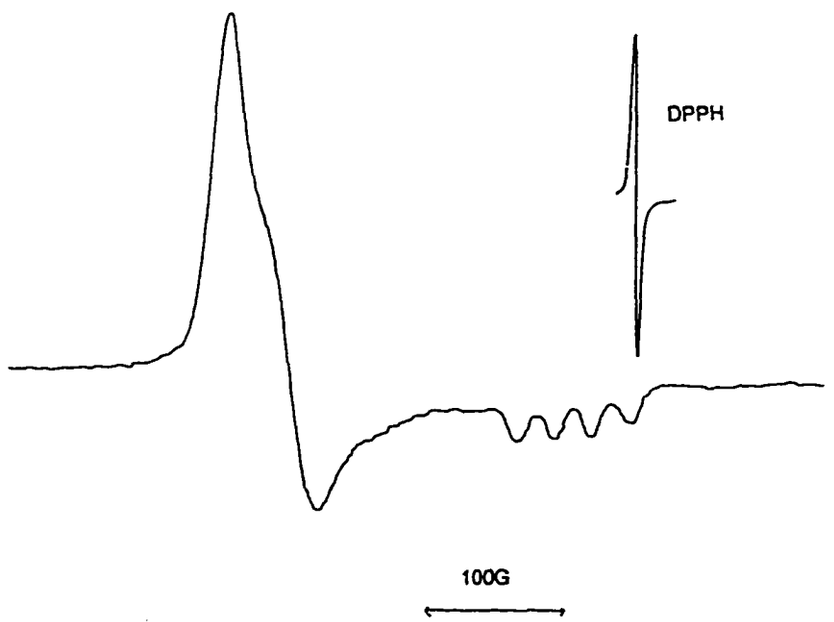

Figure 5.3: EPR spectrum of aqueous $[Ni(bicyclo[12\text{-}12]N_4O)Cl]^{2+}$ showing hyperfine coupling due to Cl^- coordination

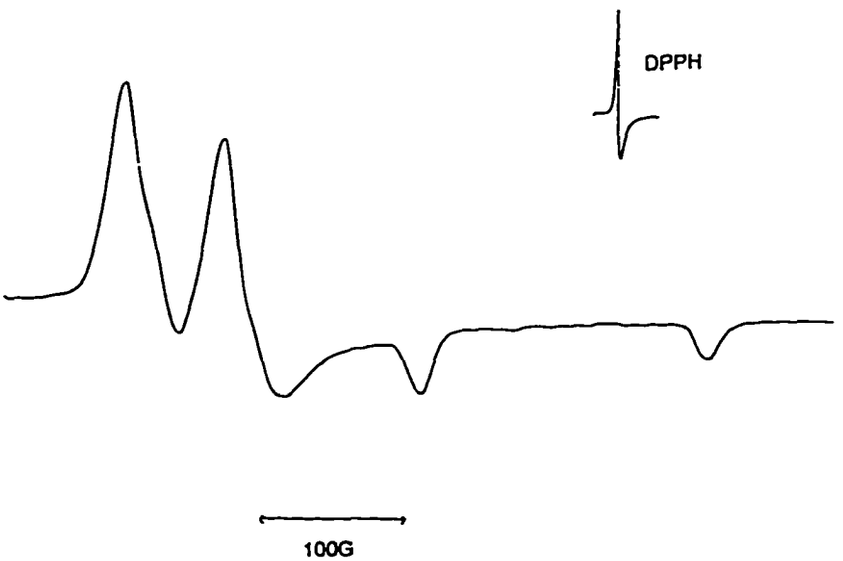

Figure 5.4: EPR spectrum of aqueous $[Ni(bicyclo[12\text{-}12]N_4O)F]^{2+}$ showing hyperfine coupling due to F^- coordination

5.4 Cyclic voltammetry

The redox data obtained for $[Ni(bicyclo[12\text{-}12]N_4O)](ClO_4)_2$ are summarised in Table 5.2. $[Ni(cyclam)]^{2+}$ is significantly easier to oxidise than the two N_4O bicycles, although this is not the case with the N_5 analogue of bicyclo[9-14]N_4O,[89] which is also readily oxidised to Ni^{III}. Similar potentials of the $Ni^{III/II}$ couple are obtained for the two N_4O bicycles, suggesting that the geometry of the two macrocycles are nearly equivalent. Why a nitrogen donor in the axial position but not an oxygen donor would stabilise the Ni^{III} state is not immediately obvious, but has been suggested to be attributable to electronic interactions.[89]

Table 5.2: Redox data for [Ni(bicyclo[12-12]N_4O)]$(ClO_4)_2$ and related compounds

Complex	Couple	$E_{1/2}$/V (vs Ag^+/Ag)	Ref
[Ni(bicyclo[12-12]N_4O)]	3+/2+	0.85 (quasi-reversible)	PW
	2+/1+	-1.79 (irreversible)	PW
[Ni(bicyclo[9-14]N_4O)]	3+/2+	0.86 (quasi-reversible)	68
	2+/1+	-1.66 (quasi-reversible)	68
[Ni(cyclam)]	3+/2+	0.59	17, 117

The redox couples are obtained in acetonitrile, apart from $[Ni(cyclam)]^{n+}$ which was obtained in 1 M $HClO_4$ solution.

An irreversible redox process was observed at 1.3 V for $[Ni(bicyclo[12\text{-}12]N_4O)]^{2+}$. This process has tentatively been assigned to either the $Ni^{IV/III}$ couple, or oxidation of the ligand to produce a ligand radical.

5.5 The rate of decomposition of $[Ni(bicyclo[12\text{-}12]N_4O)]^{2+}$ and $[Ni(bicyclo[12\text{-}12]N_4O)]^{3+}$ in aqueous acidic solution

The rate of decomposition of $[Ni(bicyclo[12\text{-}12]N_4O)]^{2+}$ was determined in aqueous 1M $HClO_4$ at 1 M ionic strength, adjusted with $LiClO_4$. The rate was monitored by UV/Visible spectroscopy at the observed maxima of 520 nm for 12 hours. No measurable decomposition

was observed during this time period.

The rate of decomposition of $[Ni(bicyclo[12\text{-}12]N_4O)]^{3+}$ in different concentrations of $HClO_4$ was monitored by UV/Visible spectroscopy at 395 nm. The rate was found to be independent of acid concentration at concentrations of $HClO_4$ between 0.2 and 1 M. This indicates that the rate of decomposition is not acid catalysed. The rate at 20°C was found to be $7.5(\pm0.2)\times10^{-4}$ s^{-1}, giving a half life of approximately 16 minutes. At 10°C, this rate was found to decrease to $2.4(\pm0.2)\times10^{-4}$ s^{-1}. This gives a half life of approximately 50 minutes, sufficiently slow to enable the monitoring of rapid substitution kinetics without interference from the decomposition rate.

The rate of $[Ni(bicyclo[12\text{-}12]N_4O)]^{3+}$ decomposition is significantly slower than that of $[Ni([10]aneN_2O)_2]^{3+}$, which has a half life of approximately 5 minutes at 20°C. Two factors account for the increase in stability of $[Ni(bicyclo[12\text{-}12]N_4O)]^{3+}$ relative to $[Ni([10]aneN_2O)_2]^{3+}$. The $[Ni([10]aneN_2O)_2]^{2+}$ complex decomposes slowly in acid, as the tridentate ligands are less stable than cyclam analogues, which have half lives for acid catalysed decomposition in the order of months or years. Also the higher potential for the $[Ni([10]aneN_2O)_2]^{3+/2+}$ couple results in water being oxidised to a greater extent by the Ni^{III}, and therefore a faster decomposition rate is observed.

5.6 Substitution reactions at the axial site of $[Ni(bicyclo[12\text{-}12]N_4O)(H_2O)]^{3+}$

Substitution reactions of transition metals can occur via a continuum of mechanisms with an

associative mechanism (A) at one extreme through to a dissociative mechanism (D) at the other. Many reactions occur via interchange mechanisms, where no intermediates can be detected, and these can be classified as associative (I_a) or dissociative (I_d) interchange, depending on the entering group effects observed.

Substitution reactions for complexes with monodentate ligands are often complicated by ligand dissociation reactions. In order to determine the mechanism of substitution at one site, five-coordinate macrocyclic ligands have been used to avoid ligand dissociation at all but the site of study. Substitution reactions at Ni^{III} centres have previously been studied, with four-coordinate ligands,[133,134] and with the $[Ni(bicyclo[9\text{-}14]N_4O_2)]^{3+}$ complex.[68] Dissociative interchange mechanisms have been suggested for these species, since the forward and reverse rates of reaction do not vary greatly, as would be expected for a interchange mechanism. The activation mechanism of the reaction has not been studied in great detail due to the limited numbers of compouunds available, although studies with substituted cyclam based ligands show an increase in rate with increasing axial crowding of the ligand[134] suggesting a dissociative interchange mechanism.

The reaction rate for Cl^- substitution at $[Ni(bicyclo[9\text{-}14]N_4O)(H_2O)]^{3+}$ was found to be dependent on the concentration of acid present. The presence of acid in the solution appreciably reduces the rate of decomposition of the $[Ni(bicyclo[12\text{-}12]N_4O)(H_2O)]^{3+}$, presumably by preventing decomposition via base catalysed pathways.[135] In order to further examine the origin of the acid dependence in this reaction, a study of the chloride substitution

kinetics at [Ni(bicyclo[12-12]N_4O)(H_2O)]$^{3+}$ was examined.

Since the Ni^{III} centre is substitution labile, reactions with chloride take place very rapidly (< 1 s) and must be followed by stopped flow methods. The change in molar absorptivity for the substitution process allows the reaction to be followed by visible spectrophotometry.

5.6.1 Determination of the equilibrium constant for the chloride substitution reaction of [Ni(bicyclo[12-12]N_4O)(H_2O)]$^{3+}$ by spectrophotometric titration

The equilibrium constant for a simple reaction such as chloride substitution of an axial solvent molecule may be determined spectrophotometrically if the reaction results in an optical density change. For the substitution reaction, $[NiL^{3+}] + Cl^- \rightleftharpoons [NiLCl^{2+}]$, the equilibrium constant, K (equation 1) may be determined using equation 2.

$$K = \frac{[NiLCl]}{[NiL][Cl]} \qquad 1$$

$$\frac{[NiL]_o[Cl]_o}{\Delta OD} = \frac{[NiL]_o + [Cl]_o}{(\Delta\epsilon)l} + \frac{1}{K(\Delta\epsilon)l} \qquad 2$$

where ΔOD is the observed optical density change at the monitoring wavelength,

$\Delta\epsilon$ is the change in extinction coefficient between the reactant and the product,

l is the path length in cm, and $[NiL]_o$ and $[Cl]_0$ are the initial concentrations of [Ni(bicyclo[12-

12]$N_4O)(H_2O)]^{3+}$ and Cl^- respectively.

A plot of $\frac{[NiL]_o[Cl]_o}{\Delta OD}$ vs $[NiL]_o + [Cl]_o$, shown in Figure 5.5 gave a good linearity over the range of the titration.

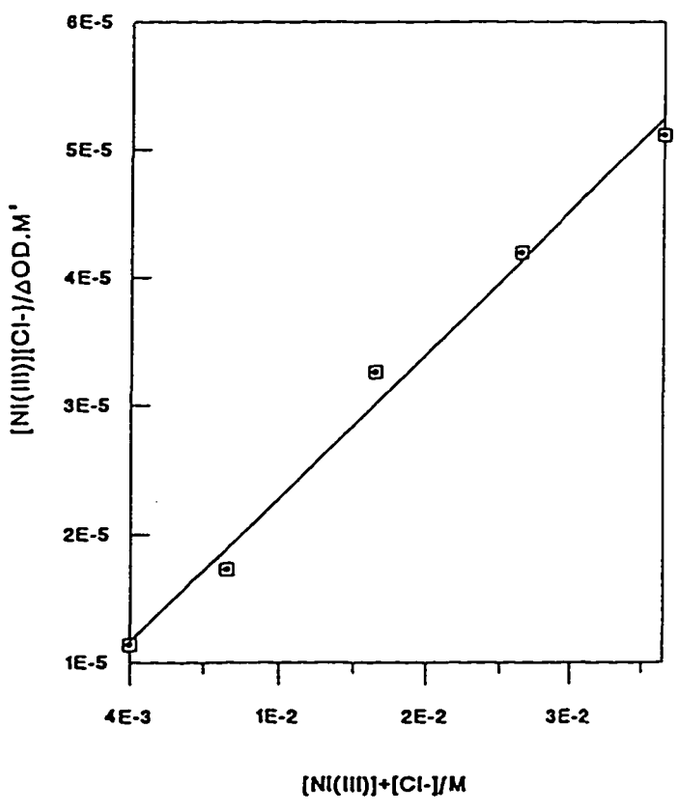

Figure 5.5: Spectrophotometric determination of the equilibrium constant for chloride substitution at the axial site of [Ni(bicyclo[12-12]$N_4O)(H_2O)]^{3+}$

The concentration of [Ni(bicyclo[12-12]$N_4O)(H_2O)]^{3+}$ was kept constant at 2.2×10^{-4} M ([H^+]

= 0.5 M, I = 1 M, adjusted with $LiClO_4$), and the absorbance changes over the range 200 to 500 nm monitored with addition of Cl^- ($7x10^{-3}$ - $8x10^{-2}$ M) at a temperature of 10°C. Adjustments were made as far as possible to account for the effect of the acid added to the solution from the $[Co(H_2O)_6]^{3+}$ solution. An isosbestic point was observed for the titration at 268 nm, with a λ_{max} value at 317 nm. From the above plot, the value of K can be determined, and was calculated to be 170±10 M^{-1}. This value is similar to the values obtained for the reaction of chloride with $[Ni(cyclam)]^{3+}$.[132]

5.6.1 The kinetics of the chloride substitution reaction of $[Ni(bicyclo[12-12]N_4O)(H_2O)]^{3+}$

The chloride substitution reaction was examined under pseudo first order conditions. In order to maintain these conditions, chloride concentrations of approximately 10 to 40 times in excess of the concentration of the $[Ni(bicyclo[12-12]N_4O)(H_2O)]^{3+}$ complex were used. Higher concentrations of chloride appeared to show a second order dependence on chloride, although the origin of this dependence is unknown. EPR spectra with large excesses of chloride and fluoride present showed coordination of one ion per nickel centre, so there is no evidence for coordination of a second chloride ion. Similarly, $[Ni(cyclam)]^{3+}$ complexes form 1:1 complexes even with large excess of chloride present. A second slow rate of reaction has also been observed for halide substitution of Ni^{III} tetraaza macrocycles.[134] In this case, the reaction was found to be independent of halide concentration, and ascribed to a rearrangement process.

The results of the rate determinations for chloride substitution at various hydrogen ion concentrations are tabulated in Table 5.3. The absorbance changes occuring on chloride substitution are very small, so appreciable errors result in the determination of the observed rate constant. The rate of substitution was followed at 430 nm, which was found to give the greatest absorbance change on substitution, with minimal noise present on the trace.

Table 5.3: Kinetic data for chloride substitution of $[Ni(bicyclo[12\text{-}12]N_4O)(H_2O)]^{3+}$ at 10°C

	$[H^+]$/M						
$[Cl^-]$/mM	0.07	0.10	0.15	0.20	0.30	0.50	0.95
	k_{obs}/s^{-1}						
3.0	4.82	4.50	4.02	3.76	3.63	3.39	3.30
5.0	5.55	5.45	4.72	4.55	4.44	4.24	3.96
8.0	6.94	6.59	6.04	5.59	5.49	5.32	5.16
10.0	7.87	7.65	6.77	6.45	6.28	5.95	5.76
12.0	8.63	8.31	7.52	7.10	6.91	6.77	6.56

The observed rate constant, k_{obs} where $-d[Ni^{III}L]/dt = k_{obs}[Ni^{III}L]$, was determined. In general the scatter of values for k_{obs} around the average value determined were in the order of ±0.2 s^{-1}. In all cases the ionic strength was maintained at 1 M by addition of $LiClO_4$. The concentration of $[Ni(bicyclo[12\text{-}12]N_4O)]^{3+}$ used was approximately $2x10^{-4}$ M, formed by

oxidising [Ni(bicyclo[12-12]N_4O)]$(ClO_4)_2$ with a deficiency of $[Co(H_2O)_6]^{3+}$. The rate measurements were determined at 10°C in order to minimise the decomposition of the $[Ni(bicyclo[12\text{-}12]N_4O)]^{3+}$ species, although this did not appreciably alter the rate constants derived, as the reaction is performed under pseudo first order conditions with excess chloride present.

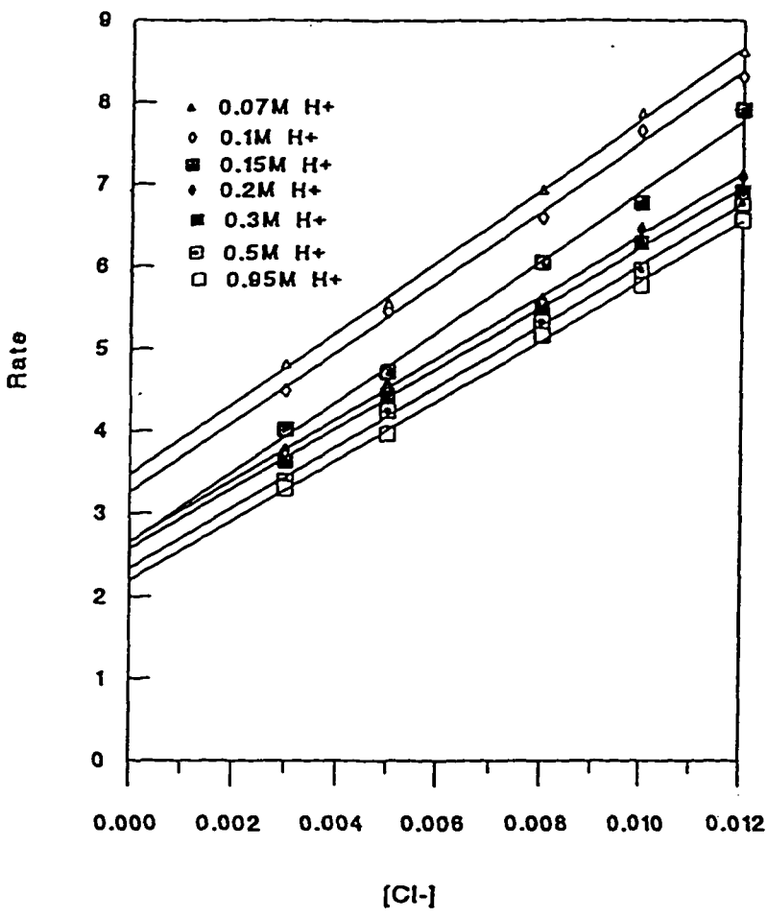

Figure 5.6: Plots of the observed rate constant for chloride substitution of [Ni(bicyclo[12-12]N_4O)(H_2O)]$^{3+}$at varying acid concentrations, T = 10°C, I = 1.0 M ($LiClO_4$)

The chloride substituted species formed is considerably more stable than the aquo species, persisting at room temperature for several hours. This increased stability of these Ni^{III} species has been observed for other Ni^{III} macrocyclic complexes with chloride in the axial position. The observed first order rate constants (k_{obs}) found to vary linearly with chloride concentration (Figure 5.6).

The intercept and slope of each curve was also found to vary inversely with acid concentration, consistent with an acid dependence of the substitution reaction. The plot of the intercepts (Figure 5.7) derived from the linear least squares fit to the above data plotted against $1/[H^+]$ was linear. However, the fit for the plot of slope vs $1/[H^+]$ (Figure 5.8) was subject to greater error. A tentative mechanism which would account for the observed acid dependence is described below.

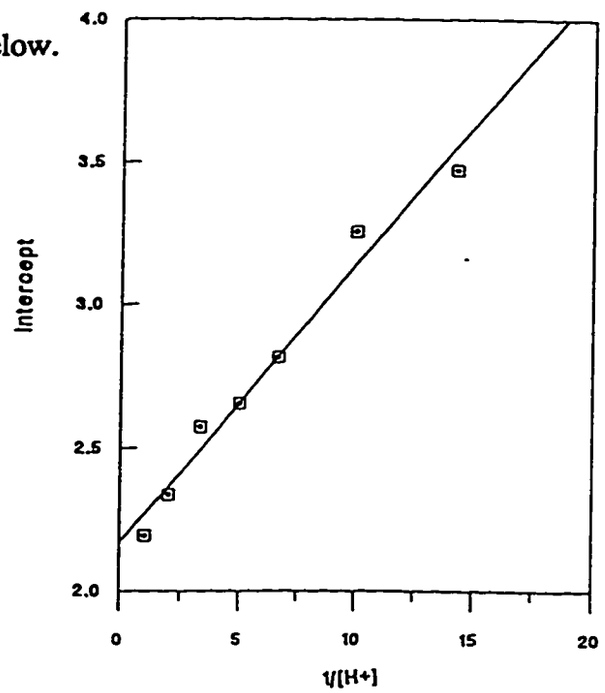

Figure 5.7: Plot of intercept vs $1/[H^+]$ for chloride substitution of [Ni(bicyclo[12-12]N_4O)(H_2O)]$^{3+}$

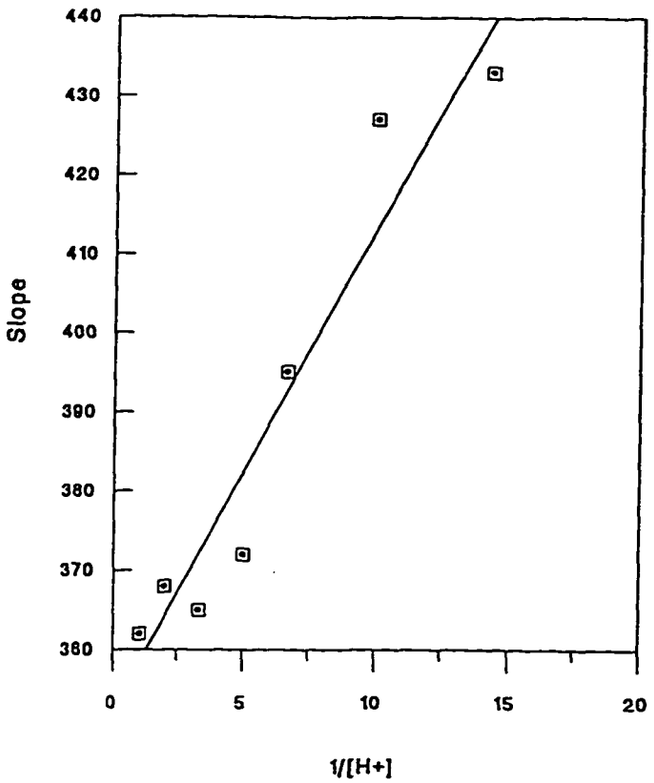

Figure 5.8: Plot of slope vs $1/[H^+]$ for chloride substitution of [Ni(bicyclo[12-12]N_4O)(H_2O)]$^{3+}$

5.6.1.1 Derivation of the observed rate law for chloride ion substitution reactions

If chloride substitution only occurs for the [Ni(bicyclo[12-12]N_4O)]$^{3+}$ complex when the complex is in the unprotonated form, two equilibria would exist as shown in Scheme 5.1.

$$NiL + H^+ \overset{K_h}{\rightleftharpoons} NiHL$$

$$H^+ + NiL + Cl^- \underset{k_{-1}}{\overset{k_1}{\rightleftharpoons}} NiLCl + H^+$$

Scheme 5.1: Chloride substitution equilibria for the unprotonated [Ni(bicyclo[12-12]N_4O)(H_2O)]$^{3+}$

$NiL = [Ni^{III}(bicyclo[12\text{-}12]N_4O)(H_2O)]^{3+}$

$NiHL = [Ni^{III}(bicyclo[12\text{-}12]N_4O + H^+)(H_2O)]^{4+}$

$NiLCl = [Ni^{III}(bicyclo[12\text{-}12]N_4O)(Cl)]^{2+}$

It can be shown that the value of k_{obs} derived from the above equilibria conforms to equation 3, which would give a linear plot of k_{obs} vs $[Cl^-]$ with slope = k_1 and an intercept with a $1/[H^+]$ dependence.

$$k_{obs} = \frac{k_{-1}K_h}{[H^+]} + k_{-1} + k_1[Cl^-] \qquad 3$$

Since a $1/[H^+]$ dependence was also observed for the slope of the curve k_{obs} vs $[Cl^-]$, this mechanism is not fully in accord with all the experimental observations.

However, If the substitution occurs involving both the protonated and unprotonated complexes, equilibria shown in Scheme 5.2 would be operative.

$$\begin{array}{ccc} NiHL + Cl^- & \underset{k_{-1}}{\overset{k_1}{\rightleftharpoons}} & NiHLCl \\ K_b \Big\uparrow\Big\downarrow & & \Big\uparrow\Big\downarrow K_a \\ NiL + H^+ + Cl^- & \underset{k_{-2}}{\overset{k_2}{\rightleftharpoons}} & NiLCl + H^+ \end{array}$$

Scheme 5.2: Protonation and substitution equilibria for chloride substitution of

$[Ni(biyclo[12\text{-}12]N_4O)(H_2O)]^{3+}$

$NiL = [Ni^{III}(bicyclo[12\text{-}12]N_4O)(H_2O)]^{3+}$

$NiHL = [Ni^{III}(bicyclo[12\text{-}12]N_4O + H^+)(H_2O)]^{4+}$

$NiLCl = [Ni^{III}(bicyclo[12\text{-}12]N_4O)(Cl)]^{2+}$

$NiHLCl = [Ni^{III}(bicyclo[12\text{-}12]N_4O + H^+)(Cl)]^{4+}$

In the above reaction scheme, chloride substitution occurs with both the protonated ligand complex and the unprotonated complex, and protonation equilibria occur for both chloride substituted and unsubstituted complexes. It can be shown (See Appendix 2 for the derivation of this equation) that the observed rate constant, k_{obs} is:

$$k_{obs} = k_{-1} + \frac{k_{-1}K_a}{[H]} + k_1[Cl] + \frac{k_1K_b[Cl]}{[H]} \qquad 4$$

As can be seen, this would result in a $1/[H^+]$ dependence for both the slope and the intercept for the plot k_{obs} vs $[Cl^-]$. This acid dependence is similar to that observed for the substitution reactions of $[Ni(bicyclo[9\text{-}14]N_4O_2)(H_2O)]^{3+}$.[67]

A fit of the observed data using equation 4 yields the values

$k_{obs} = (2.17 + 0.097/[H^+] + 352[Cl^-] + (6.11[Cl^-])/[H^+])\ s^{-1}$ and

$k_1 = 352\pm6\ M^{-1}s^{-1}$

$k_{-1} = 2.17\pm0.05\ s^{-1}$

$K_1 = 162\pm10\ M^{-1}$, $K_2 = 612\pm10\ M^{-1}$, $K_a = 0.045\pm0.005$ M, $K_b = 0.017\pm0.005$ M

The value of K_1 for substitution of the protonated complex (162 M^{-1}) is in excellent agreement with that of the equilibrium constant determined spectrophotometrically (170 M^{-1}). The plot of the calculated values of k_{obs} vs the experimental values (Figure 5.9) also shows a good correlation.

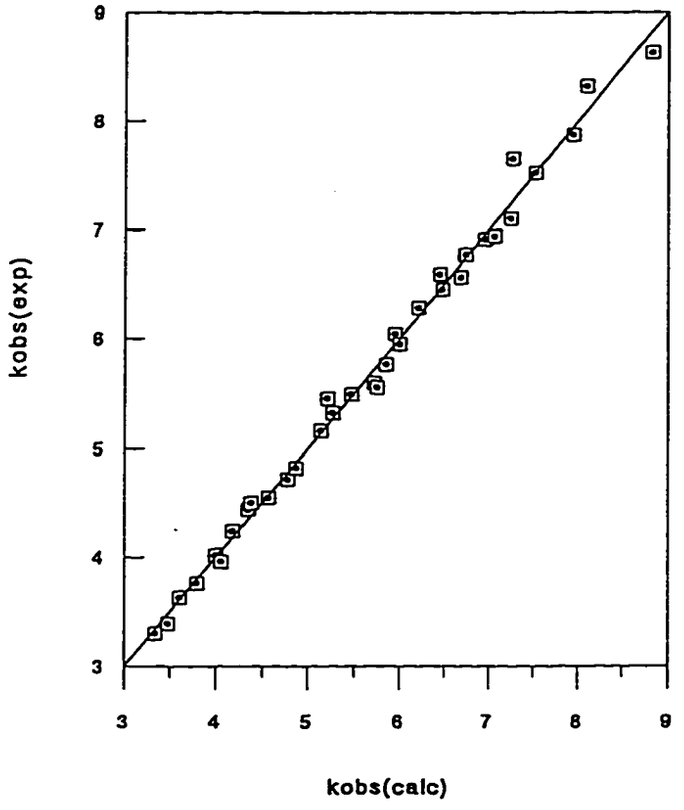

Figure 5.9: Correlation between calculated and experimental values of k_{obs}

The reaction mechanism proposed does not take into account the intimate mechanism involved in the substitution reaction. It has been proposed[133,136,137] that similar substitution processes take place via the formation of an outer-sphere complex, with subsequent replacement of the anion. Further studies of this mechanism are required in order to provide evidence for the formation of an outer sphere complex, although, based on the +3 and -1

charges of the reactants, there is no reason to presume that the outer sphere complex would not exist for the above reaction. It is at this stage not possible to determine whether the mechanism proceeds via an dissociative mechanism, since only the chloride ion substitution reaction has been studied. However since the reaction proceeds at a Ni^{III} centre, and the rates of substitution of chloride for the protonated complex are of a similar magnitude to those observed[133,134] for reactions where a dissociative interchange mechanism has been observed, it might be assumed that the substitution reactions of $[Ni(bicyclo[12\text{-}12]N_4O)(H_2O)]^{3+}$ proceed via an interchange dissociative mechanism.

5.6.1.2 The origin of the protonation equilibria for the substitution reaction

A possibility for an acid dependence is that the water molecule in the axial site is involved in a protonation/deprotonation equilibrium prior to substitution. Deprotonation is unlikely, since coordinated hydroxo groups are less labile than coordinated water. This process at the water molecule would therefore lead to decreased rates of reaction at low acid strengths, which is opposite to what has been observed in the above reaction.

There are three possible sites for protonation in the ligand, bicyclo[12-12]N_4O, namely the ether oxygen, the secondary amines, and the tertiary amines. When coordinated, it is unlikely that all of these sites could be protonated, since the lone pair of the donor is already involved in coordination to the metal. Therefore for protonation to occur, the donor must first dissociate from the metal ion.

Ether oxygen donors are very poor bases, so under the acid conditions present, it is very unlikely that the oxygen donor could be protonated. The proposed structure of the $[Ni(bicyclo[12\text{-}12]N_4O)]^{3+}$ complex would also make the lone pair of the ether oxygen virtually inaccessible to a proton. This suggests that the protonation reaction must be occuring at one of the amine sites. A proposed reaction scheme for the chloride substitution of $[Ni(bicyclo[12\text{-}12]N_4O)(H_2O)]^{3+}$ is shown in Figure 5.10.

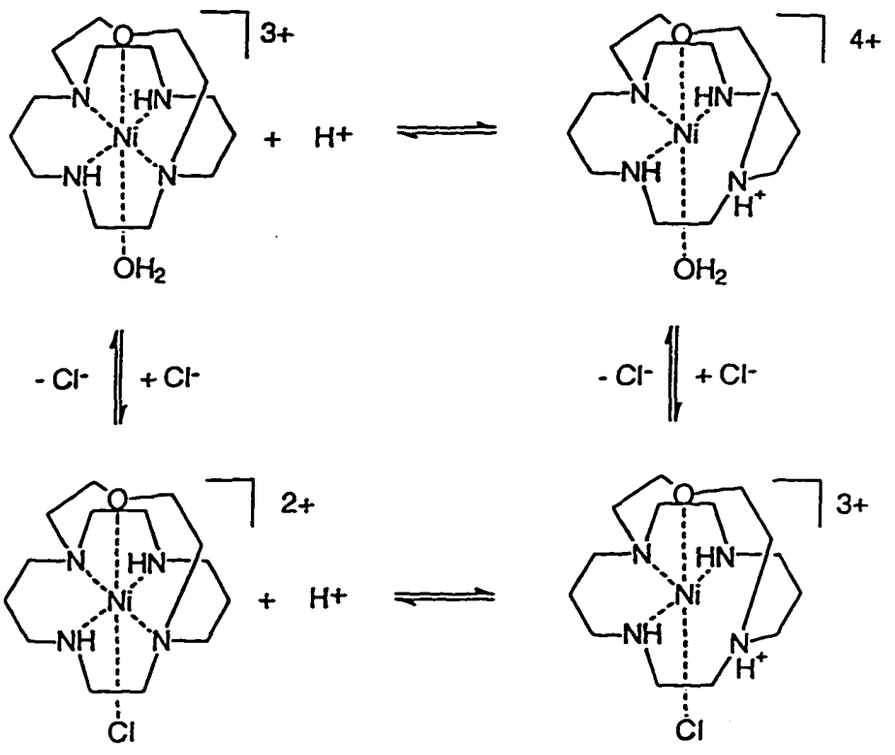

Figure 5.10: Protonation and substitution equilibria of $[Ni(bicyclo[12\text{-}12]N_4O)]^{3+}$ complex

Structural studies of the $[Ni^{II/III}(cyclam)X_2]^{n+}$ complexes[138] have shown that the oxidation of Ni^{II} to Ni^{III} results in the contraction of the tetraaza macrocycle. Ni^{III} (d^7) is Jahn-Teller distorted, therefore the equatorial bond distance contracts to a greater extent than the axial

bond distances. In the $[Ni(bicyclo[12\text{-}12]N_4O)]^{3+}$ complex, it is proposed that the equatorial contraction of the M-N bond lengths will distort the macrocyclic ligand and result in strain, especially at the bridged tertiary nitrogens. Protonation at one of the tertiary amines would diminish the strain, which may account for the low pK values observed for the protonation of the complex.

5.7 Conclusions

The acid dependence of the substitution reaction of $[Ni(bicyclo[12\text{-}12]N_4O)(H_2O)]^{3+}$ appears to be the same as that previously observed for the $[Ni(bicyclo[9\text{-}14]N_4O)(H_2O)]^{3+}$ complex. The origin of the protonation reaction is unclear, but does not appear to be due to protonation of the ether donor atom. Further studies are required to examine whether the acid dependence is general for Ni^{III} complexes with square planar tetradentate macrocycles, or is specific to bicycles of the type synthesised by this group.

CHAPTER 6

CONCLUSIONS AND SUGGESTIONS FOR FURTHER STUDIES

The synthetic procedures for several macrocycles have been recorded, along with procedures for the synthesis of several complexes of these ligands. The ligands and complexes have been characterised and the properties examined.

Further characterisation of the $[Co([10]aneN_2O)_2]^{3+}$ complex is required, as well as studies of the redox properties of this complex. The complex maybe suitable for examining the electron transfer rate exchange for the $Co^{III/II}$ couple by NMR methods. The $[Co([10]aneN_2O)_2]^{2+}$ complex may show a temperature dependent high spin - low spin equilibrium, as observed for the $[Co([9]aneN_2O)_2]^{2+}$ complex.[58a] The chromium complex of $[10]aneN_2O$ should be studied, since Cr^{III} is a hard metal, and should form stable complexes with the tridentate ligands. Unlike the softer late transition metals, the ether oxygen donor should form a strong bond with this metal.

The cobalt(III) and palladium(II) complexes of bicyclo[12-12]N_4O should be synthesised. The cobalt(III) complex would be ideal for examination of base hydrolysis kinetics and substitution kinetics as part of a series of kinetic investigations already under way in these laboratories. It would be interesting to examine whether the structure of the ligand would induce five coordinate geometry in the palladium(II) complex, since the structure of the ligand will hold the oxygen donor in the axial position close to the metal centre. The analogous ligand with a sulfur donor or a nitrogen in the axial position would be more likely to induce coordination in the axial position, and is currently under investigation.

The three bicyclic ligands, bicyclo[9-14]N_4X, bicyclo[10-14]N_4X, bicyclo[12-12]N_4X, where X = N, O, S, are suitable for examining the effect of structure on complex geometry, electronic and EPR spectra and redox processes. The three ligands have the same donor set, and are all capable of pentacoordinate geometry, so the structure of the complexes formed is governed by how the ligand backbone alters the donor position around the central metal ion.

Further investigation into the complexation of tricyclo[10-14-10]N_4O_2 is required. Crystal structures are required to determine the absolute configuration of this ligand, and investigation into the complexation of the *syn* and *anti* forms of the ligand should be examined. The synthesis of analogous complexes of the tricyclic ligand with nitrogen and sulfur donors is currently being investigated. A tricyclic ligand with propyl bridged donor atoms (Figure 6.1) has been synthesised and the complexation studies of this ligand are underway. It is possible that the larger size of this ligand may result in easier complexation to transition metals, since the steric hindrance imposed by the ligand will be reduced.

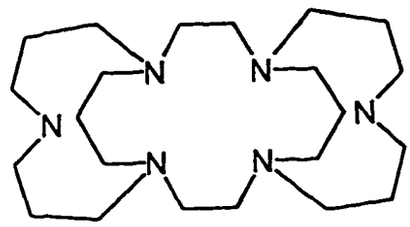

Figure 6.1: Tricyclo[12-14-12]N_6 (1,4,8,12,15,19-hexaazatricyclo[13.7.3.3]docosane)

The structure of the (N_4O_2tricycle) should be determined, since this ligand is one of the smallest cage ligands with six donors arranged in a manner that would enforce octahedral geometry. The synthesis of other transition metal complexes should be undertaken, and their structures determined. The protonation of the (N_4O_2tricycle) may compete with the metal ions for ligand binding, and should be investigated.

Should it prove possible to synthesise the nickel complex of tricyclo[10-14-10]N_4O_2, this ligand could be used as a one electron transfer reagent, provided that the Ni^{III} complex is sufficiently stable.

It may be possible to synthesise the $[Ni(tricyclo[10\text{-}14\text{-}10]N_4O_2)]^{2+}$ by using rigorously anhydrous conditions. Under these conditions there would be no competition with the protonated complex which may inhibit incorporation of the metal ion in the ligand.

The $[Cu(tricyclo[10\text{-}14\text{-}10]N_4O_2)]^{2+}$ complex may also find value as a copper sequestering agent, since the complex formed is kinetically very stable. The sulfur donor analogue of this ligand may result in an even more stable complex, since the sulfur donors have π donor capabilities which are known to stabilise Cu^{I} species.

The $[Co([10]aneS_2N)_2]^{3+/2+}$ electron transfer self-exchange reaction should be investigated. This reaction may provide insight into why no exchange was observed on the ^{59}Co NMR timescale for $[Co([10]aneS_2N$ earmuff$)]^{3+/2+}$ reaction. Crystal structures of the

[Co([10]aneS$_2$N earmuff)]$^{3+}$ and [Co([10]aneS$_2$N earmuff)]$^{2+}$ complexes would indicate whether there is a major difference in the structure of these two complexes, which would contribute to a larger than expected barrier to electron transfer due to rearrangement of the ligand during the electron transfer process.

CHAPTER 7

EXPERIMENTAL METHODS

7.1 Synthesis of Macrocyclic Ligands and Transition Metal Complexes

All starting materials used for syntheses were commercial reagent grade compounds, unless otherwise stated. DMF and acetonitrile was dried over calcium hydride and distilled prior to use. CaH has been found to decompose DMF.[139] Therefore, DMF was dried by standing over CaH at room temperature for no more than 24 hours, before distillation under reduced pressure. Compounds purchased were used without further purification.

CAUTION: Perchlorate salts used in the syntheses are potentially hazardous. Extreme care should be taken while working with these compounds.

7.1.1 Synthesis of common reagents

7.1.1.1 Lithium perchlorate

$LiClO_4$ was prepared by slow addition of solid Li_2CO_3 to aqueous $HClO_4$ until the aqueous solution was just neutral. The $LiClO_4$ was recrystallised three times from water. An approximately 3M stock solution was standardised by passing 0.4 mL through a Dowex 50W-X8 cation exchange column (7x2.5cm) in the H^+ form. The column was rinsed with deionised water until the eluent was neutral. The eluent was titrated with a standardised 0.1 M NaOH solution using phenolphthalein as the indicator.

7.1.1.2 Hexaaquacobalt(III)

A glass electrolysis cell was filled with 4 M $HClO_4$ in the cathodic compartment, and a solution of 0.4 g $Co(ClO_4)_2 \cdot 6H_2O$ in 100 mL 4 M $HClO_4$ in the anodic compartment. Using

platinum wire electrodes, the solution was oxidised at a potential of 4 V for 24 hours. While electrolysing, the solution was placed in a refrigerator. The concentration of the blue solution was determined spectrophotometrically ($\epsilon_{605nm} = 35.3\ M^{-1}cm^{-1}$).[140]

7.1.2 Synthesis of 1-oxa-4,8-diazadecane ([10]aneN$_2$O) (1)

7.1.2.1 Synthesis of 1,3-*bis*(p-tolylsulfonyl)propylenediamine (2)

1,3-*bis*(p-tolylsulfonyl)propylenediamine was synthesised as described previously.[64]

^{1}H NMR (360MHz) ($CDCl_3$): δ 1.66 (m, 2H, CH_2-C), 2.42 (s, 3H, CH_3), 3.01 (q, 2H, CH_2-N) 4.80 (t, 1H, NH) 7.31, 7.72 (d, 2+2H, Ar)

^{13}C NMR (90.6MHz) ($CDCl_3$): δ 21.6 (CH_3-Ar), 30.1 (CH_2-C), 38.0 (CH_2-N), 127.1, 129.9, 136.9, 143.7 (Ar)

7.1.2.2 Synthesis of *bis*-(2-(p-tolylsulfonyl)oxyethyl)ether (3)

Bis-(2-hydroxyethyl)ether (34.7 mL, 0.36 mol) was dissolved in 1 L dichloromethane in a 3 necked 2 L round bottom flask. The solution was cooled to 0°C, under a positive nitrogen pressure, and triethylamine (150 mL, 1 mol) was added dropwise. Over a period of 45 minutes, p-toluene sulfonyl chloride (137 g, 0.72 mol) in 500 mL dichloromethane was added. The reaction was stirred for 12 hours, initially at 0°C, then after gradual warming, at room temperature. The hydrochloride salt formed was removed by filtration, and the filtrate was washed with 750mL 2M HCl. The organic fraction was removed, and further washed with 3 x 250ml water, then with 250mL saturated aqueous sodium carbonate solution. The organic layer was dried with anhydrous sodium sulphate, and reduced to dryness. The residue

was recrystallised from hot methanol.

Yield = 127 g (85%)

^{1}H NMR (360MHz) ($CDCl_3$): δ 2.28 (s, 3H, CH_3), 3.51, 3.95 (d, 2+2H, CH_2-O), 7.26, 7.58 (d, 2+2H, Ar)

^{13}C NMR (90.6MHz) ($CDCl_3$): δ 21.6 (CH_3-Ar), 68.6 (CH_2-OTs), 68.9 (CH_2-O), 127.8, 129.8, 132.7, 144.9 (Ar)

MS (CI): m/z 415 (M+1)

7.1.2.3 Synthesis of 4,8-*bis*-(p-tolylsulfonyl)-1-oxa-4,8-diazadecane (4)

To a 5L 3-necked round bottom flask was added a solution of 1,3-(propylenediamine) ditosylate (76.4 g, 0.2 mol) in 3 L of DMF (dimethylformamide). The DMF was previously dried over calcium hydride, and freshly distilled under vacuum. The flask was fitted with an overhead stirrer, condenser, and flushed with nitrogen. Sodium hydride (60% suspension in mineral oil) (20 g, 0.4 mol) was added to the reaction vessel and stirred until the evolution of gas was complete. The solution was then heated up to 120°C, and *bis*-(2-(p-tolylsulfonyl)oxyethyl)ether (82.8 g, 0.2 mol) dissolved in 1L dry DMF was added dropwise to the vigorously stirred mixture over a period of 10 hours. The reaction mixture was then kept at 120°C for a further 12 hours. The solution was cooled, and filtered, then reduced under vacuum to a volume of 400 mL. Some of the product crystallised out of solution during this period. The slurry was added slowly to a rapidly stirred ice-water mixture (3 L). A sticky white precipitate formed immediately. The slurry was stirred for 10 minutes, then filtered. The precipitate was allowed to dry, then triturated with hexane to remove the

mineral oil. The solid was redissolved in approximately 3 L of hot methanol. Any undissolved material was filtered off. A white solid crystallised out of solution as the methanol cooled. A second crop was obtained by reducing the filtrate to approximately half the original volume.

Yield = 57 g (63%)

^{1}H NMR (360MHz) ($CDCl_3$): δ 2.23 (m, 2H, CH_2-C) 2.41(s, 3H, CH_3), 3.23 (m, 2+2H, CH_2-N), 3.74 (t, 2H, CH_2-O), 7.28, 7.64 (d, 2+2H, Ar)

^{13}C NMR (90.6MHz) ($CDCl_3$): δ 21.4 (CH_3-Ar), 29.6 (CH_2-C), 47.9 (CH_2-CH_2-CH_2-N), 51.2 (O-CH_2-CH_2-N), 70.3 (CH_2-O), 127.1, 129.7, 135.0, 143.4 (Ar)

MS (CI): m/z 452 (M+), 453 (M+1), 481 (M+29)

7.1.2.4 Detosylation of 4,8-*bis*-(p-tolylsulfonyl)-1-oxa-4,8-diazadecane to form 1-oxa-4,8-diazadecane ([10]aneN_2O) (1)

The ditosylate was dried under vacuum for at least 24 hours prior to detosylation. Concentrated sulfuric acid (20 mL) was heated to 140°C in a 100 mL round bottom flask. The ditosylate (10 g, 20 mmol) was added as a solid in small portions over a 15 minute period. The solution was stirred until the reaction was determined to be complete. (This can be determined by dropping a small portion of the solution into water. The absence of a white precipitate suggests the reaction is complete.) The reaction mixture was immediately cooled to room temperature, and added dropwise to 100 mL of ice-cold ethanol. 700 mL diethyl ether was added to complete the precipitation. The hygroscopic salt was removed by filtration, washed with diethyl ether, and transferred immediately to a beaker. Once the ether

had evaporated, the brown semi-solid was dissolved in 30 mL water and the pH was adjusted to 14 with sodium hydroxide pellets. The aqueous solution was continuously extracted with $CHCl_3$ over a period of 15 hours. The $CHCl_3$ layer was dried with anhydrous sodium sulphate, filtered and the solvent removed. The yellow oil was further dried under vacuum for 12 hours and used without further purification.

Yield = 1,5 - 2 g (~50 - 60%)

^{1}H NMR (360MHz) ($CDCl_3$): δ 1.54 (m, 2H, CH_2-C), 2.80 (m, 2+2H, CH_2-N), 3.59 (t, 2H, CH_2-O)

^{13}C NMR (90.6MHz) ($CDCl_3$): δ 27.2 (CH_2-C), 47.6 (CH_2-CH_2-CH_2-N), 48.8 (O-CH_2-CH_2-N), 69.4 (CH_2-O)

MS (CI): m/z 145 (M+1)

IR: 3272 cm^{-1} (NH stretch)

7.1.2.5 Synthesis of [10]aneN_2O·2HCl (5)

The free ligand [10]aneN_2O was dissolved in 25 mL ethanol, and ethanolic 6 M HCl was added dropwise until the pH of the solution was approximately 1. The solution was reduced in volume to about 10mL, then ether was added until precipitation commenced. The solution was allowed to cool overnight in the freezer to give pale yellow hygroscopic crystals.

Yield (from **4**) = 3.49 g (72.9%)

^{1}H NMR (300MHz) (D_2O): δ 2.05 (m, 2H, CH_2-C), 3.21 (m, 2+2H, CH_2-N), 3.80 (t, 2H, CH_2-O)

^{13}C NMR (75.5MHz) (D_2O): δ 22.8 (CH_2-C), 43.7 (CH_2-CH_2-CH_2-N), 46.0 (O-CH_2-CH_2-

N), 66.0 (CH_2-O)

MS (FAB): m/z 145.0 ($L+H^+$), 325.1 ($L_2+2H^++Cl^-$), 505.2 ($L_3+3H^++Cl^-$)

7.1.3 Synthesis of $[Cu([10]aneN_2O)_2](ClO_4)_2$ (6)

[10]aneN_2O (1.1 g, 7.6 mmol) was dissolved in 25 mL water, and $Cu(ClO_4)_2 \cdot 6H_2O$ (1 g, 2.7 mmol) was added. The solution turned a purple colour immediately, and was heated at 80°C for 1 hour to ensure complete complexation. The solution was allowed to cool overnight, during which time purple crystals formed. The crystals were removed by filtration, and washed with ethanol, then diethyl ether, and air dried. X-ray quality crystals were grown by diethyl ether diffusion into an acetonitrile solution of the crystals.

Yield = 0.95 g (65%)

UV/Vis (water): 265 nm ($\epsilon = 4620\ M^{-1}cm^{-1}$), 581 nm ($\epsilon = 50\ M^{-1}cm^{-1}$)

MS (FAB): m/z 207.0 ($Cu^{2+}(L-H^+)$), 306.0 ($Cu^{2+}L(ClO_4^-)$), 351.1 ($Cu^{2+}(L_2-2H^+)$), 450.1 ($Cu^{2+}L_2(ClO_4^-)$)

MS (Electrospray): m/z 145.1 (LH^+), 207.0 ($[Cu^{II}(L-H^+)]^+$)

Elemental analysis: Calculated(found) for $Cu(L)_2(ClO_4)_2(H_2O)$ % C 29.56 (29.11) H 6.02 (6.07) N 9.85 (9.28)

7.1.4 Synthesis of $[Ni([10]aneN_2O)_2](ClO_4)_2$ (7)

A solution of 0.67 g (1.83 mmol, 1eq) $Ni(ClO_4)_2 \cdot 6H_2O$ in 25 mL methanol was added to 0.56 g of [10]aneN_2O (3.8 mmol, 2.1eq) dissolved in 25 mL methanol. The solution was refluxed for 24 hours. A blue precipitate formed initially; however, after about 5 hours of refluxing,

a lilac precipitate started to form. After 24 hours, both a lilac precipitate and a green solution were present. The lilac precipitate is removed by filtration and washed with methanol. The precipitate was recrystallised from an acetonitrile/ether mixture.

Yield = 0.588 g (59%)

UV/Vis (water): 359 nm (ϵ = 13 $M^{-1}cm^{-1}$), 543 nm (ϵ = 20 $M^{-1}cm^{-1}$), 868 nm (ϵ = 6 $M^{-1}cm^{-1}$)

MS (FAB): m/z 301.0 ($[Ni^{II}L(ClO_4^-)]^+$), 455.1 ($[Ni^{II}L_2(ClO_4^-)]^+$)

Elemental analysis: Calculated(found) for $Ni(L)_2(ClO_4)_2$ % C 30.80 (30.82) H 5.91 (5.84) N 10.26 (10.15)

7.1.5 Synthesis of $[Pd([10]aneN_2O)_2](PF_6)_2$ (8)

A solution of palladium acetate (137 mg, 0.61 mmol) in 20 mL acetonitrile was added dropwise to a 20 mL solution of [10]aneN_2O (220 mg, 1.53 mmol) in acetonitrile. Both solutions had previously been degassed by bubbling with nitrogen, and were kept under a nitrogen atmosphere. The mixture was stirred overnight, and then refluxed for 1 hour. After filtration of the reaction mixture, the solvent was reduced to approximately 10 mL and a solution of 5 mL of saturated ammonium hexafluorophosphate in acetonitrile was added. Diethyl ether was allowed to diffuse into the acetonitrile solution. Pale yellow crystals formed which were filtered off and washed with ether.

Yield = 110 mg (26%)

UV/Vis (acetonitrile): 310 nm (ϵ = 350 $M^{-1}cm^{-1}$), 414 nm (sh)

^1H NMR (360MHz) (CD_3CN): δ 2.08 (m), 2.44 (m), 2.92 (m), 3.78 (m), 4.27 (m), 5.26 (br)

^{13}C NMR (90.6MHz) (CD_3CN): δ 28.5 (CH_2-C), 49.8 (CH_2-CH_2-CH_2-N), 53.5 (O-CH_2-CH_2-N), 70.0 (CH_2-O)

MS (FAB): m/z 393.1 ($[Pd^{II}(L_2\text{-}H^+)]^+$), 539.2 ($[Pd^{II}L_2(PF_6^-)]^+$)

Elemental Analyses: Calculated(found) for $Pd(L)_2(PF_6)_2(CH_3CN)$ % C 26.46(25.87), H 4.86(4.81), N 9.65(9.65)

7.1.6 Synthesis of $[Pd([10]aneN_2O)_2](BF_4)_2$ (9)

[10]aneN_2O (0.22 g, 1.53 mmol) was dissolved in 20 mL dry acetonitrile, and purged with nitrogen gas for 10 minutes. Solid $[Pd(CH_3CN)_4](BF_4)_2$ (0.3 g, 0.68 mmol) was added directly to the solution, which was refluxed under a nitrogen atmosphere for 1.5 hours. The solution was filtered, and the volume reduced to 2 mL. Yellow crystals formed on diffusion of diethyl ether into the acetonitrile solution. These were removed, and recrystallised from a nitromethane/ether solution, then further recrystallised from a second acetonitrile/ether solution.

Yield = 60 mg (16%)

^1H NMR (300MHz) (CD_3CN): δ 2.05 (m), 2.25 (m), 2.52 (m), 2.77 (m), 2.90 (m), 3.70, 4.11 (m), 4.49 (br)

^{13}C NMR (90.6MHz) (CD_3CN): δ 28.2 (CH_2-C), 47.6 (CH_2-CH_2-CH_2-N), 52.1 (O-CH_2-CH_2-N), 65.7 (CH_2-O)

MS (FAB): m/z 249.0 ($[Pd(L\text{-}H^+)]^+$), 393.1 ($[Pd(L_2\text{-}H^+)]^+$), 480.2 ($[PdL_2(BF_4^-)]^+$)

MS (ES): m/z 145.1 (LH^+), 249.0 ($[Pd^{II}(L\text{-}H^+)]^+$), 393.1 ($[Pd(L_2\text{-}H^+)]^+$)

UV/Vis (acetonitrile): 309 nm ($\epsilon = 359\ M^{-1}cm^{-1}$), 414 nm ($\epsilon = 31.2\ M^{-1}cm^{-1}$)

Elemental Analysis: Calculated(found) for $Pd(L)_2(BF_4)_2.½CH_3CN$ % C 30.59(30.79), H 5.73(5.85), N 10.70(10.15)

7.1.7 Synthesis of $[Co([10]aneN_2O)_2](ClO_4)_3$ (10)

$[10]aneN_2O$·2HCl (2.02 g, 9.3 mmol, 2.5eq) was dissolved in 50mL water. Solid $Na_3[Co(CO_3)_3]$[141] (1.14 g, 3.7 mmol) was added directly to the ligand solution, and refluxed for 5 hours. The solution was cooled and filtered. The complex was purified by Sephadex CM-C25 column chromatography, eluting with 0.1 M $NaClO_4$. The major maroon band was reduced in volume until the excess $NaClO_4$ crystallised and was removed by filtration.

7.1.8 Synthesis of 1,2-*bis*(1-oxa-5,8-diazacyclodecanyl)ethane ($[10]aneN_2O$ earmuff) (13)

$[Cu([10]aneN_2O)_2](ClO_4)_2$ (1.05 g, 1.9 mmol) was dissolved in 50 mL water. 1,2-dibromoethane (0.20 mL, 2.3 mmol) and sodium carbonate (0.5 g, 4.7 mmol) were added directly, and the two phase mixture was refluxed for 24 hours. The solvent and unreacted dibromoethane was removed under vacuum, and the residue was redissolved in water. The royal blue complex formed was purified by column chromatography (Sephadex CM-C25, 0.2 M $NaClO_4$ eluent). The column fractions were taken to dryness, and the product was separated from the $NaClO_4$ by extraction with 100% ethanol. The complex was recrystallised by diffusion of diethyl ether into an ethanol solution and identified as $[Cu([10]aneN_2O$ earmuff)$](ClO_4)_2$ (12)

Yield = 0.33 g (30%)

UV/Vis (water): 289 nm (ϵ = 6057 $M^{-1}cm^{-1}$), 587 nm (ϵ = 172 $M^{-1}cm^{-1}$)

MS (FAB): m/z 377.2 ($[Cu^{II}(L\text{-}H^{+})]^{+}$), 476.2 ($[Cu^{II}(L)(ClO_4^{-})]^{+}$)

Elemental Analysis: Calculated(found) for $Cu(L)(ClO_4)_2(H_2O)$ C 32.30(31.98), H 6.10(5.83), N 9.42(9.31)

The free ligand (**13**) was obtained by dissolving the copper complex (100 mg) in 20 mL water, and adding excess sodium sulfide (approximately 1 g). After complete bleaching of the solution (approximately 30 minutes), the copper sulfide formed was removed by gravity filtration. Sodium hydroxide (2 g) was added to the solution, and the free ligand was extracted with 5x20 mL dichloromethane. The organic fraction was dried with anhydrous sodium carbonate, and the solvent removed to give a pale yellow oil. Yields of approximately 50% for the free ligand were obtained.

^{1}H NMR (360MHz) ($CDCl_3$): δ 1.60 (m, 2H, CH_2-C), 2.65 (m, 6H, CH_2-N), 2.78, 2.88 (t, 2+2H, CH_2-N), 3.63, 3.68 (t, 2+2H, CH_2-O)

^{13}C NMR (90.6MHz) ($CDCl_3$): δ 25.9 (C-CH_2-C) 47.2, 48.3, 54.2, 54.6, 56.1 (CH_2-N), 68.3, 70.6 (CH_2-O) (See Figure 3.7 for peak assignment)

7.1.9 Capping of 1,4,8,11-tetraazacyclotetradecane (cyclam) using *bis*-(2-(methylsulfonyl)oxyethyl)ether as the bridging molecule

7.1.9.1 Synthesis of *bis*-(2-(methylsulfonyl)oxyethyl)ether (14)

Triethylamine (104 mL, 0.8 mol) and *bis*-(2-hydroxyethyl)ether (23.7 mL, 0.25 mol) were dissolved in 1.5 L dichloromethane under a nitrogen atmosphere. The mixture was cooled

to -10°C on an ice/salt bath. Methanesulfonylchloride (46.5 mL, 0.6 mol) in 250 mL dichloromethane was added dropwise over a period of 2 hours. The mixture was stirred overnight at room temperature. The organic fraction was washed successively with 100 mL 1 M HCl, 3 x 100 mL water, and 100 mL saturated aqueous sodium carbonate. The organic layer was dried with anhydrous sodium sulphate, and the solvent removed under vacuum. The residue was recrystallised from hot methanol to give white crystals.

Yield = 53.8 g (82%)

^{1}H NMR (360MHz) ($CDCl_3$): δ 3.05 (s, 3H, CH_3), 3.79, 4.37 (t, 2+2H, CH_2-O)

^{13}C NMR (90.6MHz) ($CDCl_3$): δ 37.6 (CH_3), 68.6 (CH_2-OMs), 68.9 (CH_2-O)

MS (CI): m/z 263 (M+1)

7.1.9.2 Synthesis of 17-oxa-1,4,8,11-tetraazabicyclo[6.6.5]tetradecane (bicyclo[12-12]N_4O) (17)

A slurry of sodium carbonate (10 g) in THF, dried over molecular sieves, was placed under an atmosphere of nitrogen. To this slurry was added cyclam[142] (1 g, 5 mmol) and *bis*-(2-(methylsulfonyl)oxyethyl)ether (1.3 g, 5mmol). The mixture was refluxed for 10 days then filtered. The solvent was removed from the filtrate under reduced pressure to give a crude mixture of the products, which was purified by formation of the copper complexes. The crude ligand mixture was redissolved in acetonitrile. $Cu(ClO_4)_2 \cdot 6H_2O$ (1.85 g, 5 mmol) in acetonitrile was added, and the mixture refluxed for 1hr. The acetonitrile was removed under reduced pressure, and the residue redissolved in water, then filtered. The copper complexes were purified using a Sephadex CM-C25 column, eluting with 0.1 M sodium perchlorate. A

long column was required to separate the complexes (3 x 30 cm). The major purple band was isolated and recrystallised from the sodium perchlorate solution, and identified as $[Cu(bicyclo[12\text{-}12]N_4O)](ClO_4)_2$ (**15**). In order to obtain pure $[Cu(bicyclo[12\text{-}12]N_4O)](ClO_4)_2$ without the presence of small amounts of $[Cu(N_4O_2tricycle)](ClO_4)_2$ impurity, the crude ligand mixture was dissolved in 25 mL 1 M HCl, and washed with 5 x 20 mL dichloromethane. The water layer was then basified to pH 13 with NaOH, then extracted into dichloromethane (5 x 20 mL). The dichloromethane layer was dried with Na_2SO_4, and taken to dryness. The complexation reaction was performed in water rather than acetonitrile. Under these conditions, the tricyclic copper complex does not form.

Yield = 1.37g (52%)

UV/Vis (water): 280 nm (ϵ = 4860 $M^{-1}cm^{-1}$), 537 nm (ϵ = 185 $M^{-1}cm^{-1}$)

MS (FAB): m/z 333.1 ($[Cu^{II}(L\text{-}H^+)]^+$ and $[Cu^{I}L]^+$), 432.1 ($[Cu^{II}L(ClO_4^-)]^+$)

MS (ES): m/z 166.6 ($[Cu^{II}L]^+$), 271.2 (LH^+), 332.1 ($[Cu^{II}(L\text{-}H^+)]^+$), 432.1 ($[Cu^{II}L(ClO_4^-)]^+$)

Elemental Analyses: Calculated(found) for $Cu(L)(ClO_4)_2(H_2O)$ % C 30.52(30.48), H 5.86(5.37), N 10.17(9.73)

The copper complex was redissolved in a minimum amount of water, and excess sodium sulfide was added. The copper(II) ion precipitated as a sulfide almost immediately. The solution was allowed to stand for half an hour, after which complete decolourisation had occurred. The copper sulfide was removed by gravity filtration, and 2 g of sodium hydroxide was added. The ligand was extracted from the aqueous layer using dichloromethane. After drying of the organic layer, and removal of the solvent, a yellow oil was obtained.

Bicyclo[12-12]N_4O:

Yield = 0.608 g (45%) (Based on yield from cyclam)

^1H NMR (300MHz) ($CDCl_3$): δ 1.38, 1.51 (m, 2+2H, CH_2-C), 2,35 (m, 20H, CH_2-N), 3.20, 3.36 (m, 2+2H, CH_2-O)

^{13}C NMR (75.5MHz) ($CDCl_3$): δ 25.5 (CH_2-C), 47.9, 51.0, 53.3, 53.6, 57.6 (CH_2-N), 67.5 (CH_2-O) (For peak assignments see Figure 3.16)

MS (CI): m/z 270 (M+), 271 (M+1), 299 (M+29), 311 (M+41)

7.1.10 Synthesis of [Ni(bicyclo[12-12]N_4O)]$(ClO_4)_2$ (18)

To a solution of bicyclo[12-12]N_4O (0.61 g, 0.2 mmol) in 25 mL acetonitrile, was added $Ni(ClO_4)_2 \cdot 6H_2O$ (0.73 g, 0.2 mmol) in 10 mL acetonitrile. The solution was refluxed for 24 hours, after which it was evaporated to dryness. The residue was redissolved in water and gravity filtered. The crude complex was purified on Sephadex CM-C25, eluting with 0.1 M $NaClO_4$. The pale purple $[Ni(bicyclo[12\text{-}12]N_4O)]^{2+}$ complex ion was separated from an initial blue band identified as $[Cu(N_4O_2tricycle)]^{2+}$ (16). The complexes were recrystallised from aqueous sodium perchlorate solution.

Yield = 0.44 g (42%)

UV/Vis (water): 339 nm ($\epsilon = 7\ M^{-1}cm^{-1}$), 520 nm ($\epsilon = 4.9\ M^{-1}cm^{-1}$), 1077 nm ($\epsilon = 2.5\ M^{-1}cm^{-1}$)

(acetonitrile): 326 nm ($\epsilon = 17\ M^{-1}cm^{-1}$), 498 nm ($\epsilon = 8\ M^{-1}cm^{-1}$), 722 nm ($\epsilon = 3\ M^{-1}cm^{-1}$), 953 nm ($\epsilon = 4\ M^{-1}cm^{-1}$)

MS (FAB): m/z 327.1 ($[Ni^{II}(L\text{-}H^+)]^+$), 427.1 ($[Ni^{II}(L)(ClO_4^-)]^+$)

Elemental analyses: Calculated(found) for $Ni(L)(ClO_4)_2.½CH_3CN$ % C 32.84(33.27), H 5.79(5.91), N 11.49(10.92)

7.1.11 Synthesis of 7,16-dioxa-1,4,10,13-tetraazatricyclo[11.5.3.3]octadecane (11)

7.1.11.1 Synthesis of 4,8-(dichloroacetyl)-1-oxa-4,8-diazadecane (19)

[10]aneN_2O (2 g, 14 mmol) was dissolved in 450 mL dichloromethane/50 mL water in a 2 L 3 necked flask. The vessel was placed under nitrogen, and cooled to 0°C. With rapid stirring, chloroacetyl chloride (10 mL, 62 mmol) in 250 mL dichloromethane and potassium carbonate (18 g, 65 mmol) in 250 mL water were added dropwise at the same rate over a period of 2 hours. After addition was complete, the solution was allowed to warm up to room temperature, and stirred for a further 2 hours. The aqueous layer was removed, and the organic layer washed with water (2x200 mL). The organic layer was dried with anhydrous sodium sulphate, and the solvent removed under reduced pressure. The residue was recrystallised from hot methanol.

Yield = 2 g (82%)

^{1}H NMR (300MHz) ($CDCl_3$): δ 2.20, 2.31 (m, 2H, CH_2-C), 3.50, 3.58 (m, 2+2H, CH_2-N), 3.68, 3.75 (m, 2H, CH_2-Cl), 4.12 (m, 2H, CH_2-O)

^{13}C NMR (90.6MHz) ($CDCl_3$): δ 27.9, 28.6 (CH_2-C), 40.8, 41.0, 41.3, 41.4 (CH_2-O), 46.2, 46.7, 46.8 48.3, 49.36, 49.40, 49.9, 50.1 (CH_2-N), 68.0, 69.5, 70.0, 70.3 (CH_2-Cl), 166.7, 167.1, 167.2 (C=O)

MS (CI): m/z 298 (M+1), 326 (M+29), 338 (M+41)

7.1.11.2 Synthesis of 7,16-dioxa-1,4,10,13-tetraazatricyclo[11.5.3.3]octadecane *bis*-amide (Tricyclo[10-14-10]N_4O_2 *bis*-amide) (20)

Into a 4 necked round bottom flask, fitted with a condenser, nitrogen inlet, and a high-speed overhead stirrer, was placed 4 L of dry acetonitrile and sodium carbonate (10 g, 94 mmol). The apparatus was fitted with tubing from a syringe pump. [10]aneN_2O (1.6g , 11.4 mmol) and 4,8-(dichloroacetyl)-1-oxa-4,8-diazadecane (3.4 g, 11.4 mmol) each in 200 mL dry acetonitrile were added dropwise at an equivalent rate over a period of 48 hours. The reaction mixture was then heated for a further 12 hours. The white solid was removed by filtration, and the solvent was removed under reduced pressure. The residue was recrystallised from a minimum amount of hot acetonitrile, to give a white crystalline solid.

Yield = 2.6 g (62%)

^{1}H NMR (300MHz) ($CDCl_3$): δ 1.46, 2.10 (m, CH_2-C), 2,52, 2.89, 3.27 (m, CH_2-N), 3.76, 4.08 (m, CH_2-O)

^{13}C NMR (75.5MHz) ($CDCl_3$): δ 23.2, 27.5 (CH_2-C), 45.4, 46.1, 56.3, 61.9, 62.1 (CH_2-N), 72.0, 73.4 (CH_2-O), 170.5 (C=O)

MS (CI): m/z 368 (M+), 369 (M+1), 397 (M+29), 409 (M+41)

7.1.11.3 Synthesis of 7,16-dioxa-1,4,10,13-tetraazatricyclo[11.5.3.3]octadecane (Tricyclo[10-14-10]N_4O_2) (11)

The *bis*-amide (0.3 g) was dried under vacuum for 24 hours. While on ice, diborane (1 M solution in THF) (15 mL) was added to the amide under nitrogen. The solution was then refluxed under nitrogen for 24 hours. The reaction mixture was cooled on ice, and excess

diborane destroyed by the slow addition of water. The THF solvent was removed, and 25 mL 6 M aqueous HCl was added. The slurry was refluxed for 3 hours, during which time the solid dissolved. The solution was basified by the addition of potassium hydroxide (pH 14), and extracted with 5 x 20 mL dichloromethane. The organic layers were combined, dried with anhydrous sodium sulfate, filtered and taken to dryness. The resulting pale yellow oil was used without further purification.

Yield quantitative

^{1}H NMR (300MHz) ($CDCl_3$): δ 1.16, 1.45 (m, 4H, CH_2-C), 2.14, 2.30 (24H, CH_2-N), 3.26, 3.38 (m, 8H, CH_2-O)

^{13}C NMR (75.5MHz) ($CDCl_3$): δ 28.1 (CH_2-C), 53.2 (CH_2-CH_2-CH_2-N), 53.4 (N-CH_2-CH_2-N), 54.5 (O-CH_2-CH_2-N), 65.7 (CH_2-O)

MS (CI): m/z 341 (M+1), 369 (M+29)

7.1.11.4 Synthesis of tricyclo[10-14-10]N_4O_2·2$HClO_4$ (21)

The free ligand, tricyclo[10-14-10]N_4O_2, was dissolved in water. To this was added 1 mL 0.1 M $HClO_4$. White crystals began to precipitate immediately. These were collected by filtration and recrystallised from hot water.

^{1}H NMR (300MHz) (D_2O): δ 1.82, 2.30 (m, 1+1H, CH_2-C), 2.60, 2.84, 3.1 (m, 8H, CH_2-N), 3.58 (m, 6H, CH_2-N and CH_2-O), 4.18 (m, 2H, CH_2-O)

^{1}H NMR (300MHz) (CD_3CN): δ 1.89, 2.35 (m, 1+1H, CH_2-C), 2.58, 2.73, 2.92, 3.17 (m, 8H, CH_2-N), 3.60 (m, 6H, CH_2-N and CH_2-O), 4.15 (m, 2H, CH_2-O), 8.82 (br, NH)

^{13}C NMR (75.5MHz) (D_2O): δ 19.0 (CH_2-C), 50.1 (C-C-CH_2-N), 53.1 (O-C-CH_2-N, N-C-

CH_2-N), 66.3 (CH_2-O)

^{13}C NMR (75.5MHz) (CD_3CN): δ 20.0 (CH_2-C), 51.3 (C-C-CH_2-N), 53.8 (O-C-CH_2-N, N-C-CH_2-N), 66.7 (CH_2-O)

MS(FAB): m/z 341.2 (LH^+), 441.2 ($[LH_2(ClO_4)]^+$)

7.1.12 Synthesis of $[Cu(tricyclo[10\text{-}14\text{-}10]N_4O_2)](ClO_4)_2$ (22)

Tricyclo[10-14-10]N_4O_2 (0.16 g, 4.8 mmol) was dissolved in 20 mL methanol. To this was added $Cu(ClO_4)_2 \cdot 6H_2O$ (0.178 g, 4.8 mmol) in 5 mL methanol. Initially a green precipitate formed, however, after 30 minutes of refluxing a royal blue solution formed, which was refluxed for a further 30 minutes. The solution was gravity filtered, and taken to dryness. The residue was redissolved in water, and purified by sephadex CM-C25 column chromatography, eluting with 0.1 M sodium perchlorate. The salt was further purified by slow evaporation of the aqueous sodium perchlorate solution to give royal blue crystals, which were further recrystallised by diethyl ether diffusion into an acetonitrile solution.

Yield = 0.265 g (92%)

UV/Vis (water): 314 nm (ϵ = 4930 $M^{-1}cm^{-1}$), 600 nm (ϵ = 147 $M^{-1}cm^{-1}$)

MS (FAB): m/z 341.2 (LH^+), 403.2 ($[Cu^{II}(L\text{-}H^+)]^+$ and $[Cu^{I}L]^+$), 502.1 ($[Cu^{II}(L)(ClO_4^-)]^+$)

MS (ES): m/z 171.1 ($[LH_2]^{2+}$), 201.6 ($[CuL]^{2+}$), 341.3 (LH^+), 403.2 ($[Cu^{II}(L\text{-}H^+)]^+$), 502.2 ($[Cu^{II}(L)(ClO_4^-)]^+$)

Elemental analysis: Calculated(found) for $Cu(L)(ClO_4)_2.½CH_3CN$ % C 36.60(36.45) H 6.06(5.95) N 10.11(9.41)

7.1.13 Synthesis of [Cu(tricyclo[10-14-10]N_4O_2)]($ZnCl_3H_2O$)$_2$ (23)

3M HCl (2 mL) was added to the [Cu(tricyclo[10-14-10]N_4O_2)](ClO_4)$_2$ residue (300 mg). Approximately 1 g of $ZnCl_2$ was added, and the mixture was heated to 80°C for 1.5 hours. Slow evaporation of the solution resulted in a viscous oil. Isopropanol was layered on top of the liquid, and allowed to diffuse into the solution. Blue plates, of X ray quality, formed over several days.

MS (ES): m/z 171.1 ($[LH]^{2+}$), 201.6 ($[CuL]^{2+}$)

MS (FAB): (negative ion) m/e 170.8 ($ZnCl_3^-$)

Elemental analysis: Calculated(found) for Cu(L)($ZnCl_3H_2O$)$_2$.½($CH_3CH_2CH_2OH$) % C 28.79(28.65) H 5.45(5.27) N 6.89(7.03)

7.1.14 Synthesis of [Cu(tricyclo[10-14-10]N_4O_2 *bis*-amide)](ClO_4)$_2$ (24)

Excess $Cu(ClO_4)_2.6H_2O$ was added to a solution of tricyclo[10-14-10]N_4O_2 *bis*-amide in acetonitrile. The solution was refluxed for 2 hours, after which the acetonitrile solution was filtered and the solvent removed under reduced pressure. The residue was dissolved in hot water, then filtered. Pale blue crystals formed on slow evaporation of the solution.

MS (FAB): m/z 289.0, 369.2 (L+1)

UV/Vis (water): 717 nm

7.1.15 Synthesis of 8-aza-1,5-dithiacyclodecane ([10]aneS_2N) (25)

7.1.15.1 Synthesis of 8-(p-tolylsulfonyl)-8-aza-1,5-dithiacyclodecane

The synthesis of tosyl-[10]aneS_2N was based on a previously published procedure.[61a] DMF

(freshly distilled over calcium hydride under reduced pressure) (2 L) and cesium carbonate (oven dried at 100°C overnight) (26.1 g, 80 mmol) was placed in a 5 L 3 necked flask fitted with a mechanical stirrer, condenser and a nitrogen inlet. The slurry was brought to a temperature of 60°C. A mixture of 2,2'-[(p-tolylsulfonyl)imino]*bis*(ethyl-p-tolylsulfonate)[64] (22.7 g, 40 mmol) and 1,3-propane dithiol (4 mL, 40 mmol) in 600 mL dry DMF was added dropwise to the slurry over a 24 hour period. The reaction was heated for a further 5 hours after addition was complete. The solution was filtered, and the volume of the filtrate reduced to approximately 100 mL. The solution was added slowly to a rapidly stirred ice/water mixture (2 L). The white solid formed was separated by filtration and air dried. The solid was recrystallised from hot ethanol to give white crystals.

Yield = 8.8 g (67%)

^{1}H NMR (300MHz) ($CDCl_3$): δ 1.87 (m, 2H, CH_2-C), 2.40 (s, 3H, CH_3), 3.06 (m, 2H, CH_2-N), 3.18 (m, 2+2H, CH_2-S), 7.28, 7,65 (d, 2+2H, Ar)

^{13}C NMR (75.5MHz) ($CDCl_3$): δ 21.4 (CH_3-Ar), 29.4 (CH_2-C), 31.3 (CH_2-CH_2-CH_2-S), 33.7 (N-CH_2-CH_2-S), 53.1 (CH_2-N), 127.6, 129.6, 133.7, 143.6 (Ar)

7.1.15.2 Detosylation of 8-(p-tolylsulfonyl)-8-aza-1,5-dithiacyclodecane to give 8-aza-1,5-dithiacyclodecane ([10]aneS_2N) (25)

Tosylated-[10]ane S_2N was dried under vacuum overnight prior to use. Phenol (6 g) was dissolved in 70 mL 30% hydrobromic acid in acetic acid, and added to tosyl-[10]aneS_2N (5.5 g, 17 mmol) in a round bottom flask fitted with a condenser and nitrogen inlet. The reaction mixture was stirred for 30 hours at 70°C. The solution was dropped in to an ice cold mixture

of ethanol/ether (100 mL/500 mL) that was vigorously stirred. A further 200 mL ether was added, and the pinkish solid was filtered off and air dried. The hydrobromide salt was dissolved in water and filtered, before adjusting the pH to 14 with sodium hydroxide. The free ligand was continuously extracted with chloroform for 24 hours. The chloroform layer was dried with anhydrous sodium sulphate, and evaporated to dryness to yield a yellow oil.

Yield = 1.94 g (66%)

^{1}H NMR (300MHz) ($CDCl_3$): δ 1.78 (m, 2H, CH_2-C), 2.68 (t, 2H, CH_2-N), 2.97 (m, 2+2H, CH_2-S)

^{13}C NMR (75.5MHz) ($CDCl_3$): δ 29.0 (CH_2-C), 30.2 (CH_2-CH_2-CH_2-S), 34.2 (N-CH_2-CH_2-S), 49.4 (CH_2-N)

7.1.16 Synthesis of $[Co([10]aneS_2N)_2](ClO_4)_2$ (26)

[10]aneS_2N (0.47 g, 27 mmol) was dissolved in 25 mL acetonitrile, and refluxed under nitrogen. $Co(ClO_4)_2 \cdot 6H_2O$ (0.45 g, 12 mmol) in 25 mL acetonitrile was added dropwise to the refluxing ligand solution, and refluxed for a further 2 hours. The solution was filtered, and evaporated to dryness. The residue was redissolved in hot water, then filtered, before bubbling with air for 1 hour. The aqueous solution was loaded onto a sephadex CM-C25 column, and two major orange bands were eluted with 0.1 M $NaClO_4$.

The first orange band (Isomer A) was recrystallised from aqueous sodium perchlorate to give orange/brown crystals. The second orange band (Isomer B), which was the major product formed, recrystallised to give orange crystals.

Isomer A (**26A**):

^{1}H NMR (300MHz) (D_2O): δ Multiplets between 1.8 and 3.65, 5.3 (m)

^{13}C NMR (75.5MHz) (D_2O): δ 15.7, 21.6, 28.2, 28.8, 32.6, 33.4, 37.0, 37.6, 40.5, 45.3, 52.0, 53.0, 54.3

MS (FAB): m/ez234.9 ($[Co^{II}(L\text{-}H^+)]^+$), 333.9 ($[Co^{III}(L\text{-}H^+)(ClO_4^-)]^+$), 412.0 ($[Co^{II}(L\text{-}H^+)(L)]^+$ and $[Co^{III}(L\text{-}H^+)_2]^+$), 510.9 ($[Co(L\text{-}H^+)(L)(ClO_4^-)]^+$)

Elemental Analysis: Calculated(found) for $Co(L_2)(ClO_4)_3$ % C 23.62(23.92), H 4.25(4.15), N 3.93(3.93)

UV/Vis (water): 272.6nm, 349.5nm, 484.8nm(sh)

Isomer B (**26B**):

^{1}H NMR (300MHz) (D_2O): δ Multiplets between 2.2 and 3.6

^{13}C NMR (75.5MHz) (D_2O): δ 15.4 (C-CH_2), 24.7, 25.8 (C-C-CH_2-S), 34.5, 34.9 (N-C-CH_2-S), 54.7, 56.0 (CH_2-N)

MS (FAB): m/z 412.0 ($[Co^{II}(L\text{-}H^+)]^+$ and $[Co^{III}(L\text{-}H^+)_2]^+$, 510.9 ($[Co^{III}(L\text{-}H^+)(L)(ClO_4^-)]^+$]

Elemental Analysis: Calculated(found) for $Co(L_2)(ClO_4)_3$ % C 23.62(23.71), H 4.25(4.22), N 3.93(3.89)

UV/Vis (water): 230 nm (ϵ = 10900 $M^{-1}cm^{-1}$), 275 nm (ϵ = 8875 $M^{-1}cm^{-1}$), 326 nm (sh), 355 nm (ϵ = 7210 $M^{-1}cm^{-1}$), 500 nm (ϵ = 235 $M^{-1}cm^{-1}$)

7.1.17 Synthesis of 1,2-*bis*(8-aza-1,5dithiacyclodecanyl)ethane ([10]aneS$_2$N earmuff) (27)

[10]aneS$_2$N (0.7 g, 4 mmol) was dissolved in 50 mL of dry acetonitrile. Sodium carbonate (2.12 g, 20 mmol) was added to form a slurry. 1,2-*bis*-(p-tolylsulfonyl)ethane[64] (0.73 g, 2 mmol) dissolved in 30 mL acetonitrile was added dropwise to the refluxing mixture under a positive nitrogen pressure. The mixture was refluxed for a further 60 hours. The suspension was filtered, and the solid washed with dichloromethane. The combined filtrate was evaporated to dryness. The residue was redissolved in chloroform and washed with 20mL of a saturated solution of sodium carbonate, and 2 x 20 mL water. The organic fraction was dried over anhydrous sodium sulphate, and the solvent removed by evaporation, to yield the crude product.

Yield (crude) = 0.7 g (94%) (~ 70% pure)

The ligand was purified by formation of the corresponding nickel(II) complex.

7.1.17.1 Synthesis of [Ni([10]aneS$_2$N earmuff)](ClO$_4$)$_2$ (28)

The crude ligand (0.7 g, 1.9 mmol) was dissolved in hot acetonitrile. To this was added Ni(ClO$_4$)$_2$·6H$_2$O (0.68 g, 1.9 mmol) in acetonitrile. The solution was refluxed for 1 hour, then evaporated to dryness. The purple complex was dissolved in hot water, and filtered to remove a red solid. The complex was purified by column chromatography (sephadex CM-C25, 0.05 M sodium perchlorate eluent). The complex was recrystallised by slow evaporation of the saturated aqueous sodium perchlorate solution.

Yield = 0.37 g (31%) Overall yield from [10]aneS$_2$N = 29%

7.1.17.2 Decomplexation of [Ni([10]aneS$_2$N earmuff)](ClO$_4$)$_2$ to give the free ligand (27)

The nickel(II) complex (0.37 g, 0.58 mmol) was dissolved in 100 mL water, and refluxed until dissolved. Sodium cyanide (0.2 g, 4.1 mmol) in 50 mL water was added to the refluxing solution. The solution was refluxed for 1 hour, and the white solid was filtered and washed with water.

Yield = 0.21 g (96%)

^{1}H NMR (300MHz) ($CDCl_3$): δ 1.90 (m, 2H, CH_2-C), 2.63 (s, 2H, N-CH_2-CH_2-N), 2.69 (t, 4H, CH_2-CH_2-CH_2-S), 2.71 (t, 4H, N-CH_2-CH_2-S), 3.14 (t, 4H, N-CH_2-CH_2-S)

^{13}C NMR (75.5MHz) ($CDCl_3$): δ 30.3 (CH_2-C), 30.8 (CH_2-CH_2-CH_2-S), 33.1 (N-CH_2-CH_2-S), 52.0 (N-CH_2-CH_2-N), 57.1 (S-CH_2-CH_2-N)

MS (CI): m/z 381 (M+1), 409 (M+29)

7.1.18 Synthesis of [Pd([10]aneS$_2$N earmuff)](PF$_6$)$_2$ (30)

[10]aneS$_2$N earmuff (0.1 g, 0.26 mmol) in acetonitrile was degassed with nitrogen and refluxed until dissolved. Pd(acetate)$_2$ (59 mg, 0.26 mmol) was dissolved in 25 mL dry acetonitrile and degassed with nitrogen. The metal was added dropwise to the refluxing ligand solution over a one hour period, then refluxed for a further hour. The orange/red solution was reduced in volume to about 10 mL, and filtered. A saturated solution of ammonium hexafluorophosphate in acetonitrile (3 mL) was added to the solution. Ether diffusion into this solution at 0°C gave red needle-like crystals, which analysed as [Pd([10]aneS$_2$N earmuff)](CH$_3$COO)(PF$_6$)(½CH$_3$CN) (29). These crystals were redissolved and more ammonium hexafluorophosphate was added. Repeated recrystallisation by heating

to dissolve the palladium complex in acetonitrile and diffusion of ether into the solution at <0°C gave the symmetrical [Pd([10]aneS$_2$N earmuff)](PF$_6$)$_2$ isomer.

Yield = 150 mg (74%)

Unsymmetrical isomer [Pd([10]aneS$_2$N earmuff)](CH$_3$COO)(PF$_6$)(½CH$_3$CN) (**30**):

^{1}H NMR (360MHz) (CD$_3$CN) (70°C): δ 1.72 (m), 2.10 (m), 2.38 (m), 2.55 (m), 2.69 (m), 2.78 (m), 3.01 (m), 3.15 (m), 3.29 (m), 3.68 (dq), 3.97 (td), 4.42 (q)

^{13}C NMR (90.6MHz) (CD$_3$CN) (70°C): δ 27.2, 29.3, 30.2, 32.8, 33.3, 34.5, 36.8, 37.6, 40.3, 47.9, 49.6, 54.1, 55.1, 55.4, 55.8, 57.1

MS (FAB):m/z 485.0 ([Pd^{II}(L-H$^+$)]$^+$)

Elemental Analysis: Calculated(found) for Pd(L)(PF$_6$)(CH$_3$COO).½CH$_3$CN C 32.07(31.58), H 5.17(5.17), N 4.92(5.48)

Symmetrical isomer [Pd([10]aneS$_2$N earmuff)](PF$_6$)$_2$ (**29**):

^{1}H NMR (300MHz) (CD$_3$CN): δ 2.00 (m), 2.60 (m), 2.90 (m)

^{13}C NMR (75.5MHz) (CD$_3$CN): δ 28.1 (S-CH$_2$-C-N), 28.8 (C-CH$_2$-C), 37.6 (S-CH$_2$-C-C), 48.3 (S-C-CH$_2$-N), 52.5 (N-C-CH$_2$-N)

UV/vis (acetonitrile): 273 nm (ε = 10750 M^{-1}cm^{-1}), 335 nm (ε = 14700 M^{-1}cm^{-1}), 459 nm (ε = 841 M^{-1}cm^{-1})

Elemental Analysis: Calculated(found) for Pd(L)(PF$_6$)$_2$ C 24.73(24.73), H 4.14(4.09), N 3.61(3.87)

7.1.19 Synthesis of [Co([10]aneS$_2$N earmuff)](ClO$_4$)$_2$ (31)

[10]aneS$_2$N earmuff (0.107 g, 0.28 mmol) was dissolved in 25 mL refluxing acetonitrile under nitrogen. Co(ClO$_4$)·6H$_2$O (103 mg, 0.28 mmol) in 20 mL acetonitrile was added dropwise, and the solution was refluxed for an hour. The solution was reduced in volume, and brown crystals were grown from an acetonitrile/ether solution.

Yield = 178 mg (quantitative)

UV/Vis (acetonitrile): 233 nm (ϵ = 6880 M^{-1}cm^{-1}), 281 nm (ϵ = 5550 M^{-1}cm^{-1}), 319 nm (ϵ = 4100 M^{-1}cm^{-1}), 503 nm (ϵ = 139 M^{-1}cm^{-1})

MS (FAB): m/z 438.1 ([Co^{II}(L-H$^+$)]$^+$), 537.0 ([Co^{II}(L)(ClO$_4^-$)]$^+$)

Elemental analysis: Calculated(found) for Co(L)(ClO$_4$)$_2$ % C 30.10(30.07) H 5.05(4.69) N 4.39(4.90)

7.1.20 Synthesis of [Co([10]aneS$_2$N earmuff)](ClO$_4$)$_3$ (32)

[Co([10]aneS$_2$N earmuff)](ClO$_4$)$_2$ (80 mg, 0.13 mmol) was dissolved in a minimum volume of acetonitrile. Nitrosyl tetrafluoroborate (15 mg, 0.26 mmol) was added, and the solution heated for 15 minutes. The solution turned red. The acetonitrile was evaporated, and the compound redissolved in a minimum amount of water. A saturated solution of sodium perchlorate (2 mL) was added. Slow evaporation gave red crystals.

Yield = 69 mg (75%)

UV/Vis (acetonitrile): 269 nm (ϵ = 7460 M^{-1}cm^{-1}), 511 nm (ϵ = 478 M^{-1}cm^{-1})

MS (FAB): m/z 439.01 ([Co^{II}(L-H$^+$)]$^+$), 538.0 ([Co^{II}(L)(ClO$_4^-$)]$^+$)

^{1}H NMR (300MHz) (D$_2$O): δ 2.21(m), 2.64(m), 2.9(m), 3.23 (m), 3.5 (m), 3.78 (m)

^{13}C NMR (75.5MHz) (D_2O): δ 19.5 (C-CH_2), 28.2, 29.5, 37.0, 40.8, 60.9, 69.3, 70.6

^{59}Co NMR (85.8MHz) (D_2O): δ 4409

Elemental analysis: Calculated(found) for $Co(L)(ClO_4)_3$ % C 26.04(25.08) H 4.37(4.08) N 3.80(3.96)

7.1.20 Synthesis of 1,9-*bis*(8-aza-1,4-dithiacyclodecane)-4,7-dione nonane (33)

7.1.20.1 Synthesis of 1,3-*bis*(chloroacetyl)propylenediamine

1,3-propylenediamine (2 ml, 31 mmol) was dissolved in 450 mL dichloromethane/50 mL water in a 2 L 3 necked flask. The vessel was placed under nitrogen, and cooled to 0°C. With rapid stirring, chloroacetyl chloride (10 mL, 62 mmol) in 250 ml dichloromethane and potassium carbonate (18 g, 65 mmol) in 250mL water were added dropwise at the same rate over a period of 2 hours. After addition was complete, the solution was allowed to warm up to room temperature, and stirred for a further 2 hours. The aqueous layer was removed, and the organic layer washed with water (2x200 mL). The organic layer was dried with anhydrous sodium sulphate, and the solvent removed under reduced pressure. The residue was recrystallised from dichloromethane.

Yield = 5.3 g (75%)

^1H NMR (300MHz) ($CDCl_3$): δ 1.74 (m, 2H, CH_2-C), 3.38 (q, 4H, CH_2-N), 4.08 (s, 4H, CH_2-Cl), 7.10 (br, 2H, NH)

^{13}C NMR (75.5MHz) ($CDCl_3$): δ 29.4 (CH_2-C), 36.4 (CH_2-N), 42.6 (CH_2-Cl), 166.9 (C=O)

7.1.21.2 Synthesis of 1,9-*bis*-(4-aza-1,8-dithiacyclononane)-4,7-diaza-2,8-dione nonane (*bis*-[10]aneS_2N amidoearmuff) (33)

[10]aneS_2N (0.5 g, 2.8 mmol) was dissolved in 50 mL acetonitrile. 1,3-*bis*(chloroacetyl) propylenediamine (0.32 g, 1.4 mmol) and sodium carbonate (1.5 g, 14 mmol) were added to the solution. The suspension was refluxed under nitrogen for 5 days. The solids were removed by filtration and washed with dichloromethane. The combined filtrate was taken to dryness. The crude ligand was purified by forming the nickel(II) complex.

Crude yield quantitative.

^{1}H NMR (300MHz) ($CDCl_3$): δ 1.80 (m, 6H, CH_2-C), 2.69 (br, 16H, CH_2-S), 3.10 (s, N-CH_2-C=O), 3.20 (t, 8H, S-CH_2-CH_2-N), 3.28 (q, 4H, CH_2-NH), 8.3 (br, 2H, NH)

^{13}C NMR (75.5MHz) ($CDCl_3$): δ 29.4 (N-CH_2-CH_2-CH_2-N), 30.1 (CH_2-CH_2-S), 31.6(S-CH_2-CH_2-N), 33.3 (CH_2-CH_2-CH_2-S), 36.6 (CH_2-CH_2-CH_2-N), 57.8 (S-CH_2-CH_2-N), 59.3 (CH_2-C=O), 170.5 (C=O)

MS (CI): m/z 509 (M+1), 537 (M+29), 549 (M+41)

7.1.22 Synthesis of [Ni_2(*bis*-[10]aneS_2N amido earmuff)](ClO_4)$_2$ (34)

The crude ligand was dissolved in methanol, and $Ni(ClO_4)_2 \cdot 6H_2O$, also in methanol, was added under nitrogen. The solution was refluxed for 1 hour, then filtered. The solution was evaporated to dryness and loaded onto a sephadex CM-C25 column. The teal green complex was eluted with 0.5 M sodium perchlorate. A lilac band, eluted initially with 0.1 M sodium perchlorate, was identified as [Ni([10]aneS_2N)$_2$](ClO_4)$_2$. Attempts to recrystallise the complex proved unsuccessful.

MS (FAB): m/z 722.9 ($[Ni^{II}_2(L\text{-}2H^+)(ClO_4^-)]^+$), 822.8 ($[Ni^{II}_2(L\text{-}H^+)(ClO_4^-)_2]^+$), 922.7 ($[Ni^{II}_2L(ClO_4)_3]^+$)

UV/Vis (water): 377 nm, 604 nm, 992 nm

7.2 Instrumentation and experimental methods

7.2.1 Spectroscopy

All high field ^1H and ^{13}C NMR spectra were recorded on either a Bruker AC300 or AMX360 spectrometer. Chemical shifts are reported relative to tetramethylsilane (TMS) at 0 ppm.

Infrared spectra were recorded on either a Bruker IFS25 spectrometer, or a Perkin-Elmer 1330 spectrometer. Samples were prepared as nujol mulls between NaCl plates or as KBr discs.

UV-Visible spectra were run on a dual beam Cary 5 UV-Vis-NIR spectrometer, as solutions in a quartz cell. The solvent was used as a background reference, and all spectra were run at ambient temperatures.

Mass spectra of organic compounds were run on a Finnegan GC 330 mass spectrograph using standard chemical ionisation methods. Mass spectra of salts were obtained using a Kratos Concept double focusing magnetic instrument as liquid secondary ion mass spectra. Ions were produced by either fast atom bombardment (FAB) or by electrospray (ES) techniques. The matrix used for FAB-MS was meta-nitrobenzylalcohol (mNBA), and all spectra were run

in the positive ion mode unless otherwise mentioned. For spectra obtained by electrospray methods, ionisation was achieved by volatilising a 10^{-4} M solution of the compound in CH_3CN/H_2O (1:1).

Elemental Analysis was provided by Canadian Microanalytical Services, Vancouver, BC.

Electron paramagnetic resonance spectroscopy was performed on either a Varian E6 EPR spectrometer or a Bruker ER200tt instrument. Microwave radiation used was in the X-band region (9.2 GHz). Diphenylpicrylhydrazyl hydrate (DPPH, g = 2.0037) was used as an external standard. Spectra were recorded in solution at ambient temperatures or at 77 K. Spectra recorded as a frozen glass at 77 K were obtained using a quartz dewar filled with liquid nitrogen.

7.2.2 Mass susceptibility measurements

Mass susceptibility measurements were determined by ^1H NMR spectroscopy using the Evan's method.[124] The indicator compound used was either the H_2O resonance in D_2O, or the $CHCl_3$ resonance in a 5% $CHCl_3$ in CD_3CN solution. The indicator solution was placed in a capillary tube, which was then fitted into a 5 mm NMR tube containing a solution of the compound of interest dissolved in the indicator solution. Concentrations of ~10^{-2} M were commonly used. The shift in the indicator resonance in the absence and presence of paramagnetic material was used to determine χ_g. No attempt was made to correct for the mass susceptibility of the solvent, or the density of the two solutions.[143] The diamagnetic contribution of the ligand was

used in calculating χ_M, and from this the magnetic moment was calculated.

7.2.3 Crystallography

$[Cu([10]aneN_2O)_2](ClO_4)_2 \cdot (H_2O)$

The crystal was mounted in a glass Lindemann tube and the unit cell and space group determined using Weissenberg and precession photography. The crystal was transferred to a Picker four-circle diffractometer automated with a PDP 11/10 computer. The unit cell was refined using 25 pairs of reflections in the 2θ range 17 - 36°. The intensity measurements were made using Zr-filtered Mo radiation, λ = 0.7093 Å. Background counting was introduced at the end of each scan. A set of three standard reflections preceded each batch of 50 measurements, with no noticeable change of intensity observed during the collection.

Solution of the phase problem was achieved via the Patterson Method using the NRCVAX crystal structure system.[144] Refinement of the system was carried out via the SHELX least squares method.[145] The perchlorate groups were forced to adopt a tetrahedral geometry, and the hydrogen atoms were placed in the calculated positions. The refinement converged with a maximum shift/esd of 0.02.

7.2.4 Electrochemistry

A Princeton Applied Research Model 273 potentiostat/galvanostat interfaced to an IBM PC computer was used for electrochemical measurements. Cyclic voltammograms were obtained using the Headstart program (Princeton). A standard three electrode electrochemical cell was

employed, with a Pt microelectrode as the working electrode, a Pt bead as the counter electrode, and a Ag^+/Ag reference electrode, linked to the cell via a salt bridge. All electrochemistry was performed in dry acetonitrile solutions containing supporting electrolyte (0.1 M) (usually 0.1 M $^tBu_4NClO_4$). Freshly prepared solutions were used, and degassed with argon prior to electrochemical measurments. The ferrocinium/ferrocene (Fc^+/Fc) couple was used as an external standard. $E_{½}$ values are reported relative to the Ag^+/Ag couple ($E_{½}$ (Fc^+/Fc) = 0.1V vs (Ag^+/Ag)).

7.2.5 Kinetic measurements

The kinetics of decomposition of Ni^{III} species were monitored using a Cary 05E spectrophotometer. The decomposition was followed at a specific wavelength, and monitored over several half lives. Decomposition rates were calculated with the use of the built in processing package with the spectrophotometer, employing a first order exponential fit of the absorbance vs time curve.

Substitution reaction kinetics measurements were determined using an Applied Photophysics DX-17MV stopped flow apparatus, equipped with an Acorn microcomputer. The reaction temperature was controlled at 10±0.2°C using a water bath. One syringe was charged with a ~4.10^{-4} M solution of the Ni^{III} complex in aqueous $HClO_4$ while the other syringe contained a LiCl solution of appropriate concentration. The ionic strength of all solutions was maintained at 1M, by addition of an appropriate amount of $LiClO_4$. The [Ni(bicyclo[12-12]N_4O)]$^{3+}$ solution was made by oxidising a Ni^{II} solution with a deficiency of

hexaaquacobalt(III) in 4 M $HClO_4$. The amount of acid added via the hexaaquacobalt (III) solution was taken into account when determining the concentration of acid present in the Ni^{III} solution. Since the Ni^{III} solution decomposed fairly rapidly, it was freshly made before each set of measurments, and kept on ice during the period of the measurements. The substitution reaction was followed at 430 nm. Pseudo-first order conditions were achieved by reacting a >10 times excess of Cl^- over the $[Ni(bicyclo[12\text{-}12]N_4O)]^{3+}$ ion. The substitution reaction rate was determined at several different concentrations of chloride and acid. Repeat determinations were made at all concentrations, and the averages used to plot the graphs. The rates of reaction were calculated using the DX-17MV software provided with the stopped flow equipment.

REFERENCES

1 I.S. Butler, J.F. Harrod; *Inorganic Chemistry*, Chp. 12, (1989) Benjamin/Cummings Publisher.

2 G.A. Melson; *Coordination Chemistry of Macrocyclic Compounds*, (1979) Plenum Press.

3 See for example,

a) F.H. Moser, A.L. Thomas; *Phthalocyanine Compounds*, (1963) Reinhold Publishing Corp.

b) G.S. Marks; *Heme and Chlorophylls*, (1969) Van Nostrand.

4 A.R. Battersby, E. McDonald in Ed. K.M. Smith; *Porphyrins and Metalloporphyrins*, (1965) Elsevier.

5 H. de Diesbach, E. von der Weid; *Helv. Chim. Acta.*, **10** (1927) 886.

6 A.B.P. Lever; *Adv. Inorg. Radiochem.*, **7** (1965) 28.

7 L.J. Boucher; in *Coordination Chemistry of Macrocyclic Compounds*, Ed. G.A. Melson, Chp 4 (1979) Plenum Press.

8 J.M. Robertson; *J. Chem. Soc.*, **1935** (1935) 615.

9 N.F. Curtis; *J. Chem. Soc.* (1960) 4409.

10 C.J. Pedersen; *J. Am. Chem. Soc.*, **89** (1967) 7017.

11 L. Horner, P. Walach, H. Kunz; *Phosphorus and Sulfur* **5** (1978) 171.

12 T. Kauffmann, J. Ennen; *Tet. Lett*,, (1981) 5035.

13 a) N. Bresciani-Pahor, M. Forcolim, L.G. Marzilli, L. Randaccio, M.F. Summers, P.J. Toscano; *Coord. Chem. Rev.*, **63** (1985) 1.

b) W.O. Parker, E. Zangrando, N. Bresciani-Pahor, L, Randaccio, L.G. Marzilli;

Inorg. Chem., **25** (1986) 3489.

c) K. Farmery, D.H. Busch; *J. Chem. Soc., Chem. Comm.*, (1970) 1091.

14 J.E. Richman, T.J. Atkins; *J. Am. Chem. Soc.*, **96** (1974) 2268.

15 M.G.B. Drew, F.S. Esho, A. Lavery, S.M. Nelson; *J. Chem. Soc., Dalton Trans.*, (1984) 545.

16 J.T. Landrum, D. Grinnett, K.J. Haller, W.R. Scheidt, C.A. Reed; *J. Am. Chem. Soc.*, **103** (1981) 2640.

17 a) D.C. Olson, J. Vasilevskis; *Inorg. Chem.*, **8** (1969) 1611.

b) D.C. Olson, J. Vasilevskis; *Inorg. Chem.*, **10** (1971) 463.

18 D.K. Cabbiness, D.W. Margerum; *J. Am. Chem. Soc.*, **91** (1969) 6540.

19 A.E. Martell, R.D. Hancock, R.J. Motekaitis; *Coord. Chem. Rev.*, **133** (1994) 39.

20 a) D. Munro; *Chem. Ber.* **13** (1977) 100.

b) C.F. Bell; *Principles and Applications of Metal Chelation*, (1977) Oxford University Press.

21 a) R.D. Hancock, S.M. Dobson, A. Evers, P.W. Wade, M.P. Ngwenya, J.C.A. Boeyens, K.P. Wainright; *J. Am. Chem. Soc.*, **110** (1988) 2788.

b) R.D. Hancock, A. Evers, M.P. Ngwenya, P.W. Wade; *J. Chem. Soc., Chem. Comm.*, (1987) 1129.

22 R.T. Myers; *Inorg. Chem.*, **17** (1978) 952.

23 E.J. Billo; *Inorg. Chem.*, **23** (1984) 236.

24 D.H. Busch, K. Farmery, V. Goedken, V. Katovic, A.C. Melnyk, C.R. Sperati, N. Tokel; *Adv. Chem. Ser.*, **100** (1971) 44.

25 B. Bosnich, C.K. Poon, M.L. Tobe; *Inorg. Chem.*, **4** (1965) 1102.

26 M.M. Bishop, J. Lewis, T.D. O'Donoghue, P.R. Raithby, J.N. Ramsden; *J. Chem. Soc., Dalton Trans.*, (1980) 1390.

27 K. Henrick, P.A. Tasker, L.F. Lindoy; *Prog. Inorg. Chem.*, **33** (1985) 1.

28 a) S. Ahrland, J. Chatt, N.R. Davies; *Quart. Rev.*, **12** (1958) 265.

b) R.G. Pearson; *J. Chem.Ed.*, **45** (1968) 581, 643.

29 L.Y. Martin, L.J. DeHayes, L.J. Zompa, D.H. Busch; *J. Am. Chem. Soc.*, **96** (1974) 4046.

30 L.Y. Martin, C.R. Sperati, D.H. Busch; *J. Am. Chem. Soc.*, **99** (1977) 2968.

31 J.E. Parks, B.E. Wagner, R.E. Holm; *Inorg. Chem.*, **11** (1972) 2652.

32 P.V. Bernhard, P. Comba, T.W. Hambley, G.A. Lawrance; *Inorg. Chem.*, **30** (1991) 942.

33 a) R.D. Hancock, G.J. McDougal; *J. Am. Chem. Soc.*, **102** (1980) 6551.

b) V.J. Thom, J.C.A. Boeyens, G.J. McDougall, R.D. Hancock; *J. Am. Chem. Soc.*, **99** (1984) 3198.

34 K.K. Nanda, R. Das, K. Venkatsubraminium, P. Paul, K. Nag; *J. Chem. Soc., Dalton Trans.*, (1993) 2515.

35 T.J. Lotz, T.A. Kaden; *Helv. Chim. Acta.*, **61** (1978) 1376.

36 J.F. Endicot, J. Lilie, J.M. Kuszaj, B.S. Ramaswamy, W.G. Schmorsees, M.G. Simic, M.D. Glick, D.P. Rillema; *J. Am. Chem. Soc.*, **99** (1977) 429.

37 C.M. Guzy, J.B. Raynor, M.C.R. Symons; *J. Chem. Soc.(A)*, **1969** (1969) 2299.

38 a) L.D. Kollmann, S.I. Cham; *Inorg. Chem.*, **10** (1971) 1978.

b) R.L. Martin, S. Mitra; *Chem. Phys. Lett.*, **3** (1969) 183.

39 G. Maki.; *J. Chem. Phys.*, **28** (1958) 651.

40 a) L. Fabbrizzi; *Inorg. Chim. Acta.*, **36** (179) L391.

b) L. Fabbrizzi; *Comments Inorg. Chem.*, **4** (1985) 33.

41 F.V. Lovecchio, E.S. Gore, D.H. Busch; *J. Am. Chem. Soc.*, **96** (1974) 3109.

42 L.F. Lindoy; *The Chemistry of Macrocyclic Ligand Complexes*, (1989) Cambridge University Press.

43 J.-M. Lehn, J.P. Sauvage; *J. Am. Chem. Soc.*, **97** (1975) 6700.

44 R.D. Hancock; *J. Chem. Ed.*, **69** (1992) 615.

45 G. Ercolani, L. Mandolini, P. Mencarelli; *J. Chem. Soc., Perkin Trans.*, **2** (1990) 747.

46 L.F. Lindoy, D.H. Busch; *Preparative Inorganic Reactions*, Ed. Jolly, W., Vol 6 (1971) Interscience.

47 M.C. Thompson, D.H. Busch, *J. Am. Chem. Soc.*, **86** (1964) 3651.

48 a) J.-M. Lehn; *Pure Appl. Chem*, **52** (1980) 2441.

b) B. Dietrich, J.-M. Lehn, J.P. Sauvage; *Tetrahedron*, **29** (1973) 1647.

49 I.I. Creaser, R.J. Geue, J. MacB. Harrowfield, A.J. Herlt, A.M. Sargeson, M.R. Snow, J. Springborg; *J. Am. Chem. Soc.*, **104** (1982) 6016.

50 A. Bencini, A. Bianchi, C. Bazzicalupi, M. Ciampolini, V. Fusu, M. Michelone, N. Nardi, P. Paoli, B. Valtancoli; *Supramolecular Chem.*, **3** (1994) 141.

51 E.J. Billo, P.J. Connolly, D.J. Sardella, J.P. Jasinski, R.J. Butcher; *Inorg. Chim. Acta.*, **230** (1995) 19.

52 P.J. Smolenaers, J.K. Beattie; *Inorg. Chem.*, **25** (1986) 2259.

53 K.L. Brown; *Inorg. Chim. Acta.*, **37** (1979) L513.

54 R. C. Drago; *Physical Methods for Chemists. 2nd Ed.*, (1992) Saunders.

55 H.A.A. Omar, P. Moore, N.W. Alcock; *J. Chem. Soc., Dalton Trans.*, (1994) 2631.

56 D.H. Evans, K.M. O'Connell, R.A. Petersen, M.J. Kelly; *J. Chem. Ed.*, **60** (1983) 290.

57 a) F.L. Wimmer, M.R. Snow, A.M. Bond; *Inorg. Chem.*, **13** (1984) 1617.

b) R.D. Rieke, H. Kojima, K. Öefle; *J. Am. Chem. Soc.*, **98** (1976) 6735.

c) K.A. Conner, R.A. Walton; *Inorg. Chem.*, **25** (1986) 4422.

58 T.J. Atkins, J.E. Richman, W.F. Oettle; *Organic Syntheses*, **58** (1978) 86.

59 a) D. Reinen, A. Ozarowski, B. Jacob, B. Pebler, H. Stratemeier, K. Wieghardt, I. Tolksdorf; *Inorg. Chem.*, **26** (1987) 4010.

b) R.D. Hancock, S.M. Dobson, J.C.A. Boeyens; *Inorg. Chim. Acta.*, **133** (1987) 221.

c) A. McAuley, S. Subramanian; *Inorg. Chem.*, **29** (1990) 2830.

d) K. Wieghardt, P. Chaudhury; *Prog. Inorg. Chem.*, **35** (1988) 329.

60 a) L.T. Taylor, S.C. Vergez, D.H. Busch; *J. Am. Chem. Soc.*, **88** (1966) 3170.

b) R. Yang, L.J. Zompa; *Inorg. Chem.*, **15** (1976) 1499.

61 a) S. Chandrasekhar, A. McAuley; *Inorg. Chem.*, **31** (1992) 2234.

b) S.M. Hart, J.C.A. Boeyens, J.P. Michael, R.D. Hancock; *J. Chem. Soc., Dalton Trans.*, (1983) 1601.

62 V.J. Thöm, M.S. Shaikjee, R.D. Hancock; *Inorg. Chem.*, **25** (1986) 2992.

63 W. Rasshofer, W. Wehner, F. Vögtle; *Justus Liebigs Ann. Chem.*, (1976) 916.

64 G.H. Searle, R.J. Geue; *Aust. J. Chem.*, **37** (1984) 2234.

65 X-M. Chen, Y-X. Yao, K-L. Shi, T.C.W. Mak; *Aust. J. Chem.*; **48** (1995) 139.

66 H.A. Jahn, E. Teller; *Proc. R. Soc. London, Ser. A.*, **161** (1937) 220.

67 a) K.A. Beveridge, A. McAuley, C.Xu; *Inorg. Chem.*, **30** (1994) 2074.

b) D.G. Fortier, A. McAuley; *Inorg. Chem.*, **28** (1989) 655.

c) P.W.R. Corfield, C. Ceccarelli, M.D. Glick, I.W.-Y. Moy, L.A. Ochrymowycz, D.B. Rorabacher; *J. Am. Chem. Soc.*, **107** (1985) 2399.

d) C.R. Lucas, S. Liu; *J. Chem. Soc., Dalton Trans.*, (1994) 185.

68 C. Xu, *PhD Thesis*, University of Victoria (1991).

69 A.A.G. Tomlinson, B.M. Hathaway, *J. Chem. Soc. (A)*, (1968) 1685.

70 R.L. Belford, M. Calvin, G. Belford, *J. Chem. Phys.*, **26** (1957) 1165.

71 B.N. Figgis in G. Wilkinson (Ed); *Comprehensive Coordination Chemistry*, **1** Pergamon Press (1987) 213.

72 A.D. Beveridge, A.J. Lavery, M.D. Walkinshaw, M.J. Schröder; *J. Chem. Soc., Dalton Trans.*, (1987) 373.

73 A.W. Addison, E. Sinn; *Inorg. Chem.*, **22** (1983) 1225.

74 A.W. Addison, M. Carpenter, L.K-M. Lau, M. Wicholas; *Inorg. Chem.*, **17** (1978) 1545.

75 F.G. Herring, R.L. Tapping; *Can. J. Chem.*, **52** (1974) 4016.

76 I. Adato, I. Eliezer; *J. Chem. Phys.*, **54** (1971) 1472.

77 L. Fabbrizzi, A. Poggi, P.J. Zannello; *J. Chem. Soc., Dalton Trans.*, (1983) 2191.

78 B.M. Hathaway in G. Wilkinson, Ed.; *Comprehensive Coordination Chemistry*, **5**

Pergamon Press (1987) 533.

79 C. Xu, A. McAuley; *Unpublished results.*

80 a) S-G. Kang, M-S. Kim, J-S. Choi, D. Whang, K. Kim; *J. Chem. Soc., Dalton Trans.*, (1995) 363.

b) V.J. Thöm, C.C. Fox, J.C.A. Boeyens, R. Hancock; *J. Am. Chem.Soc.*, **106** (1984) 5947.

81 L.J. Fabbrizzi; *J. Chem. Soc., Dalton Trans.*, (1979) 1857.

82 L.J. Zompa, T.N. Margulis; *Inorg. Chim. Acta.*, **45** (1980) L263.

83 R.D. Hancock, V.J. Thöm; *J. Am. Chem. Soc.*, **104** (1982) 291.

84 S.R. Cooper, S.C. Rawle, J.R. Hartman, E.J. Hintsa, G.A. Admans; *Inorg. Chem.*, **27** (1988) 1209.

85 J.C.A. Boeyens, A.G.S. Forbes, R.D. Hancock, K. Wieghardt; *Inorg. Chem.*, **24** (1985) 2926.

86 S.M. Hart, J.C.A. Boeyens, R.D. Hancock, *Inorg. Chem.*, **22** (1983) 982.

87 B.N. Figgis in G. Wilkinson (Ed); *Comprehensive Coordination Chemistry*, **1** Pergamon Press (1987) 213.

88 L.Y. Martin, C.R. Sperati, D.H. Busch; *J. Am. Chem. Soc.*, **99** (1977) 2968.

89 A. McAuley, D.G. Fortier, D.H. Macartney, T.W. Whitcombe, C.Xu; *J. Chem. Soc., Dalton Trans.*, (1994) 2071.

90 E.K. Barefield, G.M. Freeman, D.G.V. Derveer; *Inorg. Chem.*, **25** (1986) 552.

91 S. Chandresekhar; *Unpublished results.*

92 G. Hunter, A. McAuley, T.W. Whitcombe; *J. Am. Chem. Soc.*, **27** (1988) 2634.

93 A. McAuley, T.W. Whitcombe; *Inorg. Chem.*, **27** (1988) 3090.

94 F. Hori, M. Matsumoto, S. Ooi, H. Kuroya; *Bull. Chem. Soc. Jpn.*, **50** (1977) 138.

95 W.R. Mason, III, H.B. Gray; *J. Am. Chem. Soc.*, **90** (1968) 5721.

96 S. Chandrasekhar; *PhD Thesis*, University of Victoria (1991).

97 G.A. Lawrance, P.G. Lye; *Comments Inorg. Chem.*, **15** (1994) 339.

98 G.W. Watt, P.W. Alexander; *Inorg. Chem.*, **7** (1968) 537.

99 F. Wagner, E.K. Barefield; *Inorg. Chem.*, **15** (1976) 408.

100 J.F. Desreux, E. Merciny, M.F. Loncin; *Inorg. Chem.*, **20** (1981) 987.

101 a) Z. Kovacs, A.D. Sherry; *J. Chem. Soc., Chem. Comm.*, (1995) 186.

b) D. Parker, Ed.; *Macrocycle Synthesis*, (1996) Oxford University Press.

102 S. Buøen, J. Dale; *Acta Chem. Scand. B*, **40** (1986) 141.

103 G.R. Weisman, M.R. Rogers, E.H. Wong, J.P. Jasinski, E.S. Paight; *J. Am. Chem. Soc.*, **112** (1990) 8604.

104 G.H. Robinson, S.A. Sangokoya, W.T. Pennington, M.F. Self, R.D. Rogers; *J. Coord. Chem.*, **19** (1989) 287.

105 T. Rodopoulous; *Unpublished results.*

106 S. Kulstad, L.Å. Malmsten; *Acta Chem. Scand. B*, 33 (1979) 469.

107 C.H. Park, H.E. Simmons; *J. Am. Chem. Soc.*, **90** (1968) 2429.

108 J. Springborg, P. Kofod, C.E. Olsen, H. Toftlund, I. Søtofte; *Acta Chem. Scand.*, **49** (1995) 547.

109 R.W. Alder, R.E. Moss, R.B. Sessions; *J. Chem. Soc., Chem. Comm.*, (1983) 1000.

110 E. Müller, G. Bernardinelli, J. Reedijk; *Inorg. Chem.*, 35 (1996) 1952.

111 P.J. Connolly, E.J. Billo; *Inorg. Chem.*, **26** (1987) 3224.

112 M. Micheloni; *J. Coord. Chem.*, **18** (1988) 3.

113 K.P. Wainwright; *Inorg. Chem*, **19** (1980) 1396.

114 R. Bhula, P. Osvath, D.C. Weatherburn; *Coord. Chem. Rev.*, **91** (1988) 89.

115 a) W.N. Setzer, C.A. Ogle, G.S. Wilson, R.S. Glass; *Inorg. Chem.*, **22** (1983) 266.

b) K. Wieghardt, H-J. Küppers, H.Z. Weiss; *Inorg. Chem.*, **24** (1985) 3067.

c) S.C. Rawle, T.J. Sewell, S.R. Cooper; *Inorg. Chem.*, **26** (1987) 3769.

d) A.J. Blake, R.O. Gould, A.J. Holder, T.I. Hyde, A.J. Lavery, M.O. Odulate, M.J. Schröder; *J. Chem. Soc., Chem. Comm.*, (1987) 118.

116 D.M. Wambeke, W. Lippens, G.G. Herman, A.M. Goeminne, G.P. van der Kelen; *Polyhedron*, **11** (1992) 2989.

117 R. Haines, A. McAuley; *Coord. Chem. Rev.*, **33** (1981) 77.

118 B.L. Vallee, R.J.P. Williams; *Proc. Nat. Acad. Sci. (USA)*, **59** (1968) 498.

119 F.A. Cotton, G. Wilkinson; *Advanced Inorganic Chemistry*, 5th Ed., (1988) Wiley and Sons.

120 H. Koyama, T. Yoshino; *Bull. Chem. Soc. Jpn.*, **45** (1972) 481.

121 H-J. Küppers, A. Neves, C. Pomp, D. Ventur, K. Wieghardt, B. Nuber, J. Weiss; *Inorg. Chem.*, **25** (1986) 2400.

122 a) M. Brorson, M.R. Dyxenburg, F. Galsbøl, K. Simonsen; *Acta. Chem. Scand.*, **50** (1996) 289

b) R.A.D. Wentworth, T.S. Piper; *Inorg. Chem.*, **4** (1965) 1526.

123 S. Chandresekhar, A. McAuley; *Inorg. Chem.*, **31** (1992) 480.

124 G.H. Searle, E. Larsen, *Acta. Chem. Scand. A.*, **30** (1976) 143.

125 D.F. Evans; *J. Chem. Soc.*, (1959) 2003.

126 G. Dyer, M.O. Workman, D.W. Meek; *Inorg. Chem.*, **6** (1967) 1404.

127 K. Wieghardt, E. Schöffmann, B. Nuber, J. Weiss; *Inorg. Chem.*, **25** (1986) 4877.

128 a) S.E. Livingstone, B. Wheelahan; *Aust. J. Chem.*, **17** (1964) 219.

b) C.M. Harris, R.S. Nyholm; *J. Chem. Soc.*, (1956) 4375.

c) O.St.C. Headley, R.S. Nyholm, C.A. McAuliffe, M.L. Tobe, L.M. Venanzi; *Inorg. Chim. Acta.*, **4** (1970) 93.

129 A.J. Blake, A.J. Holder, T.I. Hyde, M. Schröder; *J. Chem. Soc., Chem. Comm.*, (1987) 987.

130 Y. Tanabe, S. Sugano; *J. Phys. Soc. Japan*, **9** (1954) 753.

131 D. Sutton; *Electronic Spectra of the Transition Metal Complexes*, (1968) McGraw-Hill.

132 M.J. D'Aniello Jr., M.T. Mocella, F. Wagner, E.K. Barefield, I.C. Paul; *J. Am. Chem. Soc.*, **97** (1975) 192.

133 R.I. Haines, A. McAuley; *Inorg. Chem.*, **19** (1980) 719.

134 M.G. Fairbank, A. McAuley; *Inorg. Chem.*, **25** (1986) 1233.

135 E.K. Barefield, M.T. Mocella; *J. Am. Chem. Soc.*, **97** (1975) 4238.

136 R.G. Wilkins; *The Study of the Kinetics and Mechanisms of Reaction of Transition Metal Complexes*, (1984) Allyn and Bacon.

137 T.W. Swaddle; *Coord. Chem. Rev.*, **14** (1974) 217.

138 A. McAuley, T. Palmer, T.W. Whitcombe; *Can. J. Chem.*, **71** (1993) 1792.

139 B.S. Furniss, A.J. Hannaford, P.W.G. Smith, A.R. Tatchell; *Vogel's Textbook of Practical Organic Chemistry, 5th Ed.*, (1989) Longman Scientific and Technical.

140 G. Davies, B. Warngvist; *Coord. Chem. Rev.*, **5** (1970) 349.

141 M. Shibata, *Modern syntheses of Co(III) complexes*, (1983) Springer Verlag.

142 E.K. Barefield, F. Wagner, A.W. Herlinger, A.R. Dahl; *Inorg. Synth.*, **16** (1976) 222.

143 D.H. Grant; *J. Chem. Ed.*, **72** (1995) 40.

144 A.C. Larson, F.L. Lee, Y. LePage, M. Webster, J.P. Charland, E.J. Gabe; *NRCVAX Crystal Structure System*, Chemistry Division, NRC, Ottawa, Canada.

145 G.M. Sheldrick; *SHELX76, Program for Crystal Structure Refinement*, (1976) University of Cambridge, Cambridge, UK.

APPENDIX 1

Crystallographic data for $[Cu([10]aneN_2O)_2](ClO_4)_2 \cdot (H_2O)$

Table A.1: Crystallographic data for $[Cu([10]aneN_2O)_2](ClO_4)_2 \cdot H_2O$

Chemical formula: $C_{14}H_{32}Cl_2CuN_4O_8 \cdot H_2O$ fw: 568.8

Space group: $P2_1/c$ (no. 14)

$a = 9.334(1)$ Å

$b = 9.411(2)$ Å

$c = 13.630(3)$ Å

$\alpha, \gamma = 90°$

$\beta = 98.75(1)°$

$V = 1183.32$ Å^3

$Z = 2$

$T = 22 \pm 2$ °C

$\lambda = 0.7093$ Å

Total No. of reflections (No. of reflections in final data set) = 1540 (1284)

$\rho_{obs} = 1.617$ g.cm^{-3}

$\rho_{calc} = 1.598$ g.cm^{-3}

$\mu = 12.09$ cm^{-1}

Transmission coefficient = 0.5028 - 0.5658

$R(F_o) = 0.0631$ $R_w = 0.0712$

Table A.2: Fractional atomic coordinates and temperature parameters for $[Cu([10]aneN_2O)_2](ClO_4)_2 \cdot H_2O$

Atom	x/a	y/b	z/c	U_{eq}
Cu(1)	0(0)	0(0)	0(0)	270(4)
N(1)	2131(6)	363(6)	661(4)	39(2)
N(2)	-180(6)	-1526(6)	1047(4)	36(2)
O(1)	1140(5)	-1893(5)	-683(3)	43(2)
C(1)	210(8)	-958(8)	2095(5)	49(3)
C(2)	1741(9)	-492(9)	2373(5)	50(3)
C(3)	2259(8)	688(8)	1719(5)	45(3)
C(4)	606(8)	-2864(6)	910(6)	47(3)
C(5)	705(9)	-3116(8)	-194(6)	53(3)
C(6)	3152(7)	-802(9)	464(6)	50(3)
C(7)	2646(8)	-1533(9)	-534(6)	55(3)
H(1)	246	131	30	50'
H(2)	-132	-181	93	50'
H(11)	0	-179	260	50'
H(12)	-48	-6	217	50'
H(21)	188	-11	313	50'
H(22)	243	-141	233	50'
H(31)	339	90	199	50'
H(32)	162	163	180	50'
H(41)	169	-280	132	50'
H(42)	4	-374	119	50'
H(51)	-35	-344	-57	50'
H(52)	148	-395	-25	50'
H(61)	421	-35	46	50'
H(62)	321	-158	105	50'
H(71)	327	-250	-57	50'
H(72)	285	-83	-112	50'
Cl(1)	38743(21)	44976(22)	15170(16)	534(8)
O(11)	2763(12)	4049(11)	851(11)	248(9)
O(12)	4290(10)	5795(8)	1348(8)	155(5)
O(13)	3259(25)	4578(17)	2363(11)	374(21)
O(14)	4890(9)	3533(10)	1711(12)	206(8)
O(15)	6737(6)	7719(8)	954(5)	84(3)

Estimated standard deviations are given in parentheses.
Hydrogen atoms have been placed in calculated positions
Coordinates $x10^n$ where n = 5,4,4,4,3,5 for Cu, N, O, C, H, Cl.
Temperature parameters $x10^n$ where n = 4,3,3,3,3,4 for Cu, N, O, C, H, Cl.
U_{eq} = the equivalent isotropic temperature parameter.
$U_{eq} = 1/3\ \Sigma_i\Sigma_j U_{ij} a_i^* a_j^* (a_i . a_j)$ $T = \exp-(8\pi^2 U_{iso} \sin^2\theta/\lambda^2)$
Primed values indicate that U_{iso} is given.

APPENDIX 2

Derivation of the observed rate law for the chloride ion substitution reaction of $[Ni(bicyclo[12\text{-}12]N_4O)(H_2O)]^{3+}$

For the equilibria:

$$\begin{array}{ccc} NiHL + Cl^- & \underset{k_{-1}}{\overset{k_1}{\rightleftharpoons}} & NiHLCl \\ K_b \Big\downarrow & & \Big\uparrow K_a \\ NiL + H^+ + Cl^- & \underset{k_{-2}}{\overset{k_2}{\rightleftharpoons}} & NiLCl + H^+ \end{array}$$

$NiL = [Ni^{III}(bicyclo[12\text{-}12]N_4O)(H_2O)]^{3+}$

$NiHL = [Ni^{III}(bicyclo[12\text{-}12]N_4O + H^+)(H_2O)]^{4+}$

$NiLCl = [Ni^{III}(bicyclo[12\text{-}12]N_4O)(Cl)]^{2+}$

$NiHLCl = [Ni^{III}(bicyclo[12\text{-}12]N_4O + H^+)(Cl)]^{4+}$

$H = H^+$, $Cl = Cl^-$

$$K_2 = \frac{[NiLCl]}{[NiL][Cl]} \qquad K_1 = \frac{[NiHLCl]}{[NiHL][Cl]}$$

$$K_a = \frac{[NiL][H]}{[NiLH]} \qquad K_b = \frac{[NiLCl][H]}{[NiHLCl]}$$

$$\frac{K_2}{K_b} = \frac{[NiLCl]}{[NiL][Cl]}\frac{[NiHLCl]}{[NiLCl][H]} = \frac{[NiHLCl]}{[NiL][H][Cl]}$$

$$\frac{K_1}{K_a} = \frac{[NiHLCl]}{[NiHL][Cl]}\frac{[NiHL]}{[NiL][H]} = \frac{[NiHLCl]}{[NiL][H][Cl]}$$

$$K_aK_2 = K_1K_b$$

$$[M]_t = [NiHL] + [NiL] + [NiHLCl] + [NiLCl] = [NiHL]_{eq} + [NiL]_{eq} + [NiHLCl]_{eq} + [NiLCl]_{eq}$$

$$\text{Rate} = d(NiHLCl)/dt = k_1[NiHL][Cl] - k_{-1}[NiHLCl] - k_b[NiHLCl] + k_{-b}[NiLCl][H]$$

$$= k_1[NiHL]_{eq}[Cl] + k_1[NiL]_{eq}[Cl] + k_1[NiHLCl]_{eq}[Cl] + k_1[NiLCl]_{eq}[Cl] - k_1[NiL][Cl]$$

$$- k_1[NiHLCl][Cl] - k_1[NiLCl][Cl] - k_{-1}[NiHLCl] - k_b[NiHLCl] + k_{-b}[NiLCl][H]$$

$$= \frac{k_1[NiHLCl]_{eq}[Cl]}{K_1[Cl]} + \frac{k_1K_a[NiHLCl]_{eq}[Cl]}{[H]\,K_a[Cl]} + k_1[NiHLCl]_{eq}[Cl]$$

$$+ \frac{k_1K_b[NiHLCl]_{eq}[Cl]}{[H]} - k_{-1}[NiHLCl] - \frac{k_1K_a[NiHLCl][Cl]}{[H]\,K_1[Cl]} - k_1[NiHLCl][Cl]$$

$$- \frac{k_1K_b[NiHLCl][Cl]}{[H]} - k_b[NiHLCl] - k_b[NiHLCl]$$

$$= k_{-1}[NiHLCl]_{eq} + \frac{k_{-1}K_a[NiHLCl]_{eq}}{[H]} + k_1[NiHLCl]_{eq}[Cl]$$

$$- \frac{k_1K_b[NiHLCl]_{eq}[Cl]}{[H]} - k_{-1}[NiHLCl] - \frac{k_{-1}K_a[NiHLCl]}{[H]}$$

$$- k_1[NiHLCl][Cl] - \frac{k_1K_b[NiHLCl][Cl]}{[H]}$$

$$= k_{obs}([NiHLCl]_{eq} - [NiHLCl])$$

$$k_{obs} = k_{-1} + \frac{k_{-1}K_a}{[H]} + k_1[Cl] + \frac{k_1K_b[Cl]}{[H]}$$